5-2011

Complex VS profiles to 100 m depth from Rayleigh waves and 3-D VS model for Las Vegas Valley

Helena Murvosh
University of Nevada, Las Vegas

COMPLEX VS PROFILES TO 100 M DEPTH FROM RAYLEIGH WAVES AND 3-D VS MODEL FOR LAS VEGAS VALLEY

by

Helena Murvosh

Bachelor of Science, Mathematics
University of Nevada Las Vegas
1990

Master of Science, Mathematics
University of Nevada Las Vegas
1993

A thesis submitted in partial fulfillment
of the requirements for the

Master of Science in Engineering
Department of Civil and Environmental Engineering
Howard R. Hughes College of Engineering

Graduate College
University of Nevada, Las Vegas
May 2011

THE GRADUATE COLLEGE

We recommend the thesis prepared under our supervision by

Helena Murvosh

entitled

Complex VS Profiles to 100 m Depth from Rayleigh Waves and 3-D VS Model for Las Vegas Valley

be accepted in partial fulfillment of the requirements for the degree of

Master of Science in Engineering
Department of Civil and Environmental Engineering

Barbara Luke, Committee Chair

Aly Said, Committee Member

David James, Committee Member

Carlos Calderon-Macias, Committee Member

Wanda Taylor, Graduate Faculty Representative

Ronald Smith, Ph. D., Vice President for Research and Graduate Studies
and Dean of the Graduate College

May 2011

ABSTRACT

Complex VS Profiles to 100 m Depth from Rayleigh Waves and 3-D VS Model for Las Vegas Valley

by

Helena Murvosh

Dr. Barbara Luke, Examination Committee Chair
Professor of Civil Engineering
University of Nevada, Las Vegas

Abstract from Manuscript 1, "Complex Shear-Wave-Velocity Profiles to 100 m Depth from Rayleigh Waves for Las Vegas, Nevada": Shear-wave velocity (VS) profiles were developed for 12 sites in the Las Vegas Valley, Nevada, which is situated on a deep alluvium-filled basin. The work was performed to support earthquake site response analyses. Data were acquired using the spectral analysis of Rayleigh-type surface waves (SASW) method. Sources used were an IVI Inc. "minivib" Vibroseis and an instrumented hammer. The combination of sources allowed VS profiles to be developed to 100 m and deeper without sacrificing resolution at shallow depths. The profiles were developed from the experimental dispersion data using straightforward linearized inversion and also following a method that incorporates the global search method of simulated annealing to optimize the starting model for linearized inversion. For all 12 sites, the two optimization processes resulted in nearly identical fits to the target dispersion curves. The VS of most layers from the two processes is within 20 percent. Resolution matrices for the two processes are comparable. Use of simulated annealing provided a measure of confidence in the correctness of the final VS profiles. Data from one site that is known to have a shallow, high-velocity inclusion were analyzed with the benefit of this independent information. The depth to and thickness of the high-velocity inclusion appear to be

modeled accurately. Overall, the VS profiles obtained are consistent with expectations based on previous earthquake microzonation of the Valley; VS values are lower for fine-grained sediments than for coarse-grained and cemented sediments. Average VS profiles previously developed for these two sediment-response units were updated; these profiles will enable refinement of previously developed earthquake ground-response projection envelopes.

Abstract for Manuscript 2, "Three-dimensional Shallow Shear-Wave Velocity Model for Las Vegas Valley": A three-dimensional (3-D) shear wave velocity (VS) model was developed for the heterogeneous shallow sediments (to nearly 400 m) of the Las Vegas Valley (LVV), Nevada. The model was based on more than 200 VS profiles and 1400 geologic well logs. Five sediment units including a cemented unit were defined from geologic log descriptions. A characteristic VS profile for four of the units was obtained by correlating between closely spaced pairs of VS and sediment data; a constant VS was assigned to the cemented unit. VS profiles were then assigned to each well location based on type of sediment according to the representative profiles. This assigned-velocity dataset was merged with measured VS profile data so that the measured data are honored in the model. The combined dataset results in a model with better resolution than a model developed using either of the two datasets independently. The software EarthVision was used to perform the 3-D interpolation of VS across the Valley. The model demonstrates the strong lateral variability of VS in the LVV. It also fits known patterns of sediment deposits: velocity in the central part of the Valley, where clay is the predominant sediment, is lower than velocity to the west and on the margins of the Valley, where

gravel is predominant. The model may be used to predict Valley-wide earthquake ground-shaking patterns.

TABLE OF CONTENTS

LIST OF TABLES

LIST OF FIGURES

ACKNOWLEDGEMENTS

I wish to thank my advisor, Dr. Barbara Luke, for the opportunity to perform this research. She provided encouragement and guidance, lifted heavy equipment in the field, and answered early morning phone calls. I also wish to thank my other committee members, Dr. Wanda Taylor, Dr. Aly Said, Dr. David James, and Dr. Carlos Calderón-Macías for their patience, advice, assistance and encouragement.

This research was sponsored in part by the U. S. Department of Energy under contract number DE-FG52-03NA99204. Stanley Consultants, Inc. (thanks to the support of Dennis Brown and David Huckle) provided funding for graduate courses and for conference travel. Additional funding for conference travel was provided by the UNLV Graduate and Professional Student Association (GPSA).

Dr. James Bay, University of Utah, programmed the analyzer and provided technical assistance for the minivib.

The following persons assisted with field data acquisition: volunteers Ryan Wilson and Ian Wilson; UNLV undergraduate students John Amato, Dianna Feica, Eduardo Gonzalez, and Richard Phillips; and Geophysical Research Associate Chris Cothrun. Sandra Saldaña provided technical assistance for data acquisition equipment. Cathy Willey of the UNLV Public Lands Institute obtained site permits.

Dr. Xiaohui Jin provided advice and technical assistance with inversion processes and many words of encouragement.

Committee member Dr. Wanda Taylor with the assistance of graduate student Jonathan Carter provided the three-dimensional sediment-lithology model of the Las

Vegas Valley. They also provided well log information and assistance with the software to plot and interpret the logs.

Catherine Snelson, National Center for Nuclear Security (NCNS), National Security Technologies, LLC (NSTEC), provided guidance for the assignments of shear-wave velocity values to bedrock and Oligocene-Miocene-aged sediments.

Jeff Wagoner, Lawrence Livermore National Laboratory, performed the velocity assignments to the sediment-lithology dataset and managed the interpolation process for model development using the computer program EarthVision. He also provided technical assistance and valuable insight for the correlation process.

Werner Helmer and Ron Lynn provided web-based access to public records archived at Clark County. The City of Henderson, Kleinfelder, Converse Consultants, Ninyo and Moore, and GeoTek also provided survey location information. UNLV students Thomas Higgins, Wilonda Quinn, Eduardo Gonzalez, Dianna Feica and Pinthep Kittipongdaja searched public records for shear-wave velocity data and compiled the data.

My gratitude to the persons listed here cannot be expressed adequately, especially to the students who assisted with the data acquisition. The excellent quality of their work and their contributions to this research cannot be overstated.

This thesis is for my family and friends who will be very excited and pleased to learn of its completion.

CHAPTER 1

INTRODUCTION

1.1. Purpose of the Study

The goal of this research is to develop a three-dimensional (3-D) shear-wave velocity (VS) model of the upper sediments, to 370 m, for the Las Vegas Valley, Nevada.

1.2. Overview of this Thesis

This thesis documents the data acquisition for and development of a three-dimensional shear-wave velocity model for the Las Vegas Valley (LVV). It consists of this introduction, two journal manuscripts, and appendices with data and supplemental information.

Following this introduction, Chapter Two is the journal manuscript "Complex Shear-Wave-Velocity Profiles to 100 m Depth from Rayleigh Waves for Las Vegas, Nevada". This manuscript describes the field data acquisition performed for this study and the development of shear-wave velocity (VS) profiles through inversion of these data. The results of different optimization methods are compared. The manuscript was written for possible submission to the Journal of Soil Dynamics and Earthquake Engineering. Co-authors will be Barbara Luke and Carlos Calderón-Macías.

Chapter Three is the journal manuscript "Three-Dimensional Shallow Shear-Wave Velocity Model for Las Vegas Valley". This manuscript documents work performed to develop a three-dimensional (3-D), VS model for the LVV. Data used for model development include, among other sources, the data described in Chapter 2. The

manuscript was written for possible submission to the Environmental and Engineering Geoscience Journal. Co-authors will be Barbara Luke, Wanda Taylor, and Jeff Wagoner.

Because chapters 2 and 3 are journal manuscripts, the references cited in each chapter are included at the end of the chapter.

Appendix A includes data and solutions for the 12 sites described in Chapter 2 where VS profiles were developed as part of this research. Aerial photos of each site's location along with the approximate location of the array and plots of nearby well logs are also included.

Appendix B includes a list of the VS measurement sites used for the correlation of velocity to sediment lithology described in Chapter 3. For each site, a list of wells within the correlation distance is also included. The VS sites that are deeper than any well within the correlation distance are listed with their nearest, deeper well.

Appendix C includes the description of the work performed to establish credible VS ranges for use in the velocity-sediment correlations performed in Chapter 3. A comparison to VS values previously published for sediments found in the Valley is also provided.

Appendix D includes graphics of the 3-D VS model created by Jeff Wagoner using EarthVision.

1.3. Summary of conclusions from this Thesis

A 3-D VS model for the LVV was developed by combining a dataset of limited VS measurements (212 measurements with irregular distribution throughout the Valley) with a larger dataset of sediment type (1400 well logs with better distribution throughout

Valley than the VS measurements) that is correlated to VS. This model provides better resolution than models developed using either of the two datasets independently. The model demonstrates strong lateral variability of VS, which reflects the Valley's depositional environment, history of secondary cementation, and faulting. As expected, VS is depth dependent. The model resolution is such that it may be used to predict Valley-wide earthquake ground-shaking patterns.

Twelve new VS profiles were developed for this research from a process that uses the average of three profiles derived through simulated annealing (SA) as an optimized starting model for linearized inversion (SA-LI). The results from this process were compared to profiles derived using linearized inversion (LI) based on a more generic starting model. For 75 percent of the sites compared, velocity differences are within 20 percent. In other words, the influence of the starting model on the inverted solution is relatively small. At a site where a high velocity layer (HVL) was known to exist, a VS profile was developed using the SA-LI approach where SA was configured for an explicit search for an HVL. This method accurately predicted the depth to the HVL and yielded a plausible result for its thickness. In all, the new profiles nearly double the number of high resolution profiles in the LVV and increase the number of profiles greater than 70 m deep by more than 10 percent. The 12 new VS profiles validate a previous microzonation performed for the LVV, demonstrating that sites located in the fine sediment response unit tend to have lower VS values compared to those for sites located in the coarse sediment response unit.

CHAPTER 2

COMPLEX SHEAR-WAVE-VELOCITY PROFILES TO 100 M DEPTH FROM RAYLEIGH WAVES FOR LAS VEGAS, NEVADA

Abstract: Shear-wave velocity (VS) profiles were developed for 12 sites in the Las Vegas Valley, Nevada, which is situated on a deep alluvium-filled basin. The work was performed to support earthquake site response analyses. Data were acquired using the spectral analysis of Rayleigh-type surface waves (SASW) method. Sources used were an IVI Inc. "minivib" Vibroseis and an instrumented hammer. The combination of sources allowed VS profiles to be developed to 100 m and deeper without sacrificing resolution at shallow depths. The profiles were developed from the experimental dispersion data using straightforward linearized inversion and also following a method that incorporates the global search method of simulated annealing to optimize the starting model for linearized inversion. For all 12 sites, the two optimization processes resulted in nearly identical fits to the target dispersion curves. The VS of most layers from the two processes is within 20 percent. Resolution matrices for the two processes are comparable. Use of simulated annealing provided a measure of confidence in the correctness of the final VS profiles. Data from one site that is known to have a shallow, high-velocity inclusion were analyzed with the benefit of this independent information. The depth to and thickness of the high-velocity inclusion appear to be modeled accurately. Overall, the VS profiles obtained are consistent with expectations based on previous earthquake microzonation of the Valley; VS values are lower for fine-grained sediments than for coarse-grained and cemented sediments. Average VS profiles previously developed for these two sediment-

response units were updated; these profiles will enable refinement of previously developed earthquake ground-response projection envelopes.

This manuscript was written for possible submission to the Journal of Soil Dynamics and Earthquake Engineering. Co-authors will be Barbara Luke and Carlos Calderón-Macías. Student contributions: Ms. Murvosh is the first author for the manuscript. She led the team that performed the data acquisition, was responsible for applying the optimization processes as described in the article to obtain the VS profiles, and performed all other data analyses described. She wrote the article and addressed all editorial comments from her co-authors.

2.1. Introduction

Rayleigh-type seismic surface wave testing was conducted to develop shear-wave velocity (VS) profiles using the spectral analysis of surface waves (SASW) method (Stokoe et al., 1994) at 12 locations in the Las Vegas Valley (LVV), Nevada (USA). Data were acquired with a hammer source and with a Vibroseis source. The data acquisition process was optimized to take advantage of the frequency ranges generated by each of these sources. Results were merged to develop VS profiles to depths on the order of 100 m.

The work was performed to expand a dataset of VS profiles in the LVV that characterize sediments to depths important to seismic site response analysis for the alluvium-filled basin for incorporation in a regional VS model for the LVV. Since 2002, many surface-wave measurements of LVV sediments have been performed, but primarily to develop VS profiles to 30 m. Few measurements have been performed to develop

deeper profiles. The measurements presented here increase the number of profiles in our VS database that extend to depths of 70 m and greater by 13 percent and nearly double the number of deep measurements that include detail near the surface. The VS profiles were combined with previously compiled data (Liu et al., 2005; Scott et al., 2006; Murvosh et al., 2006a) to develop a three-dimensional (3-D) VS map for the Valley, which will ultimately be used to model earthquake site response (Luke et al., 2008; Luke et al., 2009).

Development of VS profiles from surface-wave data in the LVV is challenging because the character of the shallow alluvial sediments can vary significantly over short distances. The challenge is greatest where high-velocity inclusions or layers (HVLs) exist at shallow depths. This study addresses challenges associated with the surface-wave signature of complex sediment columns. In this paper, we compare the results of linearized inversion to develop layered VS profiles from two starting models: 1) a straightforward, data-driven starting model and 2) a refined starting model developed from a simulated annealing optimization process. We investigate resolution matrices from the linearized inversion for their value in describing degree of confidence in the outcomes. The VS profiles resulting from the analyses are compared to nearby well logs and assessed in the context of an earthquake-response microzonation for the LVV presented by Luke and Liu (2008).

2.2. Background

For context, this section summarizes the local geologic setting, especially the heterogeneity of the sediments, earthquake risk and previous microzonation of the LVV.

The rationale for developing VS profiles deeper than 30 m in deep, sedimentary basins is discussed. The selection of test sites and the data acquisition process is presented. The background for the inversion methods is also presented.

2.2.1. Basin sediments

The LVV is located in an alluvium-filled basin in the Basin and Range geomorphic province (Wyman et al., 1993). The Spring Mountains, located on the west side of the Valley, are the primary source of alluvial deposits (Figure 2.1). Sediments become finer from west to east, with increasing distance from the source and with decreasing elevation. From the lowest elevations to the east (Frenchman and Sunrise Mountains), sediment size increases with distance. According to a geophysical study by Langenheim et al. (2001), the basin is deep and complex in shape, with the maximum depth to Paleozoic bedrock near 5 km occurring in the northeast quadrant of the basin, approximately 5 km west of Frenchman Mountain. The upper portion of the basin, to depths of 1 km, consists of Quaternary and Pliocene sediments (Taylor et al., 2008), which includes some material that engineers would consider to be rock: having VS approaching and in some cases exceeding 1000 m/s. The lower portion consists of Miocene and Oligocene material (Taylor et al., 2008).

Taylor et al. (2008) developed a 3-D geometric model of basin stratigraphy and structure from approximately 1400 well logs, geophysical measurements, and data from air photos, maps and direct field observations. The model shows that clay deposits dominate in the deep, central and south part of the basin, and coarse- and mixed-grain size deposits dominate in the shallower, western part of the basin. The model also shows that the deposits exhibit considerable vertical and lateral heterogeneity, which presents

unique challenges for development of a high resolution VS model from Rayleigh-wave data.

Cemented soils and dense sands and gravels present strong stiffness contrasts when juxtaposed with layers of clay or less dense sand and gravel. The stiffest of the sediments is locally known as "caliche". It is heavily carbonate-cemented fines, sand or gravel, which appear in lenses that can have thickness of up to 2 m or more and can occur to depths of 350 m or more (Taylor et al., 2008). Caliche has a high VS: Stone and Luke (2001) reported VS in laboratory testing of 2350 m/s; Tecle et al. (2003) reported values measured in the field from 1650 to 2000 m/s; and Werle and Luke (2007) reported measured field values from 1000 to 1500 m/s. In contrast, Sundquist (2001) reported VS values of uncemented LVV sediments between 260 and 860 m/s for clay and between 300 and 500 m/s for sand at depths less than 50 m.

2.2.2. Earthquake hazard and previous microzonation of LVV

Characterization of the VS of local sediments has become increasingly important with our developing knowledge of earthquake risk and related hazards in the LVV. Price et al. (2009) published a preliminary report that presents estimates of total economic loss, number of people needing public shelter and hospital care, and number of fatalities due to earthquakes ranging in magnitude from 5.0 to 7.0 and occurring within 50 years and 50 km of Nevada's major communities. For a magnitude 6 earthquake occurring on the central east side of the Valley (epicenter at 115.12 degrees west longitude, 36.17 degrees north latitude with a depth of 10 km), the economic loss in the Valley was estimated at 7.2 billion dollars, and the number of fatalities was estimated at 280. Four times as many fatalities were estimated for a magnitude 6.5 earthquake with the same rupture location.

As part of a broader effort to define earthquake hazard and related risks in the LVV, Luke and Liu (2008) used a preliminary geologic model and 16 VS measurements to develop a seismic microzonation for the LVV based on predominant sediment in the upper 30 m. They defined and developed characteristic profiles for two units: a coarse sediment response unit (coarse SRU) and a fine sediment response unit (fine SRU). The coarse SRU consists predominantly of gravel and also includes mixed-grain-sized deposits and cemented media that commonly occur in the alluvial fans on the margins of the Valley. The fine SRU has a lower VS overall and occurs in the areas of predominantly clay (although the presence of cemented sediments is not uncommon) in the intermediate-depth and deep parts of the basin, which are also lower in surface elevation. Luke and Liu (2008) presented ground response projection envelopes for each unit. In general, lower velocity sediments are expected to produce higher ground motions than sediments with higher velocities (e.g. Idriss, 1990); however, spectral accelerations modeled for the LVV coarse SRU were greater than those modeled for the fine SRU. Because projections for the coarse SRU were based on VS measurements from only four sites, Luke and Liu (2008) concluded that, for the coarse SRU, the velocity dataset used in their study was too sparse to permit confident comparisons. The new profiles presented in this paper allow the microzonation of Luke and Liu (2008) to be tested and the ground response projection envelopes to be refined.

2.2.3. Rationale for deep profile development

The International Building Code (IBC) provides guidance for engineers to consider VS averaged over the upper 30 m (VS(30)) for the seismic design of structures (International Code Council, 2009). However, as discussed below, research suggests that

for deep, sedimentary basins, such as the LVV, VS data deeper than 30 m are needed to accurately predict ground motion during an earthquake.

In their Next Generation Attenuation project to model earthquake ground motion for California, Abrahamson and Silva (2008) applied in tandem VS(30) and the depth to engineering bedrock, which is defined in their study as the depth where VS reaches 1000 m/s ($Z_{1.0}$), for seismic site classification. They recommended the use of the engineering bedrock parameter $Z_{1.0}$ to distinguish between shallow ($Z_{1.0} < 200$ m) and deep ($Z_{1.0} > 200$ m) "soil" sites.

In a study to investigate the influence of shallow sediments on ground motion in LVV, Luke and Liu (2007) established a preferred depth to model half-space for one-dimensional site response analyses. They compared the site response on the surface of a 1-km deep sediment column to that of a "rock" site situated at the foot of Frenchman Mountain (Figure 2.1) for small-strain motions. They projected ground surface response for sediment columns having depths to half space ranging from 50 m to 500 m. The projections were compared to weak ground motions measured at the two sites during nuclear test events and during a magnitude 5.5 earthquake. The authors found the best matches of modeled ground motion to recorded ground motion occurred for a half-space depth of 375 m.

Based on these results and considering the recommendations of Abrahamson and Silva (2008), VS profiles for the new sites would have ideally extended to 400 m depth. However, due to survey limitations discussed in the following section, maximum depths to halfspace of VS at the new study sites ranged from 60 to 130 m.

2.2.4. Test site selection, data acquisition, and dispersion curves

Test sites were selected following criteria developed by Murvosh et al. (2006b): Preference was given to sites that:

1. are located in one of the established sediment response units
2. are located near wells that are included in the 3-D geometric model of basin stratigraphy and structure (Taylor et al., 2008), for geologic ground truth
3. are located near seismic monitoring stations
4. are located near structures of importance for public safety (e.g. schools and hospitals)
5. are located where the sediment-lithology or velocity structure at depths from 400 m to 1 km were already known through other testing; tying this dataset to the more shallow data discussed in this paper will allow us to produce a more accurate 3-D map over a greater depth range than previously studied for the LVV
6. enhance geographic distribution of VS measurements across the LVV.

Practical considerations also factored into the site selection process: the availability of land with sufficient space to perform a long, linear survey; the ability to obtain permission from the land owner to study the site; and the ability to safely access the site. Site selection is described in detail by Murvosh and Luke (2008). Ultimately, eight sites in the fine SRU and four in the coarse SRU were tested. The site locations are listed in Table 2.1 and are shown with respect to the well-log database and sediment response units defined by Luke and Liu (2008) in Figure 2.1. All 12 test sites could accommodate linear arrays of at least 128 m length (distance from source to farthest receiver); six could accommodate array lengths of 200 m or more.

Data acquisition for the sites discussed in this paper was described in detail by Murvosh and Luke (2008). Key content is reviewed here.

Accepted procedures for an SASW survey, developed by Stokoe et al. (1994), were employed at each site to acquire Rayleigh-wave phase velocities. Rayleigh waves are surface waves, produced by the interaction of compression- and vertical shear-waves at the ground surface (Kramer, 1996). The SASW method is based on the dispersive nature of these waves, meaning the variation of wave velocity with frequency (or wavelength) in a layered media. In an SASW survey, a vertical source is used to produce vertical ground motions (Stokoe et al., 1994). Then, a frequency-domain analysis of the phase differences of the ground motion at two discrete points along a linear array radiating from the source is used to develop a dispersion curve (plot of velocity as a function of frequency or wavelength) for the site. The dispersion curve is assumed to consist primarily of the fundamental mode of the Rayleigh wave, but may also consist of higher modes as well as other wave types; thus it is considered an "effective" dispersion curve.

The sources used for this study were an instrumented sledge hammer (PCB impact hammer, model 086D50) and UNLV's "minivib", a servo-hydraulic vibrator built by Industrial Vehicles International (IVI) of Tulsa, Oklahoma, model T-7000W (Figure 2.2). The maximum force output of UNLV's minivib is 26.7 kN. It was designed to operate between 10 and 550 Hz, but can vibrate at lower frequencies. The minimum frequency at which data were acquired for this study was slightly below 3 Hz. Having been designed originally for seismic reflection surveying, the UNLV minivib was optimized for surface-wave measurements by lengthening the stroke of the shaft from 4.8 cm to 7.6 cm. The minivib is trailer-mounted and uses water for ballast, but is otherwise similar to the

mobile vibrator known as “Thumper”. Thumper is the smallest of three large-scale Vibroseis shakers operated by University of Texas as part of the National Science Foundation’s George E. Brown Jr. Network for Earthquake Engineering Simulation (NEES; Stokoe et al., 2006).

In an optimal SASW survey, all receiver spacings share a common centerpoint (Stokoe, 1994); however a three-receiver layout (Figure 2.3), where the distance between the second and third receivers (R2 and R3) is twice the distance between the first and second receivers (R1 and R2), is sometimes used for convenience (Gilbert 2004). Measurements performed with three receivers will not share a common centerpoint, but can reduce the time spent in the field or provide redundancy if duplicate measurements are made. We used a combination of these configurations to acquire data at our test sites.

Common-centerpoint geometry (Figure 2.4a) was used to acquire data for receiver spacings 1 to 16 m. The centerpoint, recorded using a handheld GPS unit, defined each site’s location shown in Figure 2.1. For receiver spacings 1, 2, 4 and 8 m, the source was an instrumented hammer, and the receivers were a pair of vertical geophones with 4.5-Hz resonant frequency, made by Mark Products (now Sercel). The geophones were coupled to the ground by metal spikes screwed into the bases. Data were acquired in both directions along the array by placing the source alternately on opposite sides of the receiver pair. The minimum frequency used from these measurements was 14 Hz.

For receiver spacings 16 m and longer, the minivib was used with the three-receiver arrangement. For efficiency, the minivib was fixed at a single position. It was placed 24 m from the midpoint of the shortest receiver spacings so that the 16-m spacing measurement shared the same midpoint. Each receiver spacing longer than 16 m,

however, had a different midpoint, and, therefore, sampled a different zone along the array (Figure 2.4b). Receiver spacings for minivib testing were doubled successively from 16 to 32 to 64 m. The maximum receiver spacing used was 128 m. Attempts were made at several sites to acquire data using longer arrays (to 165 m), but signal strength was not adequate to resolve frequencies lower than already acquired at the 128 m spacing. Some sites were space-limited so the maximum receiver spacings ranged between 64 and 128 m (Table 2.2).

For measurements made using the minivib, Mark Products (now Sercel) vertical geophones with 1-Hz resonant frequency were used. These geophones are flat-bottomed. Where possible, they were coupled to the ground by slightly embedding them. Some of the test sites, however, were turf lawns, where it was not appropriate to dig holes. At these locations, the geophones were placed on sandbags. Geophones were positioned using hardware-grade post levels.

The tests were conducted in summer, when LVV daily high temperatures are typically 38° C and higher. In July, temperatures frequently exceed 43° C. The temperature of the 1-Hz geophones was moderated by surrounding them with ice packs and by providing shade with buckets and reflecting foil (Murvosh and Luke, 2008). The buckets also provided wind isolation where the cable connects to the receiver.

A four-channel dynamic signal analyzer (Agilent model 3567A) was used for data acquisition. The spectral response computations, performed in the field with the analyzer, incorporated output from the source (acceleration measured on the vibrating mass of the minivib and force measured on the head of the hammer) to improve signal-to-noise ratio (Gilbert, 2004).

For the hammer-source measurements, both the cross-power spectrum and coherence, a measure of the data quality, were acquired according to standard procedures for the SASW method (Stokoe et al., 1994). The signals were stacked (summed) until additional measurements resulted in little to no observable changes in the data.

For the minivib-source measurements, data were acquired by a stepped-sine vibration method, which automatically steps down through the range of frequencies specified by the user. The user also specifies the number of measurements averaged at each frequency and the size of the frequency step. For the LVV tests, these parameters varied with each measurement and at each test site and depended upon the receiver spacing. The duration of a measurement to frequencies less than 5 Hz may be as much as 30 minutes. In the field, the user-defined, stepped-sine test parameters were adjusted manually for each measurement based on experience. For each receiver spacing, measurements were stopped once the frequency corresponding to a phase difference of π radians was established; data below this frequency are not useful because they are overly contaminated by near-field effects (Sánchez-Salinero et al., 1986). For the longest receiver spacing, the measurement was stopped before this point if the calculated phase difference became heavily distorted. When present, this excessive distortion usually occurred around 2.5 Hz.

Efficient data acquisition techniques were necessary because operating the minivib for long durations in the high summer temperatures caused the minivib's hydraulic fluid to overheat (fluid temperatures > 90.6 °C). Special precautions were taken to avoid overheating (Murvosh and Luke, 2008); however, surveys on some of the hottest days of

summer were stopped due to soaring hydraulic fluid temperatures. The UNLV minivib has since been outfitted with a supplemental radiator to mitigate this problem.

Coherence was not readily calculated by the analyzer for the stepped-sine data. Two measures were taken to compensate for this shortcoming of the data-acquisition process: (1) to provide redundancy frequency ranges for each receiver spacing were selected to overlap the range for the prior receiver spacing; and (2) additional measurements were acquired for the 32 and 64 m receiver spacings. Consistency between the overlapping data and the additional measurements was an indicator of data reliability.

The data from each receiver spacing were combined into a single dispersion curve (velocity as a function of frequency) containing more than one thousand data points. To develop a reasonable target for inversion, data were logarithmically binned with respect to frequency and a representative velocity value was assigned to each bin by averaging. This condensed representation, just 40 to 50 points, was smoothed by convolving it with a 5- to 7-point kernel (Wu et al., 2003). The smoothed curve was visually compared to the measured data to verify that it fit the general trends of the measured data and that the smoothing process did not remove what was judged to be potentially important trends.

The smoothed dispersion curves for the 12 sites are shown in Figure 2.5. For frequencies less than 50 Hz, the velocities for sites located in the fine SRU tend to be lower than those for sites located in the coarse SRU. One exception is the curve for the SFB site, which is located in the fine SRU and, from well logs and a nearby cut slope, is known to have a 1-m thick caliche lens between 2 and 3 m deep. The dispersion curve for this site exhibits anomalously high velocities for frequencies greater than 15 Hz, and, for frequencies above 30 Hz, has the highest velocities of all the sites. It is distinctly different

from the other dispersion curves, having a pronounced local maximum at 50 Hz and remaining flat to low frequencies.

Another exception is the OSH site, which is located in the fine SRU, but within 500 m of an area defined as part of the coarse SRU (Figure 2.1). This site exhibits wave velocities greater than those measured at other sites in the coarse SRU. The closest well to the site is within 0.5 km; its log indicates a mixture of clay and gravel sediments above 30 m. Three other wells are located within 1.5 km. Above 30 m depth, one of these logs shows only clay, one shows only gravel and the third shows a mixture of gravel and clay. Because of this information from nearby wells and considering uncertainty of the sediment response unit boundaries defined by Luke and Liu (2008), we assigned the site to the coarse SRU.

Key test parameters and sediment response unit are listed for all the sites tested in Table 2.2. The longest wavelength resolved was 254 m, which corresponded to a frequency of 3.3 Hz. This occurred at a site located within the coarse SRU. The ability to resolve longer wavelengths in the coarse SRU than the fine SRU is attributed to the generally higher average velocity of coarse-grained sediments with respect to fine-grained sediments (Figure 2.5; Luke and Liu, 2008) because surface waves will attenuate more gradually in stiff material than in soft material. The lowest frequency resolved for the studied sites was 3.2 Hz. This low-frequency limit was reached at two sites located in the fine SRU (LMN and MHS), where it corresponded to wavelengths of 186 and 166 m, respectively. The depth to model halfspace is also listed in Table 2.2. The method used to fix this depth is discussed later in this paper.

2.2.5. Inversion methods

For most cases, a Rayleigh-type surface-wave dispersion curve for a sediment column shows velocity increasing with decreasing frequency. This is logical because sediment stiffness, and therefore VS, increases with increasing confining pressure, which generally occurs with increasing depth. However, as illustrated for the SFB site in this paper, dispersion curves for sites containing HVL's can exhibit strong velocity reversals (decreases in velocity with decreasing frequency), which prove challenging to interpret.

A recent series of studies addressed inversion procedures to resolve layered systems containing HVL's such as the complex sediment profiles of the LVV (Luke et al., 2006; Calderón-Macías and Luke, 2007; Luke and Calderón-Macías, 2007; Jin et al., 2009). The inversion procedures incorporate two fundamental components (Menke, 1989). One is the forward model, which is used to construct a theoretical dispersion curve corresponding to a set of assumed soil properties through simulation of wave propagation. The other is the optimization algorithm, which iteratively adjusts the model parameters to reduce the misfit of the theoretical dispersion curve with respect to the target.

We selected the forward model to use for the test sites described in this paper based upon a synthetic study by Jin et al. (2009). Their study compared the effectiveness of two forward models to delineate HVL's in otherwise normally dispersive (meaning that VS consistently increases with depth), one-dimensional synthetic profiles. The first models the wave propagation along cylindrical wavefronts from a vertical disk load (cylindrical solution; Foinquinos-Mera, 1991). The second models strictly fundamental-mode (plane-wave) Rayleigh-wave propagation (fundamental-mode solution) using a program

developed by Lai and Rix (1998). The authors concluded that the simpler forward model (the fundamental-mode solution) might be more successful in resolving complex profiles from field data than the more sophisticated alternative because the higher level of interpretation of the data needed to use the cylindrical solution might not be achievable in practice. They further recommended that the fundamental mode solution be constrained within a reasonable search range fixed according to independent information about a site. In testing simulations, Jin et al. (2009) found the recommended approach to be reliable for determining the depth of an HVL; however, its velocity and layer thickness were overestimated by averages of 29 and 41 percent, respectively.

Jin et al. (2009) performed optimization by employing a method that incorporates the global search method of simulated annealing followed by linearized inversion (SA-LI; Calderón-Macías and Luke, 2007; Luke and Calderón-Macías, 2007). Simulated annealing (SA; e.g. Sen and Stoffa 1995) is a stochastic optimization process that allows the error between the target dispersion curve and the theoretical dispersion curve to increase between iterations to reduce the possibility that a solution becomes "trapped" at a local minimum in the error surface. The intent of employing two optimization methods in series is to first use SA to seek a solution that can include an HVL. This solution is constrained by a velocity search range for all layers and, if an HVL is known to exist, also by depth, thickness and velocity ranges for the HVL. Then, the linearized least-squares minimization process otherwise known as linearized inversion (LI) is used to refine the solution (Jin et al., 2009). LI is an unconstrained process where the error is forced to decrease with each iteration. The number of iterations may be in the thousands for the SA process compared to less than ten for LI. Following the SA optimization with

LI is particularly beneficial for cases when the limits used to constrain the SA solution are incorrect.

A sensitivity study performed by Luke et al. (2006) compared the results of surface-wave data inversion by SA-LI for a statistically significant number of repetitions on the same profile. Like the study performed by Jin et al (2009), the authors found that between an HVL's depth, thickness and velocity, depth was the most reliably resolved parameter. They too found that velocity was overestimated, generally by 30 percent, but as much as 80 percent for one case. In contrast to the test performed by Jin et al. (2009), they found thickness to be underestimated by approximately 25 percent.

To investigate the benefits of employing optimization by SA at locations where independent, site-specific information is not available, we developed VS profiles for the sites described in this paper using the LI method alone and also the SA-LI method. For the SFB site, which is known to have shallow caliche and where a velocity reversal is obvious in the experimental data, we used the search range capabilities of SA to converge upon a solution that explicitly addresses the HVL.

2.3. Test site profiles

Development of the VS profiles for the 12 test sites is described in this section. Results from optimization by the LI and SA-LI methods are discussed in detail for four of the sites: a representative fine SRU site; a representative coarse SRU site; a site found to have an HVL where a velocity reversal is not obvious in the target curve but where nearby geologic observations indicate stiff materials; and a site known to have shallow caliche where a velocity reversal is apparent in the experimental data. The optimization

outcomes for all 12 sites are compared to determine which optimization method resulted in the best fit to the target dispersion curve and the most reasonable VS profile with respect to independent information about the site. For the site known to have shallow caliche, development of a VS profile using the explicit SA search for an HVL is also described. For this site, the solutions from the optimization methods are discussed with respect to their success at identifying the HVL.

2.3.1. Procedure for VS profile development

For the profiles developed in this study, the VS values were optimized from a pre-assigned layer geometry, density, and Poisson's ratio. Poisson's ratio and density were assigned based on local field test results (Stone and Luke, 2001; Sundquist and Luke, 2001; Tecle et al., 2003), published ranges for soil and rocks (e.g. Sharma, 1997; Mavko et al., 1998), and values researched for other surface wave investigations in the LVV (Liu et al., 2005). We assigned a Poisson's ratio of 0.3 above the water table and 0.4 below the water table and a density of 1700 kg/m^3. The values of Poisson's ratio and density assigned to cemented layers are discussed in the section that describes the search for the HVL.

We developed layering and VS starting models using an algorithm based upon work by Liu et al. (2002). Dispersion curves were calculated for several trial starting-model VS profiles, each having different layer geometry but the same number of layers. Layer boundaries were set so that layers thicken exponentially with depth (Liu et al., 2002). Layer thicknesses increase with depth because the resolution of surface-based acquisition methods tends to decrease with depth (e.g., Luke and Calderón-Macías, 2007) and because of the unifying effect that confining pressure has on the stiffness of non-lithified

sediments. The shallowest and therefore thinnest layers used in this study are 0.5 to 1 m thick. The number of layers was assigned by trial and error. By applying LI to a small sample of layer geometries, we found that a 10-layer starting model provided a reasonable fit to the target dispersion curves with wavelengths up to roughly 100 m. For deeper sediment profiles, which correspond to sites having data to longer wavelengths, more layers are needed to maintain similar layer thicknesses near the surface. We assigned 10, 11 and 12 layers for datasets having maximum wavelengths in the range of 100 m, 150 m and 200 m, respectively. A calculated dispersion curve can be compared to the target smoothed dispersion curve developed from the experimental data using the data difference (DD; Liu et al., 2002), which is defined as the root-square sum of the squared difference between the calculated dispersion curve and the target calculated by wavelength step. Identification of the best starting model is not straightforward and different starting models may lead to different VS profiles each having dispersion curves with an equally good fit to the data (i.e. a nonunique solution). Empirical evidence showed that inversion results tend to be superior when the starting model corresponds to a dispersion curve with a low DD (Liu et al., 2002; Luke and Calderón-Macías, 2007). Further, in a study performed using synthetic data, Jin (2006) showed that a good fit to the starting model's dispersion curve at the short wavelength (high frequency) limit is particularly important. Therefore, from the six trial starting-model profiles we calculated for each target dispersion curve, we chose the starting-model VS profile that corresponded to the dispersion curve with a low DD and a satisfactory fit at the high frequency limit.

The resolution matrices from LI provide an opportunity to assess the quality of the solution obtained from the selected starting model. Calderón-Macías and Luke (2007) and Luke and Calderón-Macías (2007) describe the resolution matrix produced by the inversion process. In general, an identity matrix represents a solution with all layers perfectly resolved. The more the matrix diverges from the identity matrix, the poorer the resolution. The matrix depends on the forward model and the starting model, but not on the measured data; thus, a solution with perfect resolution is not necessarily the true solution. Solutions, therefore, can be considered nonunique.

Additionally, non-diagonal terms with relatively high amplitudes may indicate that too many layers (model parameters) are being solved for the frequency range being analyzed. In other words, rather than solving for VS of a particular layer, the inversion process is solving for this layer in combination with its neighbors. In general, resolution matrices are more diagonal when the inversion process is solving for fewer parameters. Thus, it is generally preferable to solve for the smallest number of layers that can fit the data reasonably well.

The depth to model halfspace was fixed as half the maximum wavelength in the experimental dataset. This criterion was used by Liu (2006) in resolving profiles to 300 m deep and deeper using a drop-weight source and passive-source energy at 12 locations in the LVV. We tested the resolution depth of the new profiles using a method to establish the depth to model halfspace followed by Rosenblad et al. (2007) for SASW data acquired using the NEES vibrator source "Liquidator" (designed to acquire data to frequencies below 1 Hz; Stokoe et al., 2006). The testing method was applied to three sites (Table 2.2): one site in the fine SRU, one in the coarse SRU, and the site known to

contain a high-velocity layer. For each of these sites, the theoretical dispersion curve for the VS profile resolved for the site was compared to a dispersion curve generated by increasing the VS of the profile's bottom layer by 20 percent. The changes in velocity of the dispersion curve at the lowest frequency resulting from the increase in the bottom-layer VS were between 7 and 10 percent. These changes in velocity are greater than the minimum 5 percent change accepted by Rosenblad et al. (2007); for sites where the change was less than 5 percent, they would include the bottom layer in the halfspace. Therefore, the test supported our assumption that setting the depth to halfspace equal to half the longest wavelength was reasonable for our datasets.

For each of the 12 sites, two VS profiles were obtained by applying LI and SA-LI to the starting model using the process illustrated in Figure 2.6. For SA, the search range for VS was from one-half of the starting model velocity to twice the starting model velocity. Three different VS profiles were obtained by applying SA to the starting model three times. The average of these VS profiles was calculated and used as the starting model for LI. This SA-LI procedure improves upon that recommended by Luke and Calderón-Macías (2007) in which they performed LI for each of three starting-model VS profiles obtained from SA and averaged the VS profiles from LI to obtain the final solution. A disadvantage of this procedure is that a dispersion curve generated by averaging of the three profiles might not result in an optimum fit to the target.

The minimum and maximum, or extreme, velocities resolved from the three SA runs provide a convenient measure of confidence in the VS profile resolved (Luke and Calderón-Macías, 2007).

2.3.2. Results for LI and SA-LI optimization: four case studies

The results from the four case-study sites are described here. The proximity of these sites to the nearest ground truth (geologic well logs or other local sediment information) are shown in Figure 2.7. A sediment lithology key and resolution matrix key are shown in Figure 2.8. The widths of the sediment symbols shown in the lithologic logs provide an indication of relative grain size; narrower symbols represent finer-grained sediments. For convenience, the symbols for the most of the mixed units (e.g. "Clay and Sand" and "Clay Sand Silt") are shown at maximum widths. The site data and solutions are presented in Figures 2.9 to 2.12. These figures contain dispersion curves with DD values, lithologic logs from nearby wells, VS profiles, and resolution matrices.

The results for both LI and SA-LI are plotted in Figures 2.9 to 2.12. The VS profiles display the velocity search range employed in SA and the extremes of the velocities resolved from the three SA runs ("solution range"). Table 2.3 lists the maximum VS difference found between the LI and SA-LI profiles for all 12 test sites.

Fine SRU site (LES)

The LES site is located in the north of the LVV (Figure 2.1) on a grassy field of a schoolyard. Site data and solutions are shown in Figure 2.9. Sediment lithology is available from a well located 325 m west of the site (Figure 2.7). Its log describes clay to a depth of 15 m and mixed clay, sand and silt to 98 m.

The dispersion curves for the LI and SA-LI solutions are virtually identical and have a low DD (good fit to the target). The depth to model halfspace is 63 m. VS of the LI and SA-LI solutions differ by less than 5 percent.

The range of the three SA solutions for this fine SRU site is always less than 200 m/s. The LI and SA-LI solutions fall roughly in the middle of these extremes. With the exception of the fourth and tenth (bottom) layers, which have slightly lower VS than their overlying layer, VS of the solutions increases with increasing depth. The resolution matrices for LI and SA-LI are virtually identical. Because the most important parameter controlling the matrix is layer thickness rather than velocity (Calderón-Macías and Luke, 2007) and because layer thickness is identical while velocity is relatively close for LI and SA-LI, the similarity of the matrices is not surprising. For both solutions, nine of the eleven "layers" (10 layers plus the model halfspace) have resolution greater than 0.5 along the diagonal of the matrix. The scale of the resolution matrix is 0 to 1, where 1 along the diagonal is a perfectly resolved solution. Resolution generally decreases with increasing layer depth. Resolution is poorest for the model halfspace, which, as discussed later in this paper, implies that fewer, thicker layers at depth or a shallower halfspace may produce an equally good fit to the data at the low frequencies.

Coarse SRU site (GMS)

The GMS site is located in the southwest of the LVV (Figure 2.1) on a grassy field shared by a school and a park. Site data and solutions are shown in Figure 2.10. Sediment lithology is available from a well located 460 m east of the site (Figure 2.7). Its log describes layers of strictly gravel alternating with layers of gravel that are mixed with sand or clay to a depth of 152 m, except for a thin layer from 52 to 53.5 m that is logged as mixed sand and clay.

The dispersion curves for the LI and SA-LI solutions are virtually identical. The DD values indicate a slightly poorer fit to the target with respect to the solution for the fine

SRU site, which is expected because the dispersion curve for this site is more complex than the dispersion curve for the fine SRU site. The depth to model halfspace is 127 m, twice as deep as resolved for the fine SRU and the deepest of all the sites in this study. VS of the LI and SA-LI solutions differ by at most 17 percent (Table 2.3). The range of three SA solutions is always less than 200 m/s above 85 m depth and 300 m/s below 85 m. Neither the LI nor the SA-LI solutions fall consistently within the extremes of the SA solutions. As is true for the LES site, the resolution matrices for the GMS site do not differ substantially. The SA-LI process improved the resolution of some layers, but the resolution of an equal number slightly decreased. Out of 13 layers, LI produced 9 layers with resolution greater than 0.5 along the diagonal of the matrix; SA-LI produced 10 layers with resolution greater than 0.5. The halfspace is not well resolved for either solution.

HVL site 1 (NLP)

The NLP site is located in the central part of the LVV (Figure 2.1) on a grassy field of a park. The site is in the fine SRU. Site data and solutions are shown in Figure 2.11. Sediment lithology is available from two wells, located within 700 m of the site (Figure 2.7). The closest, well number 607, is 470 m east-southeast of the site. This log shows layers of mixed materials (sand, clay and silt) to 95 m. Three shallow caliche layers are described: having thicknesses and depths respectively of 2.7 m and 4.6 m, 1.5 m and 13.1 m, and 2.4 m and 17.1 m. The next closest well, number 709, is 680 m south of the site. The log for this well describes alternating layers, 1- to 2-m thick, of clay and gravel and of stiff, higher velocity materials (stiff sediments with calcite) from the surface to 16 m. In the depth range from 16 to 68 m, according to the logs, layers of limestone from 0.5 to

22 m thick alternate with clay layers. Below this depth, layers are predominantly gravel. The static water level is 10 m.

Because of the prevalence of stiff materials reported in the nearby logs, we suspected that stiff layers might be present at the NLP site. The ground-truth information, however, was too distant to warrant using an explicit, constrained stiff-layer-search approach in SA inversion.

The dispersion curves for the LI and SA-LI solutions are virtually identical and have a low DD, slightly less than the DD of the fine SRU site. Although the target does not exhibit a strong local maximum that would indicate an HVL, both of the resolved VS profiles indicate a 4-m thick HVL at 6.5 m. The VS of this layer, 700 m/s, is 1.8 to 2 times higher than VS resolved for the surrounding layers, 350 to 400 m/s. The depth of the HVL generally corresponds to the depths of high velocity materials shown in the two closest well logs. The depth to model halfspace is 61 m, slightly less than that resolved for the fine SRU site. VS of the LI and SA-LI solutions differ by 3 percent or less for the layers above the HVL, by 8 percent at the HVL and for the two layers below the HVL, and by 4 percent or less for the deepest layers. The range of the three SA solutions is always less than 175 m/s. Neither the LI nor the SA-LI solution falls consistently within the extremes of the SA solutions. Compared to the LI profile, the SA-LI profile exhibits greater fluctuations in VS between layers, especially at the HVL. The resolution matrices are not substantially different, which, as previously discussed, is expected. The SA-LI process does not notably improve the resolution of any layer and decreases the resolution of layer 8, which is 9 m thick and 16.5 m deep. Of the 11 layers, LI produced nine with

resolution greater than 0.5 along the diagonal of the matrix, and SA-LI produced eight with resolution greater than 0.5. The halfspace is not well resolved for either solution.

HVL site 2 (SFB)

The SFB site is located in the south-central part of the LVV (Figure 2.1) on a desert-landscaped plot south of the Stan Fulton Building on the UNLV campus and 30 m south of a trapezoidal drainage swale. The swale is part of the Flamingo Wash, a significant storm-flow conduit for the LVV. The site is in the fine SRU. Site data and solutions are shown in Figure 2.12. A caliche layer approximately 1 m thick and roughly 2 to 3 m deep is visible in the side slopes of the drainage swale, which is more-or-less parallel to the survey array. Additional sediment lithology is available to 5 m depth for a borehole (designated as B-1) located approximately 150 m west of the site and to 120 m depth for a well located 370 m west of the site (number 741). The log for the borehole describes cemented material from 2.7 to 3.7 m, which roughly corresponds to the depth of the caliche observed in the swale. The log for the well, which is located farther from the site than the borehole, shows cemented materials from 6.1 to 8.2 m. Neither the presence of water nor the depth to groundwater was not noted in either log, which is surprising given the site's proximity to the wash.

Compared to the other case studies presented, the dispersion curve for the average of the SA solutions for HVL site 2 has a poor fit to the target at frequencies below 40 Hz. In spite of this poor fit, the dispersion curves for the LI and SA-LI solutions are virtually identical and have low DD values. Even with the presence of high VS contrast, the two different starting models converged to a similar VS profile. Both of the resolved VS profiles show a 2.5-m thick HVL at 3.3 m deep. The velocity of this layer, 1050 m/s, is

2.2 to 3 times higher than VS resolved for the surrounding layers, 350 to 475 m/s. The depth and thickness of the HVL roughly correspond to the depth of caliche reported in log for the nearest well and observed in the adjacent swale. The depth to model halfspace is 88 m, slightly deeper than that of the HVL site previously discussed. VS of the LI and SA-LI solutions differ by no more than 5 percent. The range of the three SA solutions, however, is as much as 550 m/s. With the exception of the HVL and the model halfspace, the LI and SA-LI profiles fall within these extremes.

Comparing the resolution matrices for LI and SA-LI solutions, SA-LI has a slightly better resolution than LI for the 3 deepest layers and the halfspace. Elsewhere these two matrices are nearly identical. Neither produces well-resolved solutions for the two deepest layers or the halfspace. Again, the similarity of the matrices is expected.

2.3.3. Comparison of LI and SA-LI results: all sites

For the four case studies presented, LI and SA-LI methods produce equivalent results considering the expected accuracy of the inversion methods. Computed dispersion curves for the two methods have virtually identical fits to the target and differences in DD are insignificant. For each layer, VS of the two solutions are within 20 percent of one another. We consider a maximum difference of 20 percent to be reasonable. At all of the case study sites, we observed relatively poor resolution of the halfspace. The decrease in resolution indicates that despite the test performed to set the depth to model halfspace, we may be claiming a higher confidence at depth than is appropriate. More studies are needed to determine limitations in predicting depth to model halfspace.

Similar patterns were observed in nine of the twelve sites tested: difference in DD values is less than 3 and maximum difference in VS between LI and SA-LI solutions is

everywhere less than 20 percent (Table 2.3). In other words, for those nine sites, the impact of refining the starting model is minor. For profiles incorporated into a regional VS model, which is the reason these profiles were developed, the goal is to capture a local trend and its effect on earthquake site response rather than a VS profile for a specific, vertical line. In this respect, surface waves are an ideal tool to develop VS profiles because they express velocity averaged over broad areas.

The three sites that do not fit this pattern are all in the fine SRU. For two of these sites, MHS and WLE, dispersion curves for the two optimization methods have virtually identical fits to the target. For the third site, SMS, the dispersion curve fits differed for frequencies greater than 90 Hz, which corresponds to the shallowest layers. For the three sites, the difference in VS was typically 20 percent or less; however, overall 30 percent of the layers had differences between 21 and 46 percent (Table 2.3; Figure 2.13). For all three sites, both the LI and SA-LI solutions appear reasonable, yielding VS profiles that are generally consistent with the other profiles developed in the fine SRU, although the SA-LI solutions show higher fluctuations of VS between layers than do the LI solutions. No wells are located at the sites to help establish which profile provides the better representation for these sites, and none of their SA-LI resolution matrices indicated an increase in resolution when compared to LI (not included for brevity). Although resolution matrices for both methods indicate slightly poorer resolution overall compared to the other nine sites.

Reasons for the diverging outcomes from LI and SA-LI procedures were discussed in previous research by Luke et al. (2003). The authors showed that the LI process applied to different starting models, such as the process described here where LI is performed

using a starting model that has been optimized using SA, can yield solutions with different VS profiles, but with equally good fits to the target. Luke et al. (2003) also showed that the difference between VS profiles generated using the two processes was greater for sites with complex dispersion curves compared to sites that are normally dispersive. The dispersion curves for the MHS, SMS and WLE sites are not substantially more complex than those at sites with consistent LI and SA-LI results. The three sites also have HVL's within the upper 10 meters, but the changes in velocity between the HVL and surrounding layers are similar to those found at the NLP and SFB sites, which had consistent results. Although not investigated in this study, we suspect that the difference in consistency of results is attributable to the complexity of sediment stiffness (vertically and perhaps laterally) and the quality of the starting model. Different solutions are not unexpected because of the nonuniqueness of the problem.

To determine the extent to which different solutions affect VS(30) and VS averaged over the total depth (VS(TD)), we calculated these averages for the 12 test sites (Table 2.4). The model halfspace was included as a layer in the calculation for VS(TD). The thickness of this layer was set to one-third of the model depth to halfspace. The depth-averaged results for the two optimization methods are virtually identical, differing by 2 percent or less.

2.3.4. Investigation of profile uncertainty

Use of resolution matrices to evaluate uncertainty of VS profiles was investigated. Generally, a poorly resolved layer, defined here as a layer having resolution less than 0.5, had a wide SA solution range, while a well resolved layer had a narrow solution range. Resolution tended to decrease with increasing depth. The most poorly resolved layers did

not always correspond to the layers with the greatest difference in VS between LI and SA-LI processes. Overall, the resolution matrices for the two optimization methods differ only slightly, which, as previously discussed, is to be expected because the layer geometry is identical.

The SA-LI process was useful to provide confidence for the LI solutions. Additionally, the range of the SA solutions also provides a measure of confidence (Calderón-Macías and Luke, 2007). For this reason and based on research to resolve HVL's previously cited in this article, we selected the VS profile from the SA-LI process to represent the final solution for the 12 test sites.

2.3.5. SA-LI with explicit search for HVL (SAES-LI; SFB site)

Because of the close proximity of the independent evidence of a shallow caliche layer, an additional VS profile was developed for the SFB site using optimization by SA specifically configured to search for an HVL. The search ranges for the depth to the HVL, 2.5 m to 4 m, and for the thickness, 0.5 m to 1.0 m, were based on the observed depths to the HVL in the nearby swale and the nearest log. We assigned a Poisson's ratio of 0.25 and a density of 2200 kg/m^3 for cemented sediments (e.g. Stone and Luke, 2001; Tecle et al., 2003).

As usual with the SA-LI approach, three SA runs were performed. To develop an "average" VS profile from this process, the stiff layer resolved for each of the runs was stripped from the profile, leaving three background profiles (underlying profile without the HVL). These background profiles were averaged to develop a base profile. From the three stiff layers we calculated an average thickness of the HVL, average depth to the middle of the HVL (midpoint depth), and average velocity of the HVL. The average

thickness and midpoint depth were then used to fix the depth to the HVL. The result, a 0.6-m thick HVL, at 3 m depth (to top), with VS of 1551 m/s, was overlain on the base profile. This combined profile was used as the starting model for LI. Its dispersion curve has a better fit to the target compared to the average of the SA profiles developed without the search for the HVL, but below 20 Hz the fit is still poor (Figure 2.12).

The dispersion curve for SA-LI resolved with the explicit search for a stiff layer (SAES-LI) is virtually identical to the dispersion curves from LI and SA-LI (Figure 2.12). The DD is slightly higher than the DD for the LI and SA-LI solutions, but the difference between all three DD values is small.

The VS profile resolved using SAES-LI (Figure 2.14) has an HVL with a VS of 1530 m/s, 1.5 to 3 times higher than that of the surrounding layers. The depth to the top of the HVL on the SAES-LI profile (3 m) is comparable to nearby sites located 30 m, 150 m, and 370 m away. The difference in thickness of the HVL between the measurement location (0.5 m thick) and the closest observation point (1 m thick) can be explained by the degree of variability in the thickness of a caliche horizon over short distances that has been observed in the Valley. For example, Stone and Luke (2001) reported a nearly 3-m difference in thickness of a shallow caliche layer in the LVV over a horizontal distance of less than 35 m.

Our conclusion that the depth of the HVL was resolved reliably is in agreement with previous research by Jin et al. (2009) and Luke et al. (2006), mentioned earlier in this paper. Because of the lateral variability of caliche, we assume thickness was estimated correctly. As previously discussed, findings from the previous studies by Luke et al. (2006) and Jin et al. (2009) conflicted, with Luke et al. (2006) reporting thickness to be

underestimated by 25 percent and Jin et al. (2009) reporting thickness as overestimated by 41 percent. Given the data available, the reliability of VS estimated for the HVL could not be determined. Recall that both Jin et al. (2009) and Luke et al. (2006) found VS of the HVL to be overestimated; thus we suspect that the same is true for this study.

For the SAES-LI process, the range of VS in the SA solutions for any single layer is as high as 525 m/s. The SAES-LI profile does not fall within the extremes of the SA search for every layer, although it does at the HVL.

Comparing SAES-LI to LI and SA-LI solutions, VS for the layers above the HVL differs by less than 20 percent. In contrast, VS of the layers below the HVL differs substantially. For layers directly below the HVL, the difference is as great as 77 percent (Table 2.3). For layers below 26 m, differences decrease to 35 percent. Immediately below the HVL, fluctuations in VS are visible in the profiles of all three solutions, but are more dramatic, as much as 400 m/s, for the SAES-LI profile. These observed fluctuations are consistent with findings of Luke and Calderón-Macías (2007). For an experimental dataset having ground truth available from nearby boreholes, they reported large fluctuations in VS for layers at and below the known depth of HVL's.

The VS resolved for the HVL using SAES-LI is 50 percent higher than the VS resolved by LI and SA-LI (Figure 2.14). However, the depth-averaged VS calculated over the range of depths of the HVL, 3.0 to 5.8 m, for the LI and SAES-LI profiles are similar, 925 m/s and 900 m/s, respectively (Recall that the LI and SA-LI profiles are virtually identical; thus an average for SA-LI was not calculated.). Because layer thickness is fixed for HVL's resolved without the stiff layer option, the VS resolved for

the HVL using LI and SA-LI apparently represents an average for a stiff layer with its surrounding layers.

VS(30) and VS(TD) were also calculated for the SAES-LI solution (Table 2.4). Both depth-averaged results differ from the LI and SA-LI results by only 2 percent.

As with LI and SA-LI, SAES-LI does not produce well-resolved solutions for the two deepest layers or the halfspace (Figure 2.12). Compared to LI and SA-LI, the resolution for SAES-LI is generally poor for most of the deeper layers and the HVL (layer 3). Ground truth, however, indicates that the HVL is properly resolved. Because of the nonuniqueness of the problem, this apparent conflict is not unusual. In the previously-mentioned sensitivity study performed by Luke et al. (2006), the authors observed the solution with the best resolution matrix did not necessarily correspond to the correct answer, although resolution matrices are still useful to assess the quality of the solution.

For the regional 3-D VS model, Luke et al. (2009) chose to use the results from the SA-LI method for this site because the authors believed the fluctuations in VS below the HVL to be more realistic than those resolved using SAES-LI. Additionally, the thickness and velocity of the HVL resolved using the SA-LI method was thought to more appropriately represent the area's sediments on a regional map than the thinner, higher-VS HVL resolved using SAES-LI.

2.4. Summary of outcomes

The VS profiles (from the SA-LI process) for all 12 test sites are plotted with respect to their sediment-response unit in Figure 2.15. Figure 2.15a shows the entire profile, while Figure 2.15b shows the upper 30 m, which, as previously mentioned in this paper,

is the depth over which the sediment-response unit classifications are based (Luke and Liu, 2008). The four coarse SRU sites generally have higher VS than the eight fine SRU sites. Exceptions include the following:

1) HVL's resolved for sites in the fine SRU generally exhibit higher VS than uncemented layers in the coarse SRU sites at the same depth (e.g. SFB, WLE).
2) For sites in the coarse SRU, at depths where well logs indicate the presence of clay, VS values are lower than other coarse SRU sites; alternatively, for sites in the fine SRU, at depths where well logs indicate the presence of gravel, VS values are higher than other fine SRU sites. For example:
    a. The low VS of coarse SRU site GMS, compared to other coarse SRU sites, is attributed to the presence of lower velocity sediments; the site is located within 800 m of a fine SRU, and the nearest available log describes the presence of clay in the gravel layers.
    b. The high VS values, greater than 1000 m/s, below 30 m for fine SRU site SMS are attributed to the presence of high velocity sediments; the log for a well located within a 150 m of the site shows a change at 45 m depth from mixed sand and clay sediments to gravel, which is expected to have higher VS than clay and sand.

Referring to Table 2.4, VS(30) and VS(TD) are typically higher for sites in the coarse SRU than those in the fine SRU. VS(30) for the coarse SRU sites are between 450 and 660 m/s. This range is within a broader range described by the IBC as seismic site classification C, very dense soil and soft rock (VS(30) between 360 and 760 m/s; International Code Council, 2009). Excluding the SFB site, VS(30) for the fine SRU sites

are between 320 and 450 m/s. This range falls between the high end of the VS(30) range for sites described as seismic site classification D, stiff soil (VS(30) between 180 and 360 m/s) and the low end for seismic site classification C.

The 12 new VS profiles are plotted with 16 others from the LVV compiled by Luke and Liu (2008) in Figure 2.16. The new site profiles are generally within the range of values previously measured in the site's sediment-response unit; although, for reasons previously discussed, VS below 40 m for the SMS site is higher than for the other profiles in the fine SRU. A representative profile for each sediment-response unit was calculated from the 28 sites by first discretizing the continuous profiles at 0.25 m intervals, then, at each depth interval, by calculating the average VS of the profiles located in each unit (10 located in the coarse SRU; 18 in the fine SRU). The representative profile is shown along with the VS profiles compiled by Liu et al. (2005) for site response analyses. Although the sediment-response units were defined based on the predominant sediment type within only the upper 30 m, the 3-D geometric model of basin stratigraphy and structure (Taylor et al., 2008) showed that the predominant sediment type above 30 m tended to be the predominant sediment type below 30 m. Thus, VS of the updated-average profile of the coarse SRU is consistently higher than that of the fine SRU over all depths. From 0 to 100 m depth, the updated-average VS profile for the coarse SRU is 25 to 400 m/s higher than that of the fine SRU. From 100 to 150 m depth, the difference between the profiles increases to 1000 m/s. The updated-average profile for the fine SRU generally has slightly higher VS values between 85 and 130 m depth than the profile developed by Luke and Liu (2008), but is otherwise not substantially different than the previous version. In contrast, the updated-average profile

for the coarse SRU has VS values that are as much as 500 m/s lower between 25 to 100 m depth. Of the relatively small number of profiles used to develop the profile for the coarse SRU, only four are as deep as 100 m (compared to ten in the fine SRU). More measurements are needed in the coarse SRU to better characterize this unit.

As depth increases the number of VS profiles decreases. Therefore, confidence in the profile averages decreases for increasing depths. The number of profiles in each of the sediment response units with respect to depth is shown in Table 2.5. Note that for the coarse SRU, the average VS below 170 m is based on only two sites (Figure 2.16).

2.5. Recommendations

Because solutions to the inversion process for Rayleigh-wave dispersion data can be nonunique, several methods may be incorporated to improve model results. These techniques include, but are not limited to, the following: acquiring complementary refraction data, especially to identify the depths to HVL's; using multi-mode surface-wave data (e.g. Casto et al., 2010); smoothing the profile (discussed below); testing for optimum layer geometry via parametric study; inverting the profile simultaneously for both depth and VS; and comparing the inverted profile to local geologic data. Not all of the additional measures are practical for general use. We recommend three for future research.

First, layers with high, non-diagonal values in the resolution matrix may be candidates for smoothing of the final VS profile. Smoothing is the process of combining layers with the goal of removing high velocity fluctuations in the final profile that are considered to be unrealistic. By using the resolution matrix to identify the parts of the

model to smooth, one is honoring the resolution in an inverted model (also referred to as "model regularization"; e.g. Hansen, 1998). In other words, model resolution might improve by smoothing the profile to have fewer layers, specifically, by combining those layers having poor resolution with adjacent layers. Because we observed relatively poor resolution of the halfspace at all the sites, the depths to model halfspace may be candidates for smoothing during model regularization.

Second, other than for the site where we observed an HVL in a nearby embankment, we did not use SA to invert for layer thickness. By simultaneously inverting for VS and layer geometry, it may be possible to increase the resolution of the SA-LI solution.

As previously discussed, future study is also needed to better set appropriate depth to model halfspace.

2.6. Conclusions

Twelve sites in the Las Vegas Valley (LVV) were surveyed using the SASW method to develop shear-wave velocity (VS) profiles to 100 m and deeper for use in seismic site response analyses. A multi-stage optimization process for developing VS profiles using the average of three profiles derived through simulated annealing (SA) as a refined starting model for linearized inversion (SA-LI) was presented and results were compared to those derived using linearized inversion (LI) based on a more conventionally developed starting model. For all 12 test sites, results from the LI and SA-LI approaches have consistently similar theoretical dispersion curves that fit the target well. Layer-velocity differences between the LI and SA-LI profiles are typically less than 20 percent. Similarity in results between the two processes is an indication that the inversion process

is robust; therefore, confidence in the outcome is enforced. For these sites where the SA-LI and the LI solution are not substantially different, the more straightforward LI approach was considered to have resolved a reasonable VS profile. At three sites, differences between LI and SA-LI profiles for the VS of some of the layers were as great as 46 percent; however, differences in depth-averaged velocity values remained small, 3 percent or less. Different solutions are not unexpected due to the nonunique nature of the problem. Large differences in velocity between the LI and SA-LI solutions likely occur because the solution to the inversion problem is non-unique. This arises because of the complexity of sediment stiffness, vertically and perhaps also horizontally. One possible solution to the problem of non-uniqueness is to improve the quality of the starting model. Large differences between solutions imply decreased confidence in results.

At a site where a high velocity layer (HVL) was known to exist, a VS profile was developed using the SA-LI approach configured for an explicit search for an HVL (SAES-LI). Excluding the HVL, differences in VS of individual layers between the LI and SA-LI profiles and the SAES-LI profile were as great as 77 percent. In contrast, the depth-averaged velocities differed by less than 3 percent. The depth averaged VS calculated over the depth of the HVL also differed by less than 3 percent and indicates that VS for the stiff layer resolved using LI and SA-LI represents an average of a stiff layer and its surrounding layers. The depth to and thickness of the HVL obtained using the SAES-LI method appeared to be well resolved.

The 12 new VS profiles generally fit expectations for the fine and coarse sediment response units in the LVV: profiles for sites located in the fine sediment response unit

typically have lower VS values compared to those from sites located in the coarse sediment response unit, and the new velocity profiles are consistent with profiles developed by others in the two sediment-response units. The new profiles were added to the VS dataset previously compiled for the sediment response units. The combined dataset was used to create updated-average profiles for use in site response analyses. Recommendations to improve data interpretation were presented for future study.

2.7. Paper-specific acknowledgements

This research was sponsored by the U. S. Department of Energy under contract number DE-FG52-03NA99204. Stanley Consultants, Inc. provided tuition assistance to the lead author. The following persons assisted with field data acquisition: John Amato, Chris Cothrun, Dianna Feica, Eduardo Gonzalez, Richard Phillips, Ryan Wilson and Ian Wilson. Cathy Willey obtained site permits with the assistance of Mr. Gonzalez and Mr. Phillips. Wanda Taylor and Jonathan Carter provided the well log database as well as assistance plotting and interpreting the logs.

2.8. Tables and Figures

Table 2.1 Test site designations and descriptions

Test site	Latitude, degree N	Longitude, degree W	Description
CCH	36.0084	114.971	Undeveloped lot west of College of Southern Nevada, Henderson, NV
CPH	35.9934	114.961	Undeveloped lot, intersection of College Dr. and Paradise Hills Dr., Henderson, NV
GMS†	36.1128	115.231	Guinn Middle School, turf
LES†	36.2368	115.069	Lowman Elementary School, turf
LMN	36.2462	115.246	Undeveloped lot southeast of Lone Mountain Rd. and Hwy I-95
MHS	36.2577	115.139	Mojave High School, turf
NLP†	36.1621	115.195	Cragin Park, turf
OSH	36.0386	115.042	Undeveloped lot south of Ocean Spray Plant, Henderson, NV
SFB†	36.1135	115.146	Stan Fulton Building, UNLV campus, gravel roadside
SMS	36.0343	115.129	Schofield Middle School, turf
SPS	36.0592	115.116	Sunset Park, undeveloped area to south
WLE	36.1492	115.088	Walter Long Elementary School, turf

† Inversion process for these sites is detailed in this paper

Table 2.2 Key test parameters, sediment response unit, and depth to model halfspace.

Test site	Frequency range, Hz		Wavelength range, m		Model halfspace depth, m	Sediment response unit	Receiver spacings, m
	min	max	min	max			
CCH	5.7	57	2.6	117	55.6	Coarse	2, 4, 8, 16, 32, 64
CPH†	6.5	214	0.6	127	63.7	Coarse	1, 2, 4, 8, 16, 32, 64
GMS††	3.3	172	0.8	254	127.0	Coarse	1, 2, 4, 8, 16, 32, 64, 128
LES††	3.7	253	0.5	126	63.1	Fine	1, 2, 4, 8, 16, 32, 64, 128
LMN	3.2	193	1.0	186	93.2	Fine	2, 4, 8, 16, 32, 50, 64, 100
MHS	3.2	76	2.7	166	83.1	Fine	2, 4, 8, 16, 32, 64, 128, 165†††
NLP††	4.6	179	0.7	121	60.5	Fine	1, 2, 4, 8, 16, 32, 64, 69
OSH	7.5	301	0.4	115	57.6	Coarse	1, 2, 4, 8, 16, 32, 54, 64, 108
SFB	3.4	192	1.8	176	87.8	Fine	2, 4, 8, 16, 32, 60, 91
SMS	4.7	155	1.2	127	63.3	Fine	2, 4, 8, 16, 32, 64
SPS	3.5	188	0.8	191	95.5	Fine	1, 2, 4, 8, 16, 32, 64, 128
WLE	3.8	92	0.7	128	64.0	Fine	1, 2, 4, 8, 16, 32, 42.5, 64, 85

† Site is located less than 1 km south of the coarse SRU's defined boundary.
†† Site used to test depth to model halfspace.
††† The lowest frequency was resolved from the data acquired at 128 m receiver spacing.

Table 2.3 Maximum difference found comparing VS layer-by-layer between the LI and SA-LI solutions.

Test site	Difference, %
CCH	9
CPH	3
GMS	17
LES	4
LMN	12
MHS	46
NLP	8
OSH	11
SFB	5 (77[†])
SMS	46
SPS	7
WLE	40

[†] Maximum difference found comparing LI solution to a solution derived using an explicit search for stiff-layer (SAES-LI).

Table 2.4 VS averaged over the upper 30 m depth (VS(30)) and averaged over the total depth (VS(TD)).

Test site	LI VS(30), m/s	SA-LI VS(30), m/s	VS(30) Difference, %	LI VS(TD), m/s	SA-LI VS(TD), m/s	VS(TD) Difference %	Sediment-response unit
CCH	463	462	0	656	657	0	Coarse
CPH	580	581	0	819	821	0	Coarse[†]
GMS	456	453	1	824	832	1	Coarse
LES	373	373	0	476	477	0	Fine
LMN	445	450	1	608	610	0	Fine
MHS	377	373	1	539	548	2	Fine
NLP	447	450	1	565	566	0	Fine
OSH	658	660	0	863	871	1	Coarse[†]
SFB	499	499	0	636	635	0	Fine
SFB[††]	499	511	2	636	646	2	Fine
SMS	314	316	1	608	616	1	Fine
SPS	324	324	0	654	658	1	Fine
WLE	338	343	1	493	501	2	Fine

[†] Assumed

[††] Explicit search for stiff-layer used in SA-LI (SAES-LI)

Table 2.5 Number of VS profiles at specific depth for the combined dataset of the 12 new profiles and the profiles presented by Luke and Liu (2008).

Depth, m	Fine SRU	Coarse SRU
30	18	10
75	15	7
100	10	4
150	5	3
200	5	2
250	3	2
350	2	2
400	1	1
> 400	N/A	1

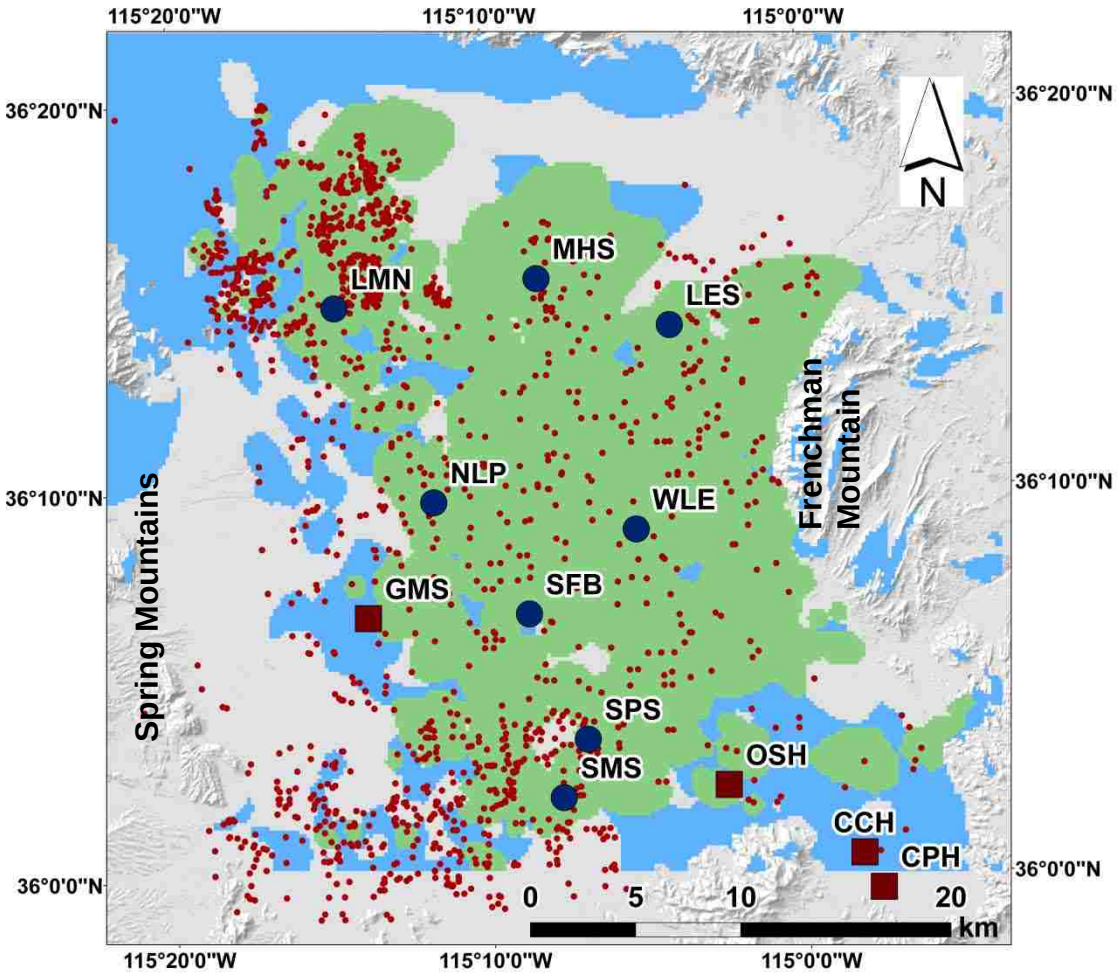

Figure 2.1 The Las Vegas Valley with test site locations (dark red squares are sites in coarse SRU; blue circles are sites in fine SRU) shown with respect to well locations (red circles) and sediment-response units according to Luke and Liu (2008; fine in green and coarse in blue).

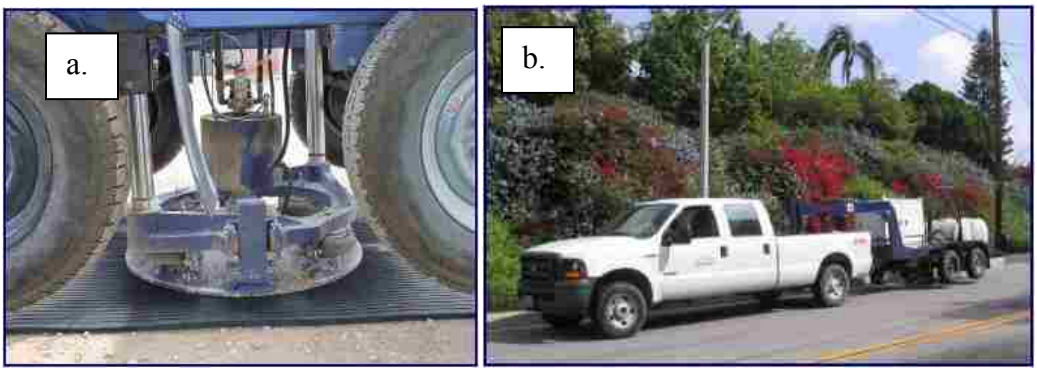

Figure 2.2 UNLV's "minivib", a trailer-mounted T-7000W servo-hydraulic vibrator built by Industrial Vehicles International: a) mass and baseplate and b) truck with trailer attached.

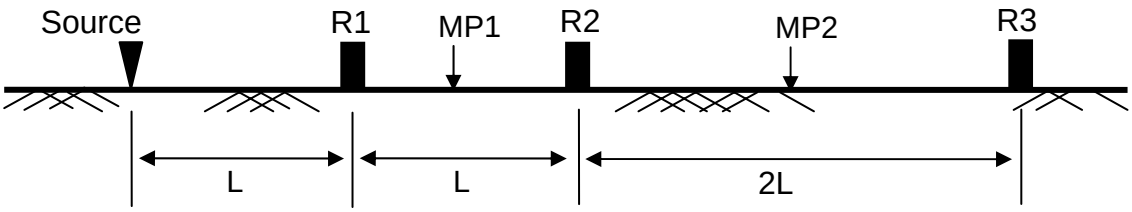

Figure 2.3 Two- and three-receiver arrangements for SASW array. For surveys performed with two receivers, receivers are centered on midpoint 1 (MP1). For the three receiver arrangement, receivers R1 and R2 are centered on MP1, and receivers R2 and R3 are centered on midpoint 2 (MP2).

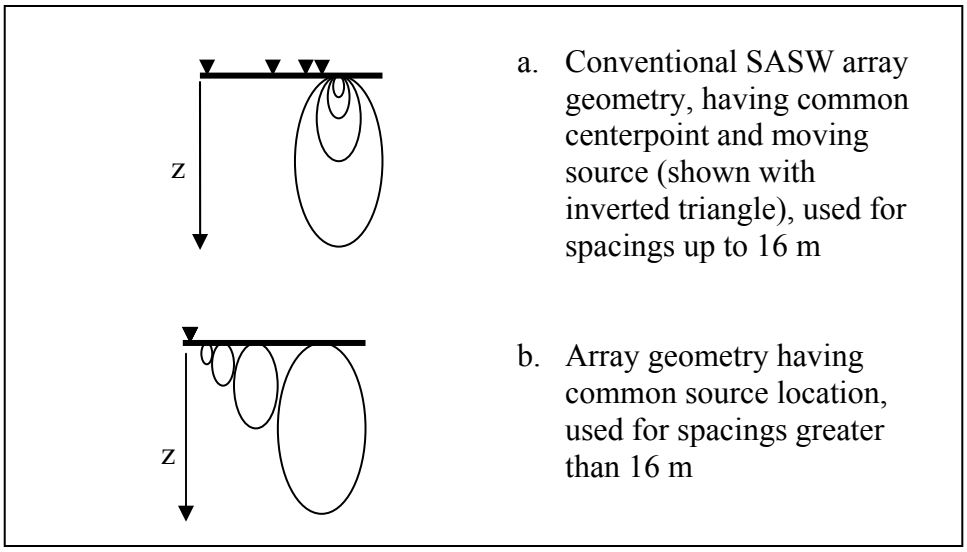

Figure 2.4 Conceptualization of zones tested (shown by ellipses) along SASW array with different receiver spacings and source-receiver geometry (z = investigation depth) (from Murvosh and Luke, 2008).

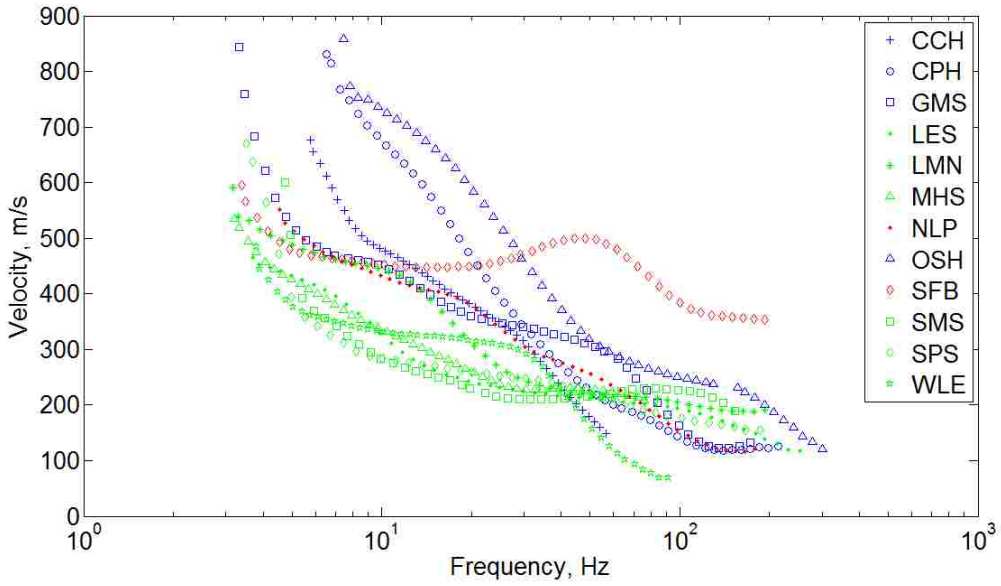

Figure 2.5 Target dispersion curves for the 12 test sites. Most of the fine SRU sites shown in green; all coarse SRU sites shown in blue. Sites in fine SRU, but known to have high velocity inclusions, are shown in red.

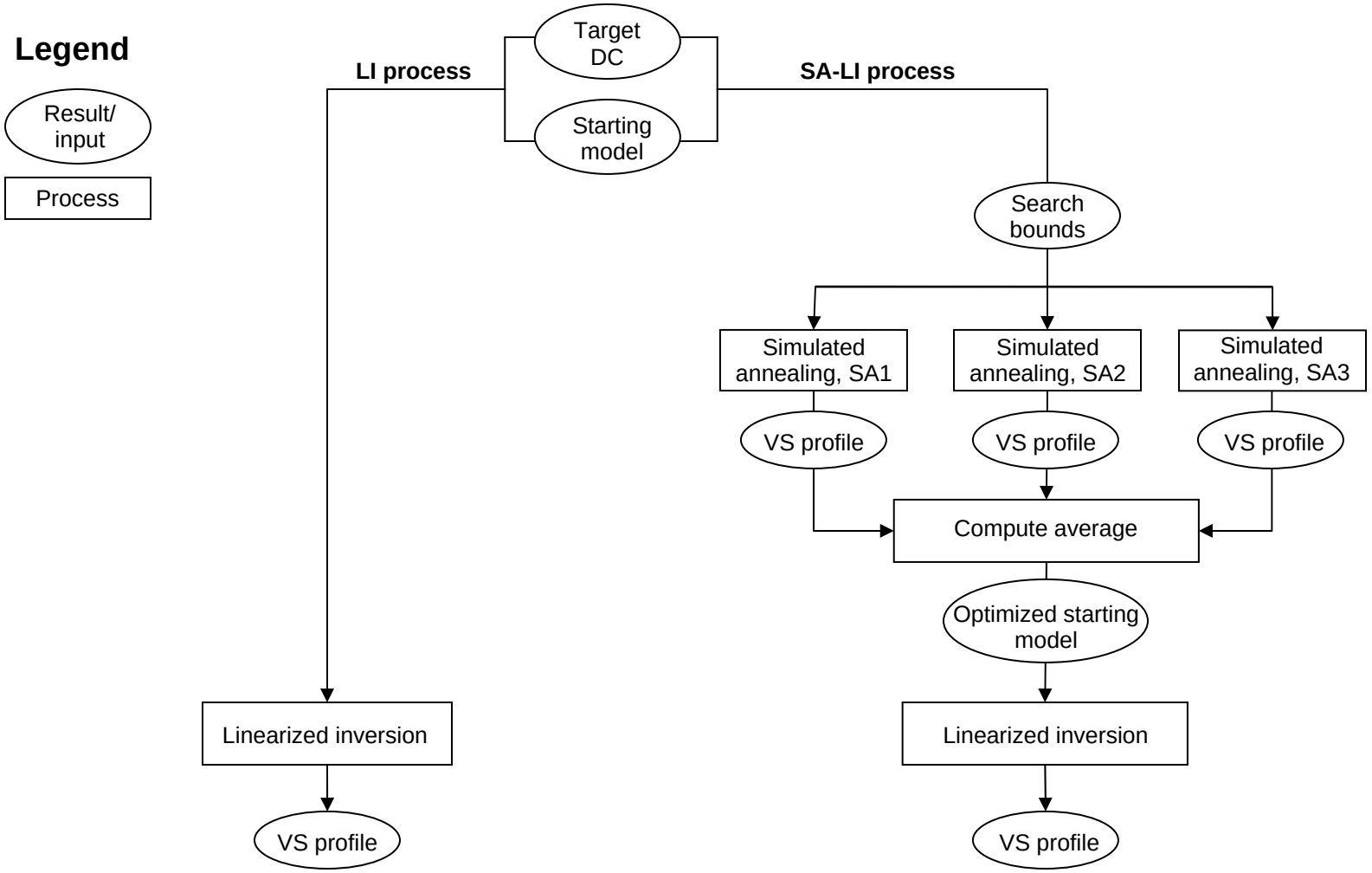

Figure 2.6 Chart illustrating the steps taken to perform optimization using LI and SA-LI methods.

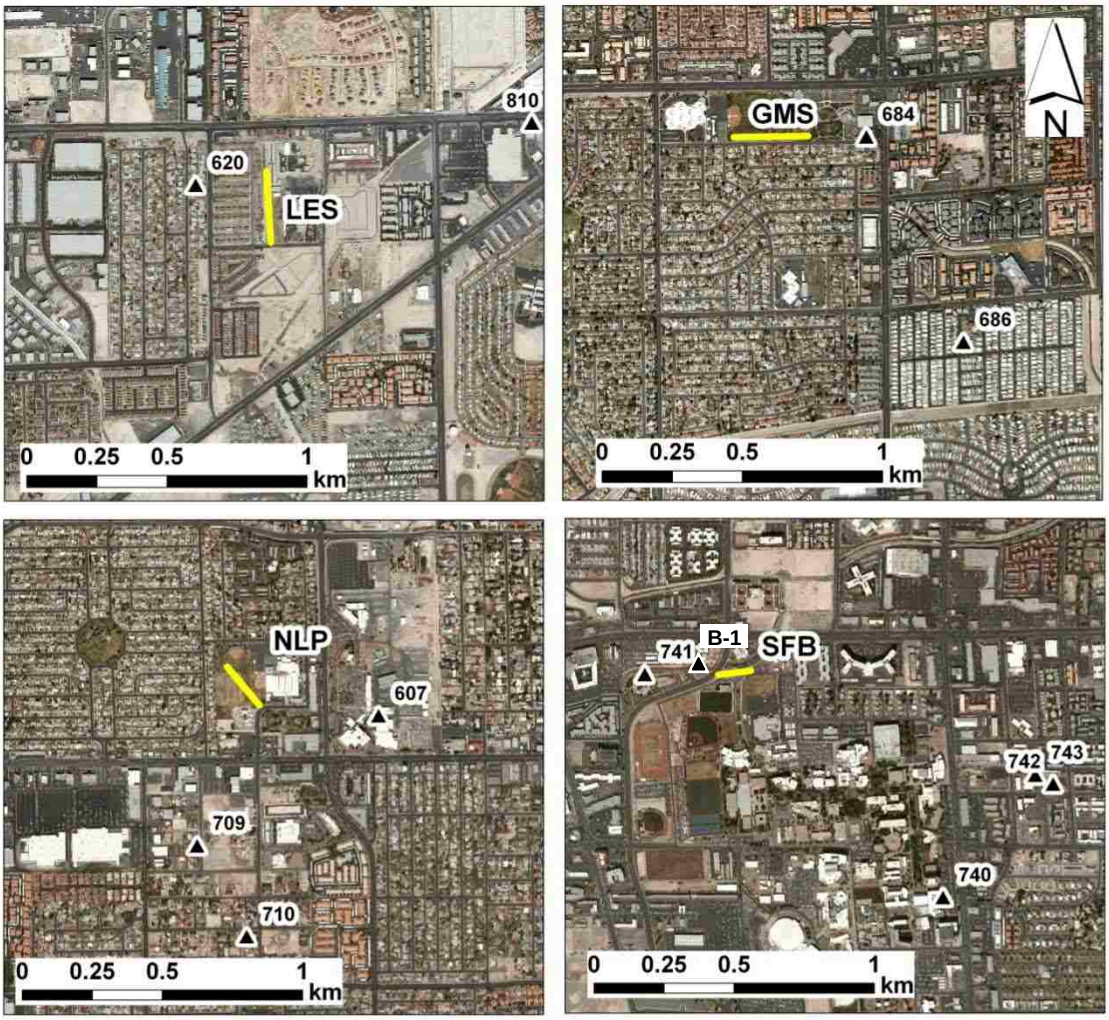

Figure 2.7 Locations of the 4 case study sites: array locations (yellow lines) with respect to nearby wells (black triangles). Latitude and longitude for each site are listed in Table 2.1.

a) b)

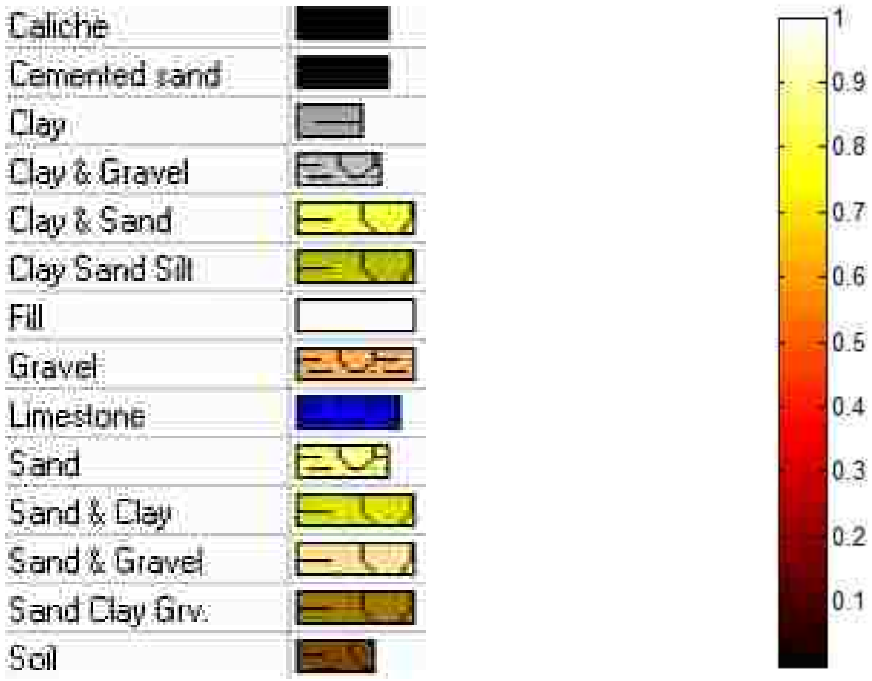

Figure 2.8 Sediment and lithology key (a) and resolution matrix key (b) (used in Figures 2.9 through 2.12). "Soil" classification used by Taylor et al. (2008) to denote areas with organic material or sediments that have experienced additional surface weathering or near surface (within upper 0.5 m) cementation.

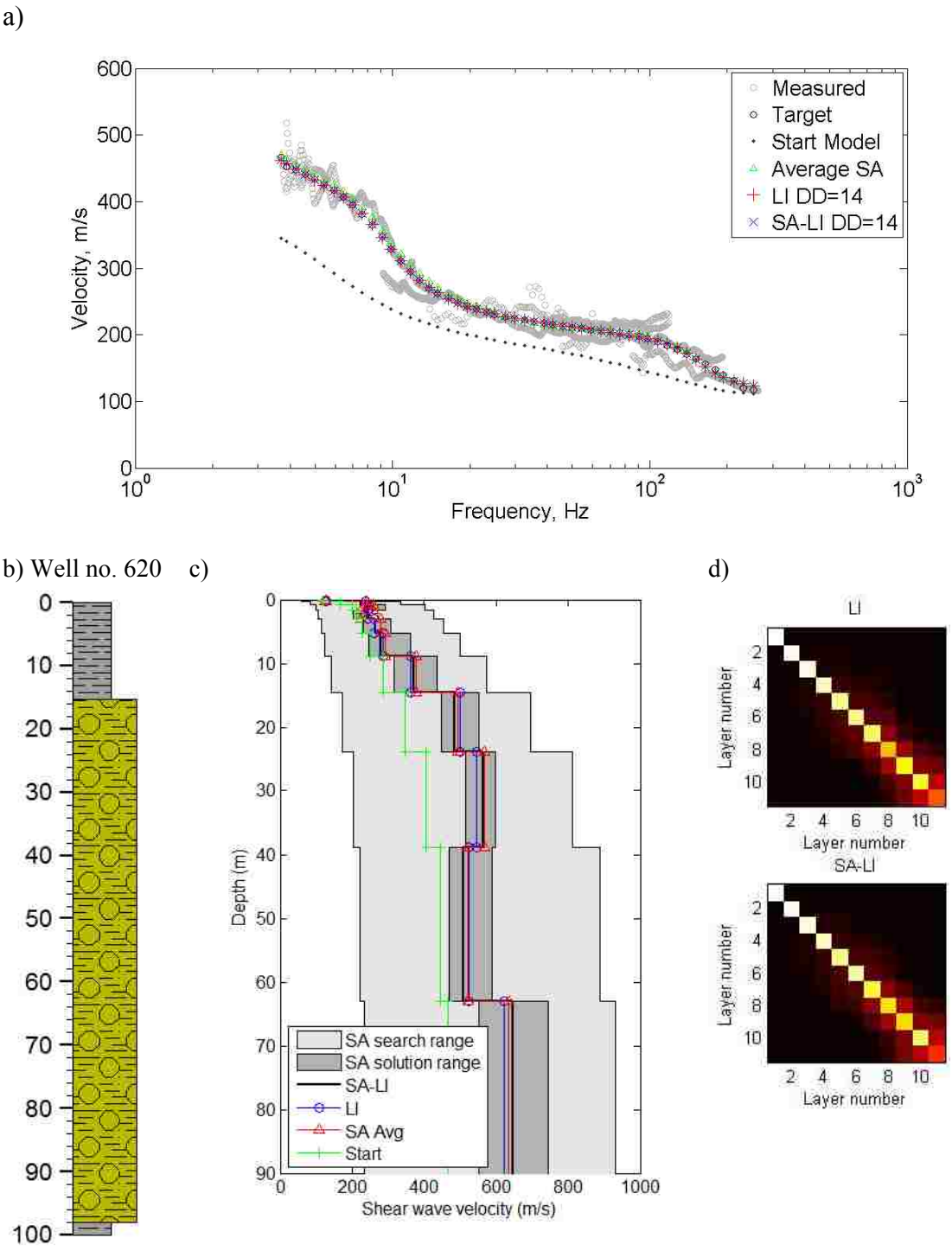

Figure 2.9 Sample fine-sediment response unit site (LES), data and solutions: a) dispersion curves, b) well log information (depth in meters), c) VS profiles, and d) resolution matrices.

a)

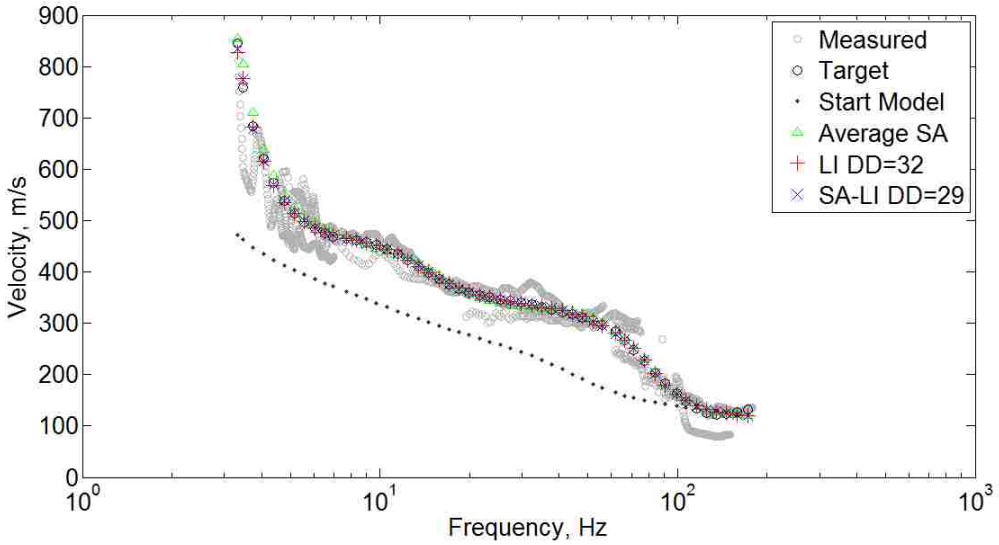

b) Well no. 684 c) d)

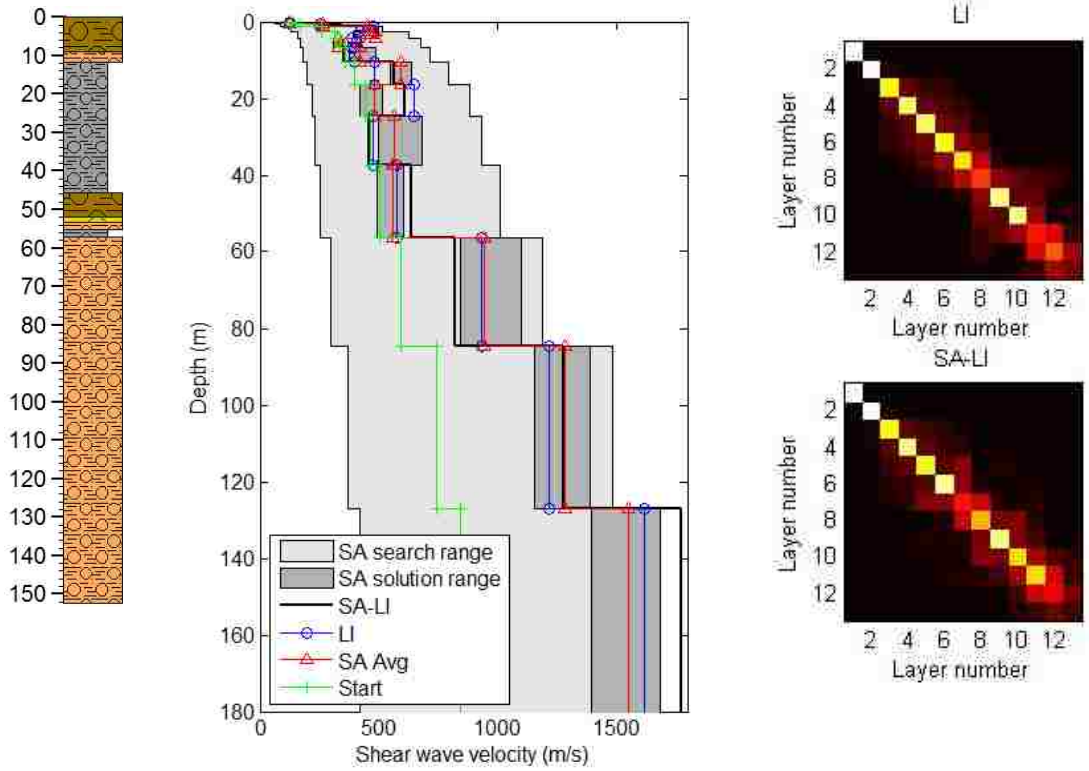

Figure 2.10 Sample coarse-sediment response unit site (GMS), data and solutions: a) dispersion curves, b) well log information (depth in meters), c) VS profiles, and d) resolution matrices.

a)

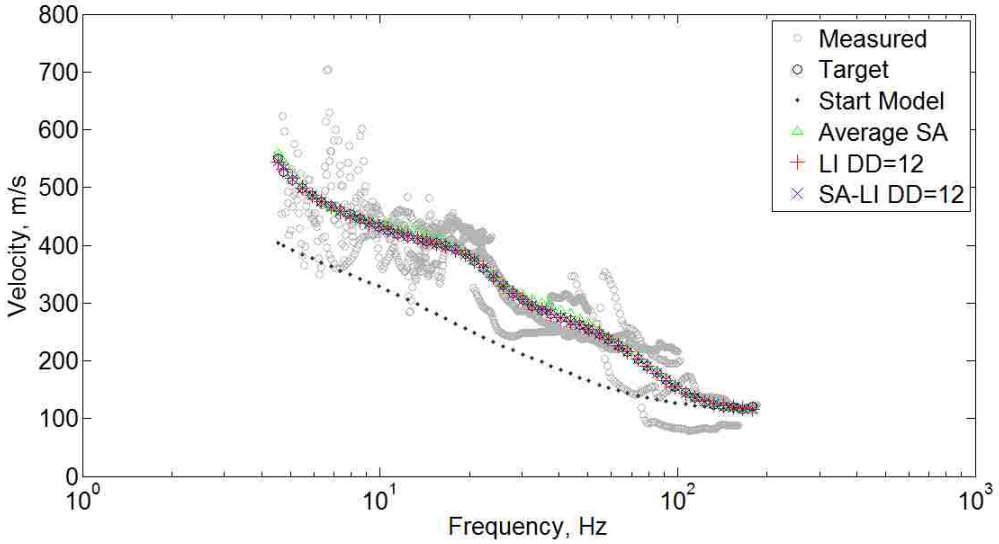

b) Well no.'s 709 (L) and 607 (R)

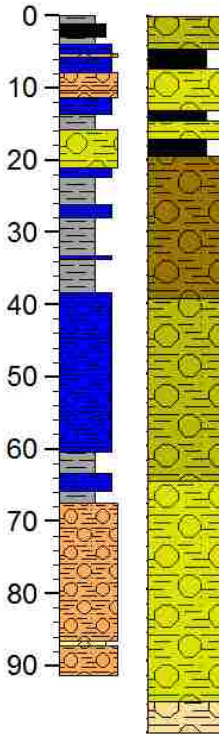

c)

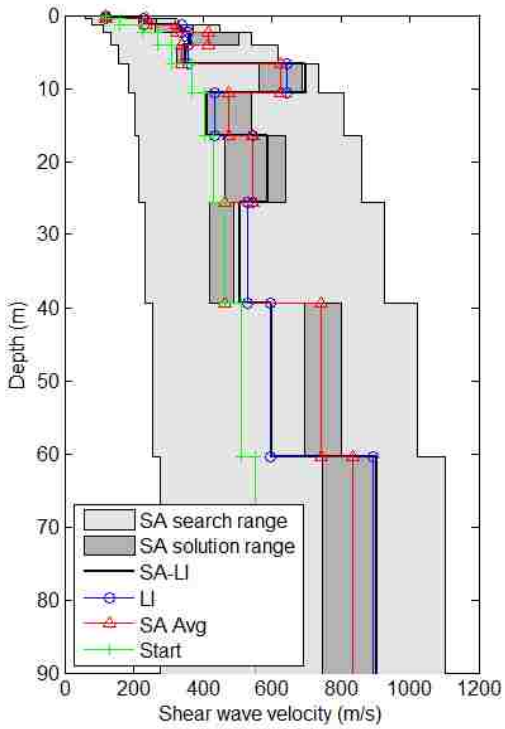

d)

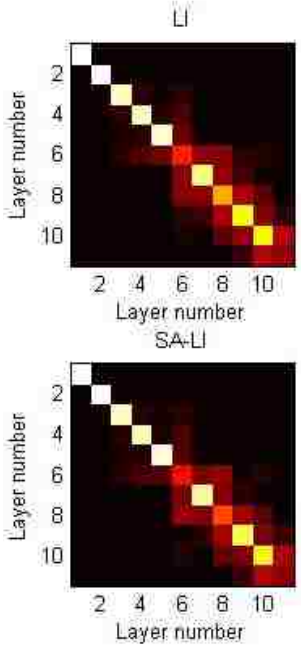

Figure 2.11 HVL site 1 (NLP), data and solutions: a) dispersion curves, b) well log information (depth in meters), c) VS profiles, and d) resolution matrices.

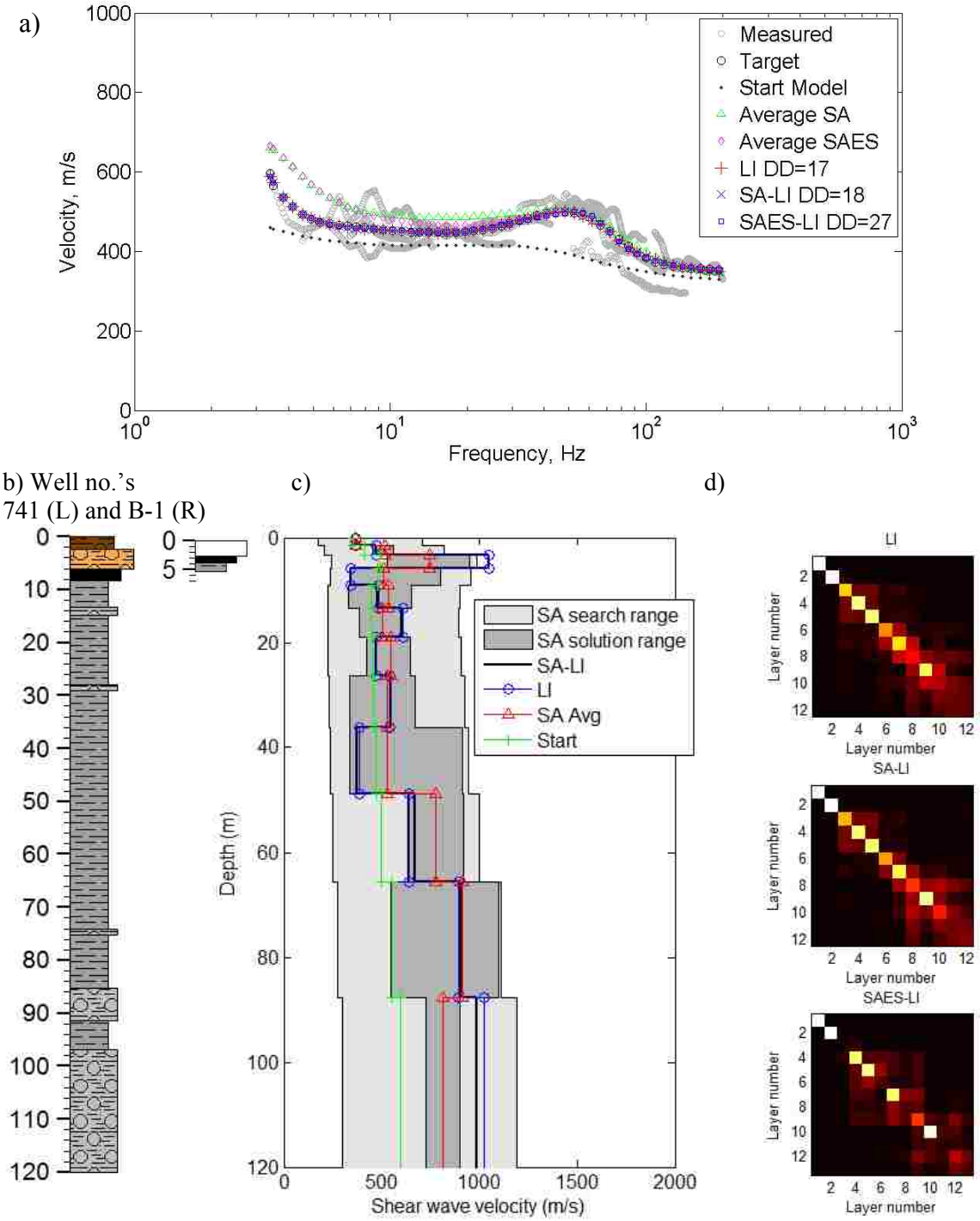

Figure 2.12 HVL site 2 (SFB), data and solutions: a) dispersion curves including curve for SA-LI with the explicit search for a stiff layer (SAES-LI, discussed in Section 2.3.5), b) well log information (depth in meters), c) LI and SA-LI VS profiles and d) resolution matrices.

MHS SMS WLE

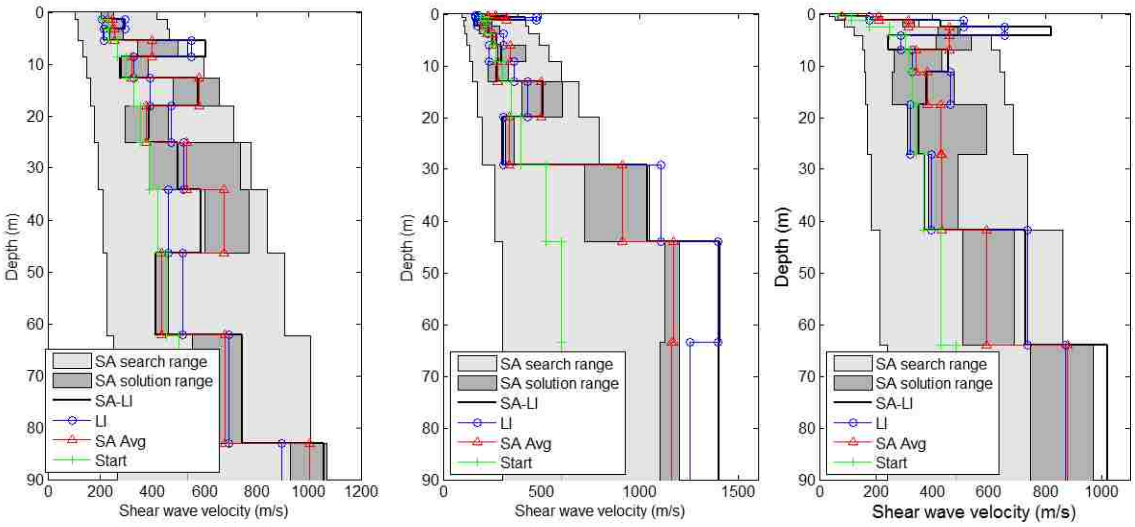

Figure 2.13 VS profiles for LI and SA-LI processes for 3 sites, all in fine SRU, where difference in VS between the methods exceeded 20 percent in at least one layer. Bottom layer shown is halfspace.

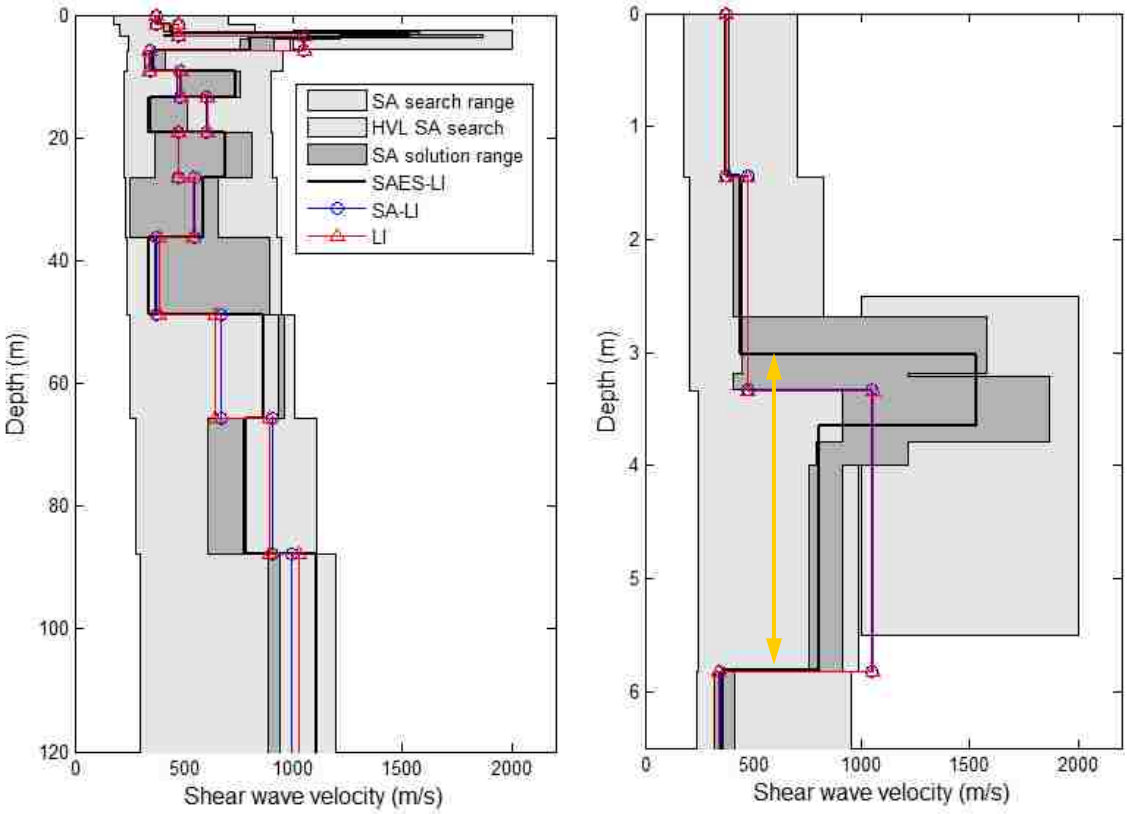

Figure 2.14 HVL site 2 (SFB), comparison of LI and SA-LI solutions (Figure 2.12) to a solution resolved using explicit search for stiff layer, (a) VS profiles from LI, SA-LI and SAES-LI and (b) expanded view of upper 6 m showing depth range over which an average velocity was calculated for the HVL (yellow arrow, see text). Note the search range for SA is the same for SA-LI and SAES-LI except that SAES-LI includes an additional search range for a stiff layer (HVL SA search). The SA solution range shown is the range for SAES-LI.

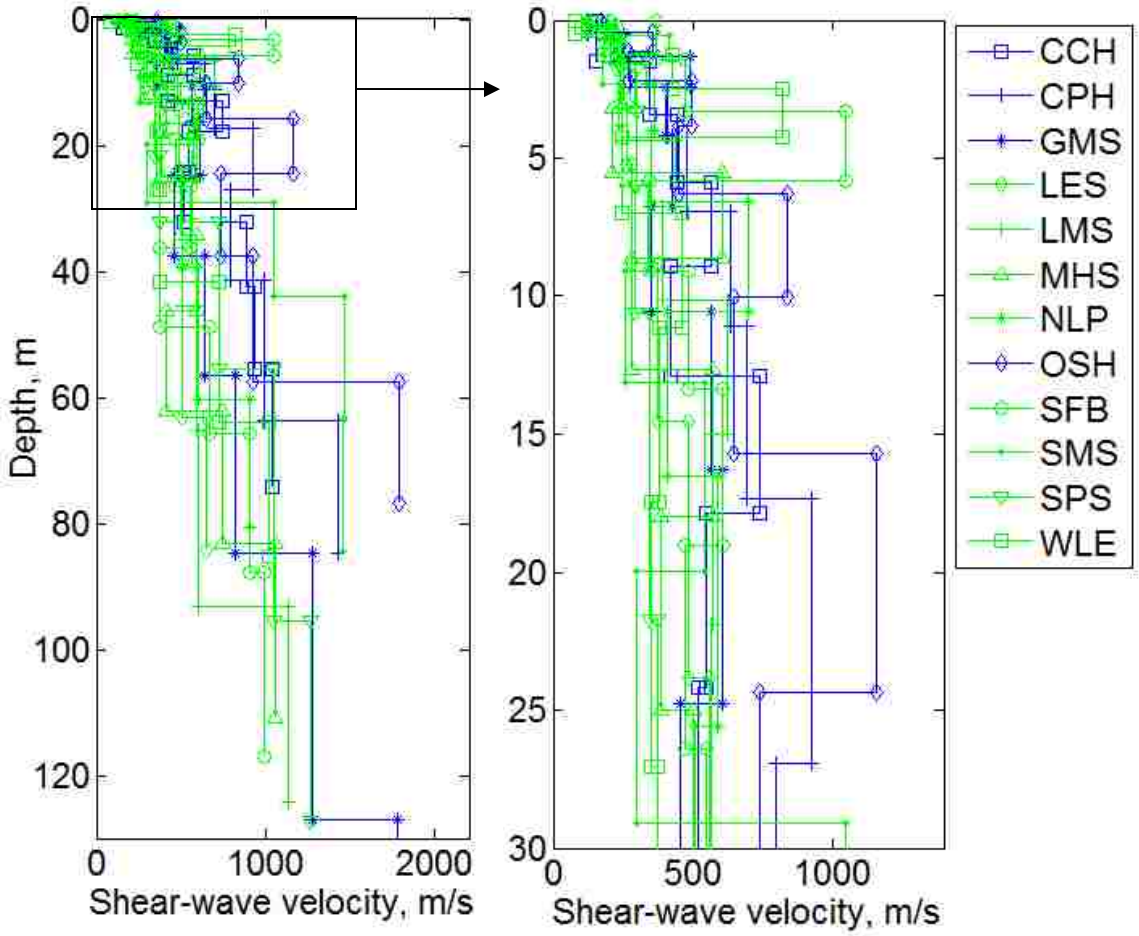

Figure 2.15 SA-LI profiles for the 12 test sites: a) to 130 m depth and b) to 30 m depth. Sites located in the fine-sediment response unit shown in green; sites in the coarse-response unit shown in blue.

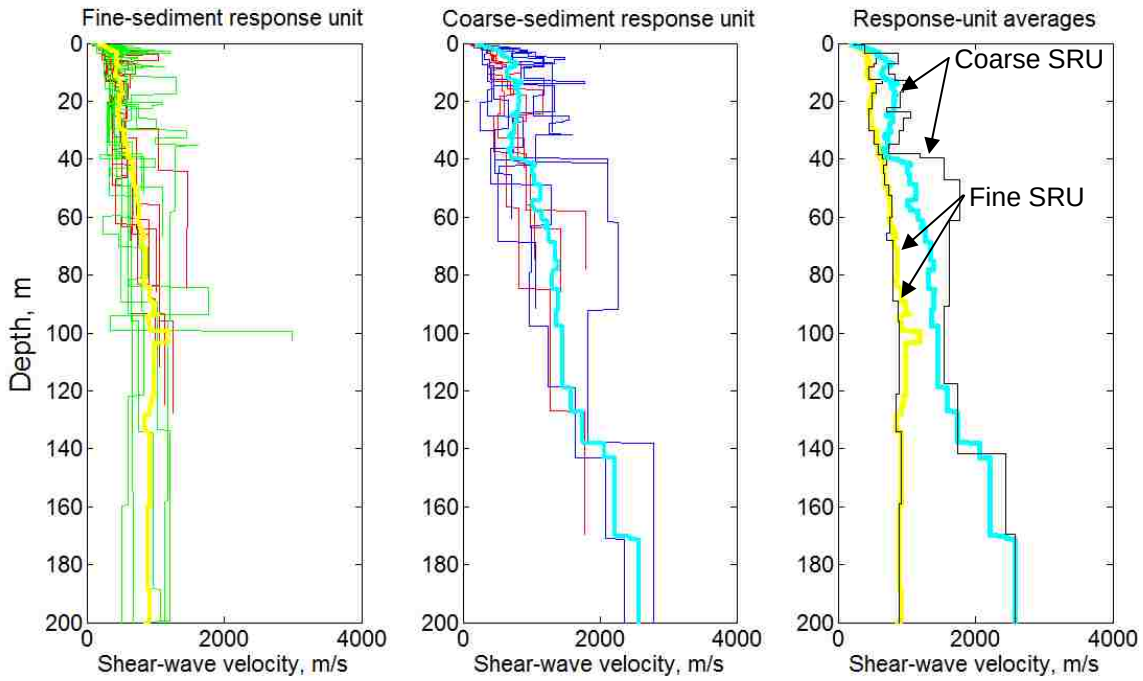

Figure 2.16 New data (red) combined with data from previous microzonation by Luke and Liu (2008): (a) VS profiles for sites in the fine sediment response unit and their average (yellow); (b) VS profiles for sites in the coarse sediment response unit and their average (cyan); and (c) updated average profiles (yellow and cyan) and previous profiles (black) originally published by Luke and Liu (2008).

2.9. References

Abrahamson, N., and Silva, W. (2008). Summary of the Abrahamson & Silva NGA ground-motion relations. *Earthquake Spectra, 24* (1), 67-97.

Calderón-Macías, C. and Luke, B. (2007). Improved parameterization to invert Rayleigh-wave data for shallow profiles containing stiff inclusions. *Geophysics, 72* (1), U1-U10.

Casto, D., Calderón-Macías, C., Luke, B., and Kaufmann, R. (2010). Improving MASW results for a site with shallow bedrock through the use of higher-mode data. In D.

Fratta, A. J. Puppala and B. Muhunthan (eds.), *GeoFlorida 2010: Advances in Analysis, Modeling and Design, Geotechnical Special Publication 199* [CD-ROM] (pp. 1360-1368). Reston, VA: American Society of Civil Engineers.

Foinquinos-Mera, R. (1991). Analytical study and inversion for the spectral-analysis-of-surface-waves method. Master's thesis, University of Texas at Austin, Austin, Texas.

Gilbert, J. W. (2004). Shear wave velocity profiling of poorly characterized geologic units in Salt Lake Valley, Utah. Master's thesis, Utah State University, Logan, UT.

Hansen, P, C. (1998). *Rank-deficient and Discrete Ill-Posed Problems: Numerical Aspects of Linear Inversion*. Philadelphia, PA: Society of Industrial and Applied Mathematics.

Idriss, I. M. (1990). Response of soft soil sites during earthquakes, In J. M. Duncan (ed.), *Proceedings, H. Bolton Seed Memorial Symposium, vol. 2* (pp. 273–289) Berkley, CA: BiTech Publishers.

International Code Council (2009). *International Building Code*. Country Club Hills, IL: International Code Council.

Jin, X. (2006). Delineating anomalous layers in soil profiles using seismic surface wave methods. Ph. D. Dissertation, The University of Nevada Las Vegas, Las Vegas, NV.

Jin, X., Luke, B., and Calderón-Macías, C. (2009). Role of forward model in surface-wave studies to delineate a buried high-velocity layer. *Journal of Environmental & Engineering Geophysics*, *14* (1), 1–14.

Kramer, S L. (1996). *Geotechnical Earthquake Engineering*. Upper Saddle River, NJ: Prentice-Hall, Inc.

Lai, C. G., and Rix, G. J. (1998). Simultaneous inversion of Rayleigh phase velocity and attenuation for near-surface site characterization. School of Civil and Environmental Engineering, Report No. GIT-CEE/GEO-98-2. Atlanta, Georgia: Georgia Institute of Technology.

Langenheim, V. E., Grow, J. A., Jachens, R. C., Dixon, G. L., and Miller, J. J. (2001). Geophysical constraints on the location and geometry of the Las Vegas Valley Shear Zone, Nevada. *Tectonics, 20* (2), 189-209.

Liu, H., Luke, B., and Calderón-Macías, C. (2002). A scheme to generate starting models for interpretation of shallow surface wave data. *Proceedings, Symposium on the Application of Geophysics to Engineering and Environmental Problems* (SAGEEP; CD-ROM, 12SEI4, p. 38), Denver, CO: Environmental and Engineering Geophysical Society.

Liu, Y. (2006). Site response projections and earthquake microzonation for the Las Vegas basin, Nevada. Ph.D. dissertation, University of Nevada Las Vegas, Las Vegas, NV.

Liu, Y., Luke, B., Pullammanappallil, S., Louie, J., and Bay, J. (2005). Combining active- and passive-source measurements to profile shear wave velocities for seismic microzonation. In R. W. Boulanger, M. Dewwolkar, N. Gucunski, C. Juang, M. Kalinski, S. Kramer, M. Manzari and J. Pauschke (eds.), *Earthquake Engineering and Soil Dynamics, Geotechnical Special Publication 133* (pp. 977-990). Reston, VA: American Society of Civil Engineers.

Luke, B., and Calderón-Macías, C. (2007). Inversion of seismic surface wave data to resolve complex profiles. *Journal of Geotechnical and Geoenvironmental Engineering, 133* (2), 155-165.

Luke, B., and Liu, Y. (2007). Effect of sediment column on weak-motion site response for a deep basin fill. *Journal of Geotechnical and Geoenvironmental Engineering, 133* (11), 1399-1413.

Luke, B., and Liu, Y. (2008). Site response zones and short-period earthquake ground motion projections for the Las Vegas basin. *Journal of Earth System Science, 117* (S2), 757-772.

Luke, B., Calderón-Macías, C., Stone, R. C., and Huynh, M. (2003).Non-uniqueness in inversion of seismic surface-wave data. *Proceedings Symposium on the Application of Geophysics to Engineering and Environmental Problems* (SAGEEP) CD-ROM[1] (pp. 1342–1347). Denver, CO: Environmental and Engineering Geophysical Society.

Luke, B., Lipinska-Kalita, K., Calderón-Macías, C., and Jin, X. (2006). Interpreting complex layered systems by constrained optimization of surface wave data. In H. Mikada (ed.), *Proceedings*, *8th SEGJ International Symposium on Imaging and Interpretation* (pp. 615-620). Tokyo, Japan: Society of Exploration Geophysicists of Japan.

Luke, B., Taylor, W., Calderón-Macías, C., Jin, X., Murvosh, H., and Wagoner, J. (2008). Characterizing anomalous ground for engineering applications using surface-based seismic methods. *The Leading Edge, 27*(11), 1330–1334.

Luke, B., Murvosh, H., Taylor, W., and Wagoner, J. (2009). Three-dimensional modeling of shallow shear-wave velocities for Las Vegas, Nevada, using sediment type. *Journal of Earth Science, 20* (3), 555-562.

Mavko, G., Mukerji, T., and Dvorkin, J. (1998). *The Rock Physics Handbook*. Cambridge, UK: Cambridge University Press.

Menke, W. (1989). *Geophysical Data Analysis; Discrete Inverse Theory*. San Diego, CA: Academic Press, Inc.

Murvosh, H., Luke, B., McLaurin, B., Higgins, T., and Quinn, W. (2006a). Research and development of Las Vegas Valley VS(30) map. *Proceedings, 40th Annual Symposium on Engineering Geology and Geotechnical Engineering* (CD-ROM: 7 p.). Pocatello, ID: Idaho State University.

Murvosh, H., Luke, B., Taylor, W., Liu, Y., and Jin, X. (2006b). Characterizing shallow shear wave velocities in fabulous Las Vegas: processes and site selections. *Proceedings, 19th Annual Symposium on the Application of Geophysics to Engineering and Environmental Problems* (SAGEEP, CD-ROM P-153: pp. 1325-1333). Denver, CO: Environmental and Engineering Geophysical Society.

Murvosh, H., and Luke, B. (2008). Summer 2007 VS data acquisition campaign in Las Vegas; lessons learned. *Proceedings, 41st Annual Symposium on Engineering Geology and Geotechnical Engineering* (CD-ROM: pp. 277-286). Pocatello, ID: Idaho State University.

Price, J. G., Johnson, G., Ballard, C. M., Armeno, H., Seeley, I., Goar, L. D., dePolo, C. M., and Hastings, J. T. (2009). *Estimated Losses from Earthquakes near*

Nevada Communities (Nevada Bureau of Mines and Geology Open-File Report 09-8). .

Rosenblad, B. L., Li, J., Menq, F. Y., and Stokoe, K. H. (2007). Deep shear wave velocity profiles from surface wave measurements in Mississippi embayment. *Earthquake Spectra, 23* (4), 791-808.

Sánchez-Salinero, I., Roesset, J. M. and Stokoe, K. H. (1986). Analytical studies of body wave propagation and attenuation. Geotechnical Engineering Report No GR86–15. Austin, TX: Civil Engineering Department, University of Texas at Austin.

Scott, J. B., Rasmussen, T., Luke, B., Taylor, W., Wagoner, J. L., Smith, S. B., and Louie, J.N. (2006). Shallow shear velocity and seismic microzonation of the urban Las Vegas, Nevada basin. *Bulletin of the Seismological Society of America*, *96* (3), 1068-1077.

Sen, M., and Stoffa, P. L. (1995). *Global Optimization Methods In Geophysical Inversion*. Amsterdam, The Netherlands: Elsevier.

Sharma, P.V. (1997). *Environmental and Engineering Geophysics* (p. 122). New York, NY: Cambridge University Press.

Stokoe, K. H., II, Wright, S. G., Bay, J. A., and Roësset, J. M. (1994). Characterization of geotechnical sites by SASW method. In R. D. Woods (ed.), *Geophysical Characterization of Sites* (pp. 15-25). New Delhi, India: Oxford and IBH Publishing Co.

Stokoe, K., Cox, B., Lin, Y., Jung, M., Bay, J., Rosenblad, B., and Wong, I. (2006). Use of intermediate to large vibrators as surface wave sources to evaluate VS profiles for earthquake studies. *Proceedings, Symposium on the Application of Geophysics*

to Engineering and Environmental Problems (SAGEEP, CD-ROM P-153, pp. 1241-1258). Denver, CO: Environmental and Engineering Geophysical Society.

Stone, R., and Luke, B. (2001). An overview of engineering with cemented soils in Las Vegas. In B. Luke, E. Jacobson and J. Werle (eds.), *Proceedings, 36th Annual Symposium on Engineering Geology and Geotechnical Engineering* (pp. 135-144). Pocatello, ID: Idaho State University.

Sundquist, B. (2001). Evaluation of geophysical methods to characterize alluvial soils in the arid environment. Master's thesis, University of Nevada Las Vegas, Las Vegas, NV.

Sundquist, B. and Luke, B. (2001). Geophysical and geotechnical investigations at the Las Vegas Springs Preserve. In B. Luke, E. Jacobson and J. Werle (eds.) *Proceedings, 36th Annual Symposium on Engineering Geology and Geotechnical Engineering* (pp. 747-754). Pocatello, ID: Idaho State University.

Taylor, W. J., Carter, J., Luke, B., Snelson, C. M., and Wagoner, J. (2008). Development of Las Vegas Basin, Nevada with implications for seismic hazards. Abstract, Cordilleran Section (104th Annual) and Rocky Mountain Section (60th Annual) Joint Meeting (Paper No. 17-4). Boulder, CO: The Geological Society of America.

Tecle, M., Giorgis, A. and Luke, B. (2003). Comparison of seismic downhole to crosshole measurements in a complex-layered system. In S. Elfass, G. Norris, and R. Watters (eds.), *Proceedings, 38th Annual Symposium on Engineering Geology and Geotechnical Engineering* (pp. 299-310). Pocatello, ID: Idaho State University.

Werle, J., and Luke, B. (2007). Engineering with heavily cemented soils in Las Vegas, Nevada. In A. J. Puppala, N. Hudyma, and W.J. Likos (eds.), *Problematic Soils and Rocks and In Situ Characterization. Geotechnical Special Publication 162* [CD-ROM]. Reston, VA: American Society of Civil Engineers.

Wyman, R., Karakouzian, M., Bax-Valentine, V., Slemmons, D. B., Peterson, L., and Palmer, S. (1993). Geology of Las Vegas, Nevada United States of America. *Bulletin of the Association of Engineering Geologists, 30* (1), 33-78.

Wu, D., Huynh, M., Luke, B., and Calderón, C. (2003).Streamlining the inversion of seismic surface wave datasets. In S. Elfass, G. Norris, and R. Watters (eds.), *Proceedings, the 38th Annual Symposium on Engineering Geology and Geotechnical Engineering* (pp. 311-318). Pocatello, ID: Idaho State University.

CHAPTER 3

THREE-DIMENSIONAL SHALLOW SHEAR-WAVE VELOCITY MODEL FOR LAS VEGAS VALLEY

Abstract: A three-dimensional (3-D) shear wave velocity (VS) model was developed for the heterogeneous shallow sediments (to nearly 400 m) of the Las Vegas Valley (LVV), Nevada. The model was based on more than 200 VS profiles and 1400 geologic well logs. Five sediment units including a cemented unit were defined from geologic log descriptions. A characteristic VS profile for four of the units was obtained by correlating between closely spaced pairs of VS and sediment data; a constant VS was assigned to the cemented unit. VS profiles were then assigned to each well location based on type of sediment according to the representative profiles. This assigned-velocity dataset was merged with measured VS profile data so that the measured data are honored in the model. The combined dataset results in a model with better resolution than a model developed using either of the two datasets independently. The software EarthVision was used to perform the 3-D interpolation of VS across the Valley. The model demonstrates the strong lateral variability of VS in the LVV. It also fits known patterns of sediment deposits: velocity in the central part of the Valley, where clay is the predominant sediment, is lower than velocity to the west and on the margins of the Valley, where gravel is predominant. The model may be used to predict Valley-wide earthquake ground-shaking patterns

This manuscript was written for possible submission to the Environmental and Engineering Geoscience Journal. Co-authors will be Barbara Luke, Wanda Taylor, and Jeff Wagoner. Student contribution: Ms. Murvosh is the first author for the manuscript.

She developed the procedures to determine the correlation distance and, with assistance, to perform the sediment-velocity correlations. She established the velocity cutoff values and performed the sediment-velocity correlations. She developed the equation to quantify the deviation of the characteristic profile and performed the statistical analysis to quantify the fit of the characteristic profiles to the data. She wrote the document and addressed all editorial comments from the co-authors.

3.1. Introduction

The Las Vegas Valley (LVV) urban area, which is in Clark County, Nevada, has a population estimated at 1.9 million and an average daily visitor population of roughly 250 thousand (Clark County, 2009). The LVV's population and geologic setting warrant studies in earthquake hazard and related risks. Price et al. (2009) performed loss estimate modeling for earthquakes that could occur in the LVV using a model developed by the Federal Emergency Management Agency. They found that a magnitude 6 earthquake occurring on the east side of the Valley could cause nearly 300 fatalities and over $7 billion in building-related economic loss. For the Las Vegas Valley fault system (LVVFS), which consists of normal faults located in the more populated central portion of the Valley, maximum earthquake magnitude estimates range from 6.3 to 6.9 (dePolo and Taylor, 2008). Earthquake events that threaten the Valley are not limited to faults located in the Valley. Su et al. (1998) found that a magnitude 7.4 event on the Death Valley Fault system, located 150 km west of LVV, is capable of inducing accelerations that could exceed 0.2 g at sediment sites in the Valley. These known hazards, the heterogeneity of Valley sediments, and the population of the Valley are reasons that

seismic hazard mapping is needed for the Valley. Development of a shear-wave velocity model is a necessary step in map development.

As part of an interdisciplinary effort to investigate earthquake hazards and related risks to human safety and structures in southern Nevada, a three-dimensional (3-D) model of shear-wave velocity (VS) was developed for the LVV. The model is intended for use in studying earthquake site response in the Valley and developing earthquake hazard maps. It was generated by correlating a relatively sparse dataset of VS profiles to a larger dataset of sediment lithology. Model development began in 2004. Model evolution has been documented by Luke et al. (2006), Luke et al. (2008), and Luke et al. (2009).

This paper describes the process used to build the model, which includes compiling VS data and lithologic well logs, determining appropriate correlation distances between pairs of VS profiles and well logs, correlating VS to sediment lithology, constructing the model, and verifying it. Images from the 3-D VS model are presented along with VS profiles queried from the model.

3.2. LVV basin geometry and shallow sediments

Situated on an alluvium-filled basin in the Basin and Range geomorphic province, the LVV is roughly 30 km across from east to west and 50 km from north to south and is surrounded by mountain ranges (Figure 3.1). The Sheep and Las Vegas ranges are located to the north; Frenchman and Sunrise mountains are located to the east; the River Mountains and the McCullough Range are located to the south; and the Spring Mountains are located to the west. Wyman et al. (1993) describe the tectonic movement that formed

the mountain ranges and basin as well as the volcanism and plutonic emplacement during the Miocene and the different periods of alluvial fan deposition. Basin geometry and alluvium, with emphasis on the shallow sediments for which VS data are needed to perform seismic site response analyses, from Wyman et al. (1993) and others (as noted) are summarized here.

A geophysical study by Langenheim et al. (2001) modeled the LVV's Paleozoic bedrock surface. The authors found a complex bedrock surface including three sub-basins, the deepest of which parallels the mapped scarps of the Frenchman Mountain fault system. Here, approximately 5 km west of Frenchman Mountain in the northeast quadrant of the basin, the depth to Paleozoic bedrock approaches its maximum of nearly 5 km (Langenheim et al., 2001). Subsequent to the study by Langenheim et al. (2001), Tkalčić et al. (2008) used data acquired from a broadband seismic array to investigate the structure of the basin. The authors' findings suggest that the location of the eastern wall of the deepest part of the basin is 2 km west of the location shown in the bedrock surface model by Langenheim et al. (2001). According to dePolo and Taylor (2008), the interaction of a right-lateral, strike-slip fault known as the Las Vegas Valley Shear Zone (LVVSZ), and the Frenchman Mountain fault created the deep sub-basin that contains the oldest material. Then, in the late Cenozoic, the LVVFS shifted the depocenter from near Frenchman Mountain towards the center of the Valley (dePolo and Taylor, 2008). The shift is significant because it indicates that the deeper parts of the Quaternary-aged sediments are located beneath a more densely populated area than previously thought.

The upper portion of the basin fill, to depths of about 1 km, consists of Quaternary and Pliocene sediments (referred to here as the Quaternary basin), while the lower portion

consists of Miocene and Oligocene material (Taylor et al., 2008). These lower sedimentary and volcanic units correlate to the Muddy Creek and Horse Springs formations, both of which contain gypsum beds (Wyman et al., 1993). Units equivalent to the Red Sandstone are also included in the lower basin fill. The Horse Springs Formation includes limestone and other sedimentary rocks, and, having accumulated during the time of active volcanism, some basalt flows and tuff beds (Wyman et al., 1993). The Quaternary basin sediments also include cemented materials, some of which, because of their high stiffness, would be classified as rock for engineering purposes.

The Valley is northwest-trending, generally subparallel to the LVVSZ (Figure 3.1; Wyman et al., 1993). It is underlain by coalescing alluvial fans. The Spring Mountains are the major source of the alluvial deposits. These deposits become increasingly finer from west to east, with increasing distance from the source and with decreasing elevation. A small coalesced alluvial fan, sourced from the Frenchman and Sunrise mountains, is located east of the lowest elevations in the Valley. Another small alluvial fan, the Pittman Fan, is located at the southeast end of the Valley and is sourced from the River Mountains and the McCullough Range, and small fans in the north are sourced from the Sheep and Las Vegas ranges (Plume, 1989). Plume (1989) describes the different host rocks of each of the alluvial fans.

Taylor et al. (2008) compiled an extensive database of the shallow basin lithology from over 1400 well logs (primarily from Nevada Division of Water Resources archives), geophysical measurements, and data from air photos, maps and the field. Well locations are shown in Figure 3.2a. Eight of the wells were greater than 1 km deep with an average depth of 2.7 km. The rest of the wells ranged in depth from 12 to 1,000 m with an

average depth of 171 m. Taylor et al. (2008) used the database to develop a 3-D geometric model of the Quaternary basin sediment-type distribution and structure (referred to here as 3-D sediment-lithology model) using the software package EarthVision, developed by Dynamic Graphics, Inc. for 3-D model building. To facilitate interpolation of the data by the program, the authors compiled well log descriptions into nine sediment-lithology units: gravel, sand, clay, gypsum, mixed, limestone, volcanic, cemented, and bedrock. A logged layer was assigned a unit based on its predominant sediment. The designation "Mixed" was assigned where no sediment was predominant. From their 3-D sediment-lithology model, Taylor et al. (2008) verified that clay deposits dominate in the deeper, central and south parts of the Quaternary basin, coarse- and mixed-grain size deposits dominate in the shallower, western, part of the basin, and coarse- and fine-grained deposits interfinger at their interfaces.

Cemented soils and medium-dense to dense sands and gravels occur in alluvial fans surrounding the Valley (Wyman et al., 1993). The most extremely cemented deposits are known locally as caliche and most probably formed as soil or ground water carbonate deposits. Werle and Luke (2007) summarized the geologic processes that occur in the LVV that result in caliche. Thicknesses of caliche lenses can range from a few centimeters to 2 to 3 m (Wyman et al., 1993), and lateral variability is high (Taylor et al., 2008). For example, Stone and Luke (2001) observed a change in thickness of approximately 3 m over a distance of less than 35 m. Caliche deposits are typically located in the western and central portions of the Valley (Wyman et al., 1993), but also occur in areas where clay deposits are predominant (Taylor et al., 2008). Taylor et al. (2008) included caliche in their 3-D sediment-lithology model (the Cemented unit) where

it was logged individually (in contrast to a logged interval description such as "gravel with caliche"). With strength and stiffness as high as concrete, a fully formed caliche deposit can be a desired bearing stratum for structural foundations or a hindrance to excavation (Werle and Luke, 2007). Caliche has a high VS: Stone and Luke (2001) reported laboratory values of 2350 m/s; Werle and Luke (2007) reported measured field values from 1000 to 1500 m/s; and Tecle et al. (2003) measured field values as high as 2000 m/s. Caliche adds significantly to the variability of the mechanical stiffness of Valley sediments and, thus, to the complexity of developing the 3-D VS model.

3.3. VS data compilation

Key to model development is adequate VS data. The acquisition, interpretation and compilation of seventy-seven of the pre-existing profiles used in this study were previously described in detail (Liu et al., 2005; Liu, 2006; Scott et al., 2006). The efforts made to acquire new measurements and to amass publicly available VS data into a VS database are described in this section. In all, 212 surveys were compiled (Figure 3.1) and are the basis for the 3-D VS model for the LVV. These include profiles developed from both body-wave and surface-wave (including active- and passive-source surveys) measurements. The velocity of the model halfspace was included as a layer in developing the 3-D VS model and in performing VS-sediment correlations. In general, the thickness of this layer was set to one-third of the model depth to halfspace. For this paper, the bottom depth of this "layer" is considered the bottom, or total depth, of the profile.

The 3-D VS model described in this paper was developed to provide detail of the shallow layers as well as information to depths of 370 m. Separate from and coincident

with the research described in this paper are two data acquisition projects for the LVV, each being performed by a different agency. The first is a project by the Clark County Building Department to acquire VS data in the unincorporated parts of the LVV over an area of approximately 1300 km^2 (Louie, 2008). This project consists of acquisition and processing of Rayleigh-type seismic surface wave data using the passive-source surface-based Refraction Microtremor method (ReMi; Louie, 2001). The data are being considered for development of a depth-averaged shear-wave velocity map for the upper 30 m (VS(30)) and other average VS maps (Nevada Earthquake Safety Council, 2009). The second project is being performed by the Nevada Seismological Laboratory, which began work in 2008 to develop a Western Basin and Range Community Velocity model (Louie et al., 2009). In combination, the three research projects will benefit the people of the LVV by providing the VS models needed to understand earthquake risk in the Valley. Coincidentally, overlapping datasets from the three projects provide opportunities to test the accuracy of the various models.

3.3.1. VS profiles from body-wave and active-source surface-wave measurements

Twenty-eight of the seismic surveys that preceded this research were acquired using either body-wave measurements, specifically downhole and crosshole seismic methods, or the active-source spectral analysis of surface waves method (SASW; Stokoe, 1994) (Liu, 2006). At 12 of these sites, Liu et al. (2005) combined active-source SASW measurements with passive-source ReMi measurements.

Downhole and crosshole seismic methods are intrusive methods that require drilling to produce VS profiles. In contrast, SASW and ReMi are methods whereby Rayleigh-wave phase velocities are acquired non-intrusively to develop a one-dimensional VS

profile through inversion. Due to their dispersive nature, Rayleigh waves of different lengths (or frequencies) excite the earth's materials to different depths, allowing different depths of a soil column to be sampled in a single spectral measurement. Both the SASW and ReMi methods employ a linear array.

Profiles developed using active-source surface wave methods typically have better resolution of shallow layers than profiles developed using passive-source methods. An active source can be used to generate the high frequency seismic waves that are needed to sample the shallow layers in relatively close proximity to the receivers. In contrast, seismic waves from ambient vibrations tend to originate far from the receiver array and, thus, the high frequency waves attenuate before reaching the receivers. In the LVV, detail of the shallow layers is desirable for characterizing the heterogeneity of LVV sediments, especially to characterize the effects of lenses of cemented material including soil carbonates (a.k.a caliche).

A disadvantage of active-source survey methods is that they require a heavy source to generate low frequency vibrations necessary to characterize deeper sediments, which may not always be practical. Ambient vibrations, however, tend to include these low frequencies.

One disadvantage of a linear array for a passive-source survey is that when a predominant signal approaches the array at an oblique angle, phase velocity estimates would be erroneously high. In contrast, active-source methods, such as SASW, by definition have a known, off-end source location so the testing is not subject to this error.

Data from active- and passive-source surveys can be combined to take advantage of the strengths of both survey types. For example, the profiles developed by Liu et al. (2005) were nearly 400 m deep and maintained detail at shallow depths.

To increase the number of VS profiles deeper than 50 m that also have shallow resolution in the LVV, 12 seismic surveys were performed during the Summer and Fall of 2007 (Murvosh et al., 2008). The surveys were performed using the SASW method and conformed to the general procedures for the method (Stokoe, 1994). These procedures typically involve placing two receivers and a source in a linear array at the ground surface such that the distance from the source to first receiver is equal to the distance separating the receivers. Vertical ground motions produced by a source applied vertically at the surface are recorded at the receivers. Receiver spacings double with each successive measurement, allowing measurements over an increasing range of wavelengths. A frequency-domain analysis of the phase differences of the ground motion between the two receivers is used to develop a dispersion curve (plot of velocity as a function of frequency or wavelength) for the site. The VS profile is developed through inversion of the dispersion data.

Because different sources produce different energy content, a variety of sources may be used. For this study, two sources were used: a "minivib" trailer-mounted Vibroseis source, designed and built by Industrial Vehicles International, and an instrumented sledge hammer. The minivib source has a maximum hold-down weight of approximately 29 kN and a maximum force output of nearly 27 kN (6,000 lbf) (Industrial Vehicles International, 2006). It was used for receiver spacings from 16 to 128 m. The sledge hammer was used for receiver spacings less than 16 m. Field data acquisition was

described in detail by Murvosh et al. (2008). Data acquired with the hammer and minivib were combined to develop the dispersion curves.

The dispersion curves were used to develop VS profiles through an optimization process that incorporates the global search method of simulated annealing followed by linearized inversion (Calderón-Macías and Luke, 2007). The new profiles were approximately 100 m in depth and were separated into 10 to 12 layers. The thinnest layers were 0.5 to 1 m thick.

3.3.2. VS profiles from passive-source surveys

Driven by building codes, geotechnical investigations performed in the Valley often include VS measurements to determine VS(30) from which seismic site classification is assigned (Table 3.1) and upon which design is based. Because of the large amount of new construction performed in LVV since the adoption of this code in 2002, a large number of surveys has been performed by private consulting firms and filed with local government agencies as part of a site's geotechnical report. While active-source measurements might be preferred for their shallow detail and potentially higher accuracy, the ReMi method is more frequently used by private firms performing site investigations because it is cost effective.

One hundred forty-five measurements, all of which were performed using the ReMi method, were compiled from geotechnical reports submitted to the building departments of unincorporated Clark County and the City of Henderson (Murvosh et al., 2006). Each of these measurements was examined to determine suitability for the VS database. Ideally, the examination would incorporate the picks made on the slowness-versus-frequency plots (p-f plots; Louie, 2001) to obtain an experimental dispersion curve.

However, in most instances, the p-f plot was either not available or its scanned black-and-white image (all that was made available in the public record) was of too poor a quality to examine the picks. Lacking this information, we established, with assistance from the developer of the ReMi method (Louie, personal communication, 2007), a process to determine from the available data in the filed reports whether or not a survey was performed in a manner consistent with standard ReMi data acquisition and analysis techniques (Louie, 2001). This consistency check was based on the following: profile depth, dispersion curves, and profile stability. Each is discussed below. Measurements deemed inconsistent were assumed unrepeatable and were not included in the VS database.

Profile depth

Considering the relationships between frequency, wavelength, velocity, and depth of resolution for surface waves propagating in a halfspace (e.g., Gazetas, 1992), the depth to halfspace of a ReMi survey is not expected to exceed its array length. Possible exceptions are locations with thick, continuous high-velocity materials, within which surface waves are likely to attenuate more gradually than in softer sediments. Because the target depth of these surveys was 30 m, most of the arrays were 100 m long. While most of the VS profiles were more than 30 m deep, only two sites had profiles with depths greater than their array lengths. One was located near a rock outcrop. The second profile was 111 m deep and located near a well log that reported cemented gravel, considered by the authors to be a high-velocity material, below 60 m. Except for the shallowest layers, both profiles consist of high, greater than 1,000 m/s, VS layers. Therefore, none of the profiles obtained from the public record were disqualified based on depth.

For eleven sites, only VS(30) was provided; no layered profile was included in the reports for these sites. With no way to perform a consistency check for depth and with no layered profile to include, we disqualified these measurements.

Dispersion curves

The experimental dispersion curves were usually included in the reports. We examined the fit of the theoretical dispersion curve corresponding to the reported VS profile to the experimental dispersion curve. Nine profiles were removed from the database due to what we judged to be a poor fit. The theoretical dispersion curves for these profiles only vaguely fit the corresponding experimental curves. Twenty-six profiles for which the dispersion curve plots were not provided were used in the model. All met the depth and stability criteria; eleven of these had at least one additional ReMi measurement taken at the same site.

We also checked the minimum frequency of each experimental dispersion curve. Based on frequency ranges published by Louie (2001) for a sensor's accuracy below its resonant frequency and for survey measurements performed using 8 Hz and lower geophones, dispersion curve picks below 2 Hz were not considered consistent with standard practices. The experimental dispersion curve for one of the profiles did not meet this criterion, having a minimum frequency pick of 1.7 Hz. We compared this profile to a second ReMi measurement taken at the same site (within 150 m) that passed the consistency test. The depths to layer boundaries for the two profiles were within 20 percent of one another; the VS of the layers themselves were also within 20 percent. The VS of the halfspaces are within 30 percent. Given that the reported accuracy of ReMi to determine VS(30) is within 20 percent (Louie, 2001), the profile was kept in the database.

Profile stability

In an otherwise homogeneous medium, VS will increase with depth due to effects of confining pressure (Kramer, 1996). At sites with caliche or other high-velocity inclusions, however, VS profiles with large fluctuations in velocity, approaching 1000 m/s, might be expected. Profiles at five sites exhibited either large velocity fluctuations between layers or consisted of a single layer for which nearby geologic information was either not available or did not substantiate the VS profile. These five sites were removed. Two of these sites were also disqualified from the database due to poor dispersion curve fits.

Final profiles used in model

Of the 145 public-record VS profiles considered 123 measurements satisfied the consistency criteria and were used for model development. An additional 49 VS profiles that were developed using ReMi measurements were also used. These measurements were performed along a 13-km transect running roughly northeast to southwest across a central part of the Valley by Louie and colleagues (Scott et al., 2006).

3.4. Establishing VS mapping approach

The approach used to develop the 3-D VS model took into consideration the specific geologic conditions of the LVV and methods previously used by others to develop VS models in the Valley and in other urban areas. This section presents the background and reasons for developing a 3-D VS model for the Valley as well as the selection of the model depth. The background for the VS-sediment correlation procedure, including brief discussion of statistical methods, is also presented.

3.4.1. Basis for depth and type of model

VS models and maps have been developed for many urban areas as part of a process to generate earthquake hazard maps (e.g. Frankel and Stephenson, 2000; Wills et al. 2000; Wong et al., 2002; Cramer et al, 2004; Frankel et al., 2007). VS data and maps are also used for seismic site classification needed for code-based design of structures. For example, both the International Building Code (IBC; International Code Council, 2009) and National Earthquake Hazards Reduction Program (NEHRP; Building Seismic Safety Council, 2009) provide recommendations for engineers to consider VS(30) for the seismic design of structures. For this reason, an increasing number of VS(30) maps and site classification maps based on VS(30), including projects previously described as being performed in the LVV, are being generated for urban areas throughout the United States (e.g. Wills et al., 2000; Louie et al., 2008).

Utility of a 3-D VS model beyond that of depth-averaged VS maps includes accurately modeling the variable depth to important stratigraphic boundaries of a complex area such as the LVV basin. A 3-D VS model of the LVV can capture the heterogeneity of the sediments and, therefore, may be used to perform the analyses necessary to predict ground motion in the LVV during an earthquake. It can be used to help explain more complex site-response phenomena observed in the LVV, such as basin amplification and near-fault effects. Of course, maps of VS averaged over any depth of interest may be developed from a 3-D model.

Recent research suggests that in deep, sedimentary basins, such as the LVV, VS profiles to depths greater than 30 m are required to accurately predict site response during an earthquake. Abrahamson and Silva (2008) classified sites using both VS(30) and the

depth to “engineering bedrock”, which they defined as the depth where VS equals 1000 m/s. By using this engineering bedrock parameter, they were able to distinguish between “shallow soil sites” (depth to engineering bedrock less than 200 m) and “deep soil sites” (depth to engineering bedrock greater than 200 m). As part of a study to investigate the influence of shallow sediments on earthquake ground motion, Luke and Liu (2007) established a preferred depth to model halfspace in the LVV. To establish this depth they modeled the one-dimensional response of two sites: a 1-km deep sediment column in the LVV and a reference site with shallow bedrock situated at the foot of Frenchman Mountain. For both sites, they used weak-input ground motions to project surface response for columns with varying depths to model half space. The projections were compared to ground motions measured at the two sites during nuclear test events and during a magnitude 5.5 earthquake. The authors reported that the best matches of modeled ground motion to recorded ground motion occurred for a model halfspace depth of 375 m. Based on this research, 400 m is the target depth for the LVV 3D VS model.

3.4.2. VS-sediment correlation procedure: background

Because vast amounts of geologic data may be available for a developed area, whereas the number of VS datasets is typically limited, VS model development regularly includes correlation of VS to local geology (e.g. Wills et al., 2000; Wong et al., 2002; Gomberg et al., 2003). Once the correlation is performed, the larger dataset including VS based upon sediment-type is used for interpolation of velocity to obtain a continuous model of VS. Different correlation methods, including those previously applied to LVV basin-fill sediments, are summarized here.

In the development of earthquake-scenario and probabilistic ground-shaking maps for Salt Lake City, Utah, Wong et al. (2002) correlated a sparse VS dataset to a larger dataset of surficial geologic units. They defined five distinct site-response units on the basis of predominant grain size. For each of the units where VS data were available, they then developed a characteristic VS profile by averaging profiles resolved at multiple locations in each unit. For one of the units, a smoothed average was used. The smoothed profile was preferred over the arithmetic mean by the authors because the mean profile exhibited local velocity reversals rather than having velocity strictly increasing with depth.

Romero and Rix (2001) used a similar method to develop characteristic VS profiles for the Mississippi embayment. They broadly defined regions based on age and type of geologic deposit. The characteristic profile for each region was based upon a subjective analysis of the profiles resolved within each area rather than the arithmetic mean of the profiles. In this manner the authors could edit features, such as local velocity reversals, that have physical significance at a specific measurement site, but were not considered representative of the overall area. As part of this research, Romero and Rix (2001) also performed site specific analyses at two sites in the greater Memphis area to assess uncertainty and randomness in VS profiles due to test-related factors and local variability of soil properties. To quantify their observations, they computed a mean VS profile for each site and its standard deviation and coefficient of variation. Both sites had seven VS profiles with depths of 20 m or deeper and with a maximum distance between any two measurement locations of 325 m. For the two sites, the authors found that standard deviation increased with depth. They noted this result was expected because, while local variations in soil properties will decrease with depth (e.g. lateral variation of VS will

decrease with increasing confining pressure), the uncertainty in measuring VS generally increases with depth. They also reported a general increase in the coefficient of variation with depth and reported ranges from a minimum around 4 percent to a maximum of 34 percent.

Wills et al. (2000) employed surficial geology to develop a seismic site-classification map for California. In contrast to Wong et al. (2002) and Romero and Rix (2001), who created characteristic profiles, Wills et al. used over 550 VS(30) measurements to assign a site classification to surficial geologic units shown on 1:250,000 scale geologic maps. The site classifications (B, C, D and E; Table 3.1) were subdivided to develop intermediate categories (BC, CD, and DE), which were applied to the surficial units with VS(30) values that straddled the boundaries of the site classifications.

A similar approach was used by Scott et al. (2006) to develop a shallow VS model for the LVV. They correlated VS(30) to surficial units using the 49 VS measurements of the 13-km transect that was previously described. Then they assigned VS(30) throughout the Valley based on surficial units. To test the map, they compared the values assigned from the surficial units to the original values measured along the roadway and to values measured at eight additional test sites not located on the roadway. Predictably, the locations on the roadway had a good correlation to the measured data; however, only three of the eight off-roadway locations had measured VS(30) values within 20 percent of VS(30) assigned as a result of the correlation. The authors then developed a model by correlating velocity at 79 locations (the 30 body-wave and active-source surface-wave measurements compiled by Liu, 2006 plus the 49 measurements of the 13-km ReMi transect) to a 3-D stratigraphic model based on six summary units: Paleozoic bedrock,

Oligocene-Miocene deposits, carbonate, gravel, sand and clay. For all units except sand, where VS data were not available, the authors developed VS(30) histograms. Each stratigraphic unit was assigned a single VS(30) value from the mode of occurrence. Then a VS(30) model of the Valley was calculated from the VS values assigned to the stratigraphic model. For this VS(30) model, four of the assigned VS(30) values were still not with 20 percent of the measured values, but were closer than those values developed using surficial units. The authors, therefore, recommended geographic partitioning (i.e. dividing the Valley geographically into areas expected to have similar velocity values) to perform the VS-sediment correlations.

Geographic partitioning was used by Wills and Clahan (2006) to refine the seismic site-classification map for California developed by Wills et al. (2000) that was previously described. Wills and Clahan used topography to subdivide the boundaries of the original map geographically into areas that were anticipated to be more homogeneous in grain size and thickness (e.g. areas where alluvium was expected to be shallow, such as narrow valleys and small basins, were separated from areas where alluvium was expected to be deep, such as the centers of major basins). They then developed a mean VS value from profiles measured within each area. The authors concluded that partitioning based on surficial geology can be used to produce a regional map (such as the one they developed for California), but that detailed subsurface information was needed to produce detailed and accurate maps on a local scale.

For the LVV, Luke and Liu (2008) used geographic partitioning to divide the Valley into two sediment response units: 1) fine (predominantly clay) and 2) coarse (predominantly gravel). Rather than rely on surficial geologic units, they incorporated

subsurface information by defining the units according to the sediments that dominate in the upper 30 m. For each unit, they calculated a representative VS profile in a manner similar to the methods of Wong el al. (2002) and Romero and Rix (2001). The authors observed that VS values in the profile developed for the fine-sediment response unit were consistently lower than those of the coarse-sediment response unit.

One challenge for applying geographic partitioning in the LVV is the extent to which the high-velocity cemented deposits (caliche) can be accurately represented in the model. Boundaries separating areas that are predominantly caliche could potentially be used to develop depth-averaged maps; however, the variable depths and thickness of caliche lenses preclude using this boundary for development of 3-D Valley-wide models.

Gomberg et al. (2003) developed a 3-D VS model for the basin environment of Memphis, TN, from a sediment-lithology model without using geographic partitioning. First, they compiled a 3-D sediment-lithology model from a database of more than 1200 well and borehole logs. Then, they used the logs to identify the depths to the interfaces between the five uppermost, major-lithologic units. Using a dataset of 76 VS profiles, the authors produced velocity histograms for each unit and then assigned VS based on the unit's mean VS, which did not differ substantially from the median. Because the lithologic units of the Memphis model are fairly homogeneous laterally, depth inherently becomes a part of the correlation despite not being specifically addressed.

In contrast to the geologic model for Memphis, TN, the geologic models for the LVV shallow sediment types (and, therefore, velocities) can vary significantly over short distances both vertically and laterally (Taylor et al., 2008). According to Luke and Liu (2007), accurate representation of variability of dynamic material properties is required to

accurately model earthquake ground motion. Thus, the correlation method used in the LVV to build a VS model from sediment lithology should preserve the complex heterogeneity of the Valley sediments where possible.

3.4.3. Geostatistical model background

The previous section discussed some of the limitations of using geologic data to predict VS. To overcome these limitations, Thompson et al. (2007) proposed a geostatistical method to develop depth-averaged VS maps. Their method accounts for horizontal variability of VS without employing correlations of velocity to sediment-lithology. For a 140 km^2 area of the San Francisco Bay, California, they developed a continuous map of VS averaged over the upper 10 m (VS(10)) from 189 sites characterized by seismic cone penetration tests (SCPT). The VS(10) estimates were made using geostatistical methods, specifically ordinary kriging and a model semivariogram determined from the measured VS(10) values. A similar method has been used to map liquefaction hazard (e.g. Baise et al., 2006) and has been shown to be useful to model other soil properties (e.g. soil moisture, Western and Blöschl, 1999; agricultural soil properties, Kravchenko, 2003).

A model seimvariogram is a function that may be used to interpolate between two data points (Henley, 1981). It is developed from the empirical semivariogram, $\gamma(h)$, defined for VS measurements in Equation 3.1, which describes the spatial structure of a dataset, specifically VS(10) in the study by Thompson et al. (2007).

$$\text{Equation 3.1} \qquad \gamma(h) = \frac{1}{2N}\sum_{i=1}^{N} [VS(s_{i+h}) - VS(s_i)]^2,$$

where h is the separation distance between the measurements,

N is the number of sample pairs, in this case VS measurements, separated by distance h, and VS(s) is the velocity at location s.

For datasets regularly distributed in space, where each sample pair is separated by a distance that is a multiple of h, $\gamma(h)$, $\gamma(2h)$, $\gamma(3h)$, etc. are calculated. Then, the successive γ values are plotted versus separation distance to obtain an experimental semivariogram, which is illustrated in Figure 3.3. For datasets that are not regularly spaced, a range of distance values may be considered together. For example, Thompson et al. (2007) used 400 m distance bins for the SCPT data.

Model semivariograms are the functions for the curves that are fit to experimental semivariograms. Henley (1981) summarizes several common semivariogram models and many geostatistical texts provide more information on the subject. One common model is the exponential model (Figure 3.3). For this model, γ increases with separation distance until a maximum γ value is reached. The separation distance where the curve flattens out is referred to as the range, and the value of γ at this distance is referred to as the sill. Beyond this point, γ is no longer a function of separation distance. The point where this theoretical curve intersects the ordinate is referred to as the nugget. For VS data, this value will ideally be zero because measurements taken at the same location should be identical.

The VS(10) data of the Thompson et al. (2007) study were fit using an exponential model. Then the authors used the model semivariogram and kriging to interpolate between the measured points and produce a continuous VS(10) map.

For the same area, Thompson et al. (2007) also attempted to develop a VS(30) map from 48 sites where SASW data were acquired. These sites were not as closely spaced as

the sites where SCPT data were acquired, nor were they as spatially extensive, being generally located in two areas. The authors noted that because geostatistics improve spatial prediction only where the data being interpolated have a spatial structure, the spacing of the VS data used for interpolation needed to be dense enough to establish that the closely spaced samples were more similar than those spaced farther apart. For the SASW measurements, Thompson et al. (2007) concluded that the dataset was too sparse to determine an appropriate semivariogram model for the interpolation.

Compared to the 48 SASW measurements in a 140 km^2 area used by Thompson et al., (2007), the ratio of the number of VS measurements in the LVV (212 profiles in 1600 km^2) is small. If LVV VS profiles were evenly spaced, only one profile would be located in every 7 km^2. While this density might be adequate, the measurement locations occur in clusters, leaving areas of the LVV without adequate coverage (Figure 3.2). The sparseness of the dataset increases with depth because, while nearly all of the VS profiles of the LVV dataset extend to 30 m depth, only 46 profiles extend to 200 m depth and only 20 extend to 300 m depth. Additionally, most of the deep profiles are located along the 13-km transect. Such clustering of data limits the applicability of geostatistical methods to interpolate velocity across the LVV. An additional limitation of using the method proposed by Thompson et al. (2007) is that it does not produce a 3-D model. We note, however, that Dawson and Baise (2005) adapted the 2-D semivariogram approach to develop a 3-D semivariogram, which they used to model volume of liquefiable soil.

In contrast to the velocity dataset, if the wells used to develop the shallow-sediment model for the LVV were evenly spaced, there would be approximately one well per every square kilometer. Despite being a denser dataset and covering a much broader area of the

Valley than the VS locations, there are still areas in the Valley with little or no sediment-lithology data (Figure 3.2). Due to the availability of a relatively rich sediment-lithology dataset and the relatively sparse number of profiles, especially with depth, and uneven distribution of the LVV VS dataset, we correlated VS to sediment lithology to develop the LVV 3-D VS model rather than applying geostatistical methods to the velocity data alone. A similar method to the one employed by Dawson and Baise (2005) may be viable in the LVV once more VS data, especially below 100 m, is available.

3.5. VS-sediment correlation procedure

Considering the advantages and disadvantages of the modeling methods previously described, we opted to correlate velocity to the 3-D sediment-lithology model developed by Taylor et al. (2008) in order to interpolate VS across the Valley. The VS measurements were directly included in the dataset. By using both measured VS and VS correlations to sediment type for map creation, we expect that velocity will be more accurately interpolated than using either of the two datasets independently.

We developed a VS-sediment correlation method similar to that used by Gomberg et al. (2003) rather than use surficial units or geographic partitioning. Correlations were performed for four of the five sediment units in the 3-D sediment-lithology model: Clay, Sand, Gravel and Mixed. Velocity histograms were created for each of these sediment units and used to assign a velocity value that is representative of each unit over an established depth range. The individual assignments culminated in depth-dependent correlations of VS to sediment unit. A constant VS was assigned to the fifth sediment unit, the Cemented unit.

Ideally, the histograms would be created using only those VS profiles that are located at sites with well logs. Because most of the well and VS data were not acquired specifically for the purpose of this research, these datasets were not co-located. Thus, we used semivariograms to study the spatial structure of VS in the Valley and determine appropriate correlation distances between VS and well locations.

The VS-sediment correlation process is described in this section. The assignment of VS to the Cemented unit (caliche), deep sediments, and bedrock is also described. The process preserves the location and depth of high VS zones, thereby capturing some of the heterogeneity of the LVV sediments.

3.5.1. Determining correlation distances

Sediment deposits tend to have a spatial structure; thus we expect that the VS of these sediments will also have a spatial structure. In the LVV, the spatial structure of the sediments is evident in the 3-D sediment-lithology model (Taylor et al., 2008), while the spatial structure of VS was demonstrated by the VS profiles developed by Luke and Liu (2008) for the two sediment response units. Based on these previous findings, we assume that VS of the LVV sediments has a spatial structure. If true, a maximum distance exists within which a VS profile can be located from a well and still be used to develop the VS-sediment correlation. This distance is referred to here as the correlation distance. Furthermore, we can use geostatistics, specifically empirical semivariograms (γ, Equation 3.1), to quantify how VS of the Valley sediments changes with distance and define the correlation distance.

Semivariogram development

We used ArcMap (Geostatistical Analyst Toolbox; version 9.3.1) to calculate γ for all possible combinations of pairs of the VS datapoints and plotted the results. The plot is known as a semivariogram cloud (Figure 3.4). For this study, semivariogram clouds were developed from depth-averaged VS for the depth intervals listed in Table 3.2. These intervals correspond to the seven layer boundaries used for the characteristic profiles; selection of the layer geometry is described later in this paper. The depth-averaged VS for these intervals are referred to as layer averages. In addition to the layer average velocities, we also calculated the depth-average VS from the ground surface to the bottom of each layer boundary, referred to as overall averages, and VS(30). For the shallowest layers, where all 212 VS measurements were used, γ was calculated for 22366 site pairs. The semivariogram clouds for the site pairs separated by less than 15 km are shown in Figure 3.4. Depth-averaged velocity values for any depth interval (avgVS) are calculated by summing the time for a wave to travel through each layer of the depth interval, then dividing the thickness of the depth interval by the sum of the travel times (Equation 3.2).

$$\text{Equation 3.2} \quad \text{avgVS} = \frac{T}{\sum_{i=1}^{N} \frac{t_i}{VS_i}},$$

where N is the number of layers in the depth interval, t_i and VS_i are, respectively, the thickness and velocity of layer i in the depth interval, and T is the thickness of the depth interval (note T is equal to the sum of all the individual layers, t, in the depth interval). To discern local trends from the overwhelming amount of data plotted in the semivariogram clouds and because the data were not regularly spaced, we grouped the semivariogram

cloud data by separation distance between velocity pairs in increments of 100 m. The results from this grouping is a mean γ value for site pairs located between 0 and 100 m, for those located between 100 and 200 m, etc., plotted in Figure 3.5. As previously discussed, distance bins were also used by Thompson et al. (2007) for their analysis of SCPT data.

Selection of correlation distance

The semivariogram clouds for both the overall average and layer average data show a broad range of γ at any distance (Figure 3.4). However, a general trend for close site pairs to have a smaller difference in VS compared to site pairs that are farther apart is apparent for the upper bounds of γ. This trend is easily observed in the semivariogram clouds for the overall averages, but is not as apparent in the semivariogram clouds of the layer averages.

Trends in VS are more apparent in the plots of the binned data (Figure 3.5). In these plots, mean γ increases with separation distance to approximately 20 km. This clear trend for the binned data indicates that once an adequate number of VS measurements is obtained, a semivariogram model could be fit to the data, and kriging could be used reliably to develop a 3-D VS model for the LVV. Beyond 20 km, scatter in the values for γ increases dramatically. Decreases in mean γ values observed for separation distances of more than 20 km appear to be a function of fewer datapoints being available for comparison and are not an indication of spatial structure.

For both the semivariogram clouds and the binned semivariograms, γ for the layer average tends to be greater than that of the overall average. The higher γ value for the

layer average is expected because VS is averaged over a smaller depth interval, which does not provide as much opportunity for high or low velocity values to average out.

The binned γ for site pairs separated by distances to 1.5 km are plotted in Figure 3.6 with error bars representing the standard deviation. Referring to this plot, for the first few hundred meters of separation distance, both mean γ and standard deviation generally (but not uniformly) increase with increasing separation distance. Compared to the rest of the data, a sharp increase in the mean γ for site pairs located 300 to 400 m apart was observed in most of the overall- and layer-average data. For the overall averages (top row of Figure 3.6), the mean and standard deviation generally decrease as the depth to the bottom of the interval increases, which, as previously mentioned, is expected because the high and low velocity values average out. For the layer averages (bottom row of Figure 3.6), the opposite is observed (γ and standard deviation increase as depth to bottom increases). This increase in γ with depth may be due in part to fewer data pairs at the deeper depths. For the layer-average data, the increase in the standard deviation with depth is consistent with findings reported by Romero and Rix (2001).

Based on our observations of the semivariograms and on data availability, we chose 300 m for the correlation distance. Sixty-four VS profiles are located within 300 m of at least one well location. For the Mixed unit, the correlation distance was increased to 500 m to provide sufficient data for correlation. This distance increased the numbers of profiles used in the correlation for that unit from 20 to 32. The locations of these profiles are shown in Figure 3.2. The number of wells within the correlation distance of each profile is also shown in Figure 3.2. A summary of the number of profiles having 1, 2, 3, or more wells within the correlation distance is in Table 3.3.

The correlation distances do not account for discrepancies between the depths of the VS profiles and the wells. Thus, eleven of the VS profiles are deeper than the deepest logged well within the correlation distance. The shallowest of these VS profiles, about 130 m, is only 14 m deeper than the nearest well. Because the profile extends into the 100-m thick, 100- to 200-m layer of the characteristic profiles, use of the bottom 14 m of the profile in the VS-sediment correlations was judged reasonable. For the ten remaining profiles, the distance to the nearest well of equal or greater depth increases with depth; however, the homogeneity of VS is expected to increase with depth due to confining pressure. Therefore, the need for a well to be located within the correlation distance is less important for these deeper measurements. Of the remaining profiles, seven have profile depths ranging from 175 to 300 m and have at least two wells that are deeper than the profile within 2 km. The other three profiles are nearly 400 m deep and have two to three deeper wells within 3 km.

3.5.2. Characteristic VS profile development

An 8-layer characteristic profile was developed for four of the sediment units (Clay, Sand, Gravel, and Mixed) in the 3-D sediment-lithology model. The profiles were developed from scatter plots of depth versus velocity and from velocity histograms. The process is described in this section and was also presented by Luke et al. (2010). This section also presents the mean, standard deviation, and coefficient of variation of VS for each sediment unit. The deviation of the characteristic profile from the measured VS data is also quantified.

Scatter plot generation and data filtering

The VS profiles were discretized for use in EarthVision. The discretization process assigned VS values at regular, fixed depth intervals, such that only one VS value was associated with any depth: VS was assigned to every 1-m depth increment in the upper 65 m, and, because layer thickness increases with depth, every 3-m depth increment below 65 m. To honor the degree of detail in the original profile, additional layer boundaries were inserted to preserve layers less than 1 m thick and to preserve the depth to the bottom of each layer. The top of each successive layer was assigned a depth 0.01 m below the bottom of its overlying layer; this increment preserves the depth of each layer boundary and is less than the precision of the measurements used to develop the profiles.

The 3-D sediment-lithology model was queried to assign a unique sediment unit at each discrete depth point of the 76 VS profiles used for the correlations. The result was a dataset pairing velocity and sediment unit with depth. This dataset was sorted by sediment unit and a scatter plot was created for each unit (Figure 3.7).

VS in the scatter plots increases with increasing depth, which, as previously noted, is expected. Ideally, this depth-dependent relationship would allow a velocity versus depth gradient (e.g. Ni et al., 1998) to be developed, which would be the characteristic profile. However, for the LVV, the scatter plots also show that even within the established correlation distance, the range of VS values for a particular sediment type at a particular depth can be more than 1000 m/s.

Anomalously high velocities are attributed to cementation and to shallow bedrock and were excluded from the correlations. As previously discussed, highly-carbonate cemented sediments may occur at any location in the Valley (i.e. in any sediment unit). Shallow

bedrock occurs at sites near the Valley margins. Because VS profiles are derived from surface wave techniques, they represent characteristics of broad volumes of earth beneath the measurement array. As profile depth increases, the volume represented by the profile also increases. Thus, deeper VS measurements in sediments on the Valley edges can be influenced by sloping bedrock in the vicinity. In contrast, a nearby well log describes only sediments. Thus, a high velocity layer of a profile located at a shallow bedrock site can be assigned to a sediment unit that is based on the nearby log, but that does not accurately describe the volume of sediment and rock measured by the surface-wave survey (Luke et al., 2010).

Cutoff velocities for the Clay, Sand and Gravel units were set based on velocity ranges observed in the scatter plots and our previous experience in the LVV. The assumptions were checked against published values of wave velocities according to sediment type and depth. For these units, all VS greater than 1300 m/s and VS greater than 1000 m/s occurring shallower than 50 m were not used for the correlation (Figure 3.7).

The Mixed unit was assigned where none of the other three sediments predominate in the well log. While this unit can include some cemented materials (Taylor et al., 2008), a thick, heavily cemented unit would be assigned to the Cemented unit. Because the Mixed unit includes materials that have higher VS than clay, sand and gravel, this unit has a potential for higher representative VS values. Therefore, we slightly modified the cutoff velocities. For this case, VS greater than 1300 m/s and VS greater than 1000 m/s occurring shallower than 5 m were excluded from the correlation (Figure 3.7).

Because the Gravel unit has the highest-measured VS, the cutoffs affected far more data in this unit than any other. These high values are expected because the Gravel unit tends to be located in the areas of the LVV with the most caliche and on the Valley margins closest to bedrock (Wyman et al., 1993).

Defining layer geometry

The layer geometry (number of layers, layer thicknesses, and depth to halfspace) for the characteristic profiles was established empirically from observation of the scatter plots and from experience. The geometry established is identical for each of the predominant sediment units. The three uppermost layers are 5 m thick. Luke et al. (2009) discussed that the geophone spacing used for the ReMi surveys compiled from the public record search (typically 7.5 m) and the maximum frequencies obtained by these surveys (roughly 50 Hz) should be adequate to resolve an average velocity for the upper 5 m of the profile. Below 15 m, layers increase in thickness with increasing depth. The depth to the halfspace is 200 m.

VS assignments from histograms and profile statistics

For each characteristic-profile layer, a representative VS was assigned manually from velocity histograms. The histograms were created for each layer of each sediment unit using the software MATLAB, by MathWorks; a normal distribution was also calculated (Figure 3.8). Velocities above the cutoffs were not plotted on the histograms or included in the calculation of the normal distribution curves. For the Mixed unit, the 5 to 10 and 10 to 15 m layer intervals were combined into a single layer because of the similarity of VS values for these layers and because of the limited number of profiles available for the correlation of these layers (as few as 5).

In general, VS assignments were made from the following: the peak of the normal distribution curve, the mode, or the median velocity for the depth interval. Additionally, VS was required to increase with increasing depth. Judgment played a considerable role in the selection process. The selected values are shown by the arrows on Figure 3.8 and listed in Table 3.4. The characteristic profile of each sediment unit is superimposed on its respective scatter plot to verify reasonable fit to the data. (Figure 3.7).

The mean VS (μ), standard deviation (σ), and coefficient of variation (COV) were calculated for each layer of the characteristic profiles for each sediment unit. Similar values for each 1-m interval of the discretized dataset (μ_{1m}, σ_{1m}, and COV_{1m}) were also calculated. These values along with the number of points in the dataset are plotted for each sediment unit in Figures 3.9 through 3.12. Although several profiles were used to set the VS value for each layer of each characteristic profile, there are 1-m interval depths for which only a single profile provides information for the sediment unit. At these depths, the single datapoint is, by definition, equal to μ_{1m}, and σ_{1m} is, therefore, equal to zero. The number of instances that these "zero" values occur increases with increasing depth, further illustrating how the data density decreases with depth (Figures 3.9 through 3.12). The mode of each layer of the velocity histograms (referred to as layer mode) is also shown.

Because the characteristic profiles were not developed strictly from the mean VS of the measured profiles, we performed an additional calculation to quantify the deviation of the characteristic profile from the dataset. This deviation was determined by substituting the VS value of each layer of each characteristic profile for the mean VS in the equation for standard deviation, Equation 3.3.

Equation 3.3 $$\sigma_{cp} = \sqrt{\frac{1}{N}\sum_{i=1}^{N}(x_i - CP)^2}$$

Where σ_{cp} is the deviation of the dataset from the characteristic profile,

N is number of data points in the sediment unit for the characteristic profile layer (e.g. the number of datapoints in the Clay unit from 0 to 5 m, from 5 to 10 m, etc.),

CP is the VS value of the layer in the characteristic profile, and

$x_1, x_2, \ldots x_N$ are the VS data for the layer (shown in the scatter plots).

We also calculated a "coefficient of variation from the characteristic profile", COV_{cp}, which is defined as the ratio of σ_{cp} to the VS of the corresponding layer of the characteristic profile. Both σ_{cp} and COV_{cp} are plotted on Figures 3.9 through 3.12. A comparison of σ and σ_{cp} is provided in Table 3.5.

Discussion of variability and trends

Referring to Figures 3.9 to 3.11, μ of the Clay, Sand and Gravel units generally tracks μ_{1m} to a depth of roughly 50 m. For the Mixed unit (Figure 3.12), μ has a poor fit to μ_{1m} in the shallow layers, due to the wide range of values of μ_{1m}, but a better fit from 15 to 50 m deep. Below 50 m, the range of values for μ_{1m} increases. This increase is expected because of the decreasing number of profiles below 50 m depth. The characteristic profile for the Clay unit has a good fit with the μ value for the unit. Thus, σ and σ_{cp} for the Clay unit are also similar, as are COV and COV_{cp}. This pattern is also true for the Sand and Mixed units. For the Gravel unit, the characteristic profile has a good fit with the mode to 15 m; below this depth, the profile has a good fit with μ. Thus, σ and σ_{cp} for the Gravel unit are similar below 15 m, as are COV and COV_{cp}. The fits of the characteristic profiles to the mean and mode values highlight the manner in which the representative VS for each layer was assigned: the shallow layers of the Gravel unit fit the mode because the

representative VS values for these layers were assigned at the mode (Figure 3.8), and the deeper layers fit the mean because they were assigned at the peak of the normal distribution.

As expected, for layers where VS for the characteristic profile was assigned from the mode, the difference between σ and σ_{cp} increases as the difference between the mode and μ increases (Table 3.5). The variability of the Valley sediments is evident by the σ and σ_{cp} values, which range from 64 to 263 m/s (Table 3.5). These values are substantially higher than those reported by Romero and Rix (2001); the authors noted a maximum σ of 102 m/s in their study performed for the Greater Memphis area. The relatively high σ and σ_{cp} values of the Valley sediments provide some measure of the uncertainty associated with assigning VS to sediment units in the LVV.

For the Clay unit, σ and σ_{1m} generally increase with depth to 50 m, while COV and COV_{1m} are generally constant (Figure 3.9). The values of σ and σ_{cp} are typically lower for the Clay unit than the other sediment units from 0 to 50 m (Table 3.5). From 50 to 200 m depth, the range of values for σ_{1m} and COV_{1m} increases as the number of datapoints in the Clay unit correlation dataset decreases. Below 200 m, the smaller range of σ_{1m} and COV_{1m} values is due to the decrease in the range of VS values in the correlation dataset (Figures 3.7 and 3.8). The layer COVs range from 20 to 34 percent. This range is consistent with the upper bound reported by Romero and Rix (2001).

For the Gravel unit, σ and σ_{1m} generally decrease with depth to 50 m along with COV and COV_{1m} (Figure 3.11). The high σ of the shallow layers of this unit demonstrates the heterogeneity of LVV sediments in locations that are predominantly gravel. The range of values for σ_{1m} for this unit increases with depth to 200 m. This increase corresponds to a

decrease in the number of profiles used for the correlation. As with the Clay unit, the smaller range of σ_{1m} values below 200 m for the Gravel unit is due to the decrease in the range of VS values in the correlation datasets (Figures 3.7 and 3.8). Values for layer COV range from 15 to 33 percent.

For the Sand and Mixed units, σ and COV generally decrease with depth to 25 m (Figures 3.10 and 3.12). In contrast, σ_{1m} and COV_{1m} do not have a consistent pattern over this depth interval, and their range of values is consistently broad between the depths of 0 and 100 m. As previously noted, the smaller range of σ_{1m} and COV_{1m} values below 100 m is due to the decrease in the range of the VS values in the correlation datasets (Figures 3.7 and 3.8). Values for COV of the Sand unit range from 13 to 44 percent; values for layer COV of the Mixed unit ranges from 12 to 46 percent. The high layer COV values for the Sand and Mixed units compared to the Clay and Gravel units are expected because the Sand and Gravel units have significantly fewer datapoints in the correlation dataset (Figure 3.13).

The characteristic profiles are shown together in Figure 3.13. For all four profiles, velocity increases with depth, which is expected given that the VS data also increases with depth and because of the manner in which VS was assigned to the sediment units. The number of profiles used for each correlation is also shown in Figure 3.13 and generally decreases with depth. Above 200 m, the numbers of profiles used to develop the characteristic profiles for the Clay and Gravel units are 1.5 to 2 times greater than the numbers used for the Sand and Mixed units. From 0 to 50 m, σ_{1m} of the Clay and Gravel units have narrower ranges than σ_{1m} of the Sand and Mixed units (Figures 3.9 through 3.12). The Clay and Gravel units also have substantially more datapoints in the

correlation dataset than the Sand and Gravel units (Figure 3.7). Therefore, the Clay and Gravel characteristic profiles are more accurate than the other two profiles, especially above 50 m, and the Clay unit, which has lower σ and σ_{cp} than the Gravel unit above 25 m, is the most accurate of the profiles.

As previously discussed, the range of σ_{1m} increases with depth (to 200 m) for all four units, which implies that variability of VS of all four sediment units increases with depth. However, the increase is in part due to a decrease in the density of the correlation data with depth (Figure 3.13) and may also be due to the selection process of VS profiles for the correlation. Recall that the basis for inclusion of a VS profile does not take depth into account and that eleven of the velocity profiles are deeper than any well log within the correlation distance. Although the distances from these profiles to the nearest deeper wells (less than 3 km) were judged acceptable because of expectations for increasing homogeneity of VS of sediments with depth, the uncertainty of the sediment-unit assignment at depth for these site pairs remains higher than that for profiles having deeper wells within the correlation distance.

The VS of the characteristic profile layers for the Clay unit are less than their corresponding layers in the characteristic profile for the Gravel unit, which was expected. The difference in VS decreases with depth, possibly due to the influence of confining pressure. The characteristic profile for clay has a large increase in velocity, about 200 m/s, at 50 m depth. A corresponding (although slightly more gradual) increase in μ_{1m} (from 50 to 65 m deep; Figure 3.9) indicates the increase may be an actual shift in the velocity of the sediments rather than an artifact due to the selection of the profile geometry. Luke et al. (2010) estimated that alluvium at 50 m was deposited about 25,000

years ago during the early stages of the last glaciation of the region (the early part of Tioga time during the Wisconsin glacial episode). The authors proposed that the increased velocities of the clays below 50 m might be related to changes in moisture, and thus, depositional environment resulting from climate change.

The characteristic profiles for the Sand and the Mixed units have a more regular increase in velocity with depth. Below 50 m, the characteristic velocities for these sediment types are lower than those for the Clay and Gravel units, by approximately 200 m/s. As previously discussed, the characteristic profiles for these units are more uncertain than for the Clay and Gravel units because of lower data density.

Overall, the variability in the data and the characteristic profiles demonstrates the degree of complexity of the Las Vegas basin sediments.

Comparison to previous profiles

The characteristic profiles described here differ from earlier versions developed for this research project and published by Luke et al. (2009) using the same VS dataset. Notably, the VS of shallowest layers are as much as 125 m/s (45 percent) higher than the previously published values and those of the deepest layers are as much as 175 m/s (25 percent) higher. Differences result from adjustments to the velocity cutoff ranges and an increase in the number of layers in the characteristic profiles from six to eight. The revised characteristic profiles have a good fit with the mean/mode profiles calculated for each sediment unit.

Seismic site classification of the characteristic profiles

VS(30), which is used to assign seismic site classifications, was calculated for each characteristic profile (Table 3.3) and was compared to the VS(30) ranges of soil

classification published in the IBC (Table 3.1). VS(30) for all four units is in the range for seismic site classification "C". These resulting classifications for the characteristic profiles are similar to findings of the study presented by Louie(2008). The author reported a prevalence of alphabetically lower (stiffer) than expected seismic site classifications in the LVV, "C" rather than "D".

Taken individually, VS(30) for the Clay, Sand and Gravel units have distinctly different values. The value for the Clay unit is at the lowest quarter of the range for seismic site classification "C". The value for the Sand unit is higher than the clay unit, but is still within the lower half of the range. In contrast, the value for the Gravel unit is nearly in the highest quarter of the range. The VS(30) for the Mixed unit (477 m/s) is essentially the same as that calculated for sand (473 m/s). This value falls between the clay and gravel values, where a mixed material without caliche would be expected. However, because the amounts of gravel and caliche included in the Mixed unit would be higher than those included in the predominantly clay or sand units, we expected the characteristic profile for the Mixed unit to have higher VS values (approximately midway between the values for Sand and Gravel).

Although the characteristic profiles all have seismic site classification of "C", VS(30) calculations of individual measurements result in some "D" and "B" as well as "C" classifications. This difference illustrates one of the limitations of a regional model based solely on VS assigned to sediment type. By including depth-dependent VS measurements in the regional model, locations with site classifications other than "C" will be more accurately represented in the model and in depth-averaged VS maps created from the model.

3.5.3. VS assignments for caliche, deep sediments, and bedrock

This section describes the selection of the VS values for the 3-D model to represent sediments and lithology that were not specifically tested as part of this study (e.g. bedrock and sediments below ~400 m).

Cemented sediments (caliche)

As previously discussed, several studies performed in the LVV have measured the VS of caliche. Caliche behaves like hard rock in that VS would not be expected to be affected significantly by confining pressure in the upper few hundred meters. We considered 1000 m/s to be a lower bound VS for caliche, because lower values more likely represented fractured rather than intact caliche. As previously mentioned, caliche is included in the 3-D sediment-lithology model only where it was logged individually (Taylor et al., 2008); therefore, we assigned caliche a VS of 1500 m/s independent of depth. This value is the midpoint of our lower bound (1000 m/s) and the highest field measurement (mentioned previously, 2000 m/s).

Deep sediments and bedrock

In order to model the entire basin, constant VS values were assigned to sediments below 370 m and to bedrock. The assignments were based on research by others and are described here. For the purposes of our model, the LVV basin Quaternary-aged deposits (Taylor et al., 2008) are subdivided into a shallow basin and an intermediate basin, while the Oligocene-Miocene-aged sediments are referred to as the deep basin.

In the model, the shallow basin is considered to be the upper portion of the basin fill. Because VS data were available for all the sediment units to roughly 370 m, this depth was set as the bottom of the shallow basin Thus, this basin extends from the surface to

370 m or to the top of Miocene (30 m to 1 km; Taylor et al., 2008), whichever is shallower. The top-of-Miocene boundary for the model was developed by Taylor et al. (2008) and does not extend Valley-wide. In places where bedrock is shallower than 370 m, therefore, the shallow basin extends to the top of bedrock. Where the bedrock is shallow, it is possible that bedrock was exposed during the Miocene and covered with sediment later than that time. The VS of the shallow basin is what was modeled using the sediment-unit and caliche correlations previously described in this paper. The 370 m maximum depth of the shallow basin is within 1 percent of the 375 m depth to halfspace that Luke and Liu (2007) recommended be used for site response analyses in the LVV.

The intermediate basin of the model represents sediments from 370 m to the top of Miocene. The deep basin represents the sediments from the top of Miocene to Paleozoic bedrock (as deep as 5 km). VS for the sediments of the intermediate and deep basins and for bedrock have been addressed in several studies (McEwan, 2005; Snelson et al., 2005; Scott et al., 2006).

McEwan (2005) developed VS profiles to depths of 1 km and deeper from earthquake data recorded in the LVV by a broadband array for five locations in the LVV. All the stations of the array were located in the deepest part of the basin, roughly, the northeast portion of the Valley. The profiles were developed through inversion of fundamental mode Rayleigh wave group velocities generated from regional earthquakes. From the five profiles, we calculated an average profile, and then determined the depth averaged VS from 370 m to 1 km. This depth-averaged value, 1,100 m/sec, was assigned to the intermediate basin.

For the deep basin, we assigned a VS value of 1,500 m/sec, which correlates well with VS values developed by others over these depths: (1) the depth-averaged VS from 1 km to 4 km calculated from the average of the five profiles developed by McEwan (2005) is 1,600 m/sec; (2) the range in VS over these depths from seismic refraction experiments performed by Snelson et al. (2005) to image the geometry of the basin is 1,400 to 2,600 m/s (considering compression-wave velocity values in the referenced study and assuming Poisson's ratio of 0.25, which is a generally accepted conversion value for these "consolidated" sediments; Snelson, personal communication, 2010); and (3) from surface-based measurements, Scott et al. (2006) used histograms of velocity to assign a constant VS value of 1,500 m/s to the Oligocene-Miocene material. The measurements by Stott et al. (2006) were previously discussed.

The VS value assigned to bedrock, 2.6 km/sec, is taken from Snelson et al. (2005), again converting the reported compression velocity from the refraction study to VS using a Poisson's ratio of 0.25. The histogram of VS developed by Scott et al. (2006) for Paleozoic bedrock shows peak velocity ranges between 2.0 and 2.7 km/s.

3.6. Model development: data interpolation

For 3-D VS model development, interpolation of the VS data was performed using EarthVision. The software's 3-D minimum tension gridding algorithm calculates a smooth surface that closely fits the input data values (Dynamic Graphics, 2009). This software and gridding method have been used by others to develop 3-D models of geologic data (e.g. Jachens et al., 2001). For the LVV 3-D VS model, east-west grid spacing is 195 m, north-south is 180 m, and depth is 1.8 m. The location and orientation

of faults in the Valley were incorporated into the model. Interpolation of VS did not extend across the faults.

Ultimately, three 3-D models were developed (Figure 3.14):

1. VS-measured, which was created solely from the database of measured VS profiles.
2. VS assigned from lithology (referred to as VS-assigned), which was created from the database where VS values from the characteristic profiles were assigned to each log in the geologic database based on the sediment type described and depth of occurrence. Assignments were made to over 1400 well logs, to create the VS-assigned dataset.
3. Final model, which was created by combining the VS-measured and VS-assigned datasets.

Combining the datasets for the final model assures a more detailed and more accurate model than one created using only the VS-measured or VS-assigned datasets. This additional detail is considered more important to accurately model the heterogeneous nature of LVV sediments. The model can be applied to develop Valley-wide predictions of earthquake ground-shaking patterns needed for earthquake hazard map development. Given the uneven and in some areas sparse distribution of VS measurements across the Valley and the uncertainty associated with the characteristic profiles, site-specific predictions would still require site-specific measurements.

A primarily top-view of each of the three models is shown in Figure 3.14. A cutaway showing the north half of the final model, including the location and orientation of several faults, is shown in Figure 3.15.

Several VS-measurement locations were queried to verify that the final model honors the measured data. Figure 3.16 shows velocity profiles for two of these locations (Figure 3.1). The plots show the discretized data of the measured profile, the profile queried from the model created from the VS-assigned dataset, and the profile queried from the final model created from the combined datasets. Logs from nearby wells are also shown on the figure, and characteristic profiles for the sediments shown in the logs are plotted with the queried profiles. The shallowest depths of the queried profiles are below 0 m depths, which is a function of the models' resolution. The gradual transitions between layers, as opposed to a step-wise looking transition, are also a function of model resolution. These plots are discussed in the next section.

3.7. Results, discussion and future work

The differences between the three 3-D VS models and the increased detail provided by the final model are apparent in Figure 3.14. All of the models indicate higher VS in the west end of the Valley compared to the east, which reflects the general locations of the higher-velocity coarse-sediment response unit and the lower velocity fine-sediment response unit (Luke and Liu, 2008). Edge effects of the model are apparent in the varying colors (red, purple and green) of the mountain ranges.

The VS-measured model has large areas with high velocities, most notably the 1,800 m/s area (yellow) in the west side of the basin, which indicates a large, contiguous area of a high-velocity material. From the 3-D sediment-lithology model (Taylor et al., 2008), which shows the heterogeneity of the Valley's sediments, we know that high-VS sediments are localized. Thus, the high-VS areas shown in this model are probably due to

a small number of VS measurements being interpolated across a large area and not a large volume of high velocity material. An exception is the high VS area (1400 m/s, green) at the southwest end of the Valley. This area is represented by several VS measurements (Figure 3.2) and is known to have caliche and cemented gravel and sands.

Because of the relatively large number of wells compared to the number of VS measurements, the VS-assigned model better represents the heterogeneous nature of the sediments compared to the VS-measured model (Figure 3.14). In the VS-assigned model, areas with high VS tend to be localized rather then spread over broad areas, a pattern that is consistent with the discontinuous nature of the sediments. From the VS-assigned model, we note the faults tend to be located along areas with high VS. Compared to the VS-measured model, the VS values in the southwest end of the Valley do not indicate high VS material. As previously discussed, the Gravel unit potentially includes greater incidences of stiff material that was either not logged, or was included in the unit because the amount of material was judged to be small. For these cases, the VS-assigned value would be lower than the actual VS of the sediment.

The final model created from the combined dataset is more similar to the VS-assigned model than the VS-measured model (Figure 3.14), which is expected given the large number of wells, 1400, compared to the number of VS measurements, 212. The influence of the measured data is prominent at the southwest end of the Valley, which has higher VS values compared to the VS-assigned model. The high VS observed at the west end of the Valley in the VS-measured model is not prominent in the final model, which is also expected because the thickness and presence of cemented sediments can vary

substantially over short distances. The final model also has more detail than the VS-assigned model along the east side of the Valley.

Referring to Figure 3.15, the magnitude of the difference in sediment volume between the Quaternary basin (primarily purple and blue), to 1 km, and the lower Oligocene-Miocene deposits (green), to 5 km, is illustrated in the figure. The intermediate basin is evident at roughly the 669000 m easting (1100 m/s; thin, blue section above the Oligocene-Miocene deposits and east of a fault located toward the center of the Valley). VS generally increases with depth. An inversion of VS values is observed above the Oligocene-Miocene boundary; this is especially notable between the 670000 and the 675000 m eastings. This inversion is unexpected and remains to be investigated further.

The two sites used to verify that the VS-measured data are being honored in the final model were selected for study based on their proximity to nearby wells and the complexity of their profiles. The LES site is relatively close to a well, within 325 m, and its VS profile generally increases with depth (Figure 3.16). In contrast, the MNL site is relatively far from its closest well, 1.3 km, and has a shallow velocity inversion at 10 m depth (Figure 3.16).

The first site, LES, is in the fine sediment response unit (Luke and Liu, 2008), and its nearby log indicates predominantly clay material to 15 m depth and a mixture of clay, sand and silt material (designated as “Mixed” in the geologic database used for the correlations) to 100 m depth (Figure 3.16a). For this site, the shallowest velocities of the profile from the VS-assigned dataset are roughly twice those of the measured profile, but from 5 to 12 m depth are consistent with characteristic profiles for the Clay unit profile. This consistency is expected because of the clay sediments described in the log and

because clay is the predominant sediment in the fine sediment response unit. From 50 m depth to the bottom of the well log, the VS-assigned dataset tracks the Mixed unit profile. Again, this consistency is expected due to the sediments described in the well log. Below 10 m depth, the measured VS profile and the profile queried from the VS-assigned model differ, but not substantially, to 50 m depth. In contrast, the VS profile queried from the final model tracks the measured data over the entire profile.

The second site, MNL, is located in the northwest end of the Valley (Figure 3.1). From 0 to 25 m depth, VS queried from the VS-assigned model is more than twice that from the VS-measured profile (Figure 3.16b). The nearest well log indicates "mixed" material (Figure 3.16); however a well located 2 km northwest of the site indicates a nearly 9-m thick lens of caliche at the surface. Taken together, the information from the two logs explains the high-VS values at shallow depth of the VS-assigned model. The difference between profiles of the VS-measured and the VS-assigned models decreases below 25 m, but is still more than the difference observed in the plots for the site in the fine sediment response unit (Figure 3.16a). As with the site in the fine sediment response unit, the profile from the final tracks the measured data to a depth of 210 m, the top of the Oligocene-Miocene boundary. Below this boundary, a constant velocity of 1500 m/s is assigned, which is represented in the profiles from the VS-assigned and final models. At the MNL site, the top of the Oligocene-Miocene boundary, 210 m deep, occurs at a depth above the top of the defined middle basin, 370 m; thus, the profiles have no constant VS assignment for the middle basin.

The profiles presented for the LES and MNL sites show that model accuracy depends upon data density. Model users should, therefore, compare the location of data queried

from the model to locations of VS measurements and wells (Figure 3.1) to assess the precision of the data queried. For example, the roughly 5-km wide band of low VS values (~300 m/s, purple; Figure 3.15) from the north to northeast along the northern mountain ranges has neither VS nor lithology data (Figure 3.1). Profiles queried within this area will, therefore, not be as reliable as profiles queried from locations near sites with measured VS profiles or well logs.

Further, independent model verification, such as verification by leave-one-out cross validation method (e.g. Thompson et al., 2010) is yet to be performed.

3.8. Conclusions

A three-dimensional (3-D), shear-wave velocity (VS) model was developed for the Las Vegas Valley (LVV) using a combination of limited VS measurements and a richer database of sediment type that is correlated to VS. Incorporating both datasets into the model provides better resolution than a model developed using either of the two datasets independently.

The assignments of VS to sediment type were based on four characteristic profiles developed by correlating velocity to four sediment-lithology units defined for the LVV. The characteristic profiles generally fit the mean VS values calculated for each sediment unit. They also fit expected patterns for VS of the sediment types, with the Clay and Sand units having lower VS than the Gravel unit. For all sediment units, accuracy of the characteristic profiles, and therefore, the accuracy of the 3-D VS models, decreases with increasing depth because the number of VS profiles available for correlation decreases. Because of the amount of data available, the correlations for the Clay and Gravel units

are considered more accurate than those for Sand and Mixed. The correlation for the Clay unit is considered more accurate than Gravel because of the greater potential for cemented material to be present in the Gravel unit.

The model is valuable for predicting Valley-wide earthquake ground-shaking patterns; however, site-specific predictions require site-specific measurements. As expected, the 3-D VS model for the LVV demonstrates strong vertical and lateral variability, the latter being related to depositional environment, secondary cementation, and faulting. It also fits known patterns of sediment deposits in that VS is lower in the central part of the Valley, where clay sediments predominate, than on the edges where gravel is predominant. Accuracy of the model is expected to be greatest at those locations with greatest data density.

3.9. Tables and Figures

Table 3.1 Seismic Site Classification definitions with respect to VS(30) (International Code Council, 2009).

Seismic Site Classification	Description	VS(30), m/s
A	Hard rock	1500 < VS(30)
B	Rock	760 < VS(30) ≤ 1500
C	Very dense soil and soft rock	360 < VS(30) ≤ 760
D	Stiff soil	180 < VS(30) ≤ 360
E	Soil profile or any profile with more than 3 m of soft clay defined as soil with plasticity index (PI) > 20, water content < 40 percent, and undrained shear strength (s_u) < 25 kPa	VS(30) < 180
F	Soils requiring site-specific evaluations: 1) Soils vulnerable to potential failure or collapse under seismic loading such as liquefiable soils, quick and highly sensitive clays, collapsible weakly cemented soils; 2) Peat and/or highly organic clays with thicknesses (H) > 3 m; 3) Very high plasticity clays, thickness > 8 m, PI > 75; and 4) Very thick, soft/medium stiff clays, H > 36 m with s_u < 50 kPa	

Table 3.2 Layer geometry of the characteristic profiles, the intervals over which depth-average shear-wave velocity (VS) was calculated to create semivariogram clouds, and the number of VS profiles included in the semivariogram cloud calculation for each layer.

Layer geometry (depth interval) for layer-average calculation, m	Depth interval for overall-average calculation, m	Number profiles incl.	Depth of shallowest profile included / number profiles shallower than layer bottom, m
0-5	0-5	212	11 / 0
5-10	0-10	212	11 / 0
10-15	0-15	211	19 / 0
15-25	0-25	210	23 / 5
Not applicable	0-30	204	29 / 2
25-50	0-50	165	46 / 37
50-100	0-100	107	74 / 38
100-200	0-200	56	169 / 10

Table 3.3 Numbers of VS profiles having one or more wells within the correlation distance.

Number of wells within correlation distance	Number of profiles
1	44
2	20
3	9
4 or more	3
Total number profiles used in correlation = 76	

Table 3.4 Layer geometry and VS for the four characteristic profiles. VS averaged over the upper 30 m (VS(30)) of each profile also listed.

	VS, m/s			
Depth range, m	Clay	Sand	Gravel	Mixed
0-5	350	400	425	400
5-10	400	450	500	
10-15	425	450	550	450
15-25	475	500	700	525
25-50	550	575	725	550
50-100	750	600	775	625
100-200	900	775	950	775
200-370	950	900	1050	900
VS(30), m/s	437	473	577	477

Table 3.5 Standard deviation (σ) and deviation of characteristic profile (σ_{cp}) for each layer of the four characteristic profiles.

	Clay		Sand		Gravel		Mixed	
Depth range, m	σ, m/s	σ_{cp}, m/s	σ, m/s	σ_{cp}, m/s	σ, m/s	σ_{cp}, m/s	σ, m/s	σ_{cp}, m/s
0-5	120	120	170	168	195	263	216	226
5-10	94	94	137	137	207	248		
10-15	115	115	104	104	193	233	179	176
15-25	125	125	67	66	205	205	152	151
25-50	147	147	171	173	134	134	64	65
50-100	234	233	137	136	201	201	133	131
100-200	230	234	224	220	202	202	230	240
200-370	187	189	235	221	167	171	171	174

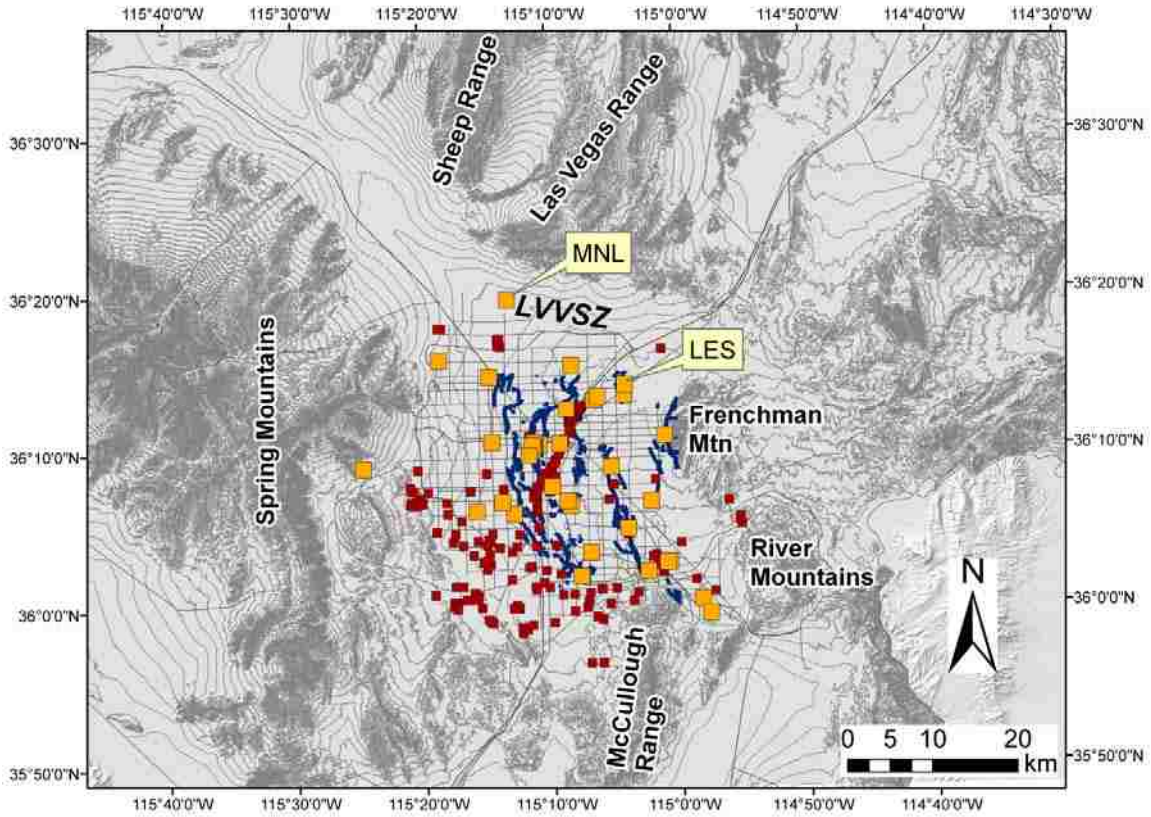

Figure 3.1 Map of Las Vegas Valley (LVV) with mountain ranges, faults (navy lines; Taylor et al., 2008), and shear-wave velocity (VS) measurement locations (body-wave and active-source surface-wave measurements as orange squares; passive-source surface-wave measurements as smaller, red squares). For the two sites labeled, measured VS profiles and profiles queried from the 3-D VS model are provided in Figure 3.16.

a) b)

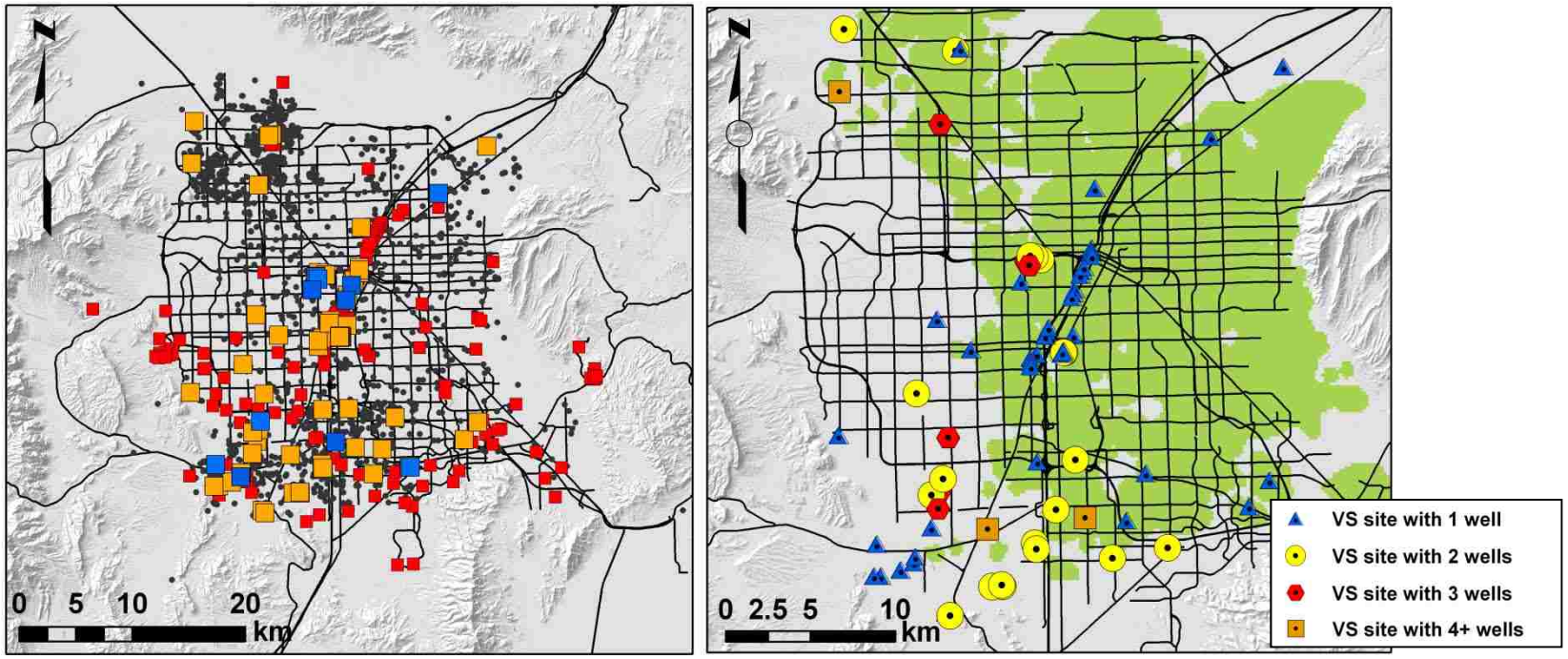

Figure 3.2 Data distribution overlying topographic map of the LVV; major streets shown in black: (a) orange squares indicate 64 VS measurements that were used to correlate velocity to sediment-lithology; blue squares indicate 12 additional velocity measurements that were used only for the mixed-sediment type correlations; red squares indicate velocity measurements that were not included in the correlations; and small dots (navy) indicate wells; (b) locations of measurement sites used for the correlations and the number of wells located within the correlation distance of each site; the fine-sediment response unit (Luke and Liu, 2008) is shown in green.

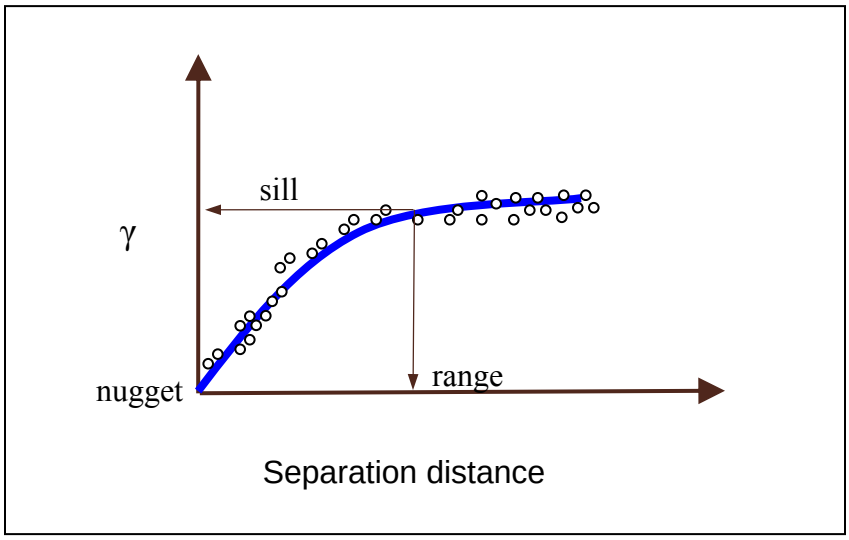

Figure 3.3 Example of an experimental semivariogram (open circles) fitted with an exponential semivariogram model (blue).

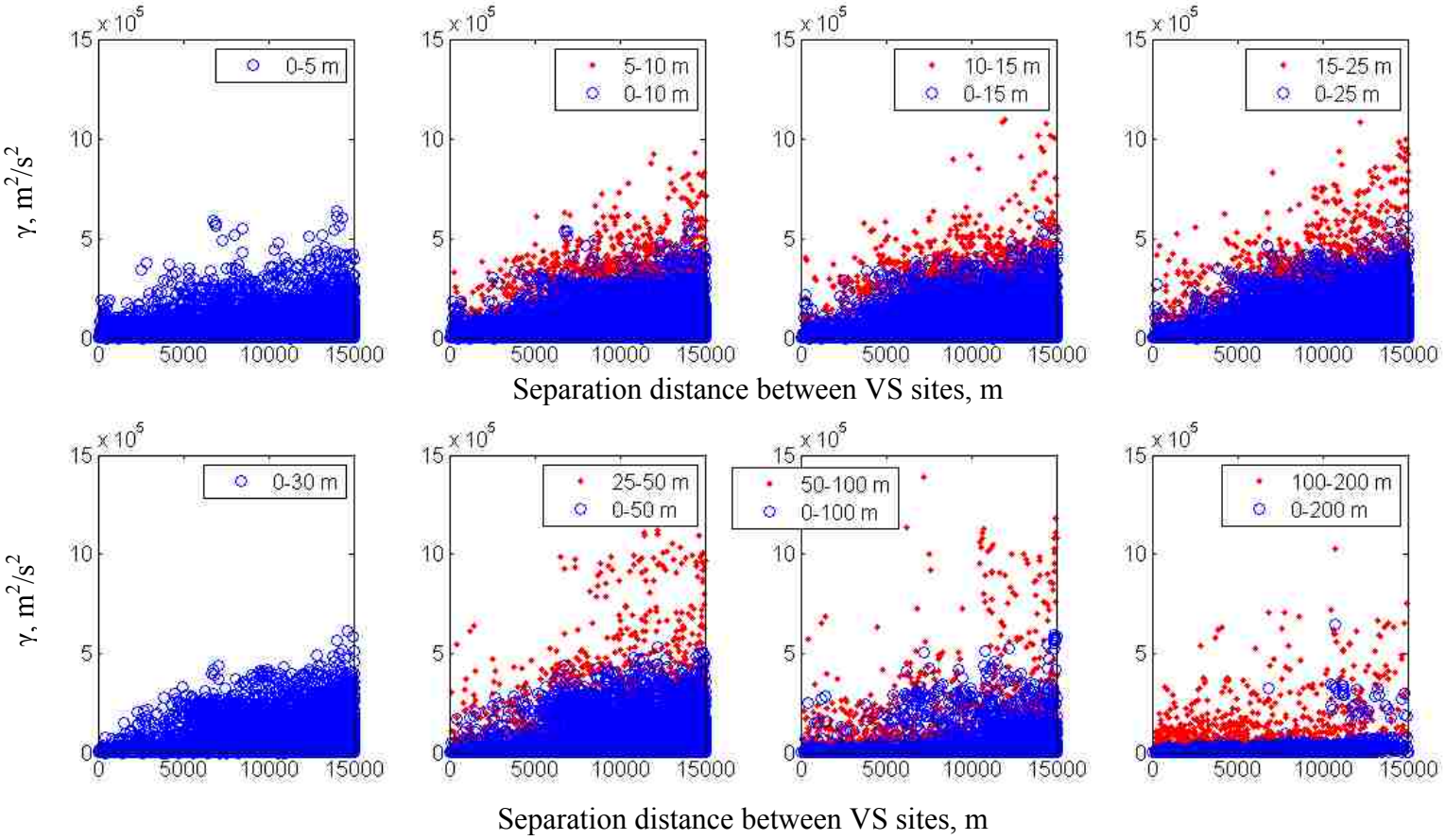

Figure 3.4 Semivariogram clouds for layers (identified by depth range). Blue circles represent the depth averaged VS from the surface to the layer bottom (overall averages); red dots represent the depth averaged VS over the layer (layer average).

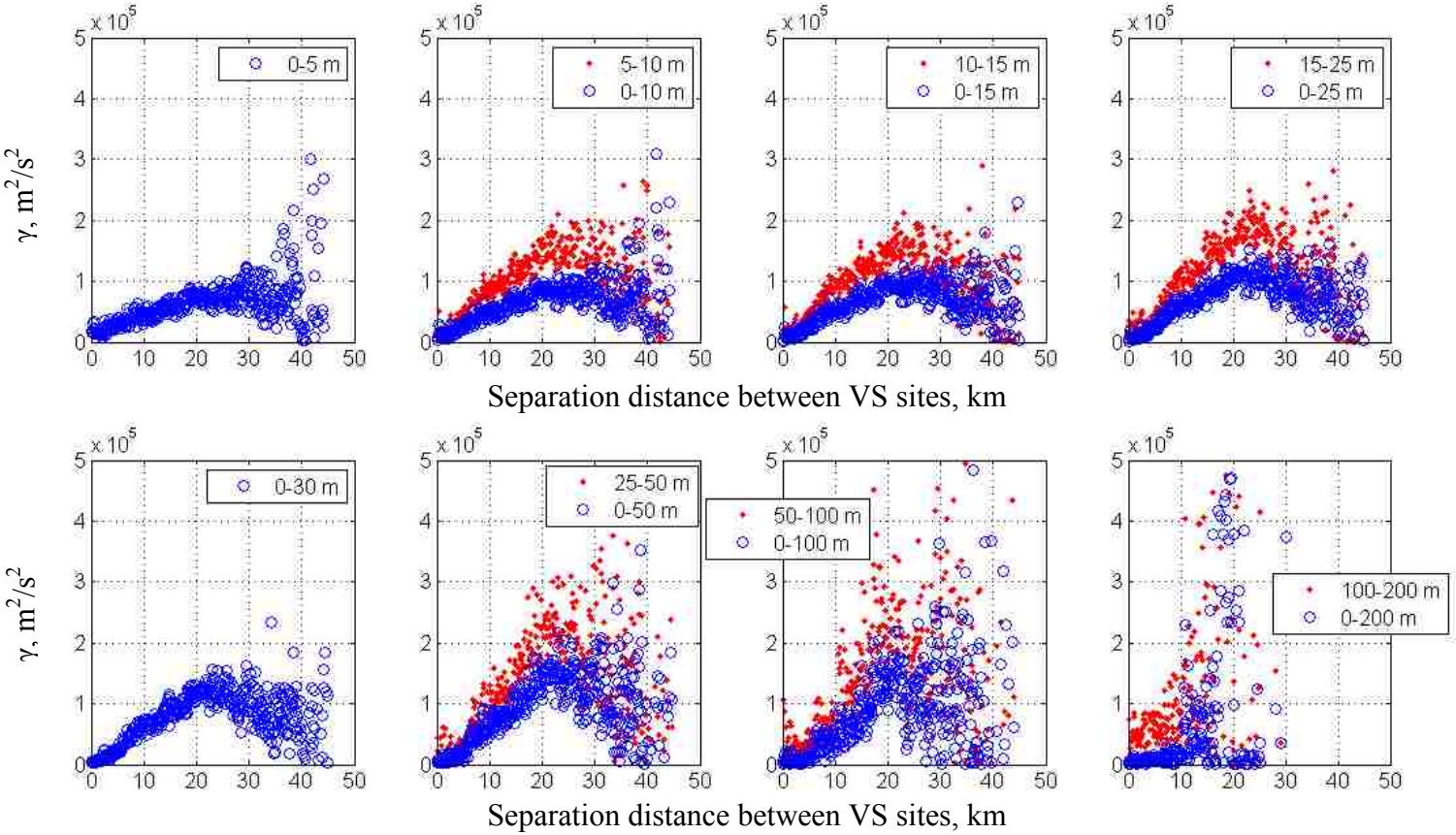

Figure 3.5 Semivariograms for layers (identified by depth range) with site pairs binned by separation distances that are multiples of 100 m. Blue circles represent the overall averages; red dots represent the layer averages.

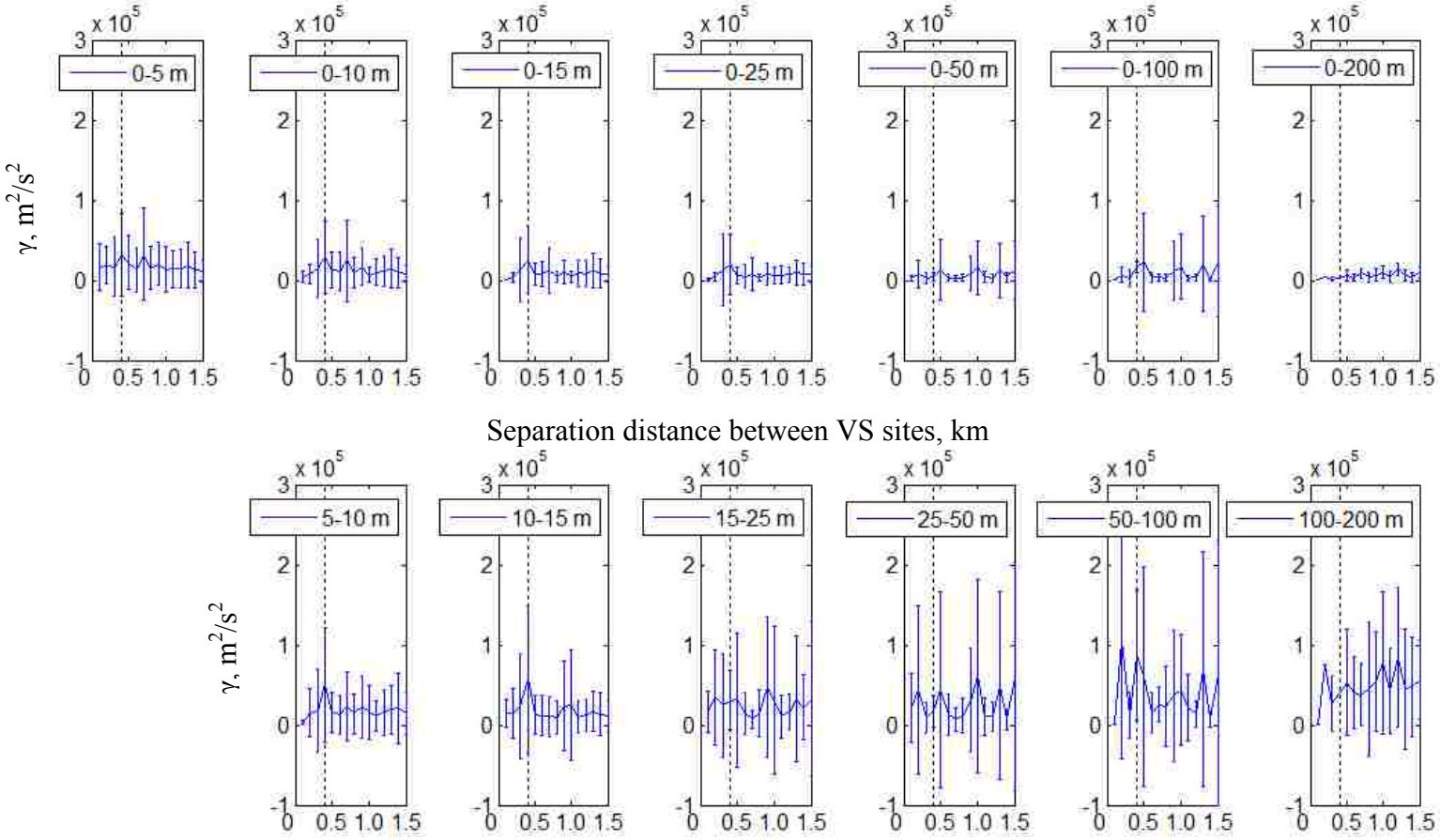

Figure 3.6 Blue curve representing mean γ for the depth ranges identified, with error bars to show the standard deviation (overall averages in top row and layer averages in bottom row). Dotted vertical line shown at 400 m is distance where γ increases for most layer intervals.

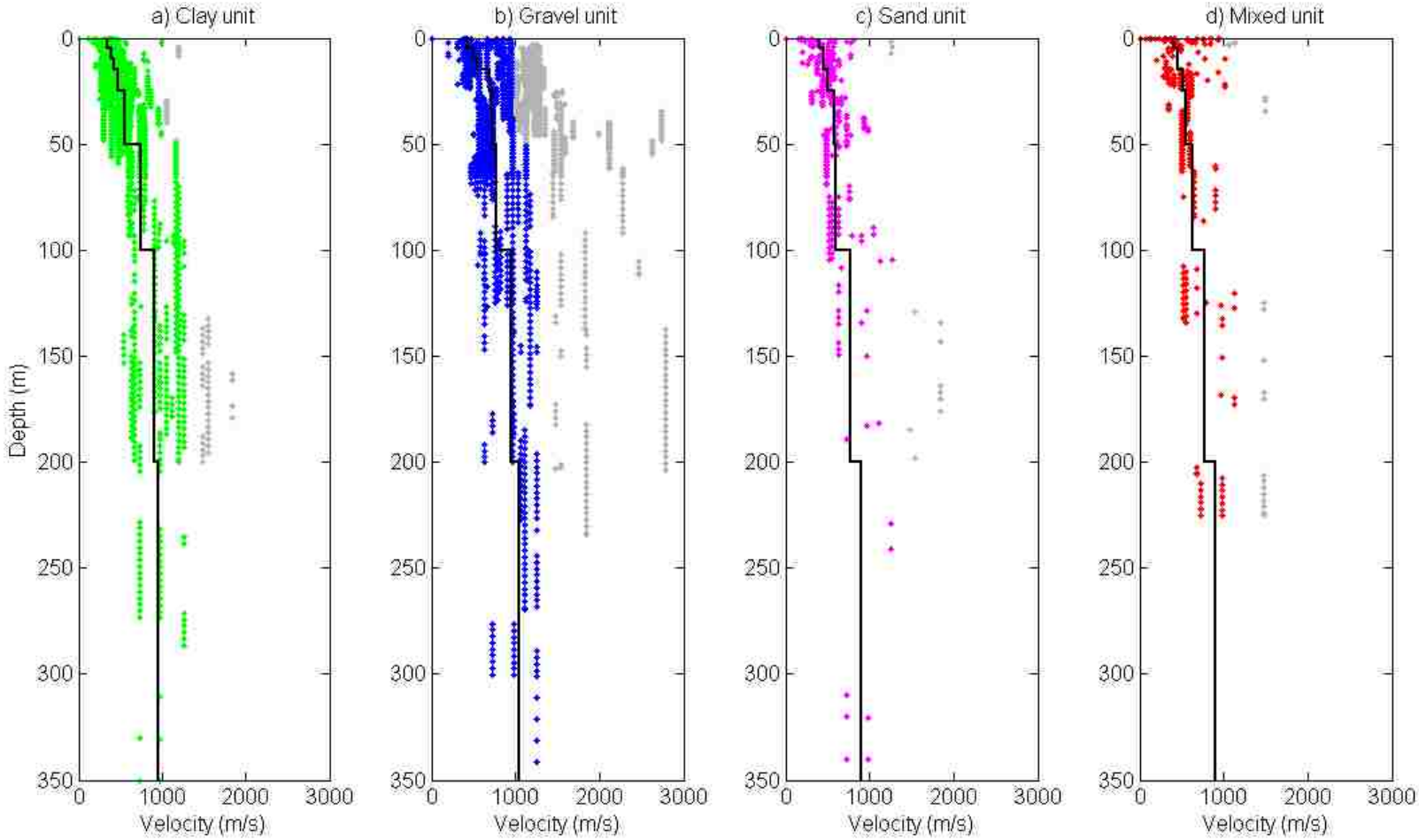

Figure 3.7 VS scatter plots for four sediment units in the 3-D sediment-lithology model. Grey dots indicate the velocity is above the cutoff boundary. The characteristic VS profile developed for each unit is shown by the black line.

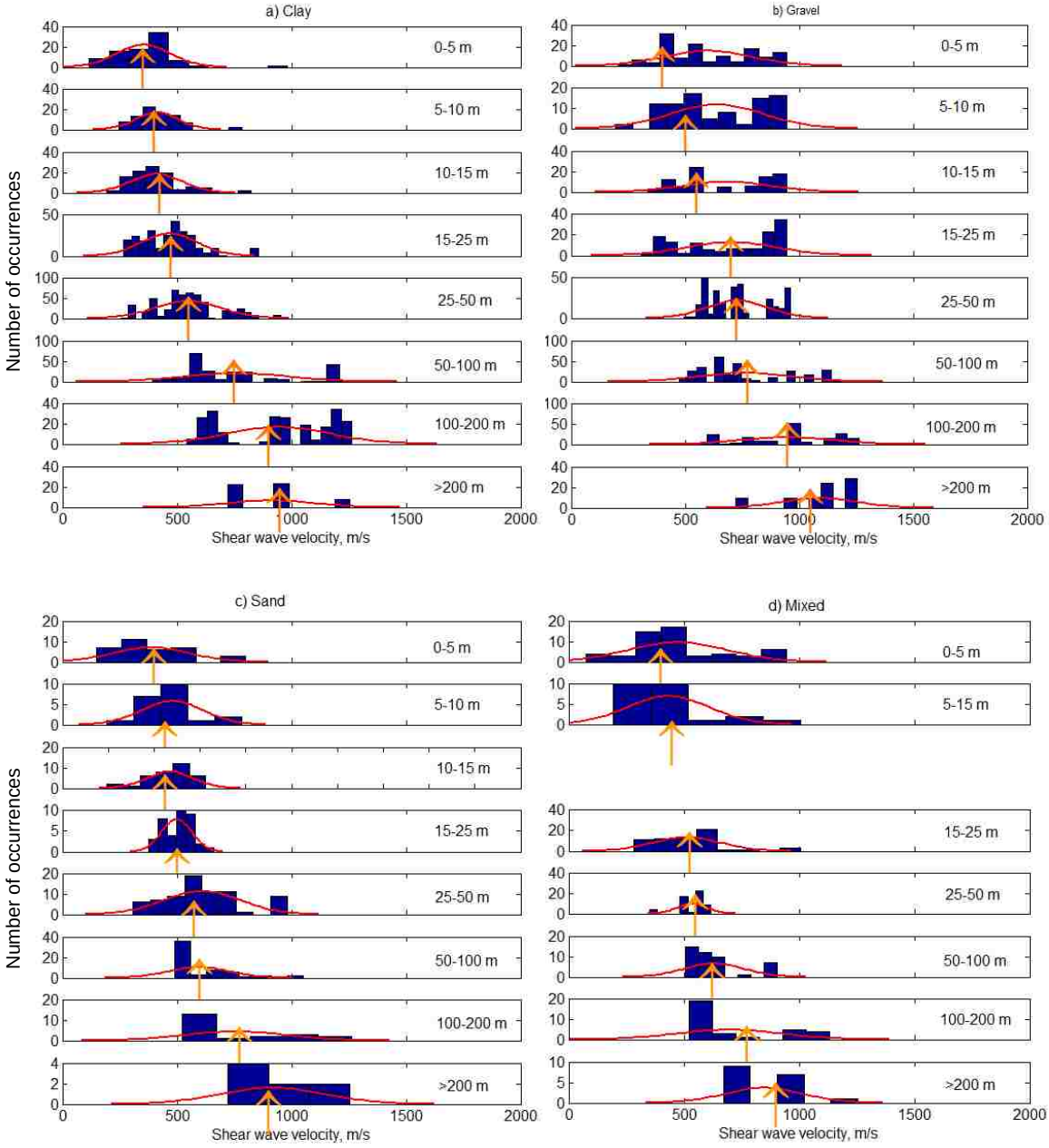

Figure 3.8 Histograms of VS (blue), calculated normal distribution (red curve) and assigned velocity (orange arrow) for each layer, identified by its depth range, of the four characteristic profiles: predominantly clay- (a), gravel- (b), sand- (c) and mixed- (d) sediment units. For the mixed sediment unit, the 5 to 10 m and 10 to 15 m layers are combined. Size of velocity bins is generated automatically by MATLAB's "histfit" function.

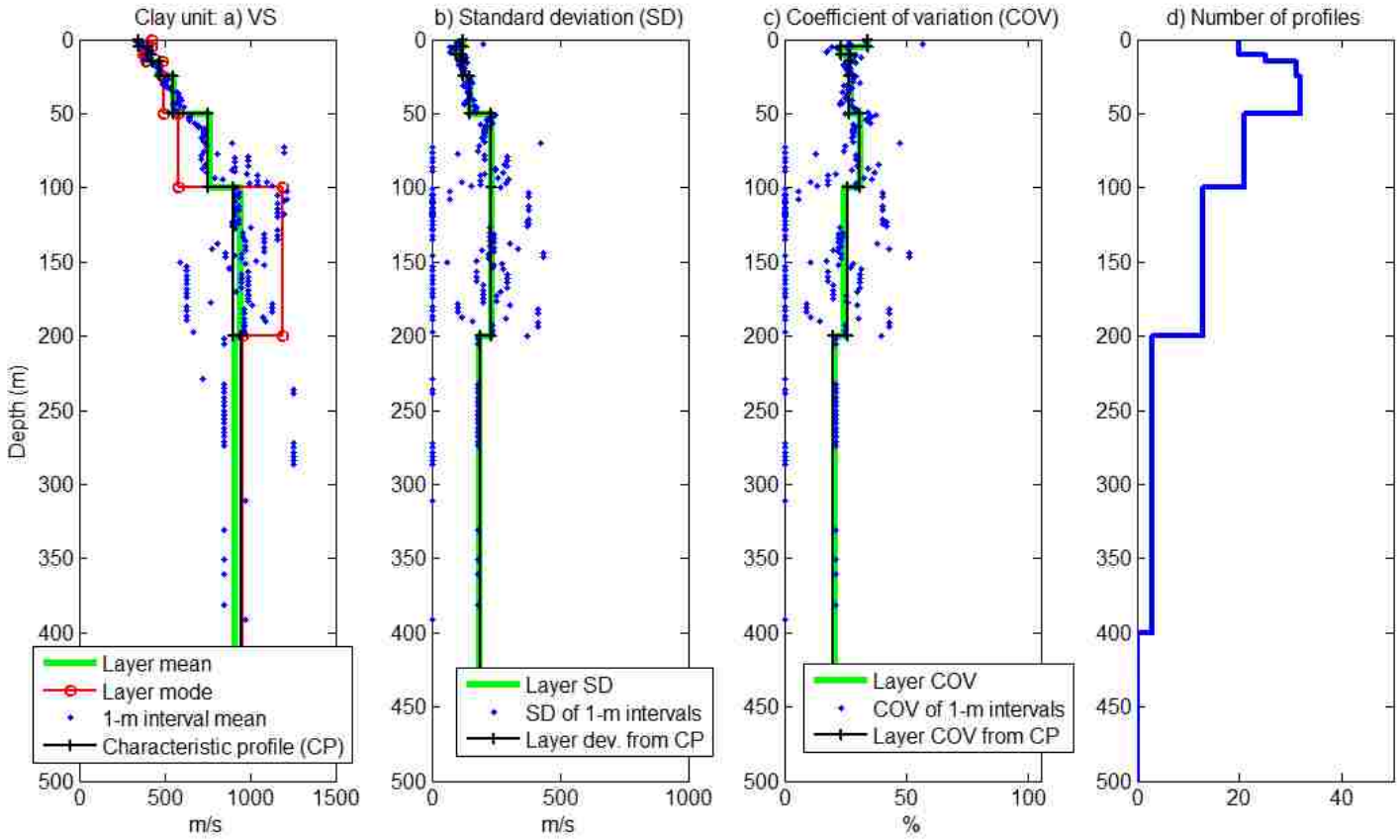

Figure 3.9 Statistics for the correlation dataset for the Clay unit: a) velocity mean, mode, and the characteristic profile (CP); b) standard deviation for each profile layer and for 1-m depth intervals and the deviation from the CP; c) coefficient of variation for the profile layers and for 1-m intervals and from the CP; d) number of profiles in each layer of the dataset.

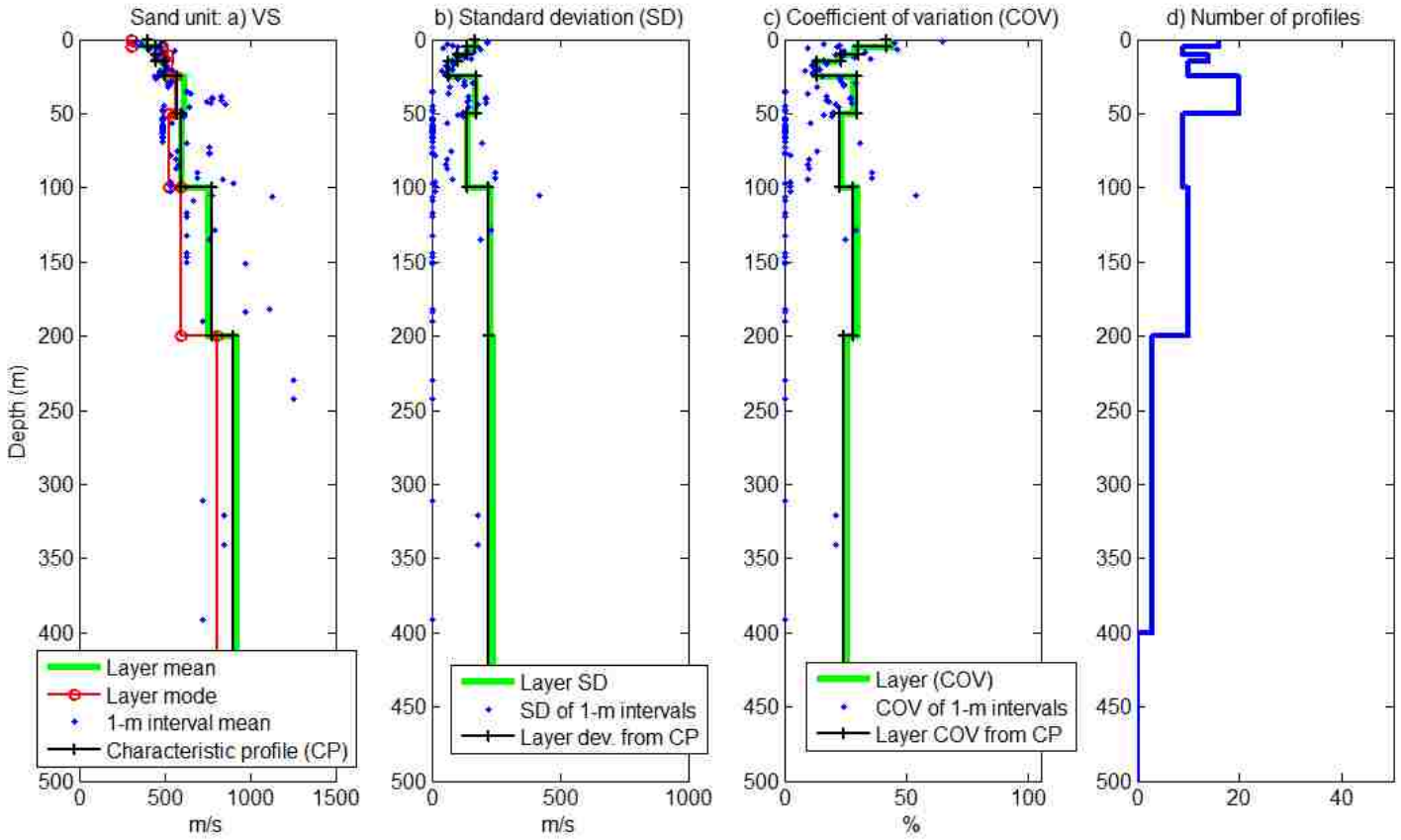

Figure 3.10 Statistics for the correlation dataset for the Sand unit: a) velocity mean, mode, and the characteristic profile (CP); b) standard deviation for each profile layer and for 1-m depth intervals and the deviation from the CP; c) coefficient of variation for the profile layers and for 1-m intervals and from the CP; d) number of profiles in each layer of the dataset.

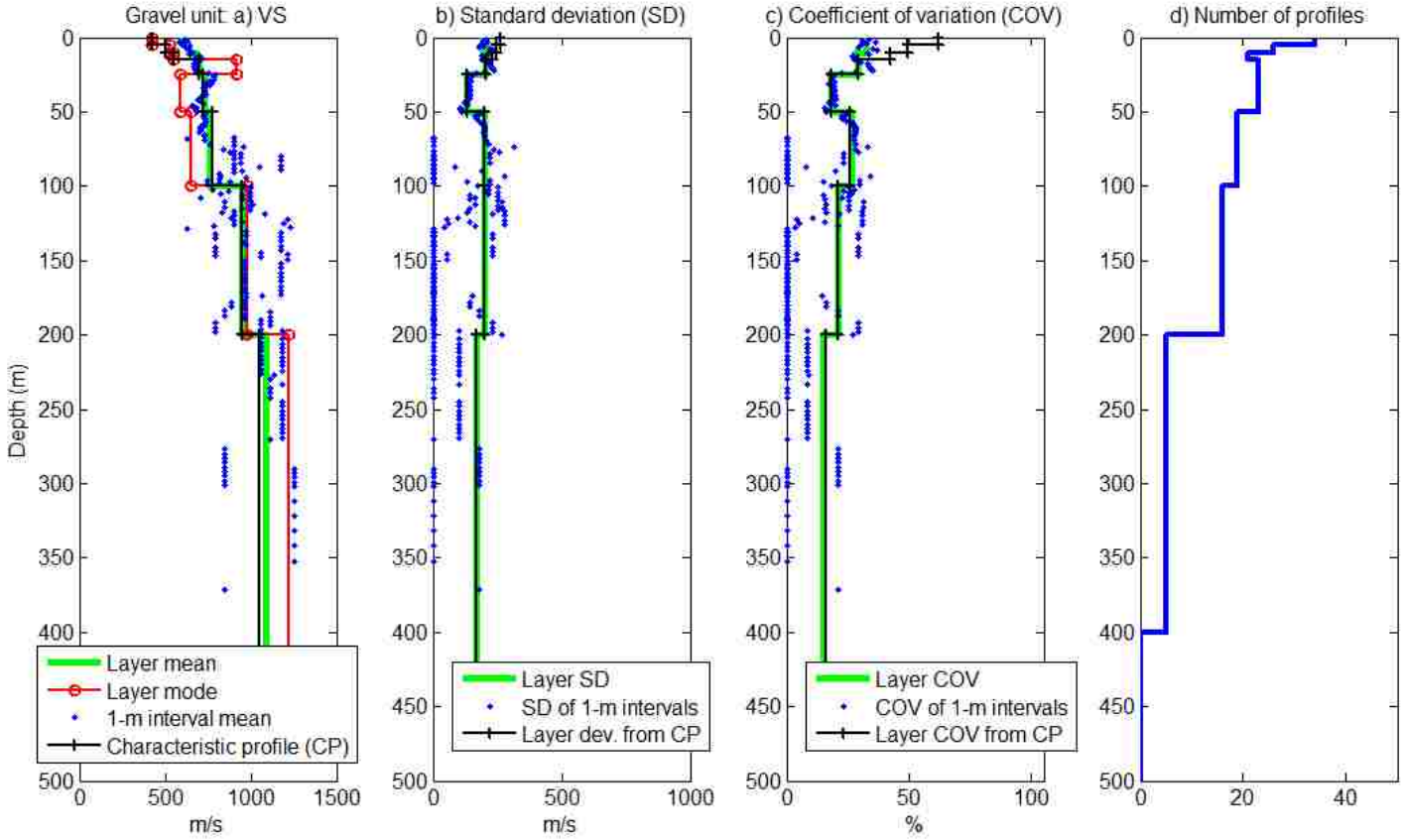

Figure 3.11 Statistics for the correlation dataset for the Gravel unit: a) velocity mean, mode, and the characteristic profile (CP); b) standard deviation for each profile layer and for 1-m depth intervals and the deviation from the CP; c) coefficient of variation for the profile layers and for 1-m intervals and from the CP; d) number of profiles in each layer of the dataset.

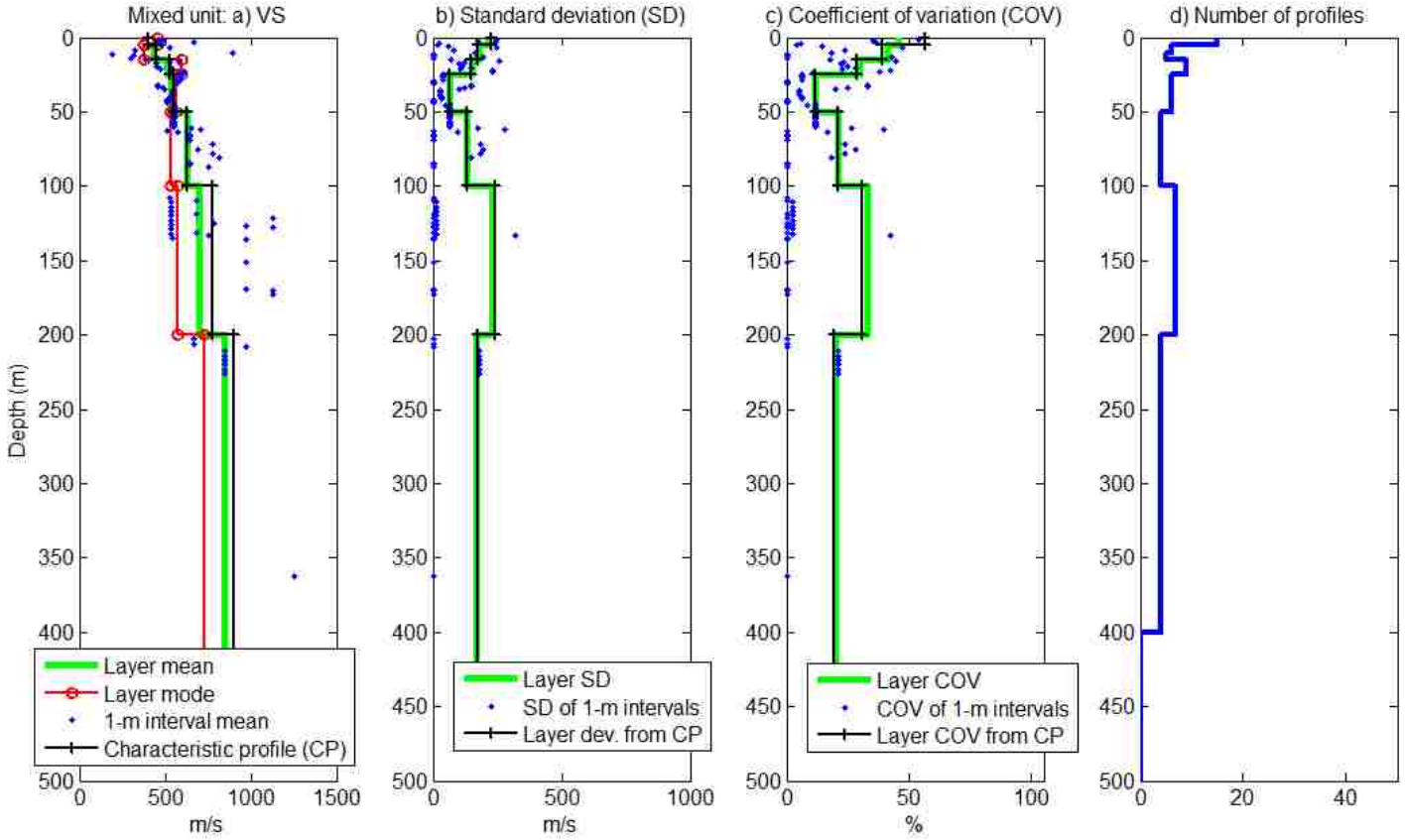

Figure 3.12 Statistics for the correlation dataset for the Mixed unit: a) velocity mean, mode, and the characteristic profile (CP); b) standard deviation for each profile layer and for 1-m depth intervals and the deviation from the CP; c) coefficient of variation for the profile layers and for 1-m intervals and from the CP; d) number of profiles in each layer of the dataset.

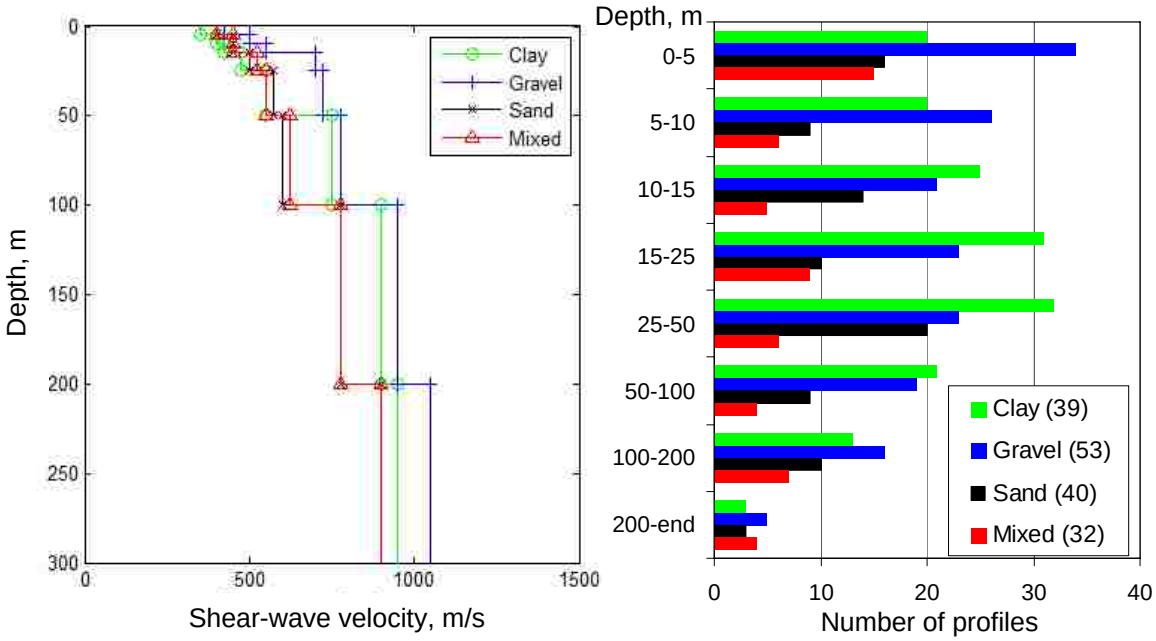

Figure 3.13 Characteristic profiles for four sediment units in the 3-D sediment-lithology model (left); number of profiles used for each correlation (right). The total number of profiles used for each unit's correlation is shown in parentheses in the legend.

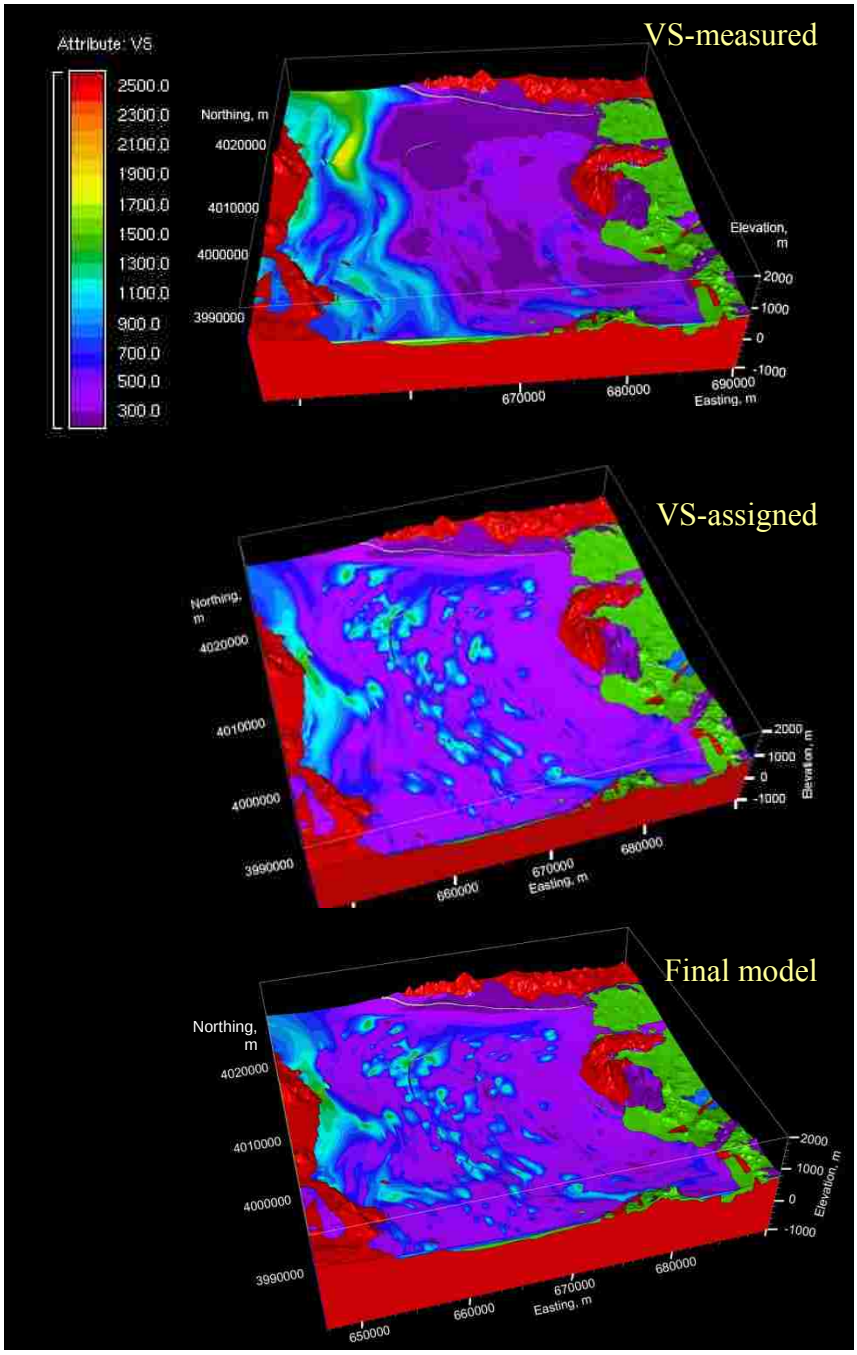

Figure 3.14 Three dimensional, shear-wave velocity models (with four times vertical exaggeration): from measured VS data (top); from data where VS was assigned to sediment-lithology (center); final model that honors VS-measured data while also using VS-assigned from sediment-lithology (bottom). The offset topography at the surface locations of the local faults appears as thin white or black lines.

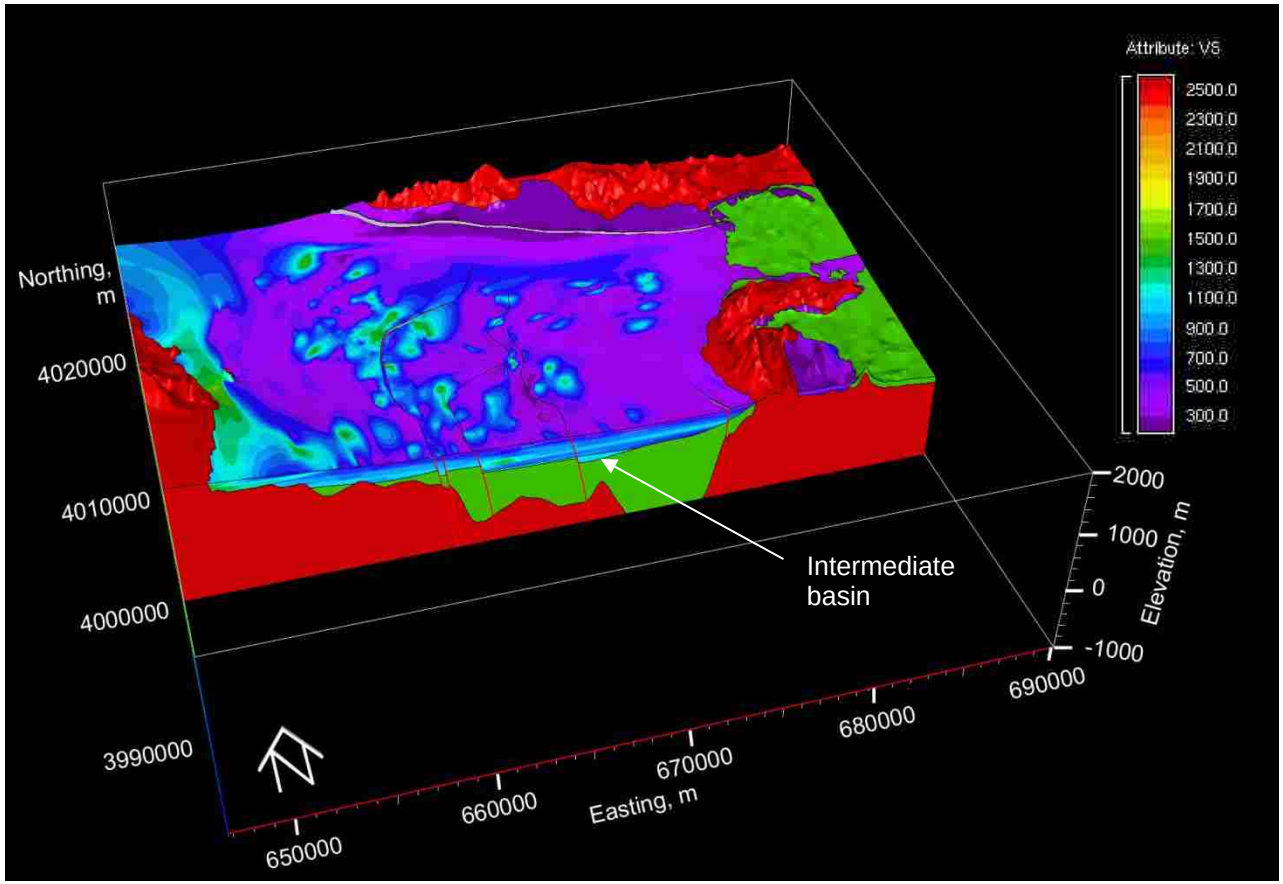

Figure 3.15 East-west cross section and surface of northern half of final 3-D VS model showing the Quaternary basin (primarily blue and purple) overlying the Oligocene-Miocene fill (green, Taylor et al., 2008) and the Paleozoic bedrock (red; Langenheim et al., 2001) and the fault locations (red lines in cross section, Taylor et al., 2008). Vertical exaggeration is four times the horizontal scales.

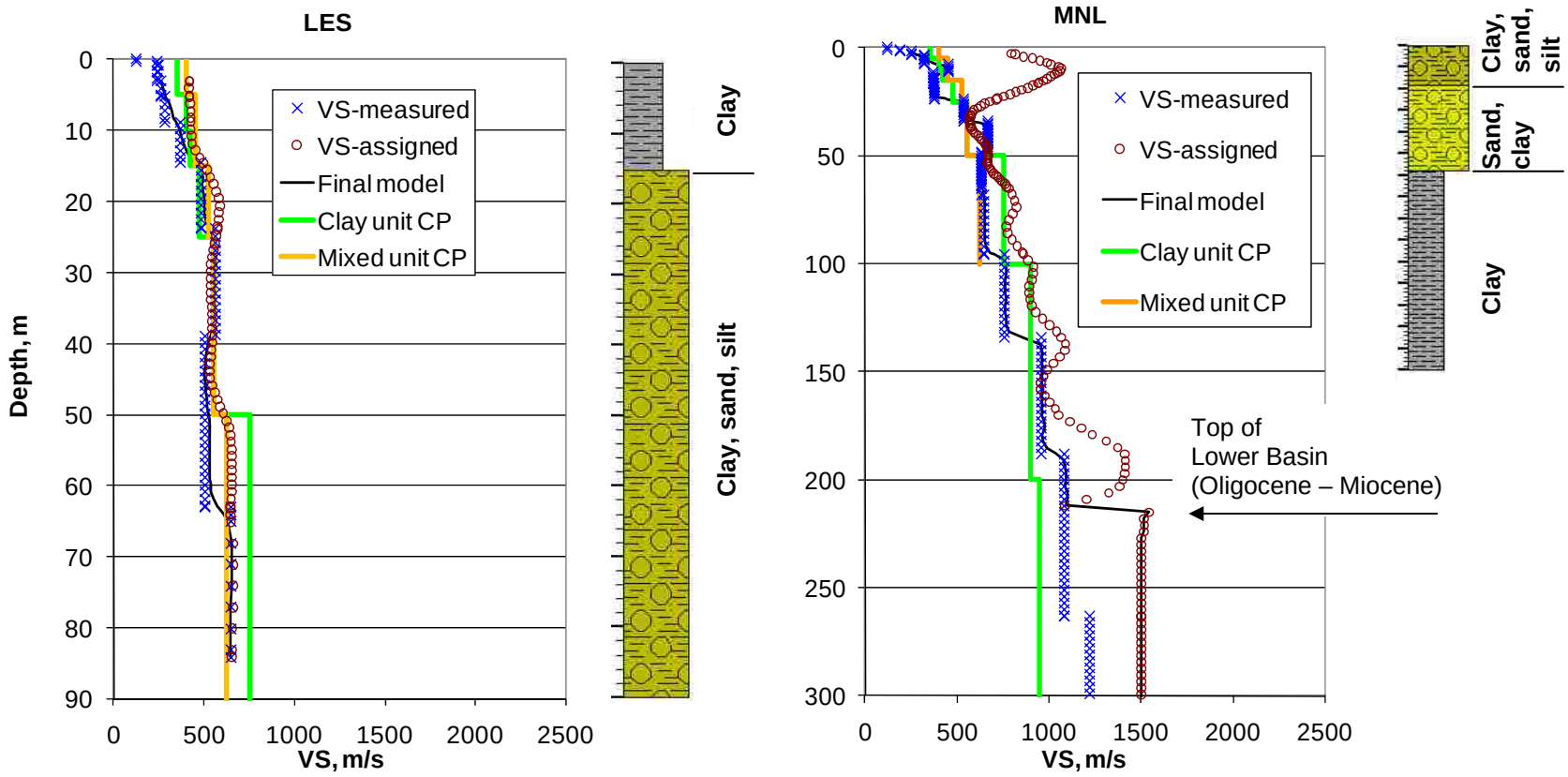

Figure 3.16 For the two sites shown in Figure 3.1, measured VS profiles, profiles queried at the site location from the 3-D VS model created from the VS-assigned dataset and from the final 3-D VS model created from the combined dataset, and log for closest well. Characteristic profiles for the predominant sediment units shown in the logs are also plotted.

3.10. References

Abrahamson, N., and Silva, W. (2008). Summary of the Abrahamson & Silva NGA ground-motion relations. *Earthquake Spectra, 24* (1), 67-97.

Baise, L. G., Higgins, R. B., and Brankman, C, M. (2006). Liquefaction hazard mapping—statistical and spatial characterization of susceptible units, *Journal of Geotechnical and Geoenvironmental Engineering 132 (6),* 705-715.

Building Seismic Safety Council of the National Institute of Building Sciences (2009). NEHRP recommended seismic provisions for new buildings and other structures (FEMA P-750). National Earthquake Hazards Reduction Program.

Calderón-Macías, C. and Luke, B. (2007). Improved parameterization to invert Rayleigh-wave data for shallow profiles containing stiff inclusions. *Geophysics, 72* (1), U1-U10.

Clark County Nevada. (2009, July). Clark County, Nevada 2009 Population Estimates. retrieved from http://www.accessclarkcounty.com/depts/comprehensive_planning/demographics/Documents/2009PlacePopulation.pdf.

Cramer, C. H., Gomberg, J. S., Schweig, E. S., Waldron, B. A., and Tucker, K. (2004). Memphis, Shelby County, Tennessee, seismic hazard maps. U.S. Geol. Surv. Open-File Rept. 04-1294, 41 pp.

Dawson, K.M., and Baise, L. G. (2005). Three-dimensional liquefaction potential analysis using geostatistical interpolation. *Soil Dynamics and Earthquake Engineering*, *25*, 369–381.

dePolo, C. M., and Taylor, W. J. (2008). Characterizing the earthquake potential of the Las Vegas Valley Fault System. Abstract, Cordilleran Section (104th Annual) and Rocky Mountain Section (60th Annual) Joint Meeting (Paper No. 17-2). Boulder, CO: The Geological Society of America (GSA).

Dynamic Graphics Inc. (2009, May). Technical specifications for EarthVision 7.5 environmental suite, retrieved from http://www.dgi.com/earthvision/techspecenvironmental.html.

Frankel, A., and Stephenson, W. (2000). Three-dimensional simulations of ground motions in the Seattle region for earthquakes in the Seattle Fault Zone. *Bulletin of the Seismological Society of America*, *90* (5), 1251–1267.

Frankel, A., Stephenson, W. Carver, D., Williams, R., Odum, J., and Rhea, S. (2007). *Seismic Hazard Maps for Seattle, Washington, Incorporating 3D Sedimentary Basin Effects, Nonlinear Site Response, and Rupture Directivity* (USGS Open-File Report 2007-1175). Retrieved from http://pubs.usgs.gov/of/2007/1175/.

Gazetas, G. (1992). Discussion of "Evaluation of in situ effective shear modulus from dispersion measurements" by C. Vrettos and B. Prange (1990, 116 (10)). *Journal of Geotechnical Engineering, 118* (7), 1120-1122.

Gomberg, J., Waldron, B., Schweig, E., Hwang, H., Webbers, A., VanArsdale, R., Tucker, K., Williams, R., Street, R., Mayne, P., Stephenson, W., Odum, J., Cramer, C., Updike, R., Hutson, S., and Bradley, M. (2003). Lithology and shear-wave velocity in Memphis Tennessee. *Bulletin of the Seismological Society of America, 93* (3), 986-997.

Henley, S. (1981). *Nonparametric geostatistics*. New York, NY: Applied Science Publishers Ltd, London, Halsted Press, a Division of John Wiley & Sons, Inc.

Industrial Vehicles International (2006, April). Minivib broad band 10 to 550 Hz vibrator T-7000. retrieved from http://www.indvehicles.com/minivibT7000.pdf.

International Code Council (2009). *International Building Code*. Country Club Hills, IL: International Code Council.

Jachens, R. C., Wentworth, C. M., Gautier, D. L., and Pack, S. (2001). 3D geologic maps and visualization: a new approach to the geology of the Santa Clara (Silicon) Valley, California. Workshop Proceedings of the Digital Mapping Techniques '01, U.S. Geological Survey Open-File Report 01-223.

Kramer, S L. (1996). *Geotechnical Earthquake Engineering*. Upper Saddle River, NJ: Prentice-Hall, Inc.

Kravchenko, A. N. (2003). Influence of spatial structure on accuracy of interpolation methods. *Soil Science Society of America Journal, 67*, 1564-1571.

Langenheim, V. E., Grow, J. A., Jachens, R. C., Dixon, G. L., and Miller, J. J. (2001). Geophysical constraints on the location and geometry of the Las Vegas Valley Shear Zone, Nevada. *Tectonics, 20* (2), 189-209.

Liu, Y. (2006). Site response projections and earthquake microzonation for the Las Vegas basin, Nevada. Ph.D. dissertation, University of Nevada Las Vegas, Las Vegas, NV.

Liu, Y., Luke, B., Pullammanappallil, S., Louie, J., and Bay, J. (2005). Combining active- and passive-source measurements to profile shear wave velocities for seismic microzonation. In R. W. Boulanger, M. Dewwolkar, N. Gucunski, C. Juang, M.

Kalinski, S. Kramer, M. Manzari and J. Pauschke (eds.), *Earthquake Engineering and Soil Dynamics, Geotechnical Special Publication 133* (pp. 977-990). Reston, VA: American Society of Civil Engineers.

Louie, J. N. (2001). Faster, better: shear-wave velocity to 100 meters depth from refraction microtremor arrays. *Bulletin of the Seismological Society of America*, *91*(2), 347-364.

Louie, J. N. (2008). Earthquake Hazard Class Mapping by Parcel in Unincorporated Urban Clark County. Abstract, Cordilleran Section (104th Annual) and Rocky Mountain Section (60th Annual) Joint Meeting (Paper No. 17-6). Boulder, CO: The Geological Society of America (GSA).

Louie, J. N., Tibuleac, I., Cashman, P., Trexler, J., Stephenson, W. J., Odum, J., Pullammanappallil, S. K., Pancha, A., and Magistrale, M. (2009). Gathering critical data toward the western basin and range CVM. *Proceedings and abstracts Southern California Earthquake Center Annual Meeting, 19*, 95-196.

Luke, B., and Liu, Y. (2007). Effect of sediment column on weak-motion site response for a deep basin fill. *Journal of Geotechnical and Geoenvironmental Engineering, 133* (11), 1399-1413.

Luke, B., and Liu, Y. (2008). Site response zones and short-period earthquake ground motion projections for the Las Vegas basin. *Journal of Earth System Science, 117* (S2), 757-772.

Luke, B., Taylor, W., Liu, Y., Wagoner, J., and Su, Q. (2006). Correlating a sparse seismic data set with lithology for site amplification investigations. In Y. Xu, J. Xia, and C. Chen (eds.), *Proceedings of the 2nd International Conference on*

Environmental and Engineering Geophysics, Geophysical Solutions for Environmental and Engineering Vol. 1 (pp. 10-23). Monmouth Junction, NJ: Science Press USA Inc.

Luke, B., Taylor, W., Calderón-Macías, C., Jin, X., Murvosh, H., and Wagoner, J. (2008). Characterizing anomalous ground for engineering applications using surface-based seismic methods. *The Leading Edge, 27*(11), 1330–1334.

Luke, B., Murvosh, H., Taylor, W., and Wagoner, J. (2009). Three-dimensional modeling of shallow shear-wave velocities for Las Vegas, Nevada, using sediment type. *Journal of Earth Science, 20* (3), 555-562.

Luke, B., Murvosh, H., Taylor, W., and Wagoner, J. (2010). Characteristic shear velocity profiles for predominant sediment fill units in the Las Vegas Basin. In D. Fratta, A. J. Puppala and B. Muhunthan (eds.), *GeoFlorida 2010: Advances in Analysis, Modeling and Design, Geotechnical Special Publication 199* [CD-ROM]. Reston, VA: American Society of Civil Engineers.

McEwan, D. J. (2005). A seismological study of the Las Vegas basin, NV: investigating basin depth and shear velocity structure. Master's Thesis, University of Nevada, Las Vegas, Las Vegas, NV.

Murvosh, H., Luke, B., McLaurin, B., Higgins, T., and Quinn, W. (2006). Research and development of Las Vegas Valley VS(30) map. *Proceedings, 40th Annual Symposium on Engineering Geology and Geotechnical Engineering* (CD-ROM: 7 p.). Pocatello, ID: Idaho State University.

Murvosh, H., and Luke, B. (2008). Summer 2007 VS data acquisition campaign in Las Vegas; lessons learned. *Proceedings, 41st Annual Symposium on Engineering*

Geology and Geotechnical Engineering (CD-ROM: pp. 277-286). Pocatello, ID: Idaho State University.

Nevada Earthquake Safety Council (2009). Summary minutes for November 9, 2009, meeting, retrieved from http://www.nbmg.unr.edu/nesc/nov09.pdf.

Ni, S. D., Siddharthan, R. V., and Anderson, J. G. (1997). Characteristics of nonlinear response of deep saturated soil deposits. *Bulletin of the Seismological Society of America, 87* (2), 342-355.

Plume, R.W. (1989). Ground-water in Las Vegas Valley, Clark County, Nevada, part 1, hydrogeologic framework. US Geological Survey Water Supply Paper 2320-A, 15 pp.

Price, J. G., Johnson, G., Ballard, C. M., Armeno, H., Seeley, I., Goar, L. D., dePolo, C. M., and Hastings, J. T. (2009). *Estimated Losses from Earthquakes near Nevada Communities* (Nevada Bureau of Mines and Geology Open-File Report 09-8). Retrieved from http://www.nbmg.unr.edu/dox/of098/Scenarios/OpenFileReport09-8.pdf .

Romero, S., and Rix, G. J. (2001). Regional variations in near surface shear wave velocity in the greater Memphis area. *Engineering Geology, 62* (2001), 137-158.

Scott, J. B., Rasmussen, T., Luke, B., Taylor, W., Wagoner, J. L., Smith, S. B., and Louie, J.N. (2006). Shallow shear velocity and seismic microzonation of the urban Las Vegas, Nevada basin. *Bulletin of the Seismological Society of America, 96* (3), 1068-1077.

Snelson C., McEwan, D., and Zaragoza, S. (2005). Velocity structure of the Las Vegas Basin: Results from recent seismic refraction experiments. *AEG News, 48* (program with abstracts), 92.

Stokoe, K. H., II, Wright, S. G., Bay, J. A., Roësset, J. M. (1994). Characterization of geotechnical sites by SASW method. In R. D. Woods (ed.) *Geophysical Characterization of Sites* (pp. 15-25). New Delhi, India: Oxford and IBH Publishing Co.

Stone, R., and Luke, B. (2001). An overview of engineering with cemented soils in Las Vegas. In B. Luke, E. Jacobson and J. Werle (eds.), *Proceedings, 36th Annual Symposium on Engineering Geology and Geotechnical Engineering* (pp. 135-144). Pocatello, ID: Idaho State University.

Su, F., Anderson, J., Ni, S. and Zeng, Y. (1998). Effect of site amplification and basin response on strong motion in Las Vegas, Nevada. *Earthquake Spectra, 14*, 357-376.

Taylor, W. J., Carter, J., Luke, B., Snelson, C. M., and Wagoner, J. (2008). Development of Las Vegas Basin, Nevada with implications for seismic hazards. Abstract, Cordilleran Section (104th Annual) and Rocky Mountain Section (60th Annual) Joint Meeting (Paper No. 17-4). Boulder, CO: The Geological Society of America.

Tecle, M., Giorgis, A. and Luke, B. (2003). Comparison of seismic downhole to crosshole measurements in a complex-layered system. In S. Elfass, G. Norris, and R. Watters (eds.), *Proceedings, 38th Annual Symposium on Engineering Geology*

and Geotechnical Engineering (pp. 299-310). Pocatello, ID: Idaho State University.

Thompson, E. M., Baise, L. G., and Kayen, R. E. (2007). Spatial correlation of shear-wave velocity in the San Francisco Bay Area sediments. *Soil Dynamics and Earthquake Engineering 27*, 144–152.

Tkalčić, H ., Rodgers, A. J., Rawlinson, N., McEwan, D. J., and Snelson, C. M. (2008). Teleseismic travel-time delays in the Las Vegas Basin. *Bulletin of the Seismological Society of America*, *98* (4), 2047–2060.

Werle, J., and Luke, B. (2007). Engineering with heavily cemented soils in Las Vegas, Nevada. In A. J. Puppala, N. Hudyma, and W.J. Likos (eds.), *Problematic Soils and Rocks and In Situ Characterization. Geotechnical Special Publication 162* [CD-ROM]. Reston, VA: American Society of Civil Engineers.

Western, A. W., and Blöschl, G. (1999). On the spatial scaling of soil moisture. *Journal of Hydrology*, *217* (1999), 203–224.

Wills, C. J., and Clahan, K. B. (2006). Developing a map of geologically defined site-condition categories for California. *Bulletin of the Seismological Society of America, 96* (4A), 1483–1501.

Wills, C. J., Petersen, M., Bryant, W. A., Reichle, M., Saucedo, G. J., Tan, S., Taylor, G., and Treiman, J. (2000). A site-conditions map for California based on geology and shear-wave velocity. *Bulletin of the Seismological Society of America, 90* (6B), S187–S208.

Wong, I., Silva, W.J., Olig, S., Thomas, P., Wright, D., Ashland, F., Gregor, N., Pechmann, J., Dober M., Christenson, G., and Gerth, R. (2002). Earthquake

scenario and probabilistic ground shaking maps for the Salt Lake City, Utah, metropolitan area. Misc. Publ. MP-02-05, Utah Geological Survey.

Wyman, R., Karakouzian, M., Bax-Valentine, V., Slemmons, D.B., Peterson, L., and Palmer, S. (1993). Geology of Las Vegas, Nevada United States of America. *Bulletin of the Association of Engineering Geologists, 30* (1), 33-78.

APPENDIX A

SHEAR-WAVE VELOCITY MEASUREMENT LOCATIONS, DATA AND SOLUTIONS

Data and results for the 12 sites where Spectral Analysis of Surface Waves (SASW) surveys were performed in the Las Vegas Valley, Nevada, are included in this appendix. The following are included for each site:

- A map showing the array location and nearby well data
- A table of the starting models for the inversion process, the linearized inversion solution (LI), the solution obtained using the average of three simulated annealing runs as the starting model for LI (SA-LI), and the solution for the one site where an explicit search for a high-velocity layer was performed (SAES-LI) are listed
- A plot containing the experimental dispersion curve and the dispersion curves for the solutions
- Well log information
- A plot containing the profiles for the starting model and solutions as well as the search and solution ranges
- Resolution matrices for the solutions

Keys for the sediments in the well logs and for the resolution matrices are also included at the end.

Data and solutions for CCH site

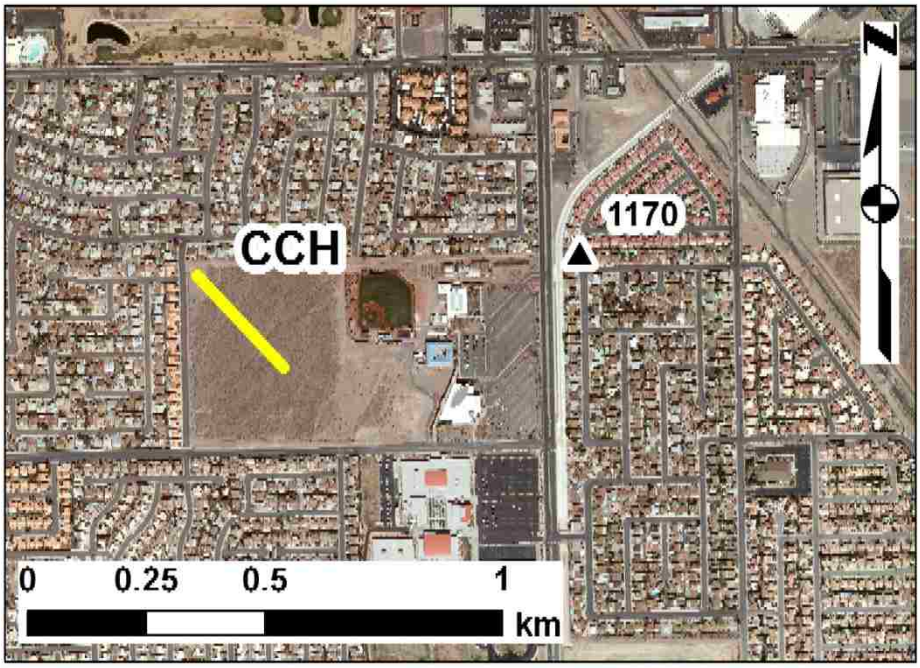

Figure A.1. Location of CCH, a coarse sediment-response-unit (coarse SRU) site: array locations (yellow lines) with respect to nearby wells (black triangles). Longitude and latitude listed on Table 2.1.

Table A.1. VS starting model and solutions for CCH site.

Layer number	Poisson's ratio	Density, kg/m^3	Thickness, m	Starting model VS, m/s	Solutions	
					LI VS, m/s	SA-LI VS, m/s
1	0.3	1700	1.50	145	157	156
2	0.3	1700	1.91	213	341	344
3	0.3	1700	2.43	296	451	442
4	0.3	1700	3.09	354	545	569
5	0.3	1700	3.93	394	437	423
6	0.3	1700	5.00	433	736	740
7	0.3	1700	6.35	468	509	547
8	0.3	1700	8.07	502	566	518
9	0.3	1700	10.26	555	817	889
10	0.3	1700	13.05	622	927	931
Halfspace	0.3	1700	N//A	656	1050	1039

a)

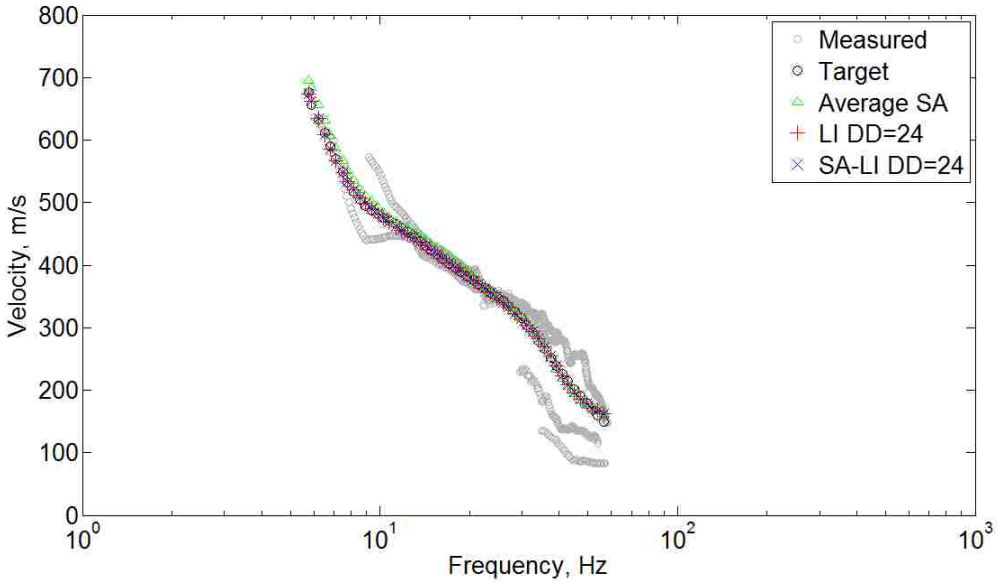

b) Well no. 1170 c) d)

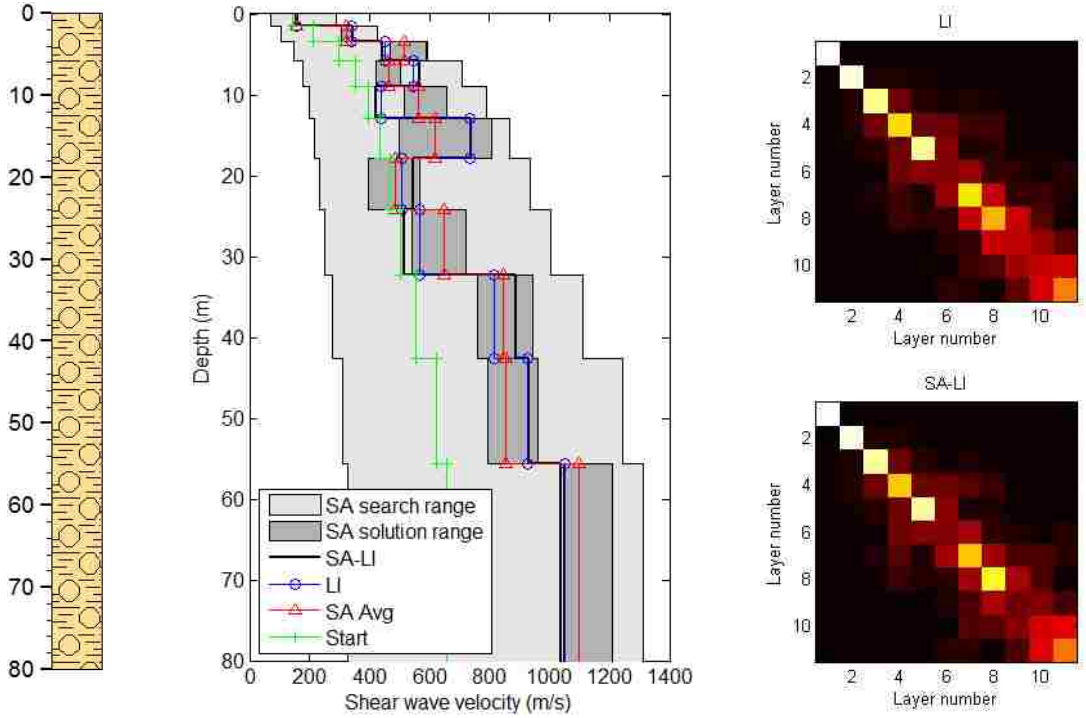

Figure A.2. Coarse SRU site CCH, data and solutions: a) dispersion curves, b) well log information (depth in meters), c) VS profiles, and d) resolution matrices.

Data and solutions for CPH site

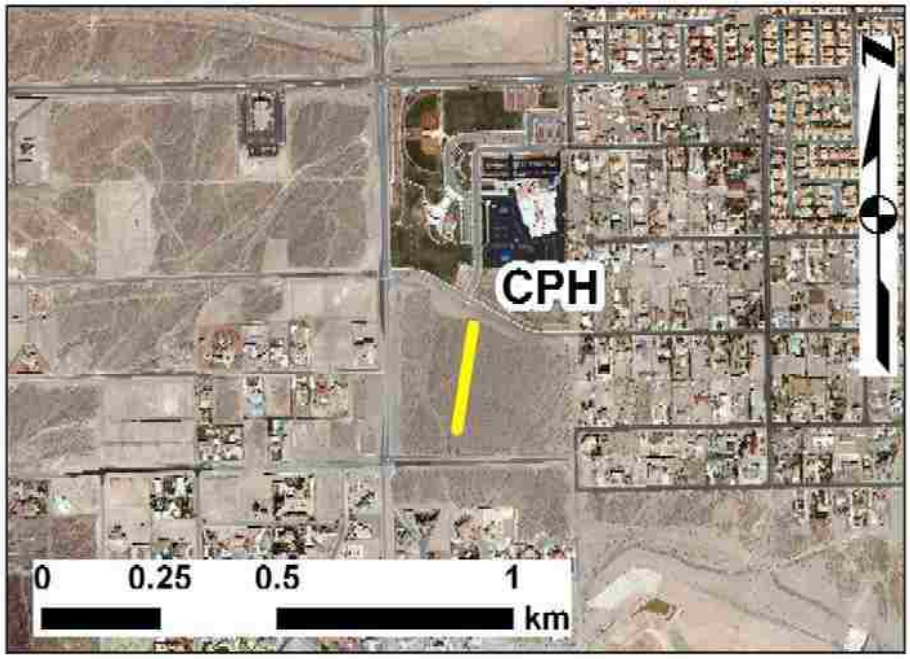

Figure A.3. Location of CPH, a coarse SRU site: array locations (yellow lines) with respect to nearby wells (black triangles). Longitude and latitude listed on Table 2.1.

Table A.2. VS starting model and solutions for CPH site.

Layer number	Poisson's ratio	Density, kg/m^3	Thickness, m	Starting model VS, m/s	Solutions	
					LI VS, m/s	SA-LI VS, m/s
1	0.3	1700	0.51	126	122	122
2	0.3	1700	0.77	158	216	218
3	0.3	1700	1.17	209	279	276
4	0.3	1700	1.78	269	403	411
5	0.3	1700	2.71	339	495	482
6	0.3	1700	4.13	417	615	636
7	0.3	1700	6.29	506	715	694
8	0.3	1700	9.57	599	908	928
9	0.3	1700	14.60	677	798	796
10	0.3	1700	22.20	766	1003	988
Halfspace	0.3	1700	N/A	831	1381	1429

a)

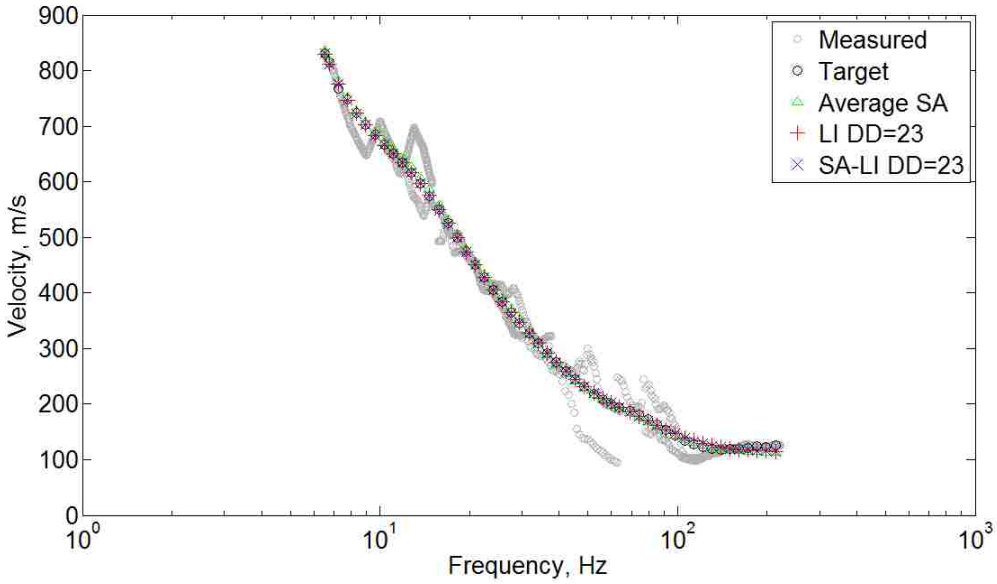

b)

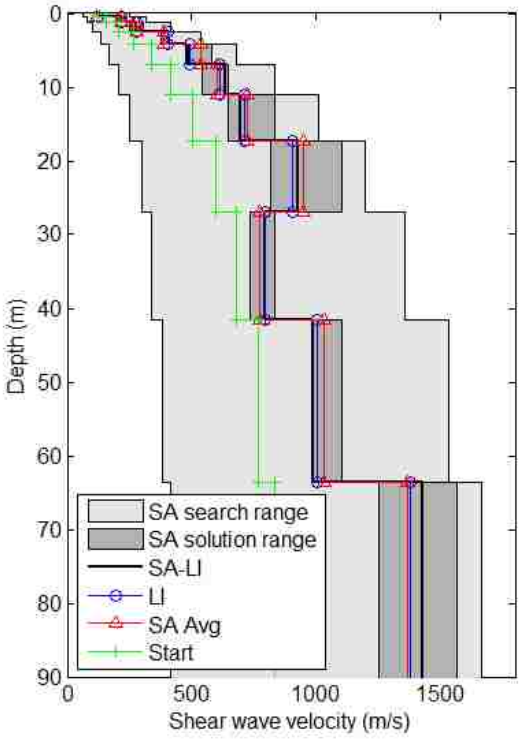

c)

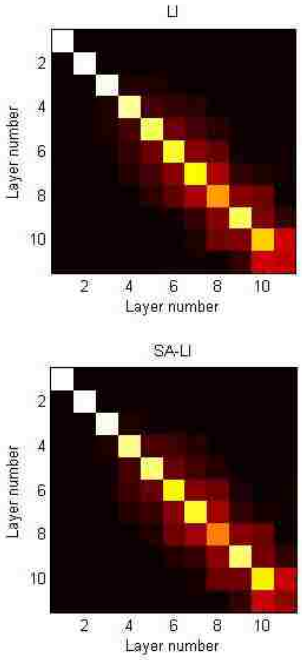

Figure A.4. Data and solutions for CPH site: a) dispersion curves, b) VS profiles, and c) resolution matrices. Site is 1,800 m south of its nearest well (no. 1170; Figure A.3), 1,900 m southwest of CCH site, and 700 m north of rock outcrops.

Data and solutions for GMS site

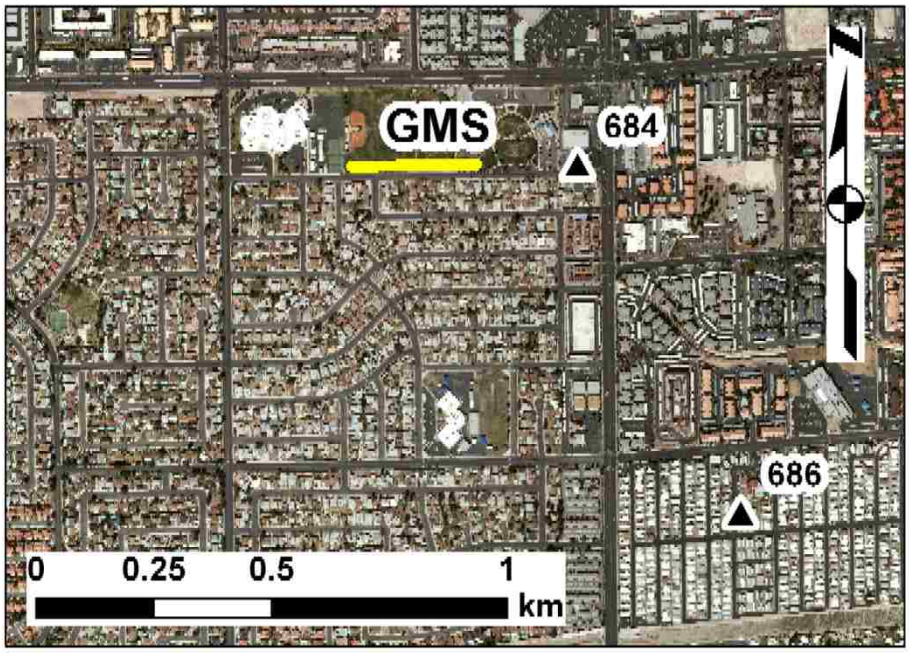

Figure A.5. Location of GMS, a coarse SRU site: array locations (yellow lines) with respect to nearby wells (black triangles). Longitude and latitude listed on Table 2.1.

Table A.3. VS starting model and solutions for GMS site.

Layer number	Poisson's ratio	Density, kg/m^3	Thickness, m	Starting model VS, m/s	Solutions	
					LI VS, m/s	SA-LI VS, m/s
1	0.3	1700	0.52	133	125	126
2	0.3	1700	0.77	172	255	254
3	0.3	1700	1.15	257	477	490
4	0.3	1700	1.72	313	422	401
5	0.3	1700	2.57	338	387	426
6	0.3	1700	3.83	358	397	352
7	0.3	1700	5.71	396	482	565
8	0.3	1700	8.52	442	647	608
9	0.3	1700	12.71	466	478	457
10	0.3	1700	18.96	505	579	639
11	0.3	1700	28.29	596	936	824
12	0.3	1700	42.20	744	1218	1280
Halfspace	0.3	1700	N/A	844	1618	1777

a)

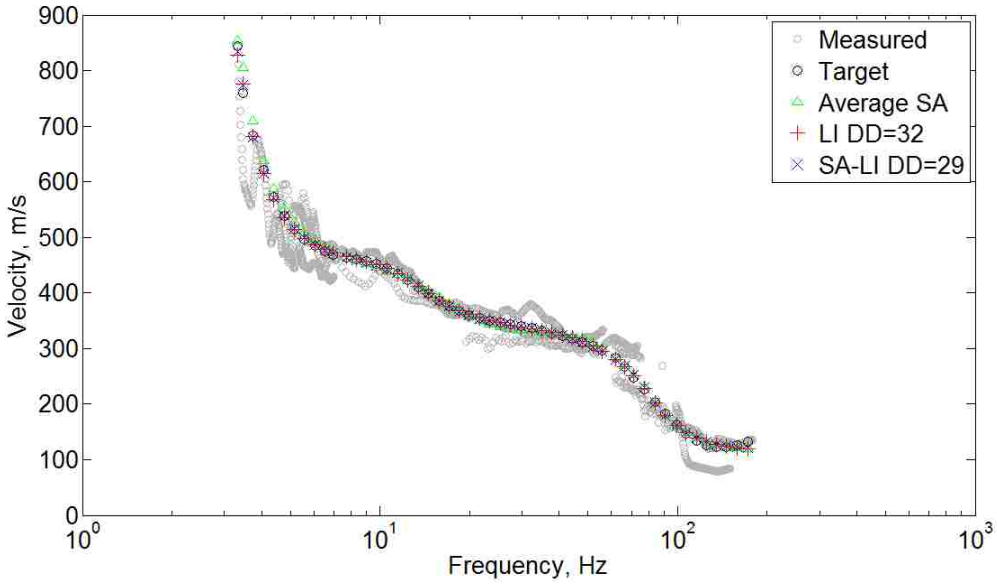

b) Well no. 684 c) d)

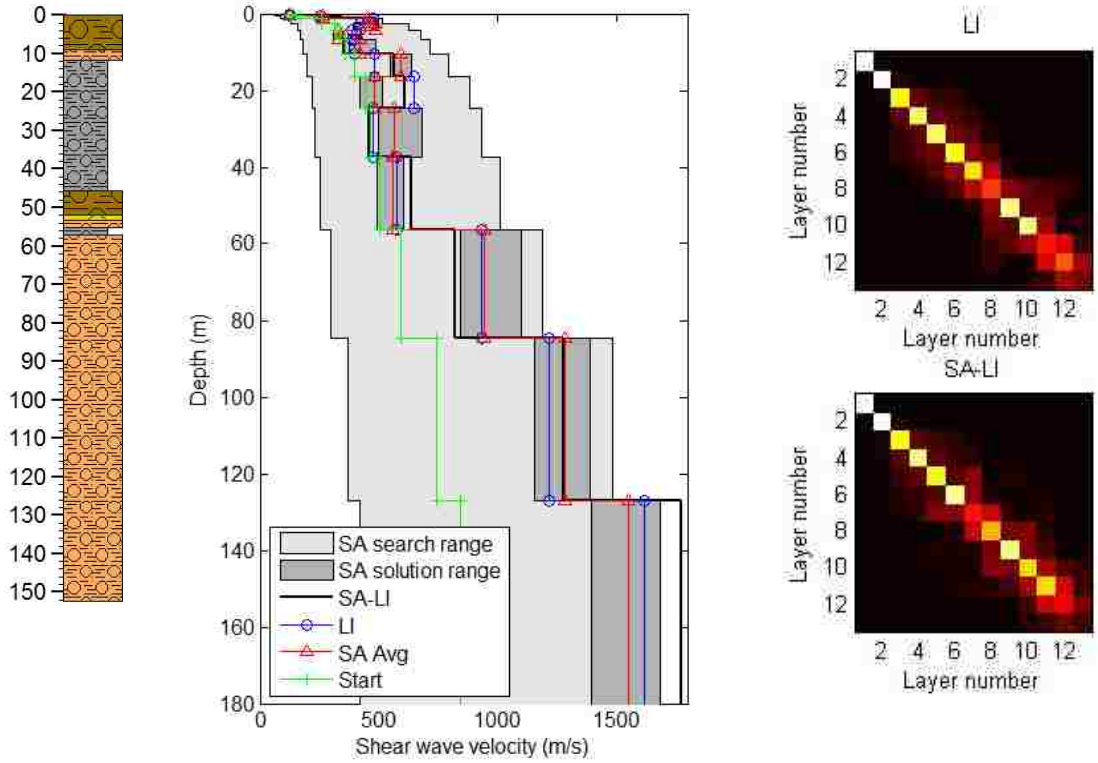

Figure A.6. Data and solutions for GMS site: a) dispersion curves, b) well log information, c) VS profiles, and d) resolution matrices.

Data and solutions for LES site

Figure A.7. Location of LES, a fine sediment-response-unit (fine SRU) site: array locations (yellow lines) with respect to nearby wells (black triangles). Longitude and latitude listed on Table 2.1.

Table A.4. VS starting model and solutions for LES site.

Layer number	Poisson's ratio	Density, kg/m^3	Thickness, m	Starting model VS, m/s	Solutions	
					LI VS, m/s	SA-LI VS, m/s
1	0.3	1700	0.32	117	127	126
2	0.3	1700	0.52	168	238	237
3	0.3	1700	0.84	202	245	246
4	0.3	1700	1.36	214	244	242
5	0.3	1700	2.20	228	261	264
6	0.3	1700	3.56	249	285	281
7	0.3	1700	5.75	287	364	372
8	0.3	1700	9.29	348	500	485
9	0.3	1700	15.01	406	545	563
10	0.3	1700	24.25	444	524	508
Halfspace	0.3	1700	N/A	466	622	646

a)

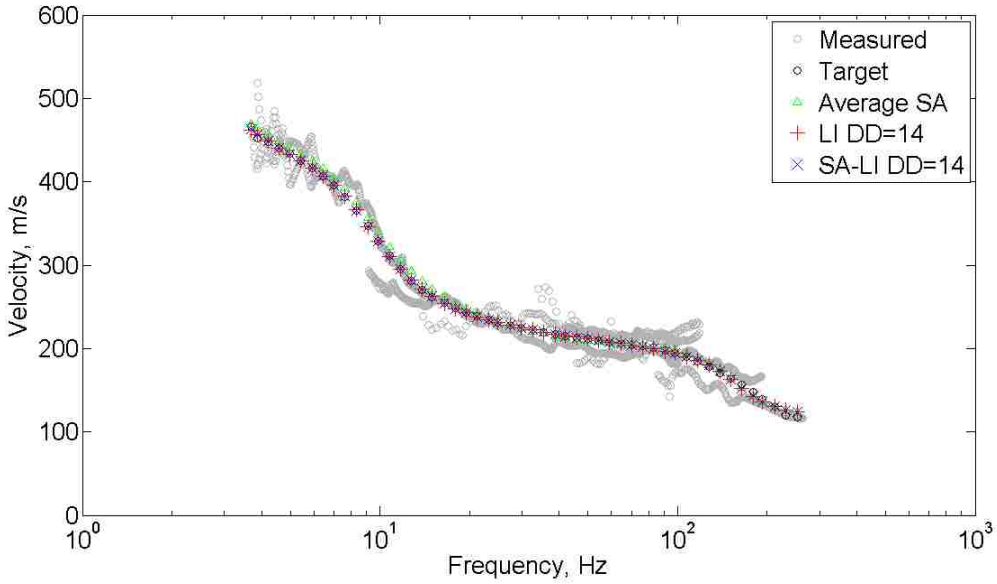

b) Well no. 620 c) d)

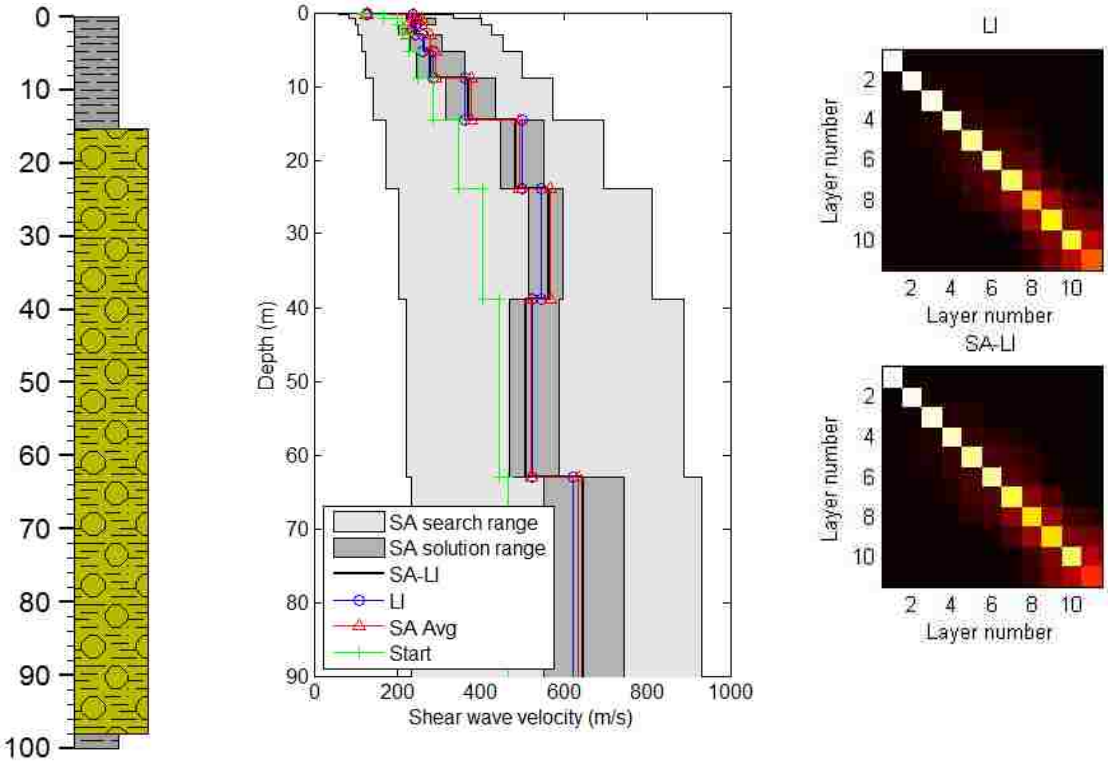

Figure A.8. Data and solutions for LES site: a) dispersion curves, b) well log information, c) VS profiles, and d) resolution matrices.

Data and solutions for LMN site

Figure A.9. Location of LMN, a fine SRU site: array locations (yellow lines) with respect to nearby wells (black triangles). Longitude and latitude listed on Table 2.1.

Table A.5. VS starting model and solutions for LMN site.

Layer number	Poisson's ratio	Density, kg/m^3	Thickness, m	Starting model VS, m/s	Solutions	
					LI VS, m/s	SA-LI VS, m/s
1	0.3	1700	0.59	191	194	193
2	0.3	1700	0.84	204	239	239
3	0.3	1700	1.20	217	251	251
4	0.3	1700	1.70	235	244	244
5	0.3	1700	2.41	271	431	436
6	0.3	1700	3.42	323	404	395
7	0.3	1700	4.85	380	589	626
8	0.3	1700	6.89	430	613	572
9	0.3	1700	9.78	453	519	564
10	0.3	1700	13.87	471	570	511
11	0.3	1700	19.69	498	532	595
12	0.3	1700	27.94	536	671	603
Halfspace	0.3	1700	N/A	591	1011	1132

a)

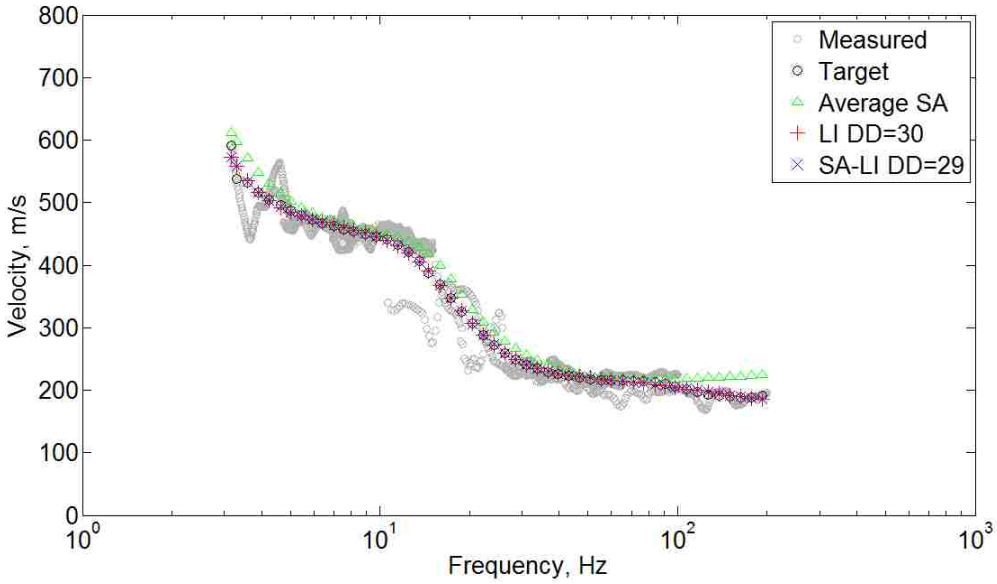

b) Well no. 454 c) d)

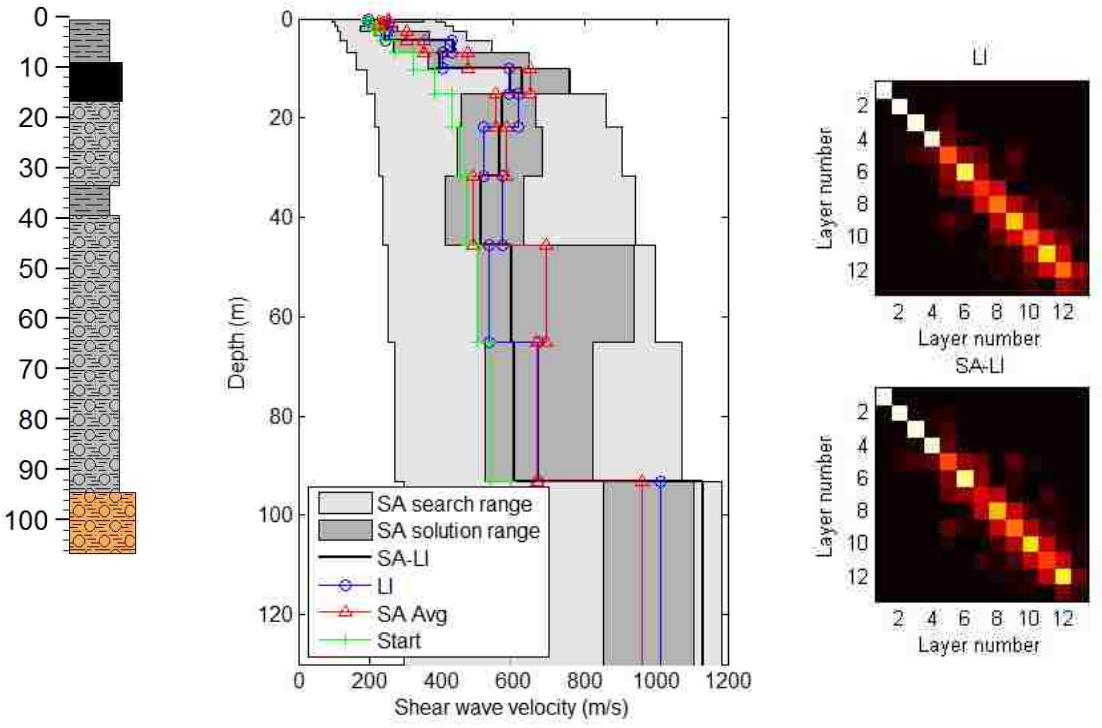

Figure A.10. Data and solutions for LMN site: a) dispersion curves, b) well log information, c) VS profiles, and d) resolution matrices.

Data and solutions for MHS site

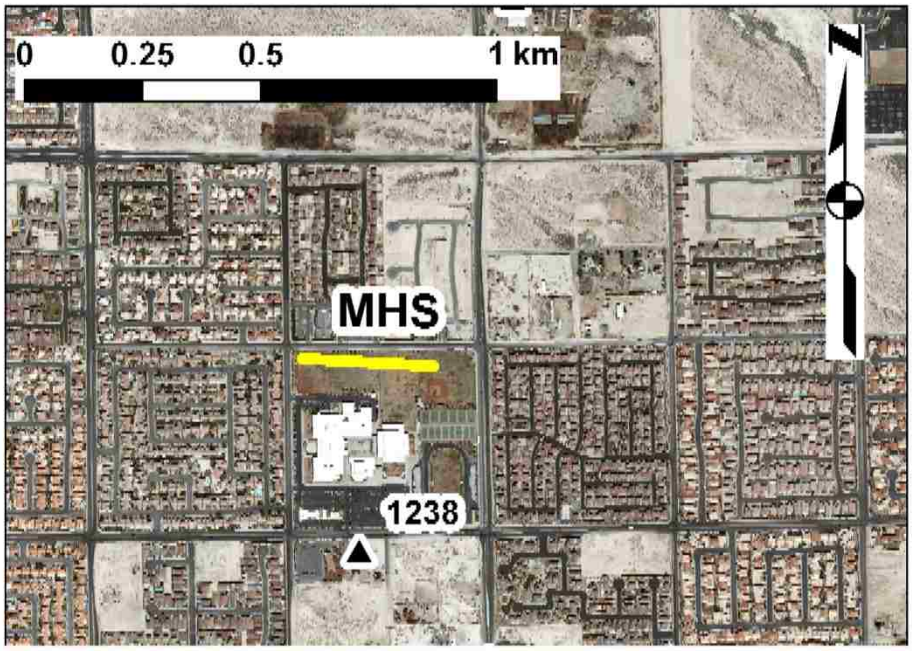

Figure A.11. Location of MHS, a fine SRU site: array locations (yellow lines) with respect to nearby wells (black triangles). Longitude and latitude listed on Table 2.1.

Table A.6. VS starting model and solutions for MHS site.

Layer number	Poisson's ratio	Density, kg/m^3	Thickness, m	Starting model VS, m/s	Solutions	
					LI VS, m/s	SA-LI VS, m/s
1	0.3	1700	1.37	208	208	209
2	0.3	1700	1.79	229	296	296
3	0.3	1700	2.36	233	215	214
4	0.3	1700	3.09	267	551	607
5	0.3	1700	4.06	299	329	282
6	0.3	1700	5.34	329	393	574
7	0.4	1700	7.01	356	473	387
8	0.4	1700	9.21	390	521	500
9	0.3	1700	12.10	420	460	588
10	0.3	1700	15.89	453	518	413
11	0.3	1700	20.88	504	693	745
Halfspace	0.3	1700	N/A	535	898	1059

a)

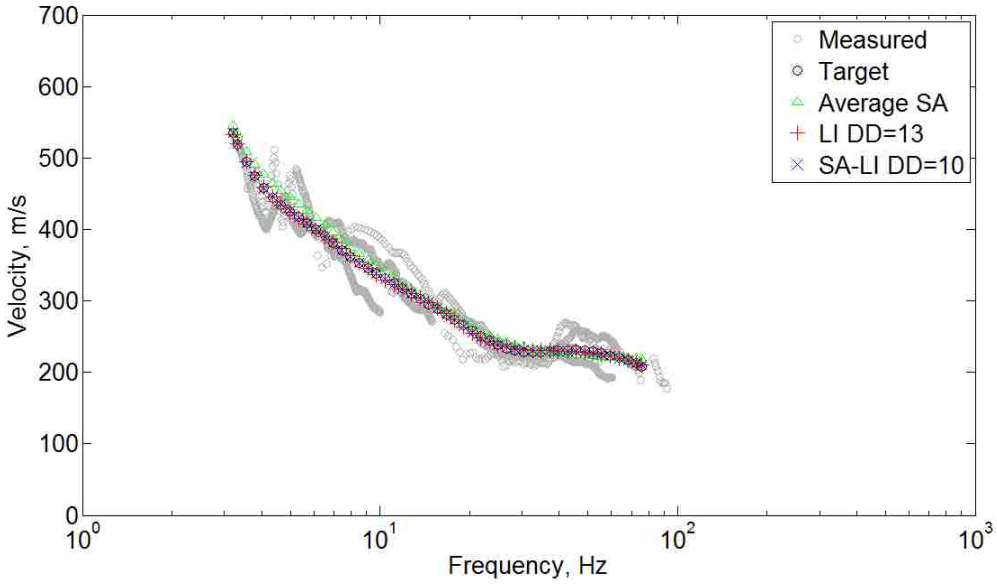

b) Well no. 1238 c) d)

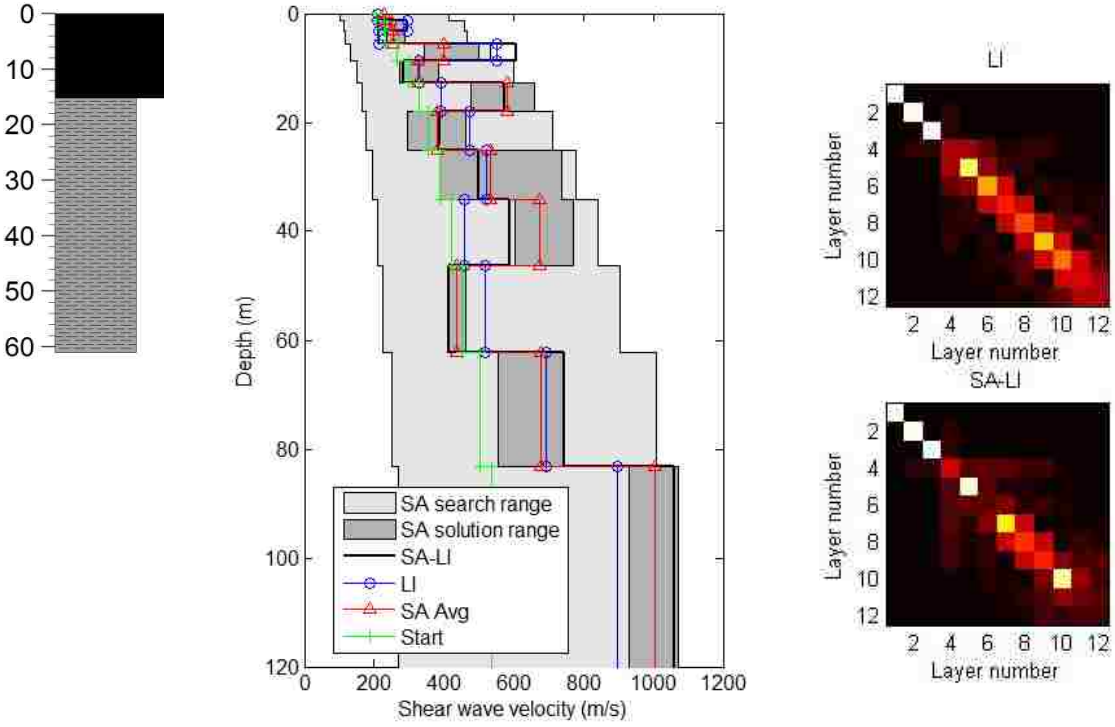

Figure A.12. Data and solutions for MHS site: a) dispersion curves, b) well log information, c) VS profiles, and d) resolution matrices.

Data and solutions for NLP site

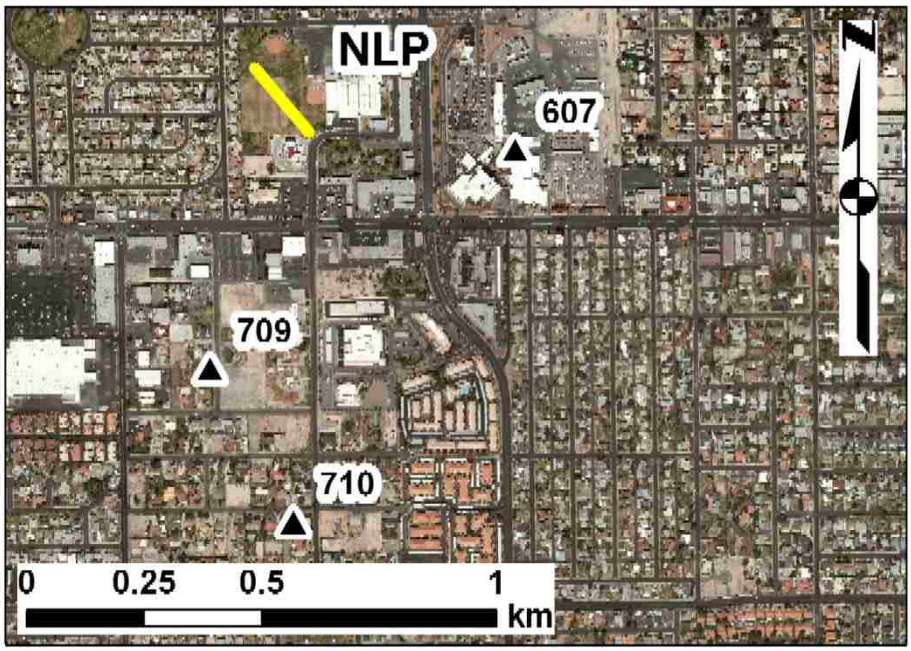

Figure A.13. Location of NLP, a fine SRU site: array locations (yellow lines) with respect to nearby wells (black triangles). Longitude and latitude listed on Table 2.1.

Table A.7. VS starting model and solutions for NLP site.

Layer number	Poisson's ratio	Density, kg/m^3	Thickness, m	Starting model VS, m/s	Solutions	
					LI VS, m/s	SA-LI VS, m/s
1	0.3	1700	0.48	121	120	120
2	0.3	1700	0.73	161	229	230
3	0.3	1700	1.11	225	339	335
4	0.3	1700	1.69	271	357	364
5	0.3	1700	2.58	310	359	349
6	0.3	1700	3.93	367	646	700
7	0.3	1700	5.98	405	437	412
8	0.3	1700	9.09	430	545	590
9	0.3	1700	13.84	463	529	509
10	0.3	1700	21.07	512	597	601
Halfspace	0.3	1700	N/A	551	894	905

a)

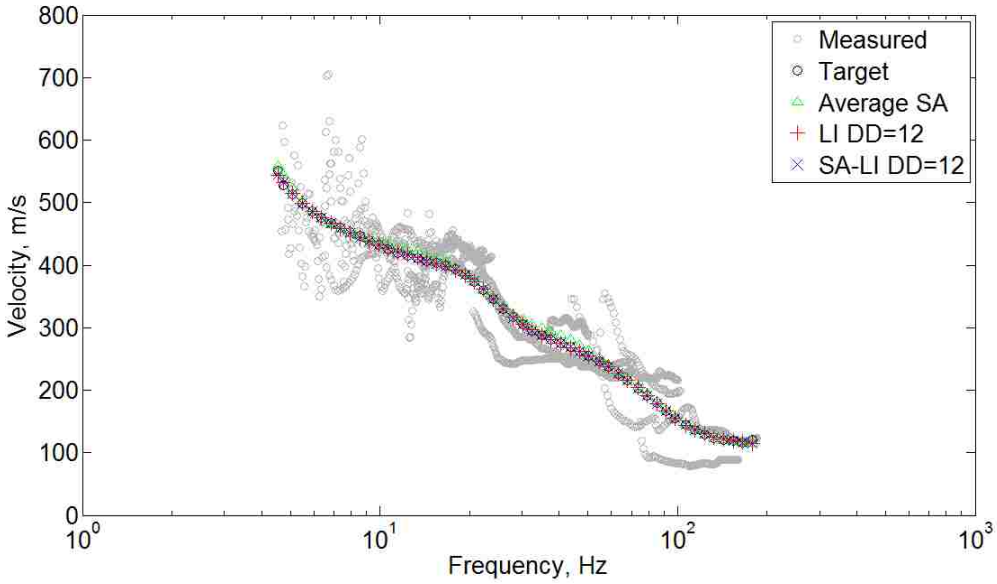

b) Well no.'s 709 and 607

c)

d)

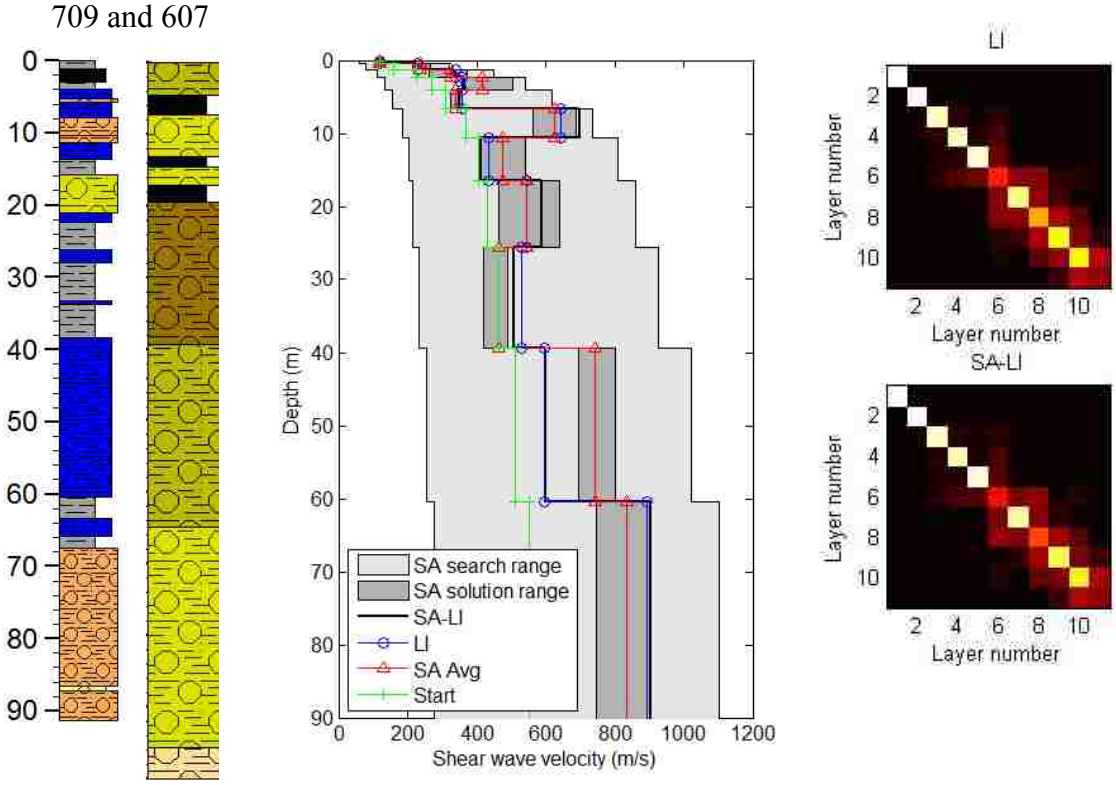

Figure A.14. Data and solutions for NLP site: a) dispersion curves, b) well log information, c) VS profiles, and d) resolution matrices.

Data and solutions for OSH site

Figure A.15. Location of OSH, a coarse SRU site: array locations (yellow lines) with respect to nearby wells (black triangles). Longitude and latitude listed on Table 2.1.

Table A.8. VS starting model and solutions for OSH site.

Layer number	Poisson's ratio	Density, kg/m^3	Thickness, m	Starting model VS, m/s	Solutions	
					LI VS, m/s	SA-LI VS, m/s
1	0.3	1700	0.46	130	172	172
2	0.3	1700	0.70	234	359	360
3	0.3	1700	1.06	266	274	273
4	0.3	1700	1.61	312	485	496
5	0.3	1700	2.45	385	465	453
6	0.3	1700	3.74	471	789	840
7	0.3	1700	5.69	564	680	649
8	0.3	1700	8.65	646	1079	1161
9	0.3	1700	13.17	710	762	738
10	0.3	1700	20.05	765	926	922
Halfspace	0.3	1700	N/A	858	1614	1789

a)

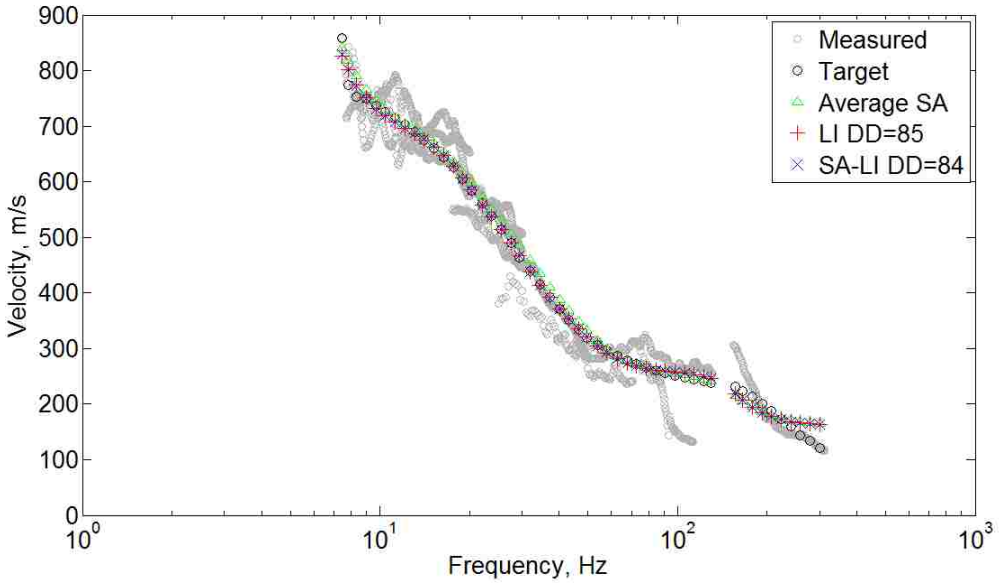

b) Well no. 1152 c) d)

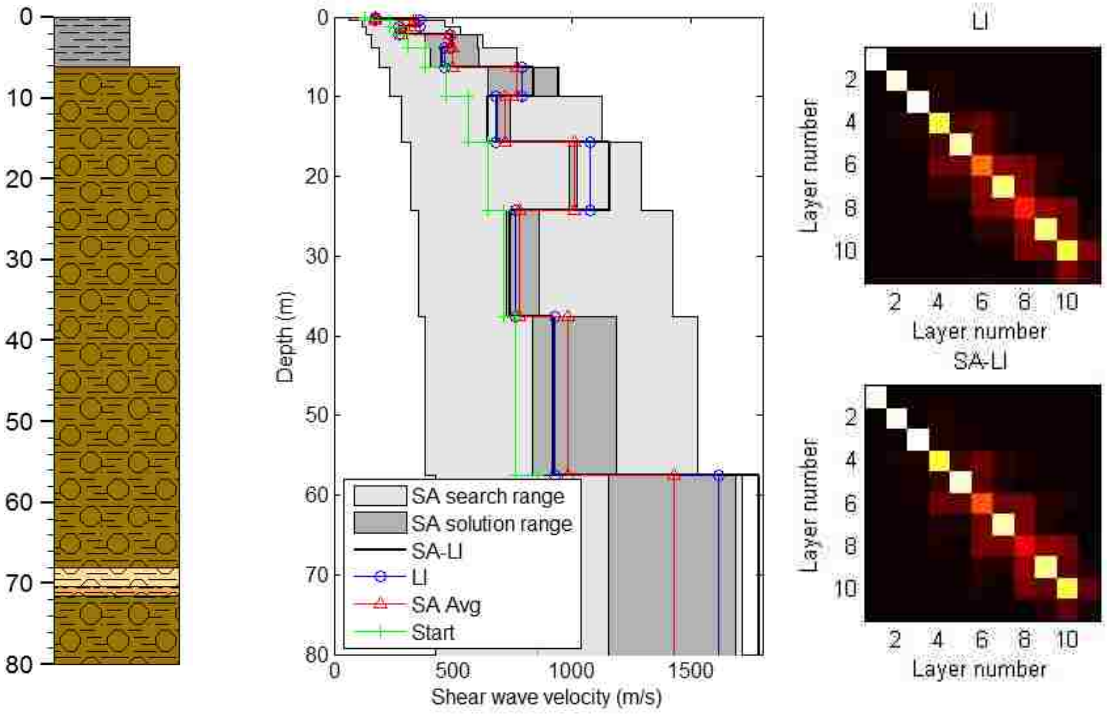

Figure A.16. Data and solutions for OSH site: a) dispersion curves, b) well log information, c) VS profiles, and d) resolution matrices.

Data and solutions for SFB site

Figure A.17. Location of SFB, a fine SRU site: array locations (yellow lines) with respect to nearby wells (black triangles). Longitude and latitude listed on Table 2.1.

Table A.9. VS starting model and solutions for SFB site.

Layer number	Poisson's ratio	Density, kg/m^3	Thickness, m	Starting model VS, m/s	Solutions	
					LI VS, m/s	SA-LI VS, m/s
1	0.3	1700	1.44	353	370	370
2	0.3	1700	1.89	412	475	474
3	0.3	1700	2.49	494	1052	1047
4	0.3	1700	3.27	477	343	346
5	0.3	1700	4.29	450	485	483
6	0.3	1700	5.64	448	607	605
7	0.3	1700	7.41	452	473	472
8	0.3	1700	9.73	462	540	550
9	0.3	1700	12.78	471	387	376
10	0.3	1700	16.78	501	640	669
11	0.3	1700	22.05	555	892	907
Halfspace	0.3	1700	N/A	595	1025	990

a)

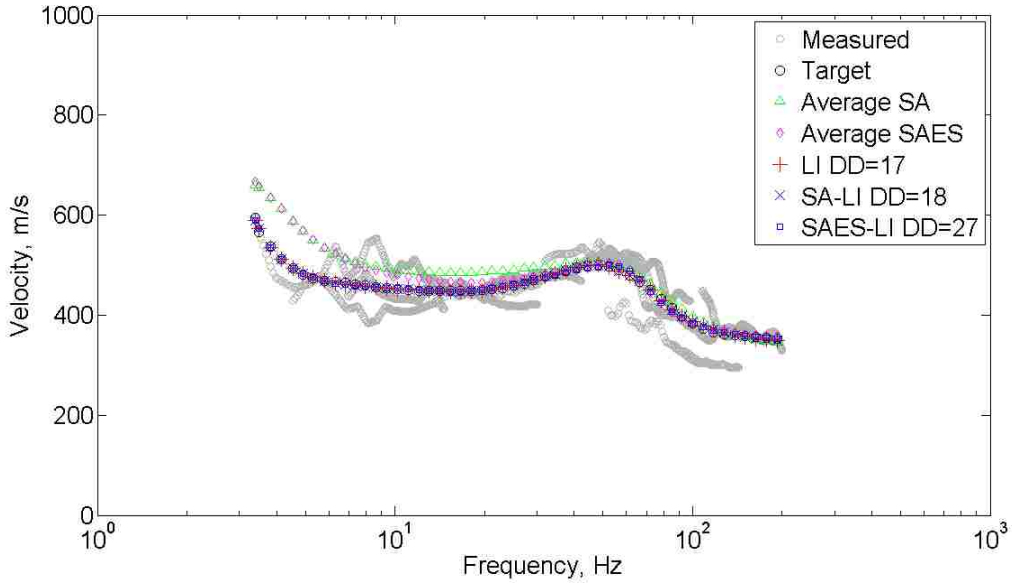

b) Well no. 741 and B-1

c)

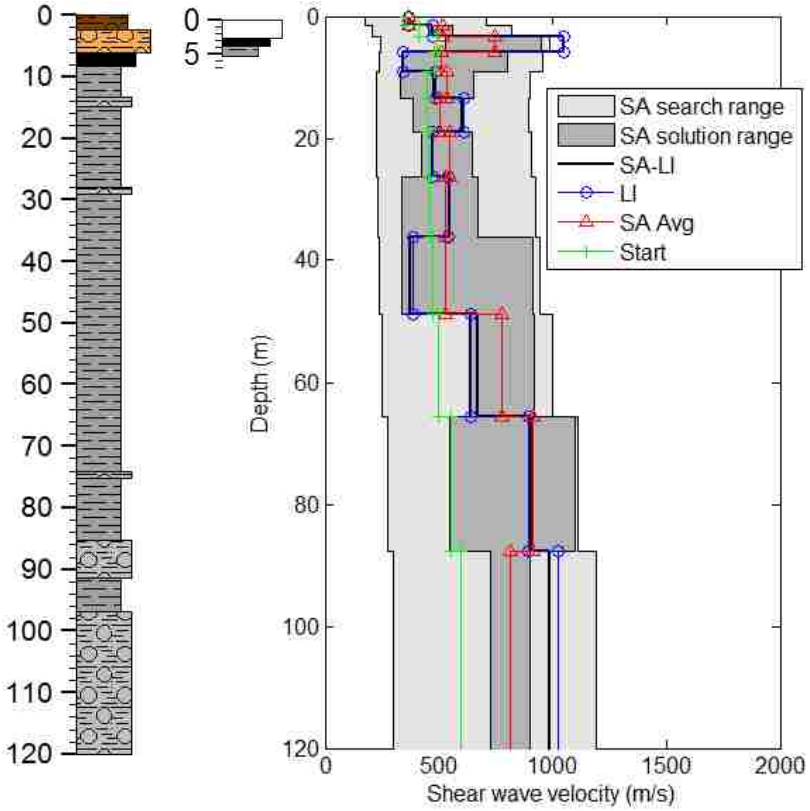

d)

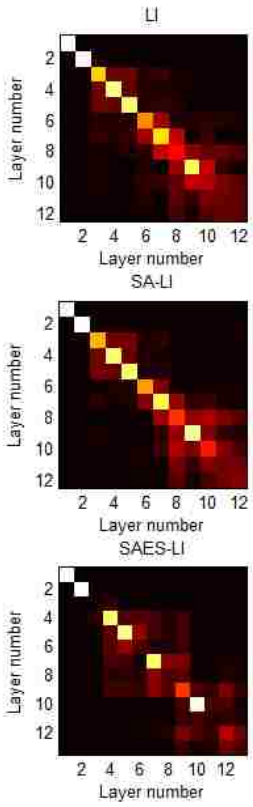

Figure A.18. Data and solutions for SFB site: a) dispersion curves, b) well log information, c) VS profiles, and d) resolution matrices.

Table A.10. VS starting model and solution for SFB site with an explicit search performed for the stiff layer.

Layer number	Poisson's ratio	Density, kg/m^3	Thickness, m	SAES-LI Solution VS, m/s
1	0.3	1700	1.44	375
2	0.3	1700	1.58	443
3	0.25	2200	0.63	1529
4	0.3	1700	2.16	802
5	0.3	1700	3.27	359
6	0.3	1700	4.29	736
7	0.3	1700	5.64	343
8	0.3	1700	7.41	692
9	0.3	1700	9.73	586
10	0.3	1700	12.78	337
11	0.3	1700	16.78	861
12	0.3	1700	22.05	782
Halfspace	0.3	1700	N/A	1109

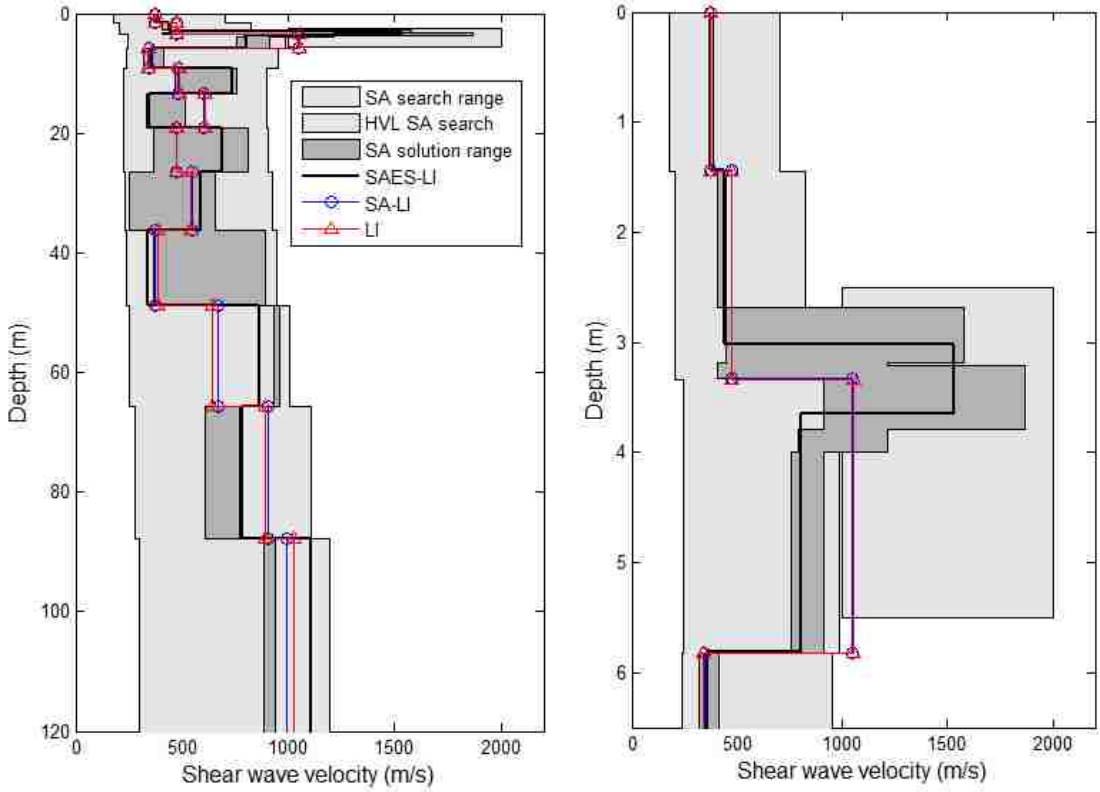

Figure A.19. HVL site 2 (SFB), comparison of LI solution to solution resolved using explicit search for stiff layer, (a) VS profiles from LI and SAES-LI and (b) expanded view of upper 6 m.

Data and solutions for SMS site

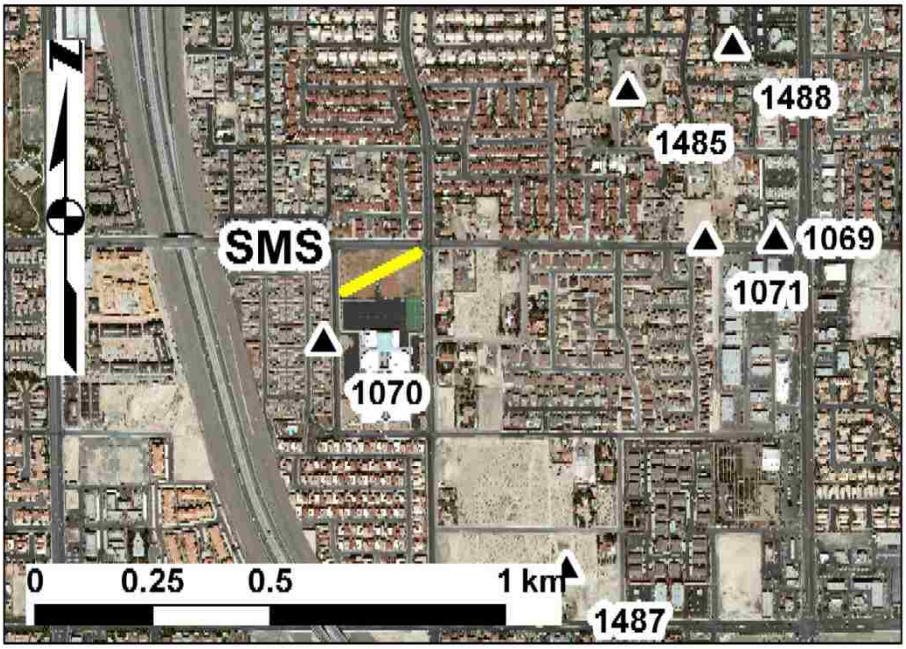

Figure A.20. Location of SMS, a fine SRU site: array locations (yellow lines) with respect to nearby wells (black triangles). Longitude and latitude listed on Table 2.1.

Table A.11. VS starting model and solutions for SMS site.

Layer number	Poisson's ratio	Density, kg/m^3	Thickness, m	Starting model VS, m/s	Solutions	
					LI VS, m/s	SA-LI VS, m/s
1	0.3	1700	0.22	190	180	224
2	0.3	1700	0.35	190	166	192
3	0.3	1700	0.69	229	475	417
4	0.3	1700	1.06	211	173	176
5	0.3	1700	1.51	217	230	236
6	0.3	1700	2.17	245	305	246
7	0.3	1700	3.11	268	234	339
8	0.3	1700	4.00	301	362	259
9	0.3	1700	6.85	345	431	541
10	0.3	1700	9.16	396	305	302
11	0.3	1700	14.90	524	1107	1048
12	0.3	1700	19.34	600	1397	1463
Halfspace	0.3	1700	N/A	600	1252	1452

Table A.12. VS profiles derived from the average of three separate SA-LI runs for SMS site. Method used to obtain better fit of target DC. SA-LI AVG was used in 3-D VS model.

Layer number	Thickness, m	Solutions			
		SA-LI 1	SA-LI 2	SA-LI 3	SA-LI AVG VS, m/s
1	0.22	201	191	280	224
2	0.35	162	166	249	192
3	0.69	475	423	353	417
4	1.06	170	199	160	176
5	1.51	236	212	259	236
6	2.17	263	257	217	246
7	3.11	297	331	390	339
8	4.00	271	249	256	259
9	6.85	518	595	510	541
10	9.16	299	294	312	302
11	14.90	1066	1160	920	1048
12	19.34	1476	1499	1413	1463
Halfspace	N/A	1467	1483	1408	1452

a)

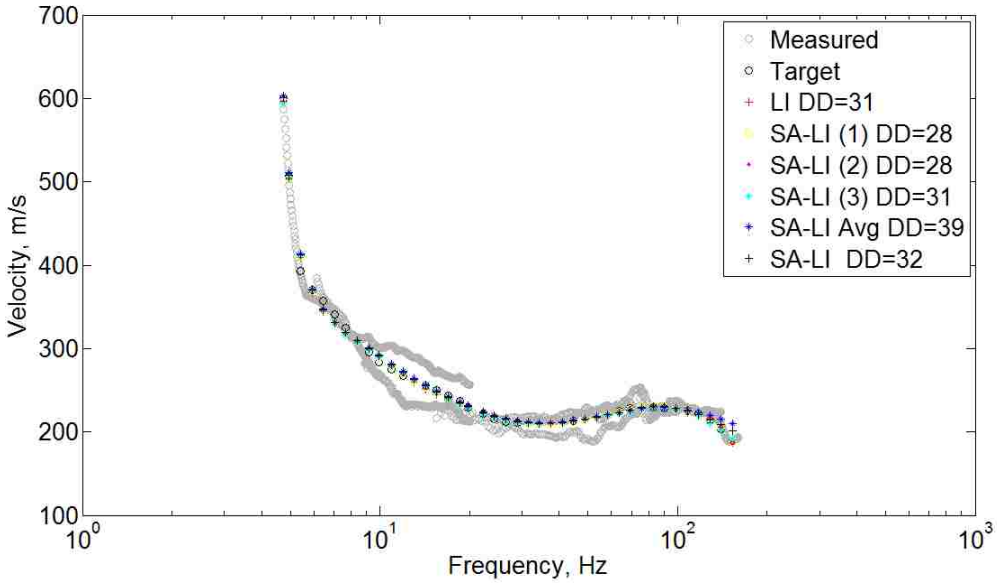

b) Well no. 1070 c)

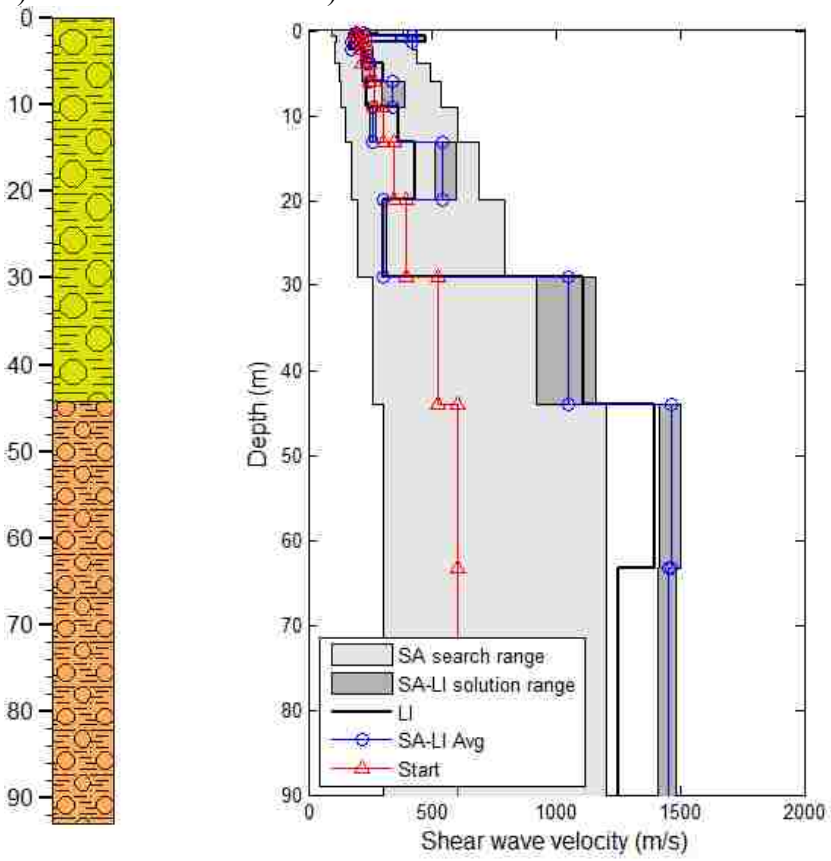

Figure A.21. Data and solutions for SMS site: a) dispersion curves, b) well log information, c) VS profiles.

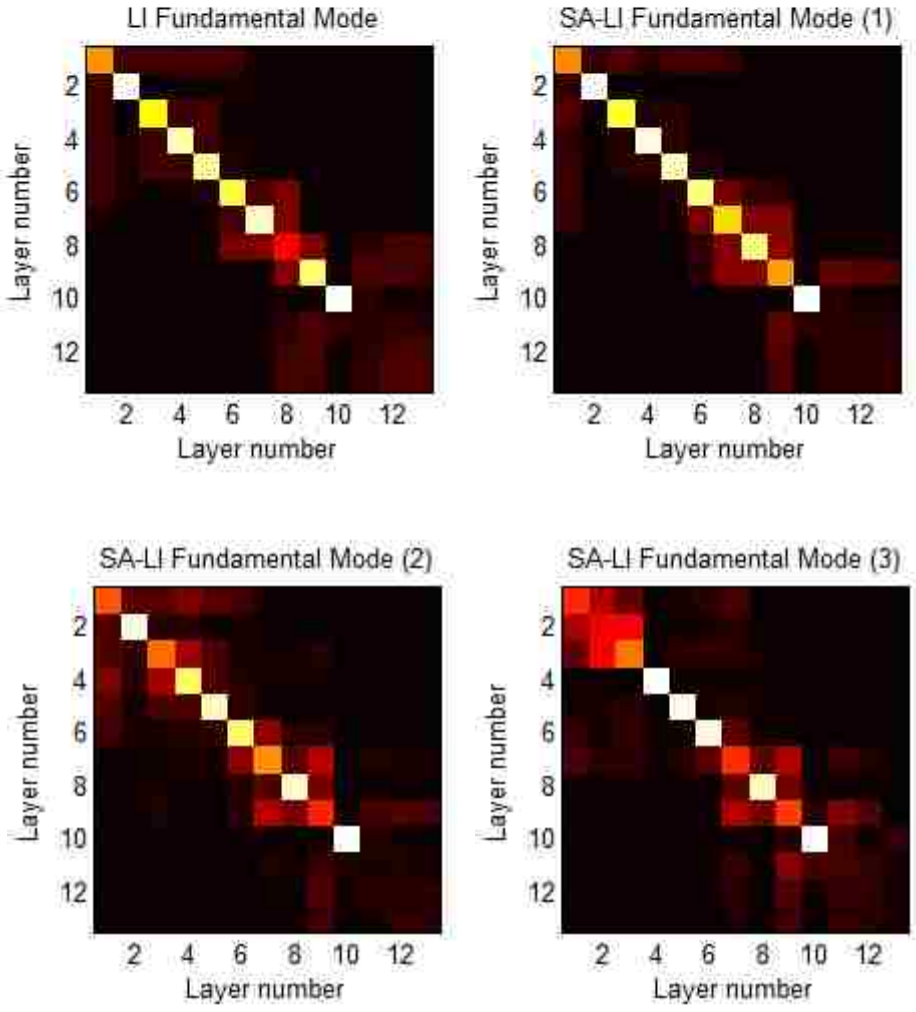

Figure A.22. Resolution matrices for SMS site: LI and SA-LI optimizations 1, 2, and 3.

Data and solutions for SPS site

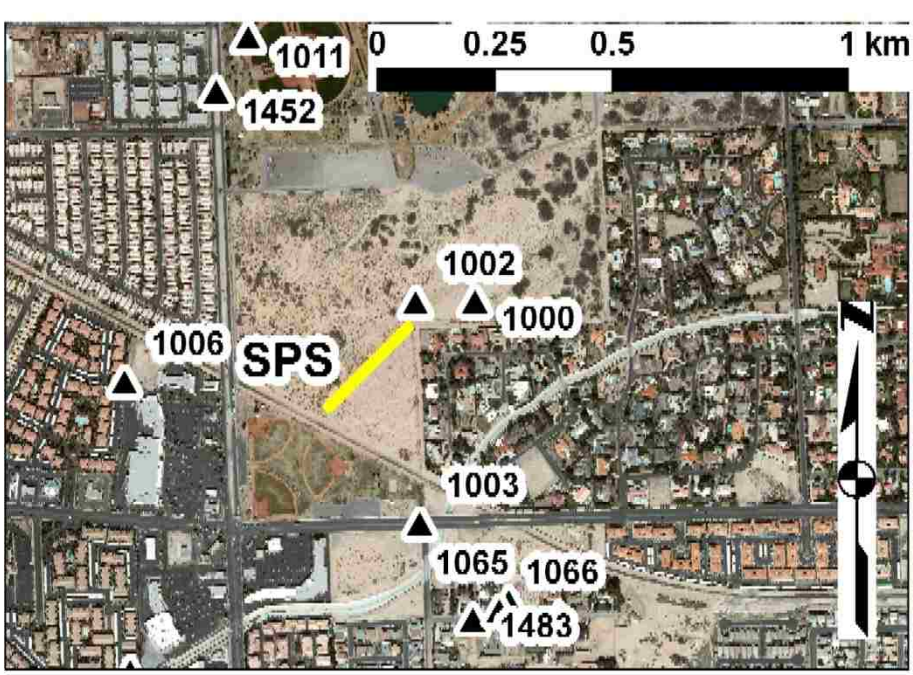

Figure A.23. Location of SPS, a fine SRU site: array locations (yellow lines) with respect to nearby wells (black triangles). Longitude and latitude listed on Table 2.1.

Table A.13. VS starting model and solutions for SPS site.

Layer number	Poisson's ratio	Density, kg/m^3	Thickness, m	Starting model VS, m/s	Solutions	
					LI VS, m/s	SA-LI VS, m/s
1	0.3	1700	0.31	155	151	150
2	0.3	1700	0.53	164	187	189
3	0.3	1700	0.91	191	235	232
4	0.3	1700	1.57	229	291	298
5	0.3	1700	2.69	249	311	302
6	0.3	1700	4.62	267	288	296
7	0.3	1700	11.07	308	355	347
8	0.3	1700	10.45	331	367	375
9	0.3	1700	23.33	420	738	729
10	0.3	1700	40.03	592	1067	1052
Halfspace	0.3	1700	N/A	670	1175	1262

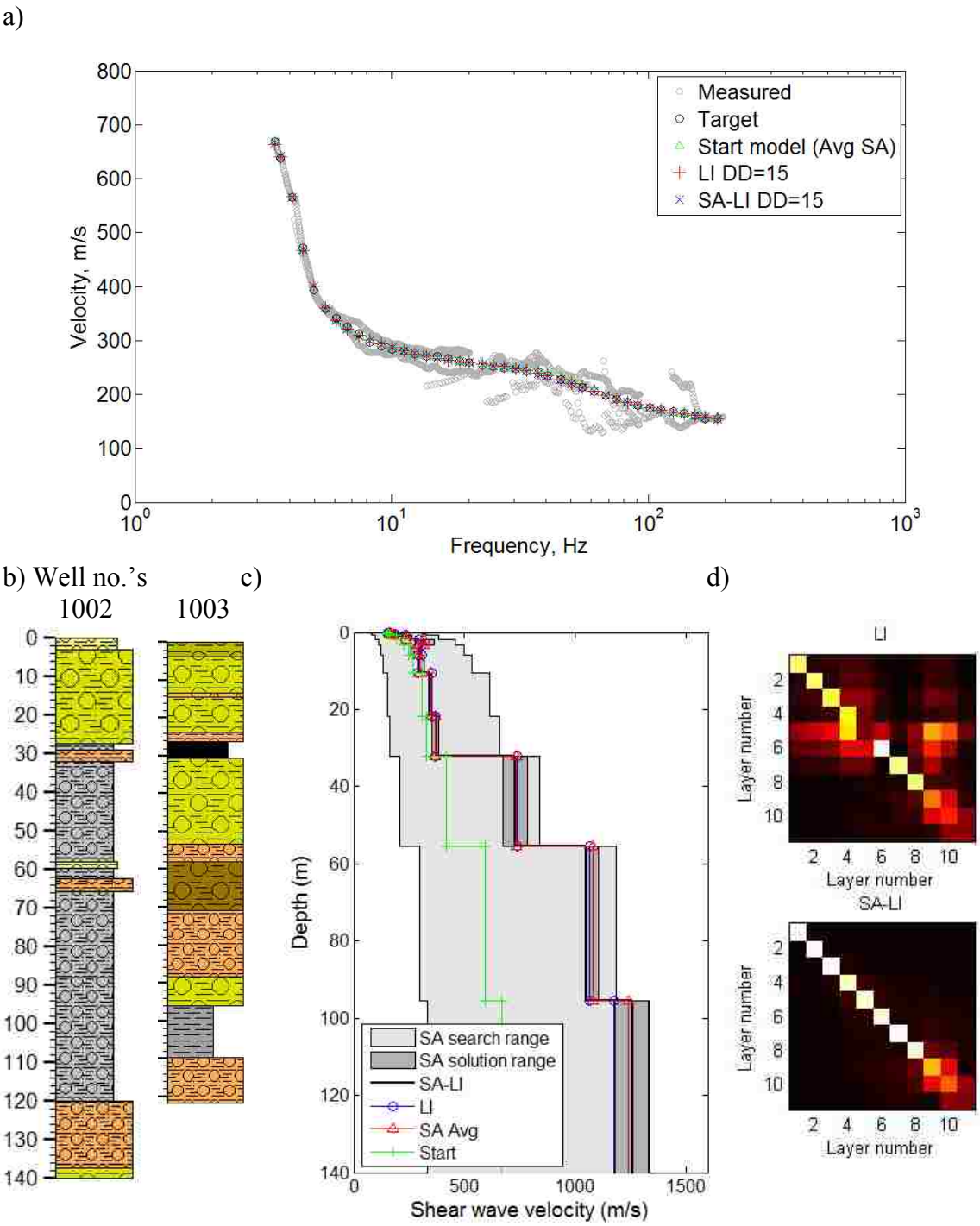

Figure A.24. Data and solutions for SPS site: a) dispersion curves, b) well log information, c) VS profiles, and d) resolution matrices.

Data and solutions for WLE site

Figure A.25. Location of WLE, a fine SRU site: array locations (yellow lines) with respect to nearby wells (black triangles). Longitude and latitude listed on Table 2.1.

Table A.14. VS starting model and solutions for WLE site.

Layer number	Poisson's ratio	Density, kg/m^3	Thickness, m	Starting model VS, m/s	Solutions	
					LI VS, m/s	SA-LI VS, m/s
1	0.3	1700	0.51	68	79	79
2	0.3	1700	0.77	112	179	181
3	0.3	1700	1.18	177	512	429
4	0.3	1700	1.79	248	658	820
5	0.3	1700	2.73	304	289	245
6	0.3	1700	4.15	320	329	459
7	0.3	1700	6.32	328	465	379
8	0.3	1700	9.62	344	323	354
9	0.3	1700	14.64	369	396	373
10	0.3	1700	22.28	432	736	729
Halfspace	0.3	1700	N/A	485	873	1019

a)

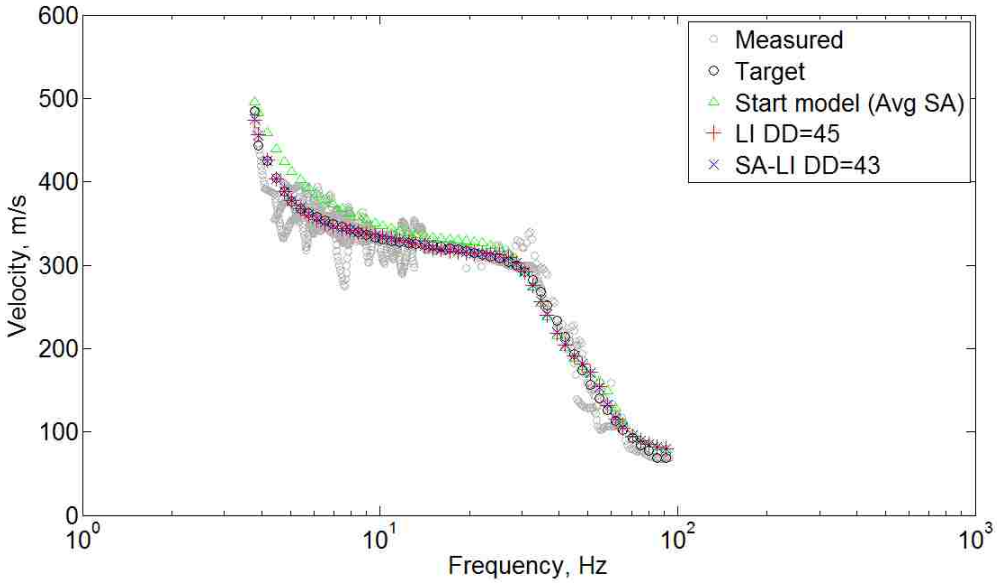

b) Well no. 840 c) d)

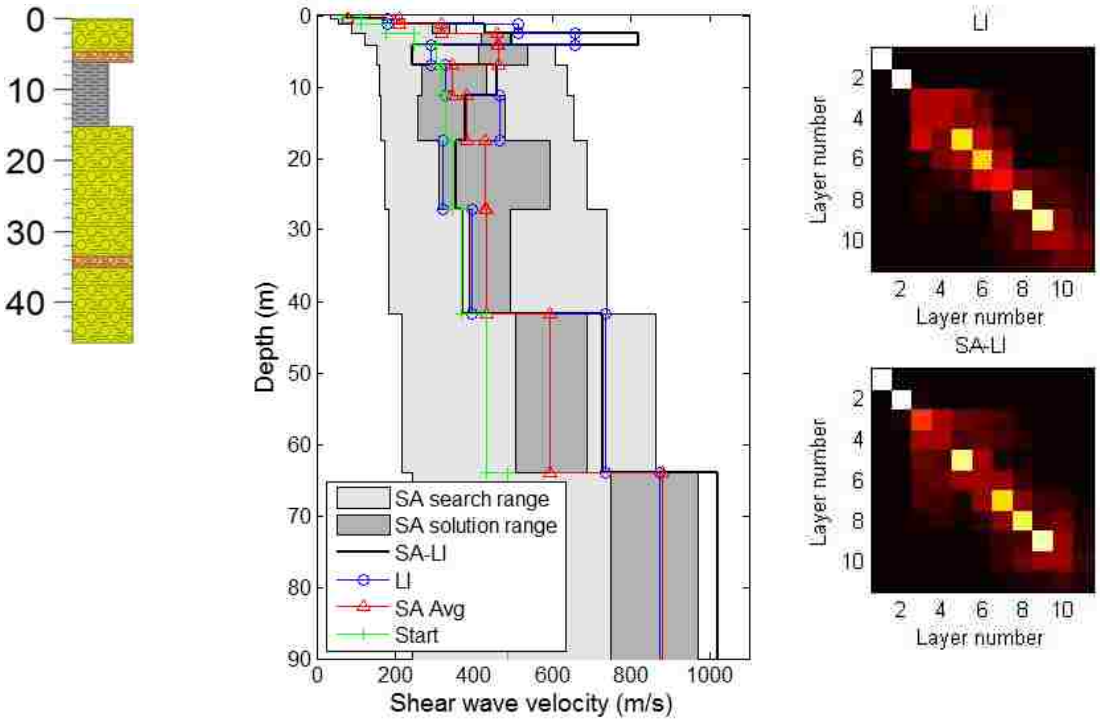

Figure A.26. Data and solutions for WLE site: a) dispersion curves, b) well log information, c) VS profiles, and d) resolution matrices.

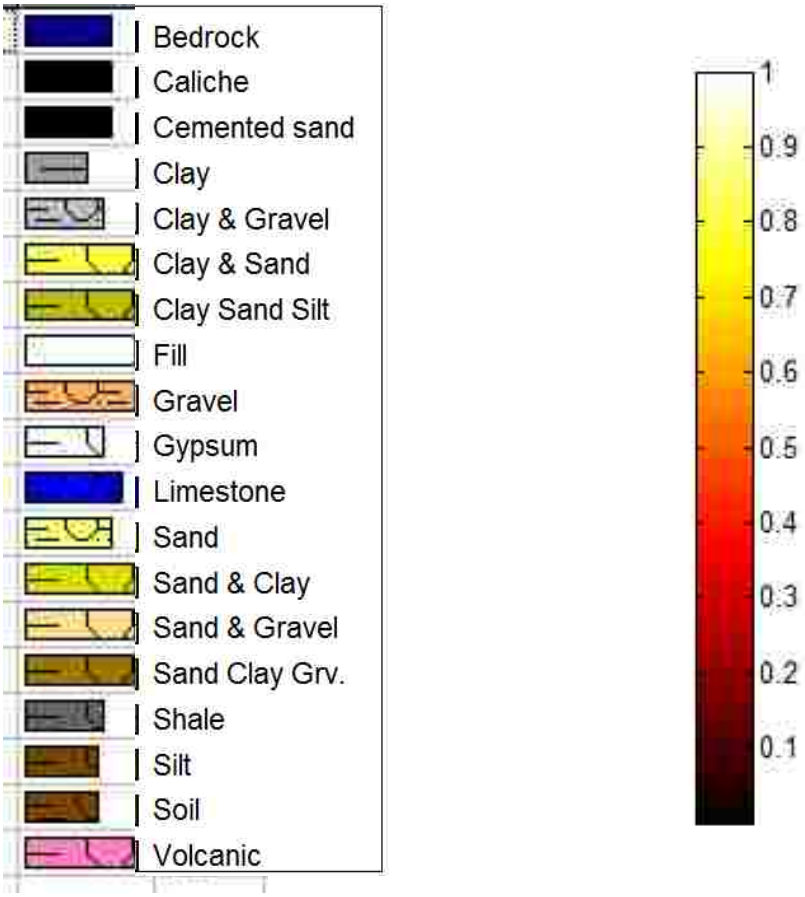

Figure A.27. Sediment and lithology key (left); resolution matrix key (right).

APPENDIX B

CORRELATION DATASET

VS measurement locations used in the correlation dataset and their nearest wells are listed in this appendix.

Table B.1 List of shear-wave velocity profiles used in the VS-sediment correlation, and wells within the correlation distance.

	VS measurement site				Well site				
	Site designation	**Longitude, degree W**	**Latitude, degree N**	**Total depth, m**	**UNLV well no.**	**Longitude, degree W**	**Latitude, degree N**	**Total depth, m**	**No. wells in correlation distance**
1	034RS1	115.31673	36.08219	30.48	D6	115.319	36.08361	578.23	1
2	038RS1	115.24438	36.07978	45.72	695	115.246	36.07780	182.88	3
					1380	115.245	36.07783	182.88	
					1545	115.247	36.07860	153.92	
3	0P3RS2	115.26872	36.01415	38.1	D12	115.268	36.01778	215.49	1
4	0P3RS3	115.26785	36.01716	45.72	D12	115.268	36.01778	215.49	1
5	0P4RS1	115.18892	36.02309	45.72	1093	115.188	36.02500	91.44	2
					1577	115.188	36.02111	60.96	
6	0P4RS2	115.18794	36.02000	45.72	1577	115.188	36.02111	60.96	2
					1578	115.186	36.02111	106.68	
7	142RS1	115.16158	36.13312	76.20	715	115.161	36.13560	397.76	1
8	211RS1	115.21044	36.00052	60.96	967	115.211	36.00073	131.06	2
					1428	115.213	35.99972	131.06	
9	211RS2	115.21391	36.00050	60.96	966	115.217	36.00097	139.00	3
					967	115.211	36.00073	131.06	
					1428	115.213	35.99972	131.06	
10	213RS2	115.29299	36.02430	45.72	984	115.293	36.02077	182.88	1
11	221RS2	115.25046	36.05153	54.86	D5	115.250	36.04889	495.91	3
					903	115.251	36.05000	192.02	
					1547	115.249	36.05110	194.46	

	VS measurement site				Well site				
	Site designation	Longitude, degree W	Latitude, degree N	Total depth, m	UNLV well no.	Longitude, degree W	Latitude, degree N	Total depth, m	No. wells in correlation distance
12	221RS3	115.25605	36.04964	54.86	1389	115.255	36.05055	192.02	2
					1548	115.255	36.05028	198.12	
13	221RS4	115.25169	36.04218	111.25	902	115.251	36.04030	201.17	3
					1390	115.250	36.04111	201.17	
					1549	115.254	36.04194	216.41	
14	222RS1	115.15562	36.03602	76.20	1560	115.156	36.03805	76.20	10
					1561	115.156	36.03778	67.06	
					1563	115.156	36.03694	39.62	
					1564	115.157	36.03610	76.20	
					1566	115.157	36.03833	76.20	
					1567	115.158	36.03583	91.44	
					1568	115.159	36.03583	121.92	
					1569	115.157	36.03556	85.34	
					1570	115.156	36.03444	91.44	
					1571	115.157	36.03805	82.30	
15	252RS1	115.27755	36.01021	45.72	977	115.276	36.00830	190.20	1
16	253RS1	115.30810	36.29761	45.72	280	115.307	36.29805	181.36	2
					284	115.307	36.29580	198.12	
17	291RS1	115.21952	36.03097	38.10	907	115.219	36.03060	152.40	5
					1391	115.219	36.03095	136.55	
					1394	115.222	36.03083	123.75	
					1550	115.221	36.03167	143.26	
					1554	115.220	36.03361	152.40	

	VS measurement site				Well site				
	Site designation	Longitude, degree W	Latitude, degree N	Total depth, m	UNLV well no.	Longitude, degree W	Latitude, degree N	Total depth, m	No. wells in correlation distance
18	312RS1	115.16859	36.12424	45.72	726	115.169	36.12444	256.03	1
19	312RS2	115.16698	36.12400	45.72	726	115.169	36.12444	256.03	2
					727	115.165	36.12444	257.56	
20	312RS3	115.16762	36.12410	45.72	726	115.169	36.12444	256.03	2
					727	115.165	36.12444	257.56	
21	312RS4	115.16950	36.12343	45.72	726	115.169	36.12444	256.03	1
22	312RS5	115.16829	36.12501	45.72	726	115.169	36.12444	256.03	1
23	312RS6	115.16898	36.12416	28.65	726	115.169	36.12444	256.03	1
24	331RS1	115.17468	36.04065	60.96	1045	115.179	36.04170	67.67	2
					1054	115.172	36.04376	91.44	
25	342RS2	115.21751	36.00049	76.20	966	115.217	36.00097	139.00	2
					1427	115.218	36.00027	139.00	
26	342RS3	115.21103	36.00121	76.20	967	115.211	36.00073	131.06	2
					1428	115.213	35.99972	131.06	
27	351RS1	115.18682	36.06654	45.72	1461	115.187	36.06611	91.44	1
28	ANNSS1	115.31144	36.26443	409.72	118	115.315	36.26490	230.12	4
					125	115.310	36.26270	152.40	
					1313	115.311	36.26264	152.40	
					1314	115.311	36.26666	214.27	
29	C02RS1	115.10285	36.02007	45.72	1516	115.105	36.02083	91.44	1
30	C09RS1	115.04869	36.04045	30.48	1152	115.046	36.04030	213.36	1
31	C24RS1	115.24844	35.98711	65.53	1443	115.247	35.98583	201.17	1

	VS measurement site				Well site				
	Site designation	Longitude, degree W	Latitude, degree N	Total depth, m	UNLV well no.	Longitude, degree W	Latitude, degree N	Total depth, m	No. wells in correlation distance
32	C24RS2	115.24532	35.98539	91.44	989	115.246	35.98330	201.17	2
					1443	115.247	35.98583	201.17	
33	C49RS1	115.24829	36.05810	36.58	895	115.246	36.05586	198.12	2
					1384	115.245	36.05583	198.12	
34	D11RS1	115.25693	36.03245	30.48	915	115.256	36.03223	213.36	1
35	D13RS1	115.29055	36.00720	38.10	1434	115.294	36.00694	201.17	1
36	D13RS2	115.29504	36.00723	38.10	1434	115.294	36.00694	201.17	1
37	D17RS1	115.22888	36.12646	45.72	1374	115.227	36.12861	237.74	1
38	D1HRS1	115.10207	36.01938	30.48	1106	115.103	36.01670	121.92	2
38					1516	115.105	36.02083	91.44	
39	D32RS1	115.23487	36.28515	76.20	298	115.236	36.28320	178.31	2
					336	115.236	36.28550	178.31	
40	D32RS2	115.23211	36.28627	76.20	332	115.231	36.28690	121.92	1
41	D35RS1	115.25081	36.14304	76.20	666	115.252	36.14200	129.54	1
42	D3FRS1	115.02038	36.27352	30.48	1208	115.018	36.27444	137.16	1
43	D50RS1	115.13831	36.01446	45.72	1099	115.138	36.01250	91.44	2
					1509	115.138	36.01499	91.44	
44	DOESS1	115.14576	36.21086	205.63	857	115.147	36.21098	60.96	1
45	E16RS2	115.03499	36.05408	76.20	1154	115.038	36.05280	73.15	1
46	E48RS1	115.16137	36.06696	45.72	1021	115.161	36.06810	152.40	2
					1458	115.160	36.06528	48.77	
47	GRPSS1	115.26452	36.10362	52.51	682	115.263	36.10580	283.46	2
					1544	115.263	36.10583	228.60	

	VS measurement site				Well site				
	Site designation	Longitude, degree W	Latitude, degree N	Total depth, m	UNLV well no.	Longitude, degree W	Latitude, degree N	Total depth, m	No. wells in correlation distance
48	LESSS1	115.06879	36.23682	84.13	620	115.072	36.23850	304.80	1
49	LMNSS1	115.24608	36.24623	124.24	450	115.244	36.24520	106.68	3
					451	115.244	36.24620	110.34	
					454	115.243	36.24690	106.68	
50	LVSCS1	115.18957	36.171619	30.00	606	115.188	36.17380	365.46	1
51	lvspref	115.19116	36.172305	49.85	603	115.186	36.17390	304.80	3
					605	115.196	36.17390	305.41	
					606	115.188	36.17380	365.46	
52	LVSRS1	115.18163	36.17355	200.00	554	115.180	36.17440	390.14	2
					557	115.182	36.17360	393.19	
53	LVSSS1	115.18698	36.17524	32.50	603	115.186	36.17390	304.80	3
					603	115.186	36.17390	304.80	
					606	115.188	36.17380	365.46	
54	LVSSS2	115.18532	36.17501	19.27	603	115.186	36.17390	304.80	2
					606	115.188	36.17380	365.46	
55	LVSSS3	115.19113	36.17275	58.67	603	115.186	36.17390	304.80	3
					605	115.196	36.17390	305.41	
					606	115.188	36.17380	365.46	
56	LVSSS4	115.18846	36.175501	41.71	603	115.186	36.17390	304.80	2
					606	115.188	36.17380	365.46	
57	LVSSS6	115.18921	36.17039	47.00	603	115.186	36.17390	304.80	3
					606	115.188	36.17380	365.46	
					608	115.188	36.16760	341.38	

	VS measurement site				Well site				
	Site designation	Longitude, degree W	Latitude, degree N	Total depth, m	UNLV well no.	Longitude, degree W	Latitude, degree N	Total depth, m	No. wells in correlation distance
58	NLPSS1	115.19516	36.16206	80.67	607	115.190	36.16040	362.71	1
59	SMSSS1	115.12914	36.03428	84.46	1070	115.130	36.03335	92.96	1
60	SPSSS1	115.11587	36.05920	127.36	1002	115.114	36.06110	152.40	1
61	transect2002A	115.14854	36.17900	148.20	892	115.149	36.17712	281.94	1
62	transect2002B	115.14854	36.17693	200.00	892	115.149	36.17712	281.94	1
63	transect2002C	115.14854	36.17486	176.80	892	115.149	36.17712	281.94	1
64	transect2102A	115.16019	36.15739	400.00	707	115.160	36.15690	164.59	1
65	transect2102B	115.16113	36.15537	400.00	707	115.160	36.15690	164.59	1
66	transect2102C	115.16206	36.15334	197.10	707	115.160	36.15690	164.59	1
67	transect2200A	115.17900	36.13524	400.00	713	115.177	36.13470	152.40	1
68	transect2200B	115.17987	36.13301	202.30	713	115.177	36.13470	152.40	1
69	transect2201C	115.17775	36.13733	226.90	713	115.177	36.13470	152.40	1
70	transect2203C	115.18558	36.12345	269.70	1438	115.188	36.12295	76.20	1
71	transect2501A	115.19000	36.12146	173.50	1438	115.188	36.12295	76.20	1
72	transect2501B	115.18992	36.11921	200.00	1437	115.187	36.11815	158.50	1
73	transect2501C	115.18983	36.11696	234.20	1437	115.187	36.11815	158.50	1
74	transect2502A	115.15530	36.16715	225.00	610	115.157	36.16880	268.83	1
75	transect2502B	115.15623	36.16500	179.60	610	115.157	36.16880	268.83	1
76	transect2503C	115.15386	36.16909	187.20	610	115.157	36.16880	268.83	1

Table B.2 List of shear-wave velocity profiles that are shallower than any well within the correlation distance. Nearby wells that are deeper than the profile and their approximate distance from the profile are also listed.

VS measurement location and bottom depth			Closest well location and depth and closest, deeper well				
Easting, UTM	**Northing, UTM**	**Profile bottom, m**	**UNLV well No.**	**Latitude, degree N**	**Longitude, degree W**	**Well bottom, m**	**Separation distance, m**
666166.821	3989316.740	76	1563	36.037	115.156	40	104
			1564	36.036	115.157	76	within 300 m
			1569	36.036	115.157	85	within 300 m
			1570	36.034	115.156	91	within 300 m
676995.826	3991532.950	76	1154	36.053	115.038	73	267
			well depth is within 3 m of profile depth				
657595.015	4012484.805	124	451	36.246	115.244	110	223
			595	36.251	115.242	175	within 700 m
662892.863	3998735.945	174	1438	36.123	115.188	76	257
			729	36.128	115.173	367	within 2000 m
			730	36.130	115.196	259	within 2000 m
			733	36.110	115.177	332	within 2000 m
662905.010	3998486.490	200	1437	36.118	115.187	158	291
			729	36.128	115.173	367	within 2000 m
			730	36.130	115.196	259	within 2000 m
			733	36.110	115.177	332	within 2000 m
663780.897	4000034.795	202	713	36.135	115.177	152	291
			714	36.136	115.166	436	within 2000 m
			729	36.128	115.173	367	within 2000 m
			730	36.130	115.196	259	within 2000 m

VS measurement location and bottom depth			Closest well location and depth and closest, deeper well				
Easting, UTM	**Northing, UTM**	**Profile bottom, m**	**UNLV well No.**	**Latitude, degree N**	**Longitude, degree W**	**Well bottom, m**	**Separation distance, m**
666685.074	4008728.965	206	857	36.211	115.147	61	69
			586	36.209	115.148	223	within 325 m
			587	36.216	115.140	372	within 800 m
663966.140	4000517.476	227	713	36.135	115.177	152	293
			714	36.136	115.166	436	within 2000 m
			729	36.128	115.173	367	within 2000 m
			730	36.130	115.196	259	within 2000 m
662917.157	3998237.034	234	1437	36.118	115.187	158	291
			729	36.128	115.173	367	within 2000 m
			730	36.130	115.196	259	within 2000 m
			733	36.110	115.177	332	within 2000 m
663286.254	3998964.298	270	1438	36.123	115.188	76	209
			729	36.128	115.173	367	within 2000 m
			730	36.130	115.196	259	within 2000 m
			733	36.110	115.177	332	within 2000 m
665500.411	4002772.495	400	707	36.157	115.160	165	54
			607	36.160	115.190	363	within 3000 m
			600	36.178	115.169	270	within 3000 m
			601	36.178	115.168	274	within 3000 m
665420.392	4002546.445	400	707	36.157	115.160	165	190
			717	36.139	115.146	622	within 3000 m
			554	36.174	115.180	390	within 3000 m

VS measurement location and bottom depth			Closest well location and depth and closest, deeper well				
Easting, UTM	**Northing, UTM**	**Profile bottom, m**	**UNLV well No.**	**Latitude, degree N**	**Longitude, degree W**	**Well bottom, m**	**Separation distance, m**
663853.957	4000283.259	400	713	36.135	-115.177	152	156
			729	36.128	-115.173	367	within 1000
			714	36.136	-115.166	436	within 1200 m
651686.498	4014399.398	410	1313	36.263	-115.311	152	208
			118	36.265	-115.315	230	within 300 m
			1314	36.267	-115.311	214	within 300 m

APPENDIX C

ESTABLISHING CREDIBLE VS RANGES FOR LVV SEDIMENT TYPES

Correlations were made between shear-wave velocity (VS) and sediment lithology using a 3-D sediment model of the Las Vegas Valley (LVV), created from over 1400 well logs and other available geologic information (Taylor et al., 2008), and a dataset of 74 VS profiles developed for the LVV (Luke et al., 2010). As part of the correlation process, credible shear-wave velocity ranges were established for the Clay, Gravel, Sand and Mixed units of the sediment-lithology model. As discussed below, the VS ranges were needed because of the heavily carbonate-cemented fines, sand or gravel, locally known as caliche, that occur in the LVV. While caliche is typically located in the western and central portions of the valley (Wyman et al., 1993), it has also been found at other locations throughout the valley (Taylor et al., 2008). Thicknesses can range from a few centimeters to 2 to 3 m (Wyman et al., 1993) and can vary within relatively short distances (e.g. Taylor et al., 2008; Stone and Luke, 2001). The strength and stiffness of caliche can be as high as concrete; thus caliche can have a high in situ VS, 1000 to 2000 m/s (Werle and Luke, 2007; Tecle et al., 2003).

The heterogeneous nature of caliche can result in anomalously high VS values for the sediment units in the correlation dataset because a cemented layer occurring at a site where VS was measured may not be present at the nearest well site. In other words, a high velocity is measured and then extrapolated to the well site that does not have high-velocity cementation. Additionally, the wells were logged for various reasons and by different people; therefore, a well site may have heavy cementation that was not logged.

By establishing credible ranges for VS, we can filter the high VS values that do not represent the uncemented clay, gravel, sand and mixed units of the 3-D sediment-lithology model from the data used for sediment-lithology correlation.

To establish the credible VS ranges, depth versus velocity scatter plots were created by querying the 3-D sediment model (Taylor et al., 2008) at each VS profile located within a specified distance (referred to as the correlation distance) of a well log: 300 m for the Clay, Gravel and Sand units; 500 m for the Mixed unit (Luke at al., 2010). From these plots, shown in Figure C.1, and from site specific information, typical ranges of VS were visually identified. These ranges were depth dependent; therefore, we defined depth-dependent upper boundaries of VS. These boundaries were used to filter data from the correlation dataset that appeared to be non-representative of the uncemented sediments.

Once defined, the upper-limit velocity boundaries were checked against VS depths and ranges for clay, gravel and sand reported in the literature (Table C.1 and Figure C.2). For the reported values, we observed that VS ranges overlapped across the different sediment types and that the ranges reported for a sediment type varied depending upon the reference (Figure C.2). For cases where depth was reported, VS tended to increase with depth. Overall, we determined the boundaries we established for credible VS ranges for sediments in the LVV were supported by the velocity ranges reported in the literature.

The following sections describe the selection of upper-limit velocity boundaries for each sediment unit and compare the values to VS values previously published.

Clay-sediment velocity:

The scatter plot developed for the Clay unit consists of data from 39 VS profiles (Figure C.1). In general, VS for the Clay unit tends to increase with depth. Above 50 m, VS is typically between 100 and 1000 m/s; below this depth VS is typically between 400 and 1300 m/s. Locations of sites with data that are outside these ranges are shown in Figure C.3. Three sites have VS greater than 1000 m/s for depths between 0 and 50 m. Two of these are located near the margins of the valley and both are within 1 km of a rock outcrop. The third is located in the fine-sediment-response unit (fine SRU; Luke and Liu, 2008) near the center of the valley (the I515/I15 interchange). Three additional sites have VS greater than 1300 m/s for depths below 50 m. All three are located in the fine SRU along Las Vegas Blvd near the center of the valley.

For the sites near rock outcrops, we expect that the relatively high VS values are representative of the rock and not the nearby clay. For sites in the fine SRU, we expect that the relatively high VS values are local to these sites due to the nature of caliche formation, especially, its lateral variability. In other words, the high VS values are more likely a measurement of a dense material at the site rather than being generally representative of the Clay unit.

In a study comparing geophysical methods to characterize alluvial soils in the Las Vegas Valley, Sundquist (2001) developed VS profiles for nine sites within a 0.3 km^2 area at the Las Vegas Springs Preserve, a location in the predominantly clay area of the valley, using the Spectral Analysis of Surface Waves method (SASW; Stokoe et al., 1994). He reported a range of VS values for clay between 260 and 860 m/s over depths from the ground surface to 30 m. The velocities in the individual profiles generally

increased with depth; however, the velocity at a specific depth at one site did not closely match the velocity at that same depth at another site. For example, one site had a VS of 400 m/s at 10 m deep while another had a VS of 300 m/s. Wong et al. (2002) present average VS profiles for four surficial geologic units, which were developed from downhole and surface-based measurements as part of their study to develop ground shaking maps for Salt Lake City. For the lacustrine-alluvial silt and clay profile, VS increases from roughly 150 m/s to 320 m/s over depths of 0 to 60 m. Sharma (1997) provides a table summarizing ranges of compression-velocity (VP) values for various sediment and rock types. He reported compression-velocity (VP) values for clay between 1100 and 2500 m/s. No depths or locations were provided by Sharma; therefore, we varied Poisson's ratio from 0.3 (representative of sediments in LVV; Liu et al., 2005) to 0.45 (increased to represent a more saturated clay) to estimate a range of VS from the VP values. Given the assumptions needed to determine VS, we consider that the calculated range of VS, from 330 and 1340 m/s, provides only a rough estimate of velocity. Mavko et al. (1998) reported VS values for kaolinite, Gulf clays, and mixed clays of 900 m/s, 1640 to 1880 m/s, and 160 m/s, respectively. Depths and locations of the values were not reported.

Sand-sediment velocity:

The scatter plot developed for the Sand unit consists of data from 40 VS profiles (Figure C.2). Although the number of profiles is about the same as for the Clay unit, fewer datapoints are assigned to a "sand" than to "clay" because most of the locations within the correlation distance are located in areas shown to be either predominantly clay or predominantly gravel (Taylor et al., 2008; Luke and Liu, 2008).

As expected, VS for the Sand unit tends to increase with depth. Above 50 m, VS is typically between 150 and 1000 m/s; below this depth VS is typically between 490 and 1300 m/s. Locations of sites with data that are outside these ranges are shown in Figure C.3. Four sites have VS greater than 1000 m/s for depths between 0 and 50 m; specifically, the high VS values occur at depths above 10 m. All four sites are located in areas where caliche has been observed (Taylor et al., 2008). Three additional sites have VS greater than 1300 m/s for depths below than 50 m. They are the same three sites located along Las Vegas Blvd. that exhibit relatively high VS below 50 m for the Clay unit.

For the sites located in areas where caliche has been identified, we expect that the relatively high VS values are representative of caliche rather than the nearby sand. For the same reasons as discussed in the previous section, we expect that the relatively high VS values below 50 m depth are more likely a measurement of a cemented material at the site rather than being generally representative of the Sand unit.

Sundquist (2001) reported VS values for sand, measured at the Las Vegas Springs Preserve, between 300 and 500 m/s from 0 to 20 m deep. Velocity generally increased with depth in each profile, but, as with the clay profile, velocity at a specific depth at one site did not necessarily match that at another site. This range is within the VS range he reported for clay. In their Salt Lake City study, Wong et al. (2002) present an average VS profile for lacustrine sand. VS in this profile increases from roughly 180 m/s to 760 m/s over depths of 0 to 60 m. This range is slightly higher than the range they reported for clay and within the range they reported for gravel. Sharma (1997) reported VP values for dry alluvium and water-saturated sand ranging respectively from 300 to 1000 m/s, and

1200 to 1900 m/s. For a Poisson's ratio of 0.3, VS values calculated from the VP for dry alluvium range from 160 to 530 m/s. For a Poisson's ratio of 0.4, VS values calculated from the VP for water-saturated sand range from 490 to 780 m/s.

Gravel-sediment velocity:

The scatter plot developed for the Gravel unit consists of data from 53 VS profiles (Figure C.1). VS for the Gravel unit tends to increase with depth; however, this unit exhibits a significantly broader range of VS values. Nineteen sites have VS greater than 1000 m/s between depths of 0 and 50 m. Their locations are shown in Figure C.3. All are located along the margin of the LVV and are either near rock outcrops or in areas where caliche has been observed. Ten sites have VS greater than 1300 m/s for depths below 50 m; seven are included in the 19 sites previously discussed. The three additional sites, also shown in Figure C.3, are the same sites described in the Clay and Sand sections.

In their Salt Lake City study, Wong et al. (2002) present an average VS profile for lacustrine-alluvial gravel. VS in this profile increases from roughly 150 m/s to 800 m/s over depths of 0 to 45 m. These values are higher than the values they reported for clay; however, the minimum is lower than the minimum clay VS reported by Sundquist (2001); no gravel values were reported by Sundquist. Burger (1992) reported a VP range for alluvium from 500-2000 m/s. No depths or locations were reported. For a Poisson's ratio of 0.3 (Liu et al., 2005), the corresponding VS is roughly 270-1070 m/s. We note that the maximum VP value reported by Burger might be representative of a stiff sediment with a lower Poisson's ratio and, thus, a higher VS value.

Credible sediment ranges:

Based on the ranges reported by others and those measured in the LVV, VS values greater than 1000 m/s and occurring from 0 to 50 m depth were not considered representative of either Clay, Gravel or Sand units and were filtered from the correlation dataset. For depths greater than 50 m, VS values greater than 1300 m/s were not considered representative of these sediment types and were also filtered from the dataset. A lower-bound VS filter was not applied to any of the sediment units.

Selection of credible velocity ranges for Mixed unit:

For their 3-D model of VS sediment, Taylor et al. (2008) defined a Mixed unit to describe layers where none of the three sediment types is predominant. Thus, the range of VS values used for the correlation of mixed-sediment type is based on those used for clay, gravel and sand. "Mixed" layers as defined by Taylor et al. (2008) may also include cemented materials, which would result in a higher VS value for the layer; therefore, the upper bound for reasonable values was assumed higher than those of the other sediment types. For the mixed sediment type, VS values greater than 1000 m/s occurring between 0 and 5 m, were not considered credible. For depths greater than 5 m, values greater than 1300 m/s were not considered credible and were filtered from the correlation dataset. A lower bound-filter was not applied.

Because only 20 VS profiles with mixed-unit layers were located within 300 m of a well, the scatter plot for this unit was developed from profiles located within 500 m of a well. Thus the plot consists of data from 32 wells (Figure C.1). The scatter plot for the mixed unit was not specifically used to determine the cutoff boundary, but is included to show the relationship of the boundary to the dataset. Of the four defined units, the Mixed

unit had the fewest profiles and datapoints with which to perform the correlations. The locations of the four sites from which data were filtered from the correlation dataset for the Mixed unit are shown in Figure C.3.

Table C.1 Shear-wave velocity (VS) ranges

Sediment unit	Range used in correlation [1]		VS values from previously published studies		
	Depth, m	VS, m/s	Depth range, m	VS m/s	Reference
Clay	0-50	100-1000	0-30	280-690	Sundquist, 2001
	50-400	300-1300	0-60	160-320	Wong et al., 2001
			not provided	330-1340 [2]	Sharma, 1997
			not provided	900	kaolinite; Mavko et al., 1998
			not provided	1640-1880	Gulf clays; Mavko et al., 1998
			not provided	160	mixed clays; Mavko et al., 1998
Sand	0-50	150-1000	0-20	300-400	Sundquist, 2001
	50-400	490-1300	0-60	180-760	Wong et al., 2001
			not provided	160-530 [2]	Sharma, 1997
			not provided	490-780 [2]	Sharma, 1997
Gravel	0-50	190-1000	0-45	150-800	Wong et al., 2001
	50-400	470-1300	not provided	270-1070 [2]	Burger, 1992

[1] Minimum values reported are lowest VS measured VS value for the unit

[2] VS listed was calculated from a reported VP

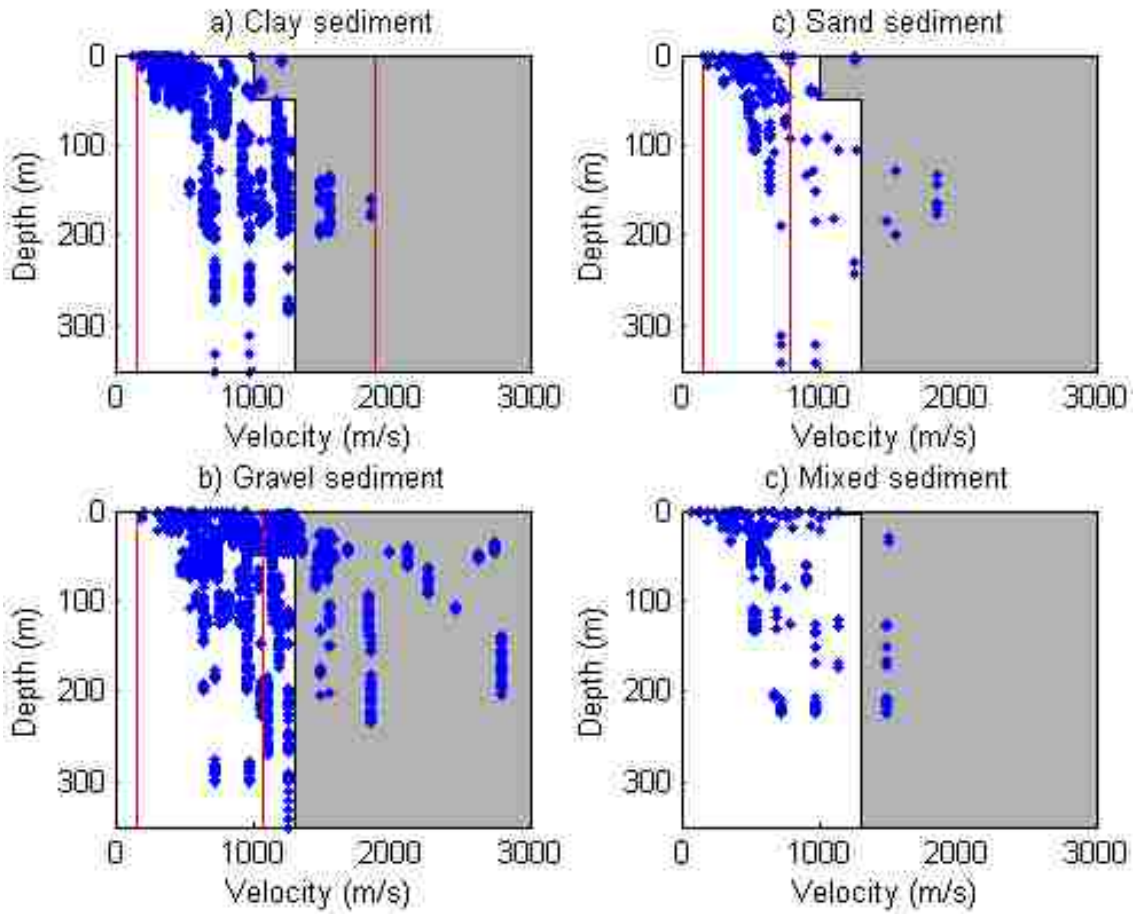

Figure C.1 Discretized VS with respect to depth for LVV predominant sediment units (blue symbols). Values greater than cutoff values derived from these datasets are superimposed on the grey background. Minimum and maximum values from literature shown for Clay, Gravel, and Sand (red).

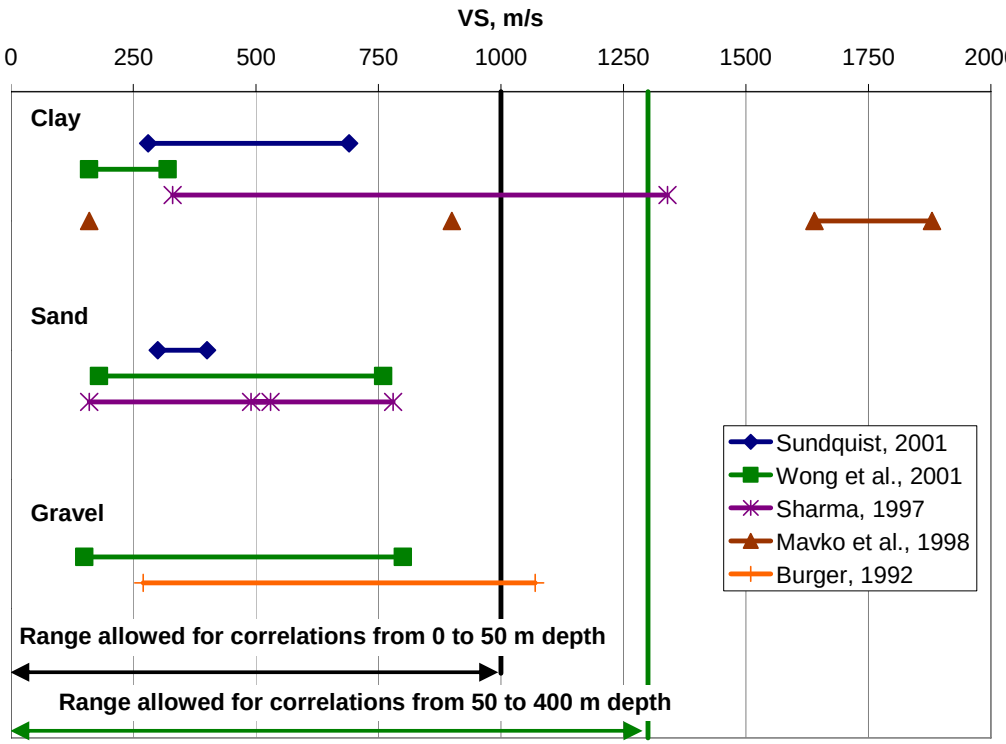

Figure C.2 VS ranges reported in the cited references and the range of VS allowed in the correlation dataset.

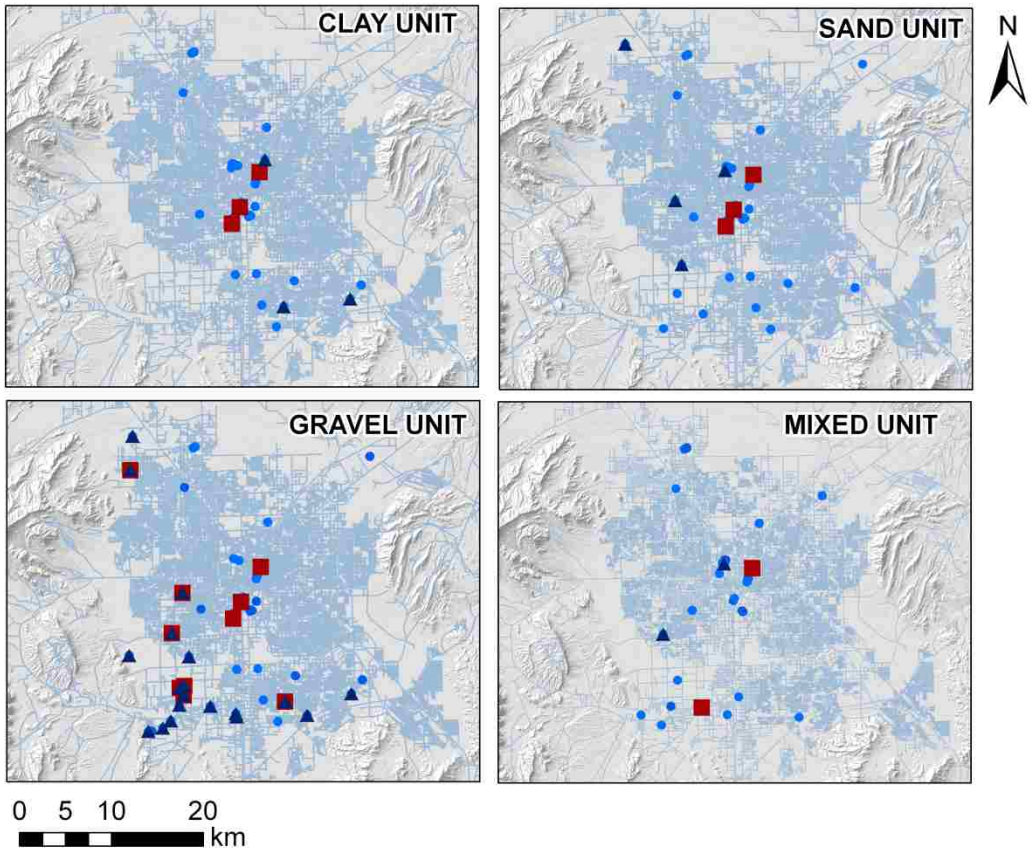

Figure C.3 Locations of shear-wave velocity (VS) profiles used for the correlation of VS to lithology for each of the sediment units. Locations where no data was filtered from the correlation dataset (blue circles), and where were filtered from the correlation dataset. For the Clay, Sand and Gravel units, filtered values are VS greater than 1000 m/s occurring between depths of 0 and 50 m (blue triangles) and VS greater than 1300 m/s for depths below 50 m (red squares). For the mixed unit, VS greater than 1000 m/s occurring between depths of 0 and 5 m (blue triangles) and VS greater than 1300 m/s for depths below 5 m (red squares) were filtered.

APPENDIX D

3-D VS MODEL

This appendix includes graphics of the 3-D VS model created using EarthVision. The vertical exaggeration shown in the figures is four times the horizontal (northing and easting) scales.

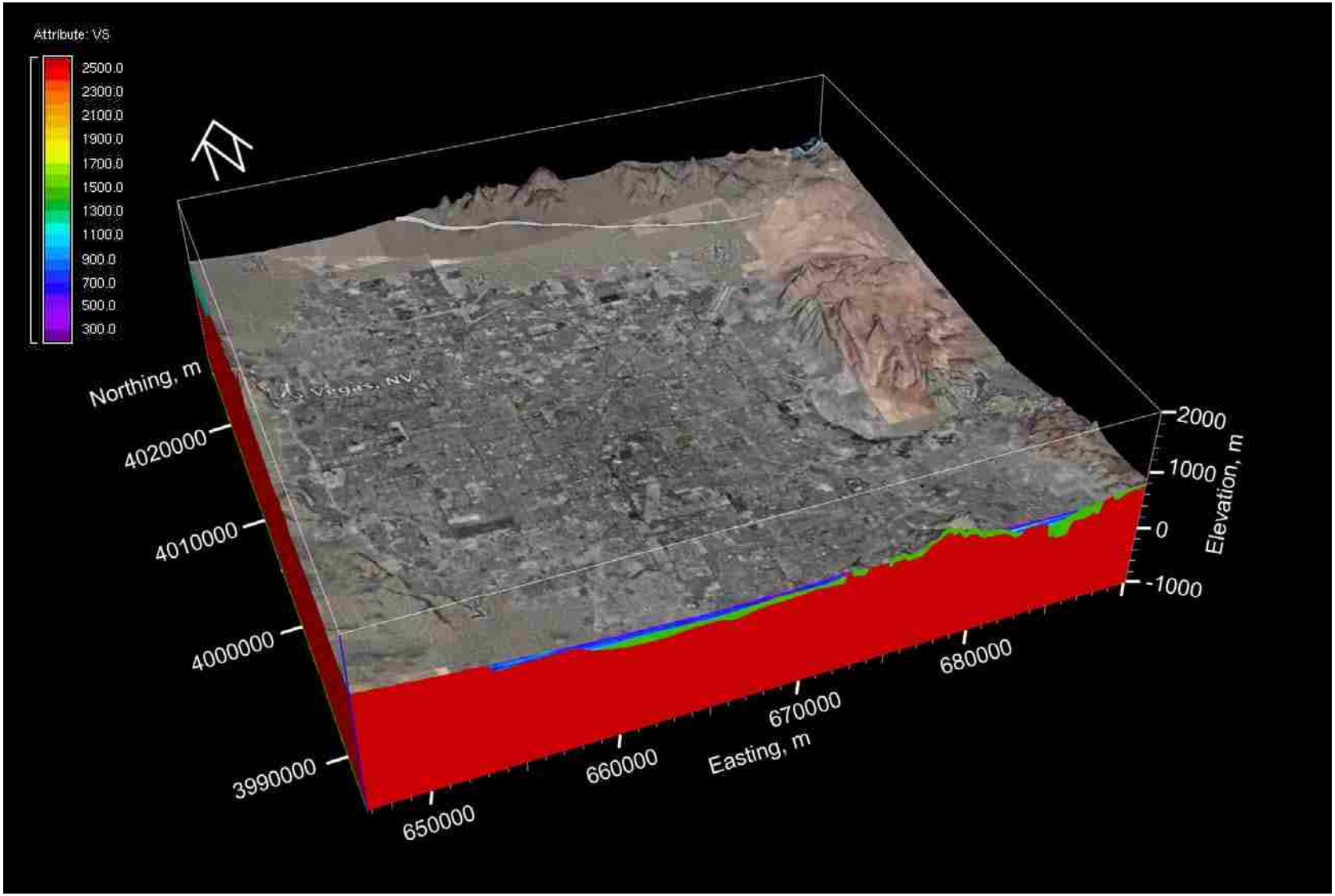

Figure D.1 Aerial view of Las Vegas Valley (LVV) overlayed on three-dimensional (3-D) shear-wave velocity (VS) model.

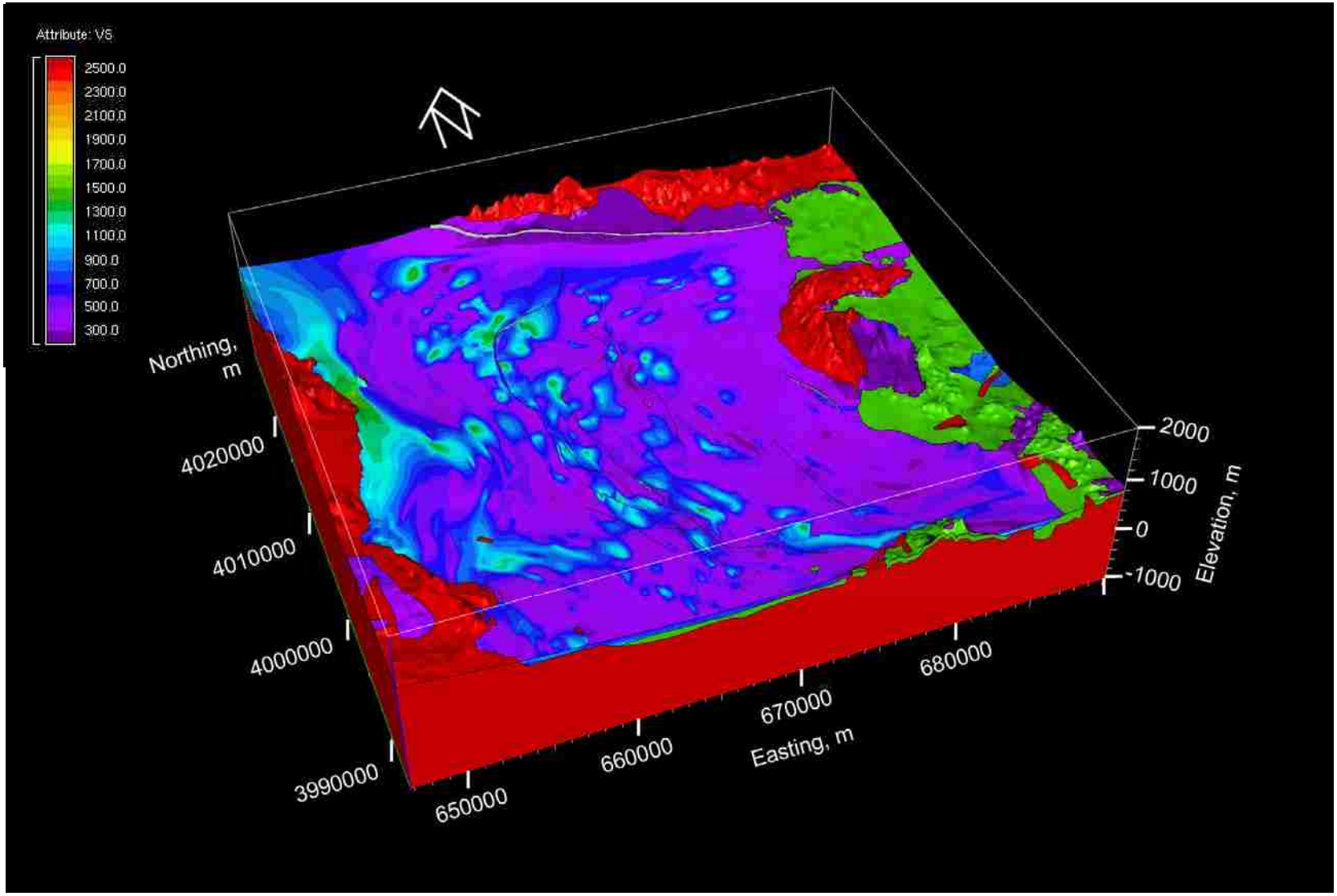

Figure D.2 3-D VS model with both VS measured and VS assigned data

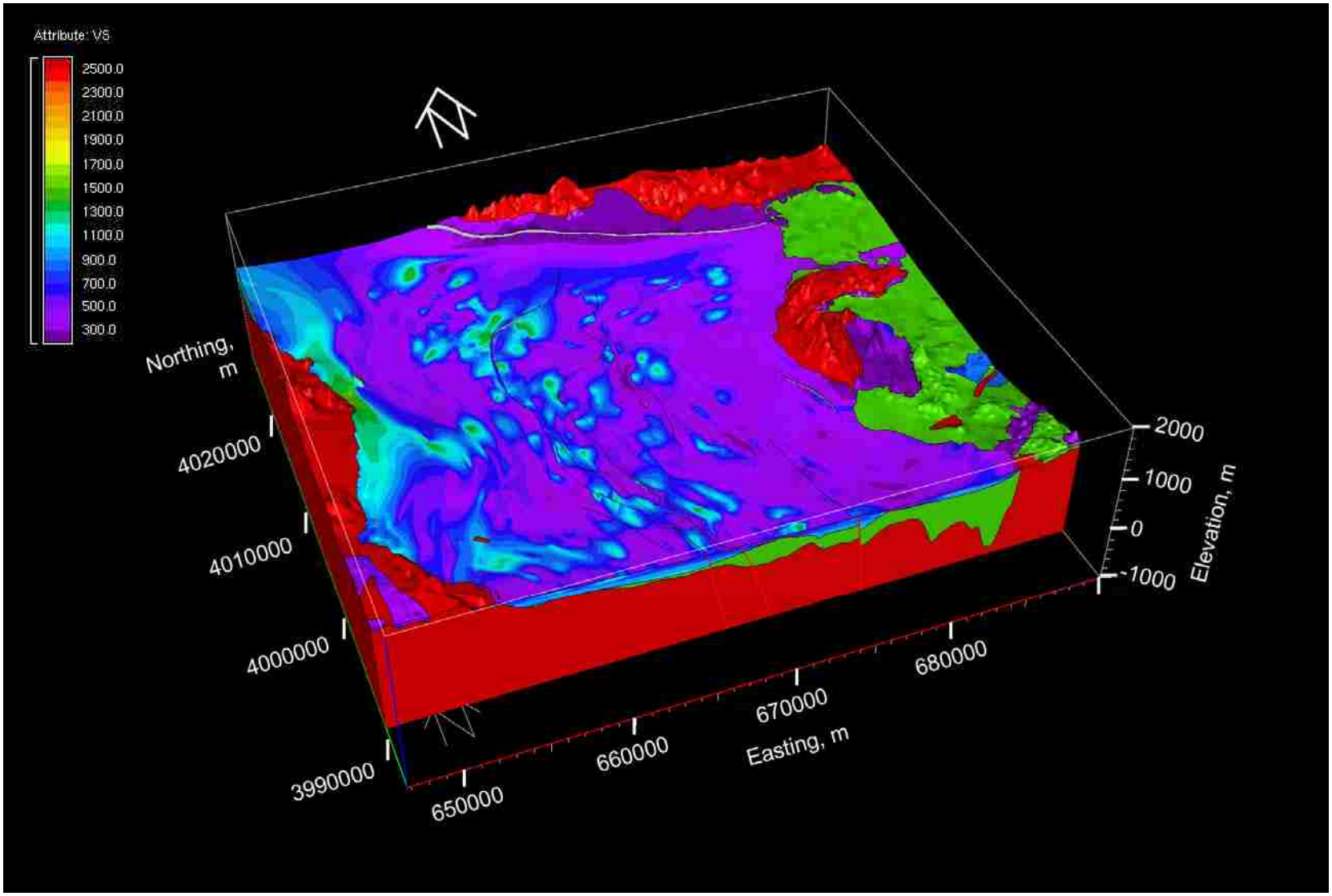

Figure D.3 3-D VS model with east-west view of below surface sediments.

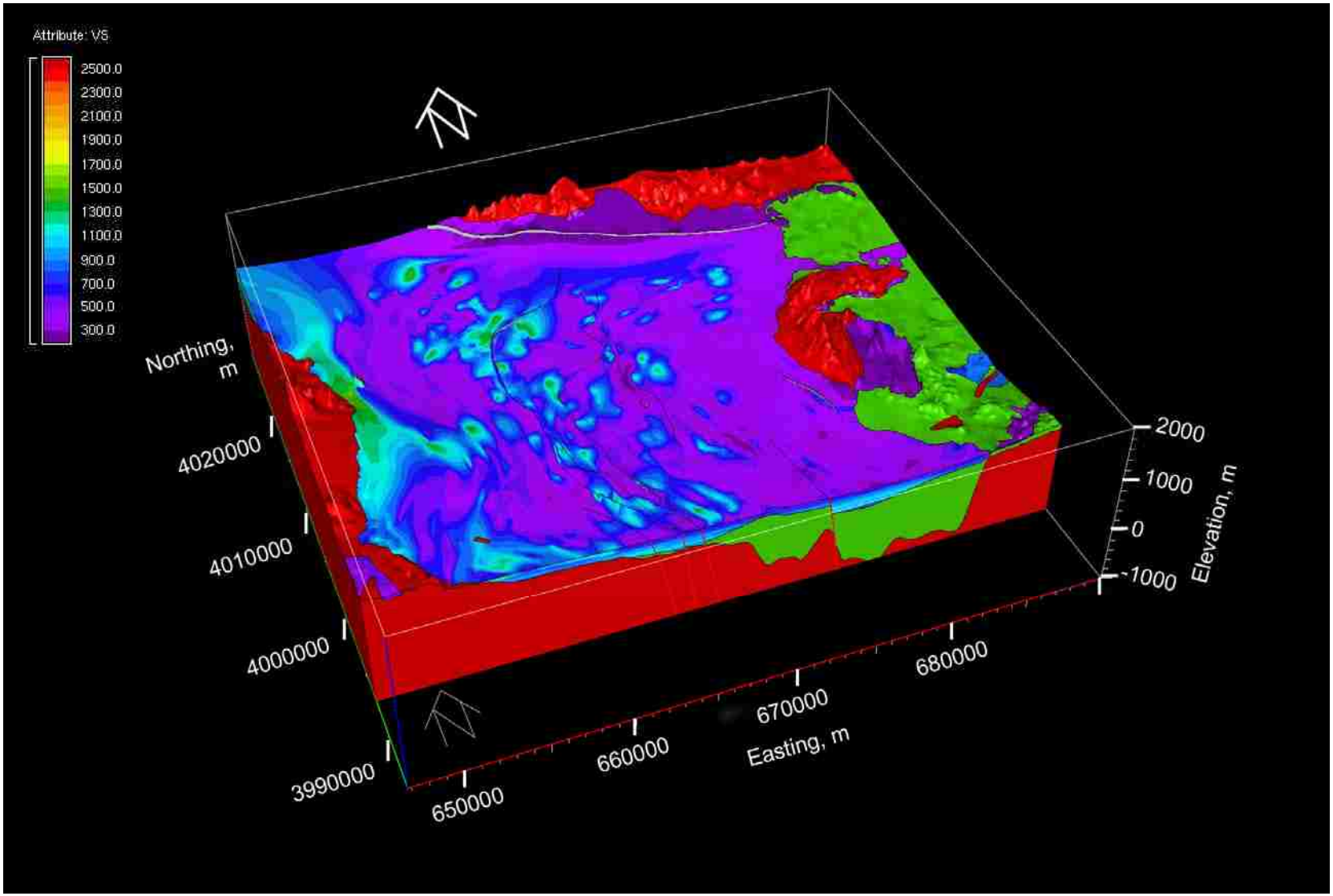

Figure D.4 3-D VS model with east-west view of below surface sediments.

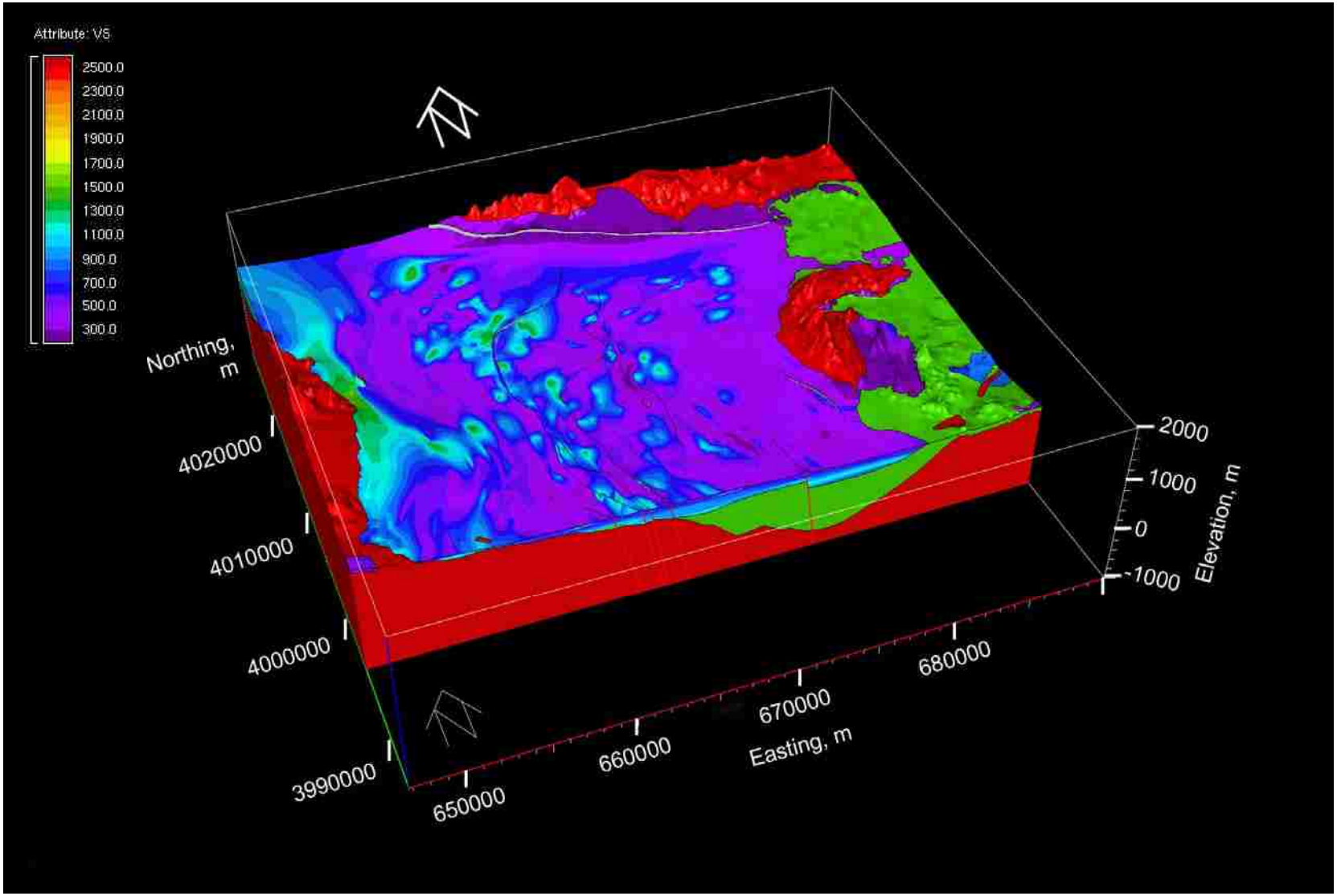

Figure D.5 3-D VS model with east-west view of below surface sediments.

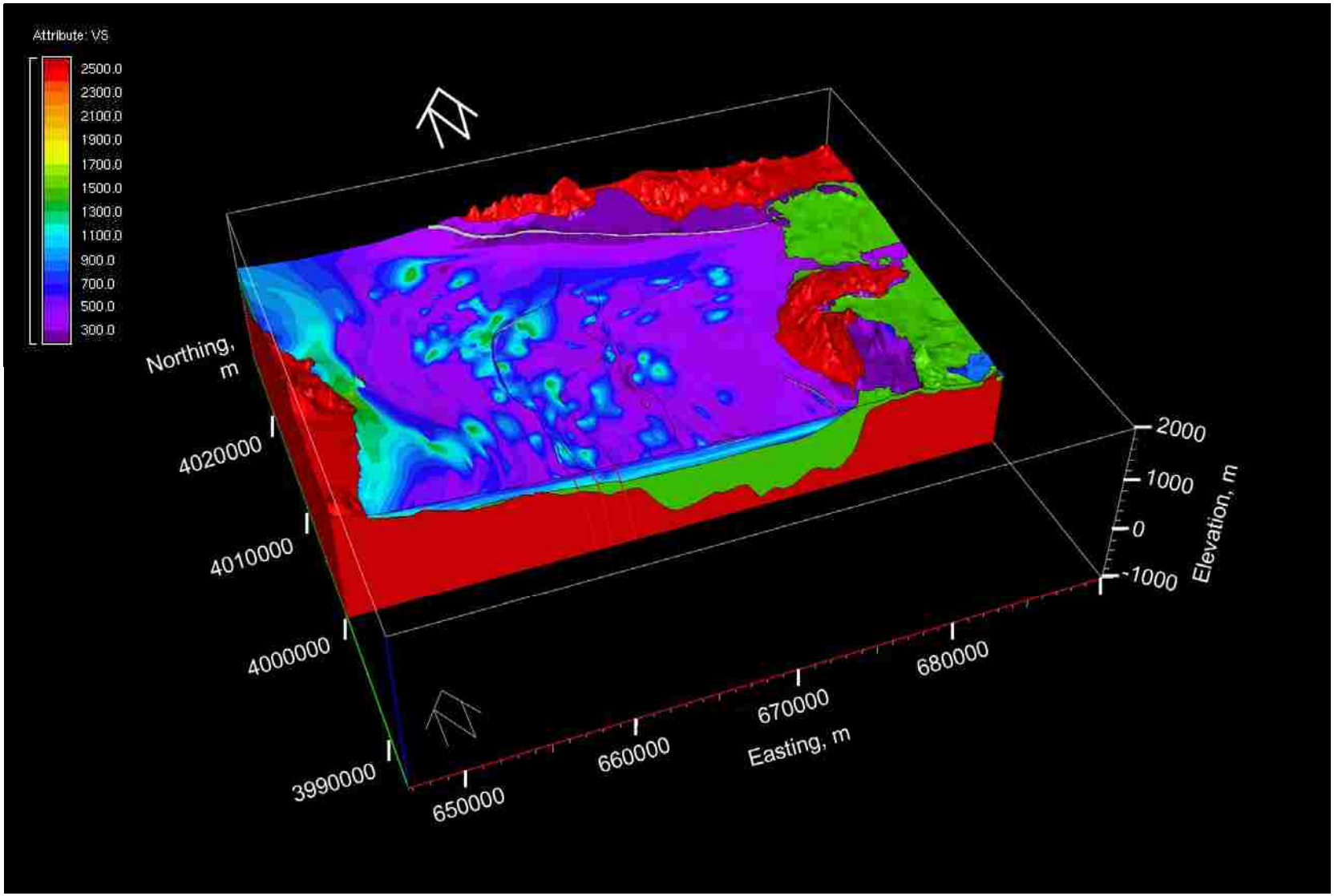

Figure D.6 3-D VS model with east-west view of below surface sediments.

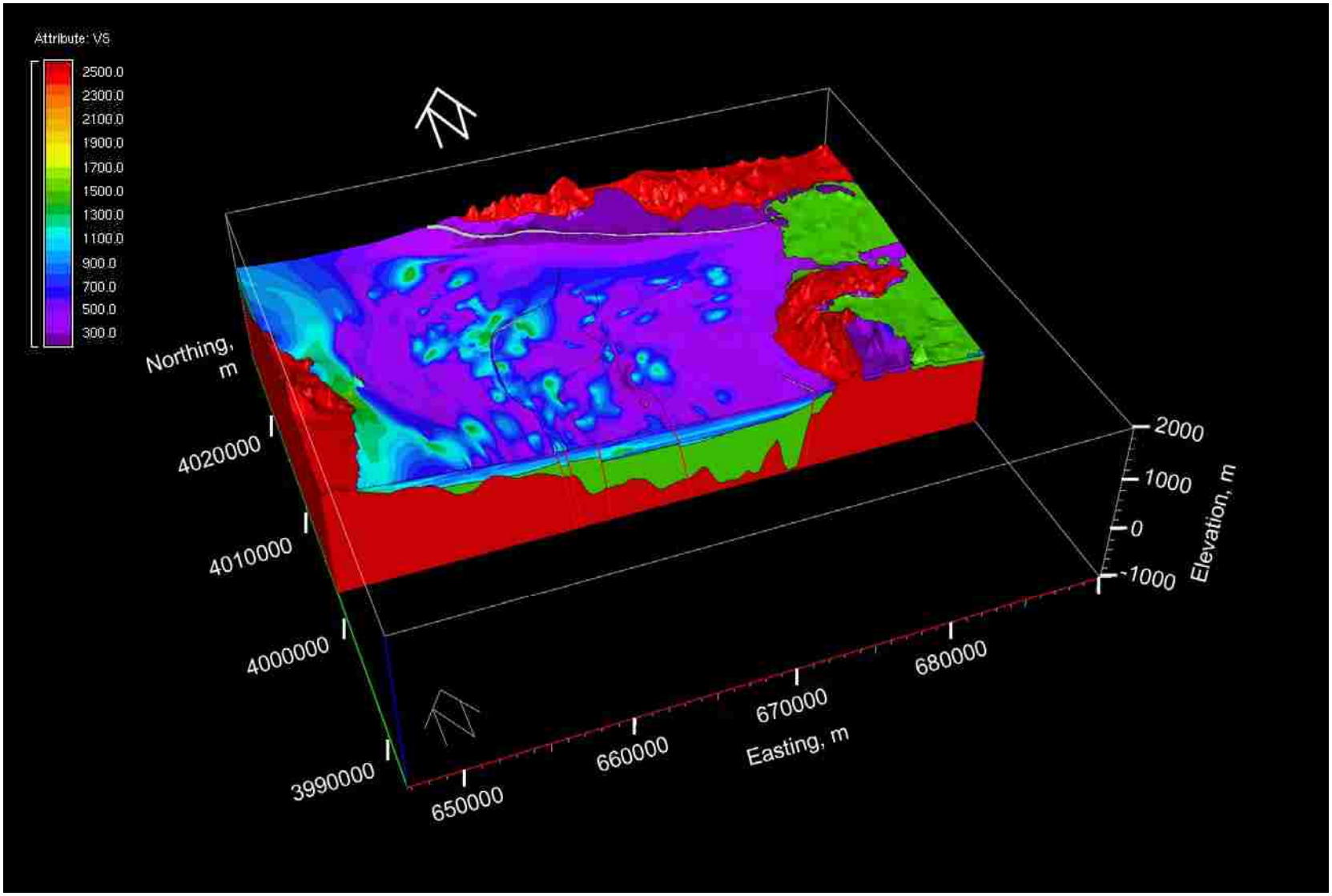

Figure D.7 3-D VS model with east-west view of below surface sediments.

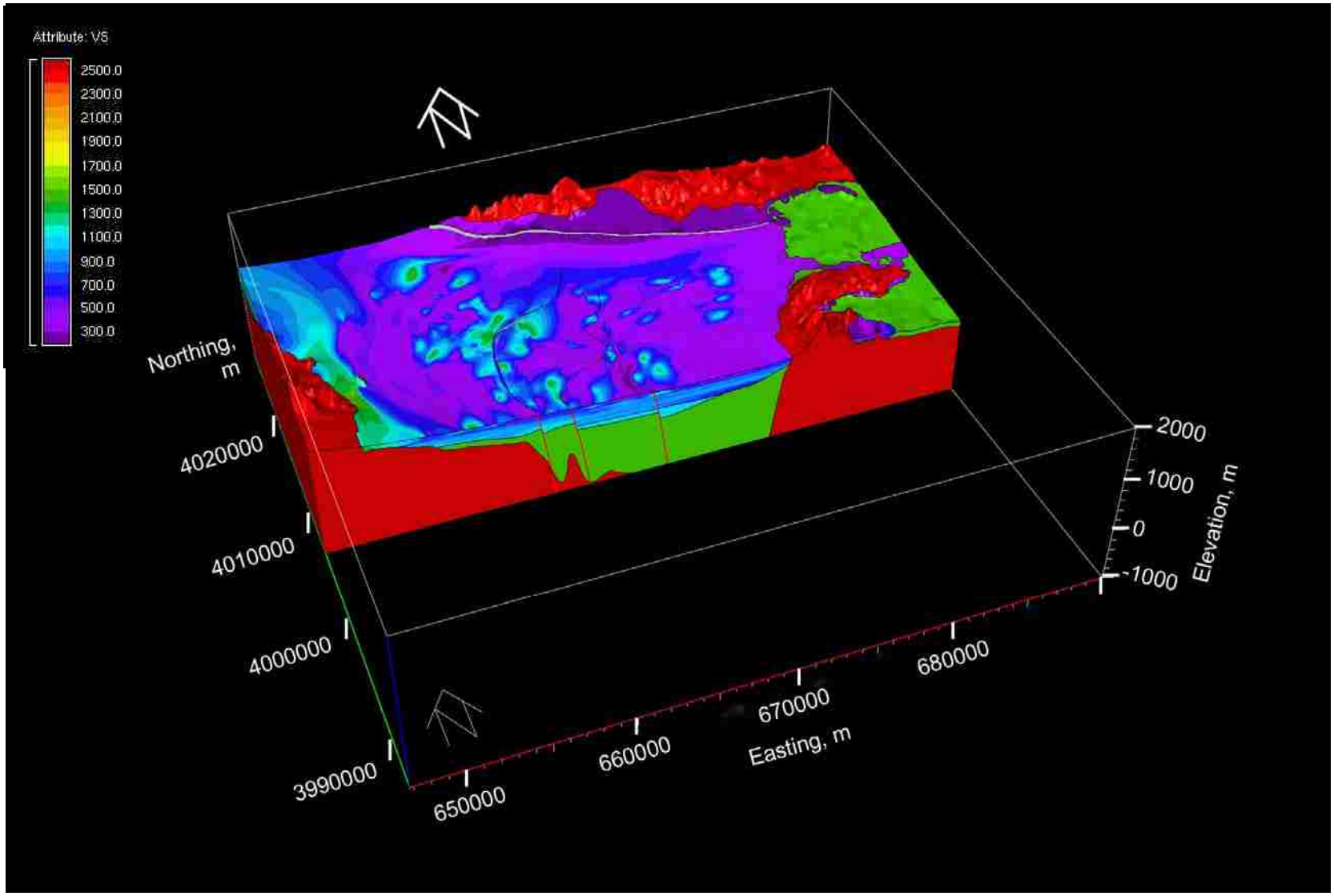

Figure D.8 3-D VS model with east-west view of below surface sediments.

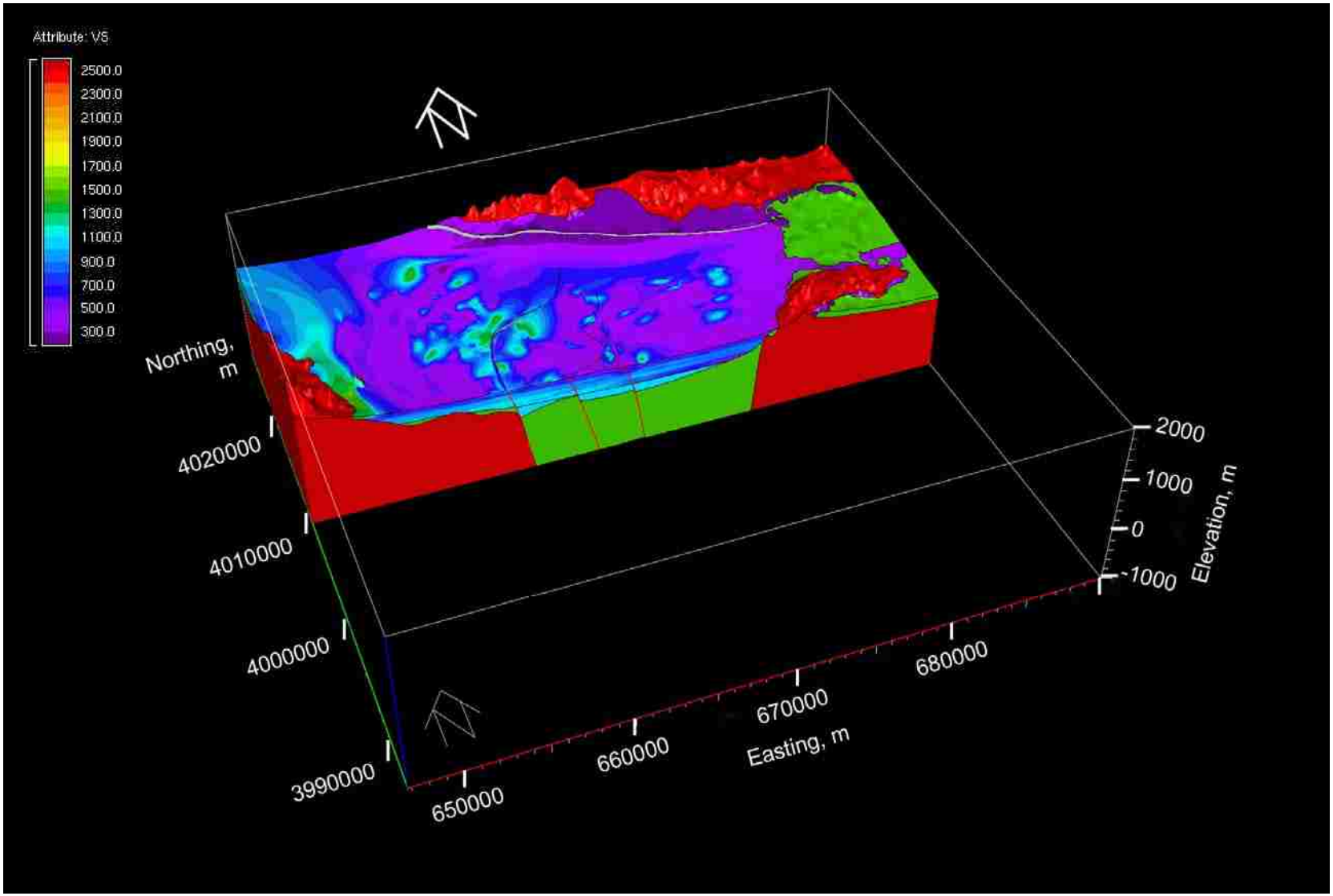

Figure D.9 3-D VS model with east-west view of below surface sediments.

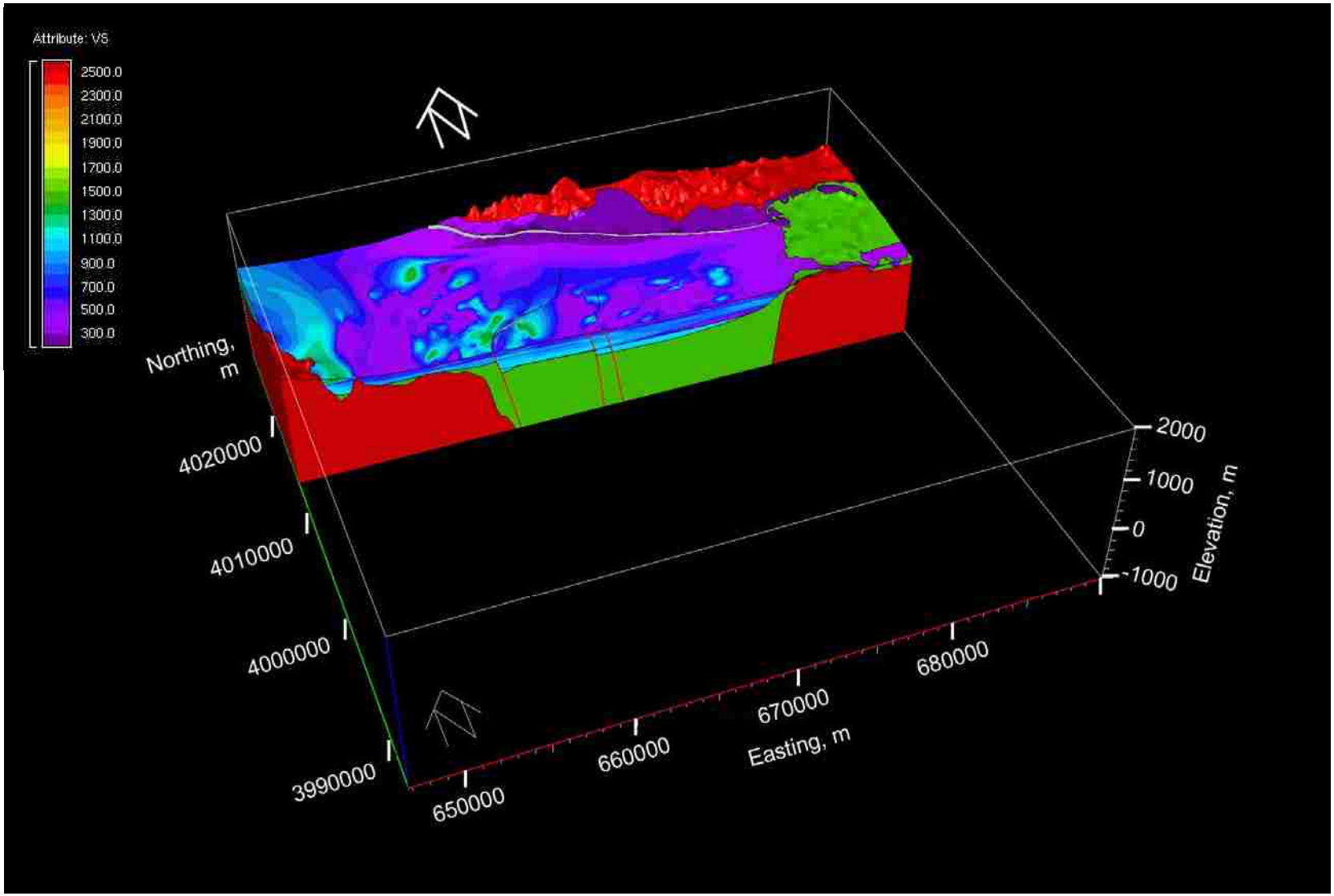

Figure D.10 3-D VS model with east-west view of below surface sediments.

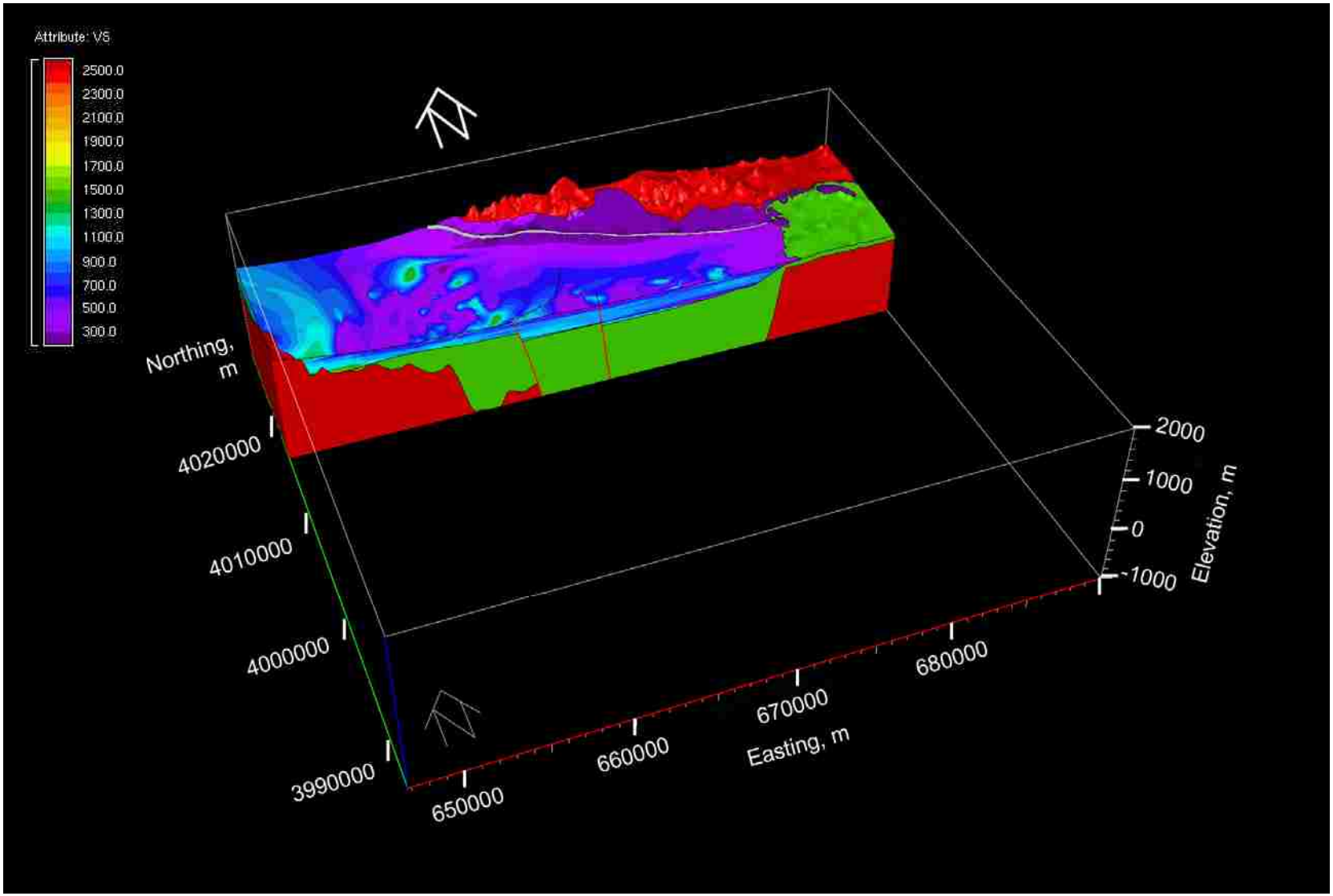

Figure D.11 3-D VS model with east-west view of below surface sediments.

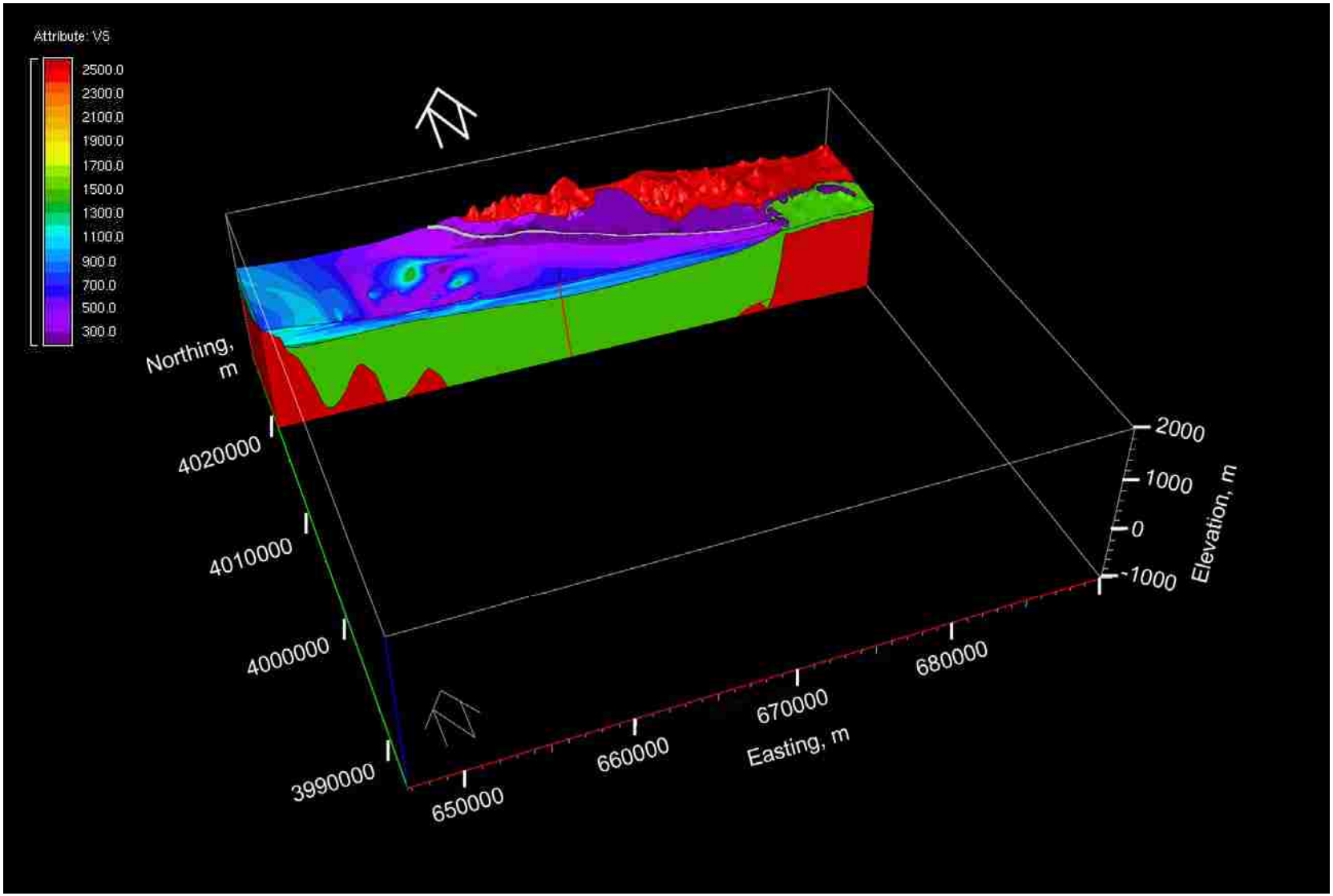

Figure D.12 3-D VS model with east-west view of below surface sediments.

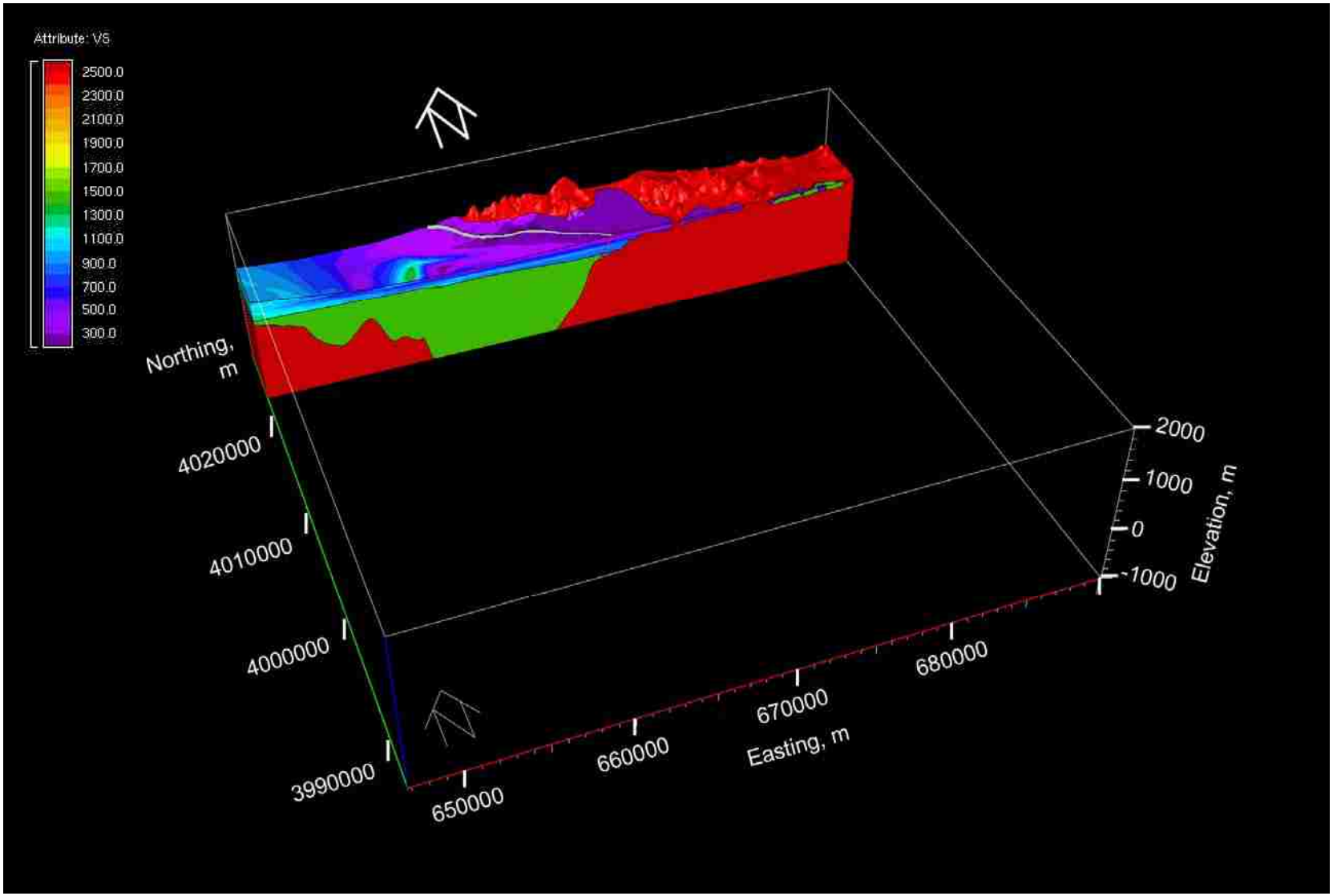

Figure D.13 3-D VS model with east-west view of below surface sediments.

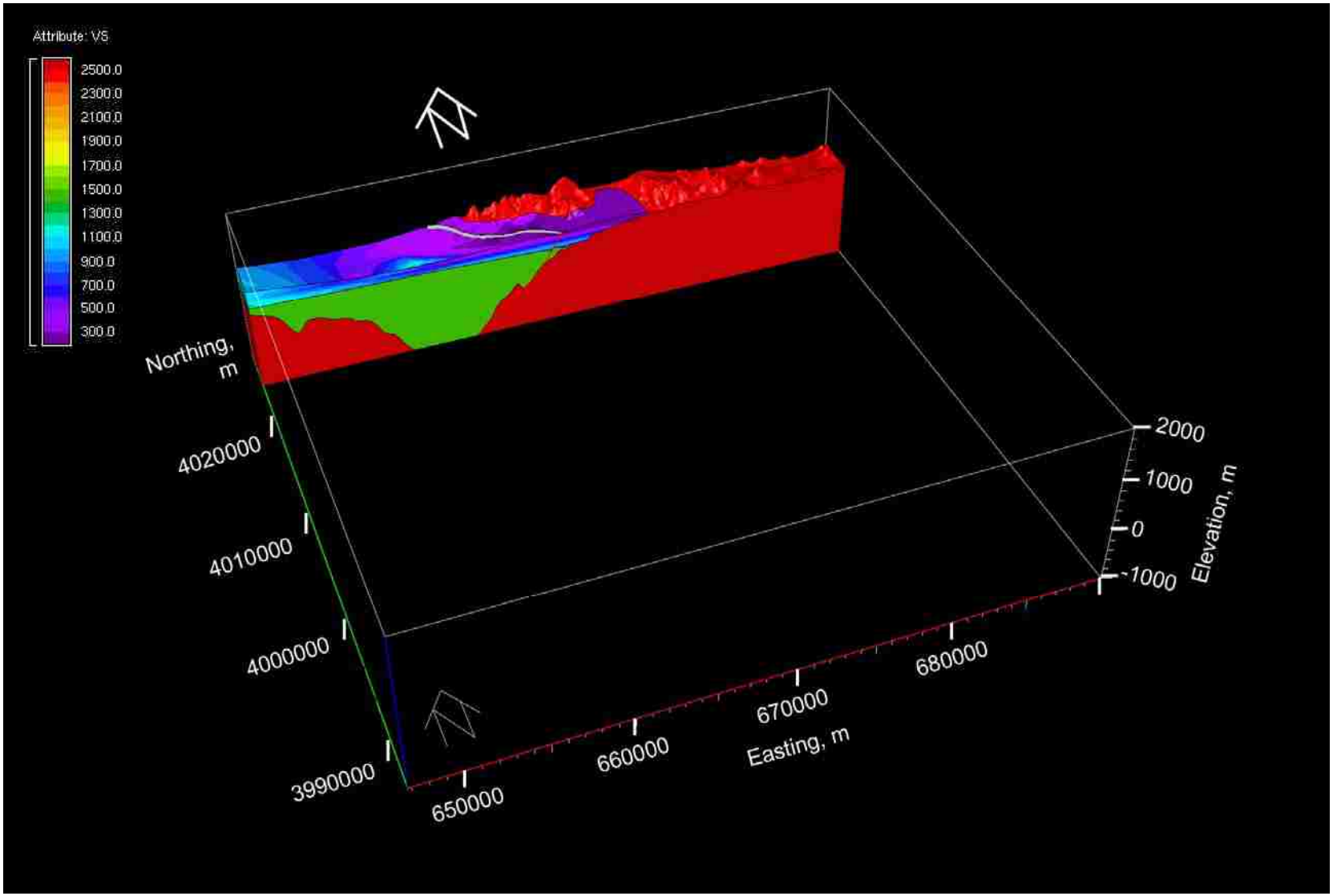

Figure D.14 3-D VS model with east-west view of below surface sediments.

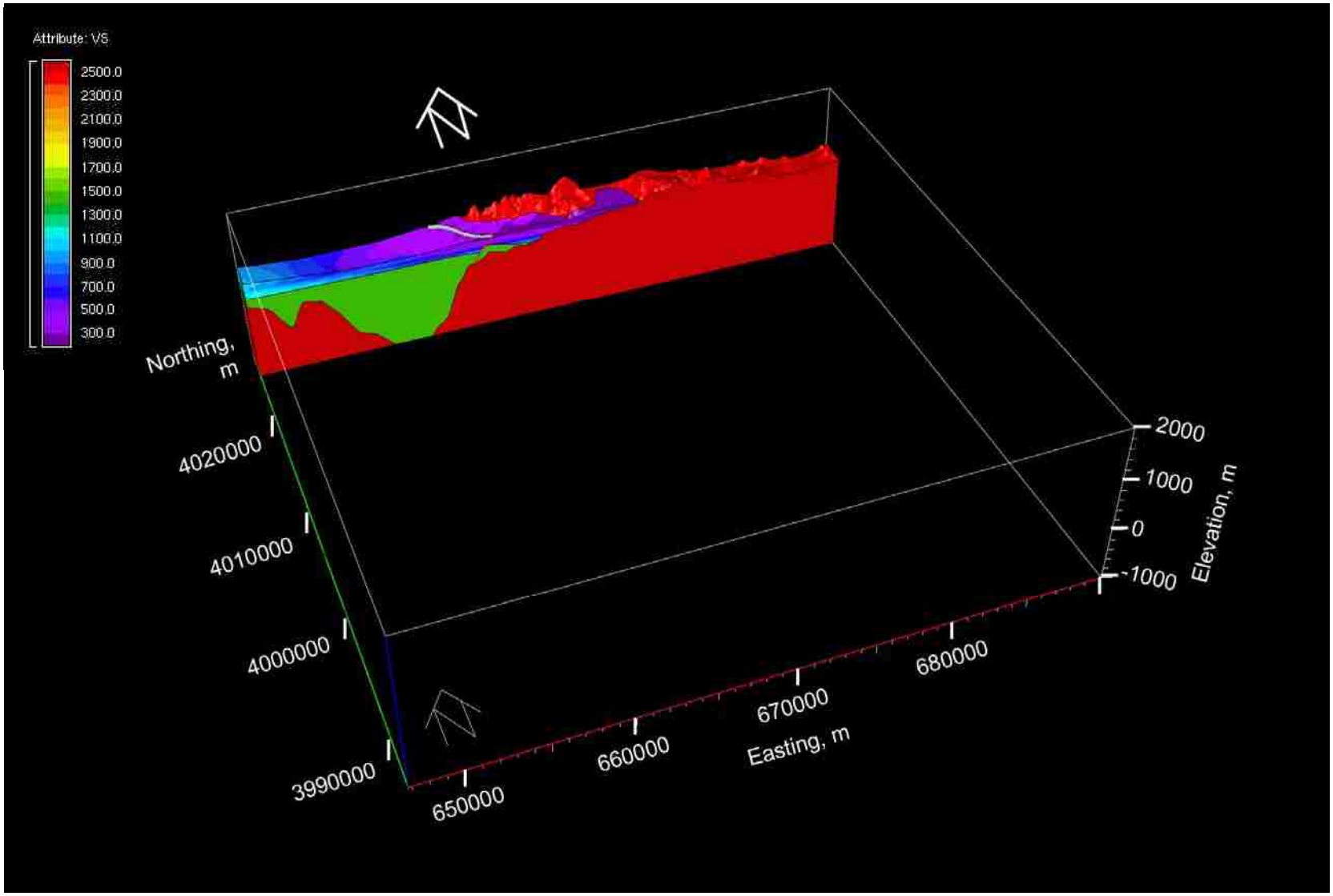

Figure D.15 3-D VS model with east-west view of below surface sediments.

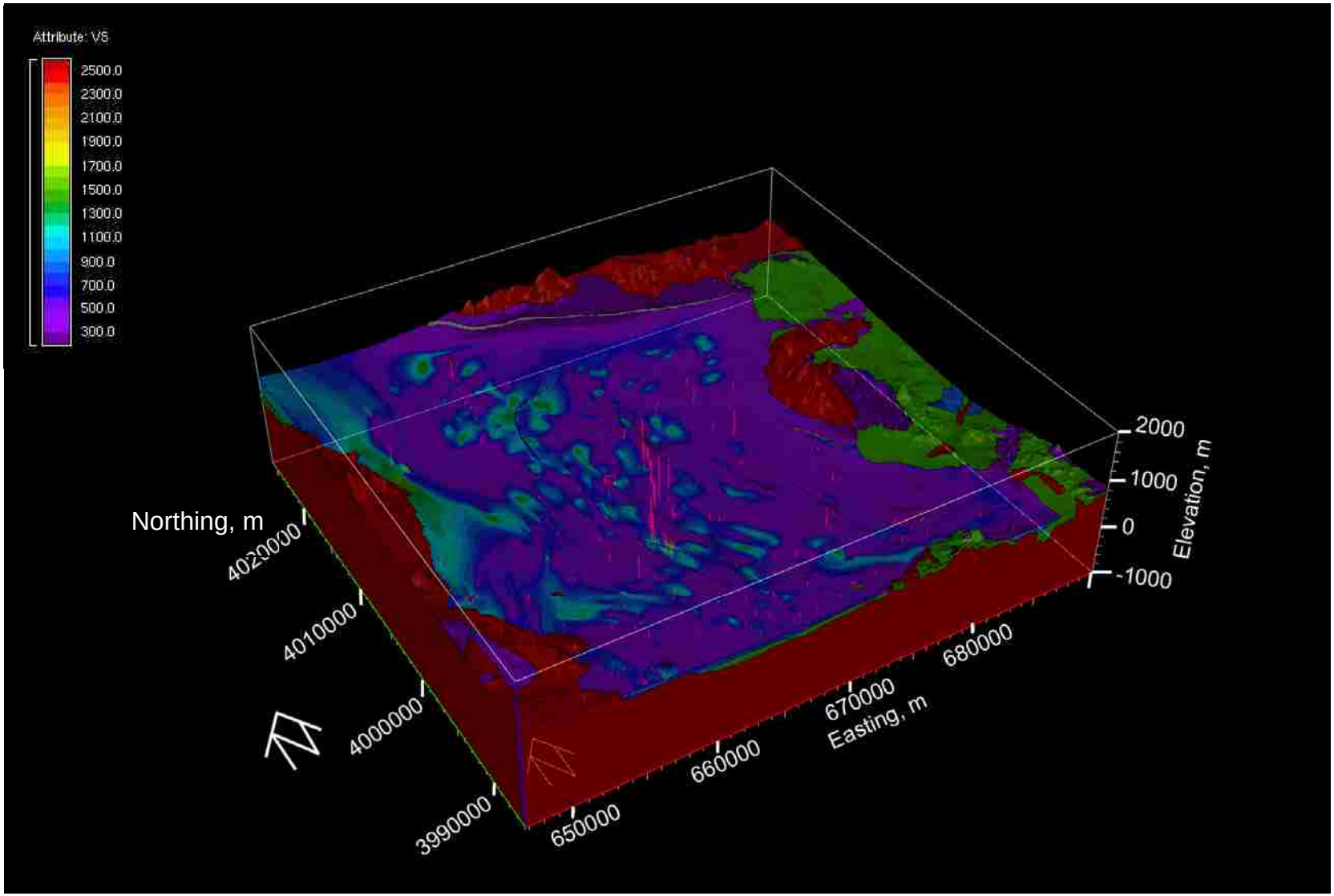

Figure D.16 3-D VS model with location of VS profiles shown in pink.

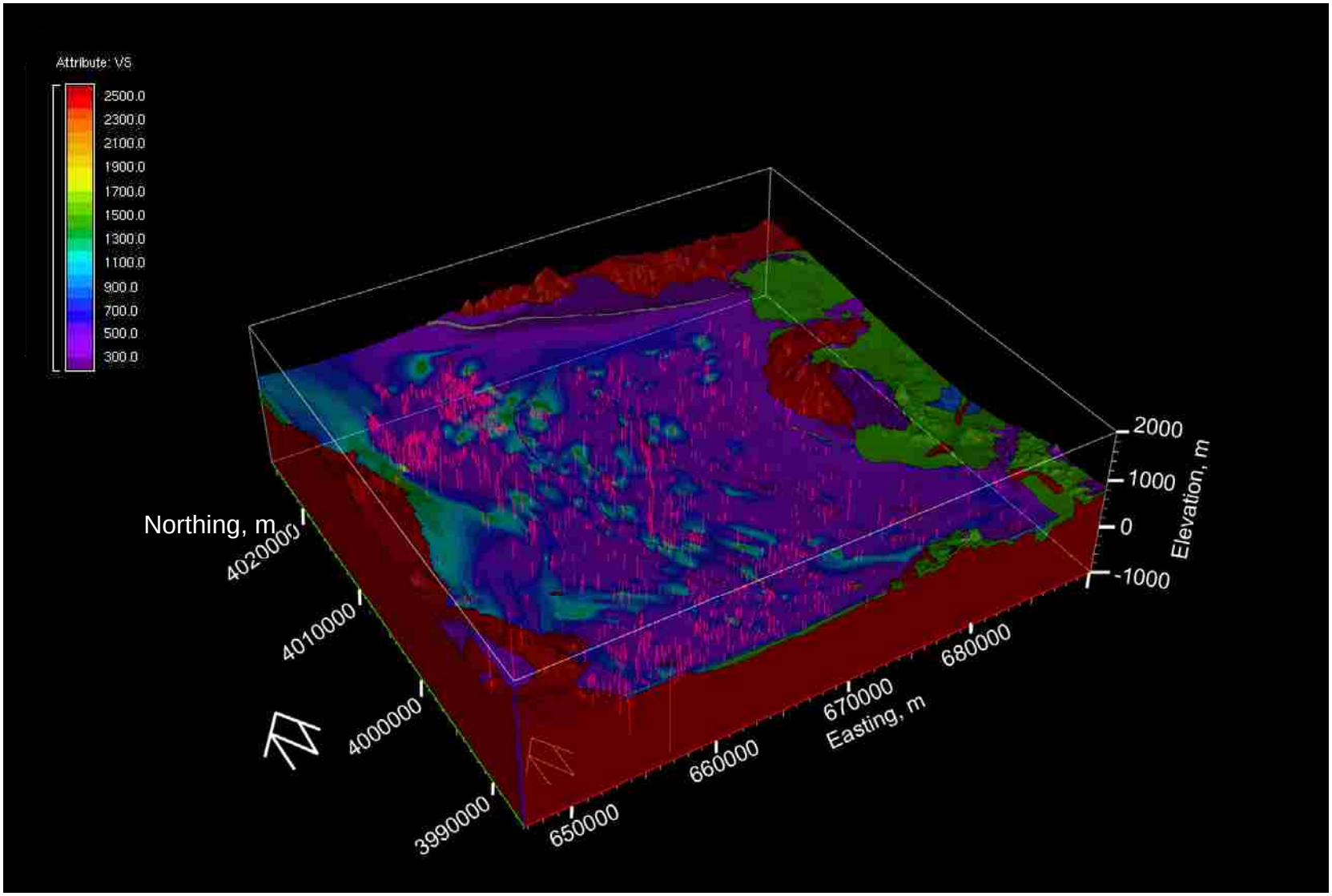

Figure D.17 3-D VS model with location of VS profiles and VS assigned to well lithology shown in pink.

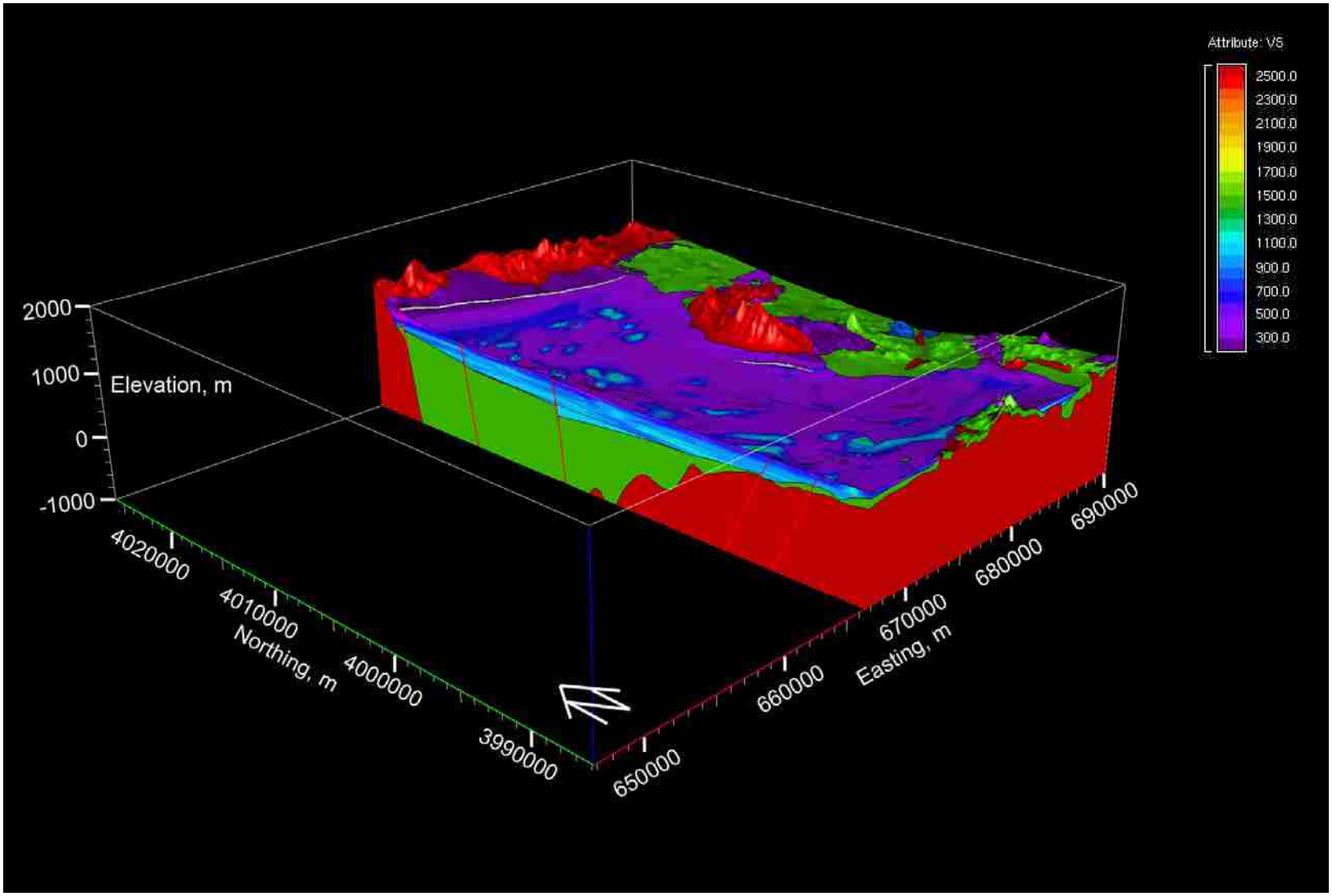

Figure D.18 3-D VS model with north-south view of below surface sediments.

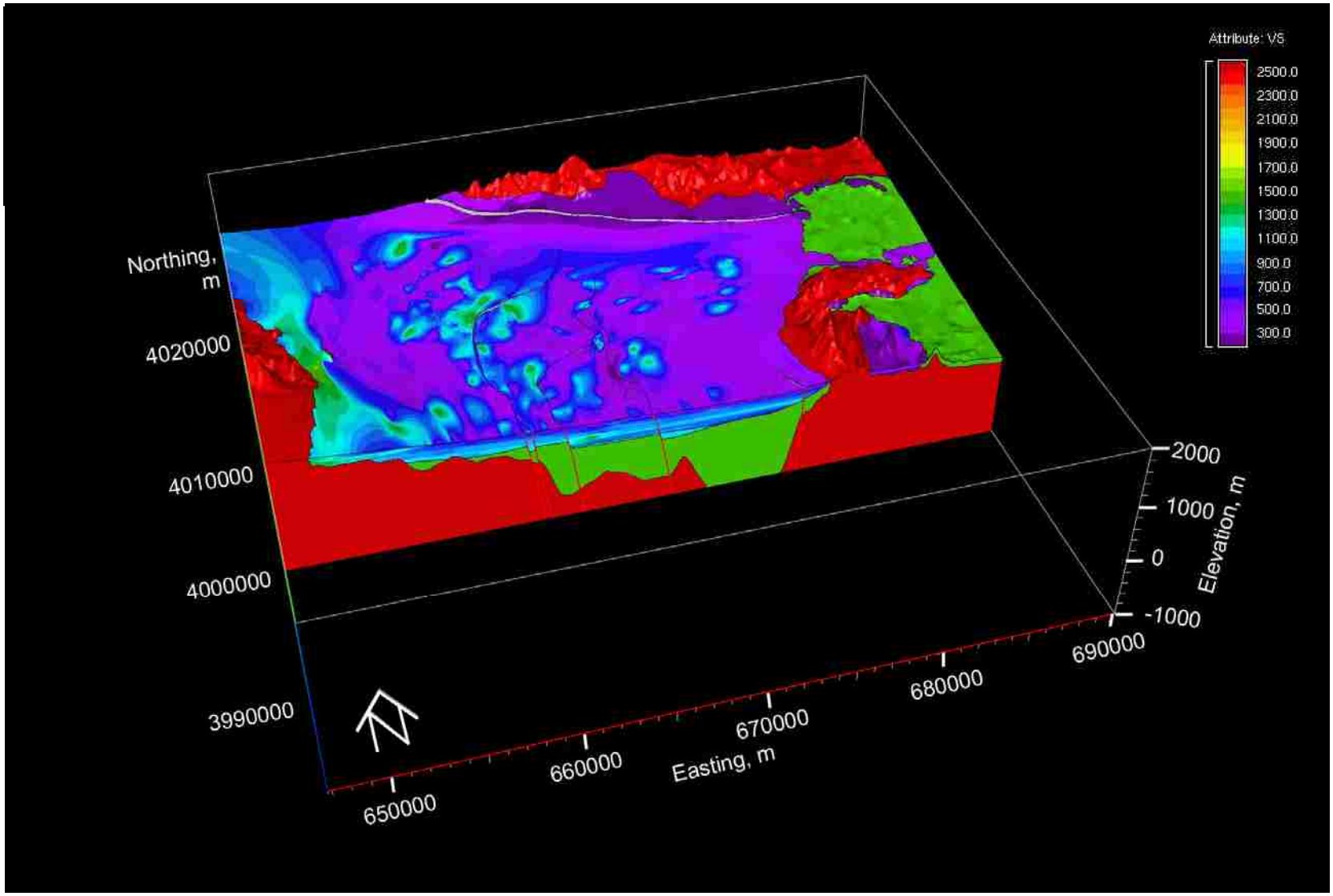

Figure D.19 3-D VS model with east-west view of below surface sediments.

VITA

Graduate College
University of Nevada, Las Vegas

Helena Murvosh

Degrees:

Bachelor of Science in Mathematical Sciences, 1990
University of Nevada, Las Vegas

Master of Science in Mathematical Sciences, 1993
University of Nevada, Las Vegas

Special Honors and Awards:

Travel grant, Spring 2007, UNLV Graduate and Professional Student Association.

Publications:

Luke, B., **Murvosh, H.**, Kittipongdaja, P., Karasa, A., Tamrakar, P., and Taylor, W. J., (2010). Rayleigh-wave dispersion curves for long, linear arrays at a predominantly-gravel site. *Proceedings, Symposium on the Application of Geophysics to Engineering and Environmental Problems (SAGEEP), 23rd Annual Meeting* [CD-ROM] (pp. 742-750). Denver: Environmental and Engineering Geophysical Society.

Luke, B., **Murvosh, H.**, Taylor, W., and Wagoner, J. (2010). Characteristic Shear Velocity Profiles for Predominant Sediment Fill Units in the Las Vegas Basin. In D. Fratta, A. J. Puppala and B. Muhunthan (eds.), *GeoFlorida 2010: Advances in Analysis, Modeling and Design, Geotechnical Special Publication 199* [CD-ROM; ISBN 978-0-7844-1095-0]. Reston, VA: American Society of Civil Engineers.

Karasa, A., **Murvosh, H.**, Luke, B., (2009). Seismic surface-wave dispersion curves for long, to 750-m, linear arrays. *Proceedings, 42nd Symposium on Engineering Geology and Geotechnical Engineering.* Pocatello, ID: Idaho State University.

Luke, B., **Murvosh, H.**, Taylor, W., and Wagoner, J. (2009). Three-dimensional modeling of shallow shear-wave velocities for Las Vegas, Nevada, using sediment type. *Journal of Earth Science*. 20(3), 555-562.

Luke, B., Taylor, W., Calderón-Macías, C., Jin, X., **Murvosh, H.**, and Wagoner, J. (2008). Characterizing anomalous ground for engineering applications using surface-based seismic methods. *The Leading Edge 27*(11), 1330–1334.

Murvosh, H., and Luke, B. (2008). Summer 2007 VS Data Acquisition Campaign in Las Vegas; Lessons Learned. *Proceedings, 41st Annual Symposium on Engineering Geology and Geotechnical Engineering* [CD-ROM Murvosh1.pdf]. Pocatello, ID: Idaho State University.

Gonzales, E., **Murvosh, H.**, and Luke, B. (2008). Sediment Lithology as a Surrogate for VS(30) in Seismic Site Classification. *Proceedings, 41st Annual Symposium on*

Engineering Geology and Geotechnical Engineering [CD-ROM Gonzalez.pdf]. Pocatello, ID: Idaho State University.

Murvosh, H., Luke, B., and Taylor, W. (2007). Testing Geologic Boundaries for VS Mapping in Las Vegas, Nevada. In K. D. Pitilakis (ed.) *Proceedings, 4th International Conference on Earthquake Geotechnical Engineering*, Thessaloniki, Greece [CD-ROM 1275.pdf].

Murvosh, H., Luke, B., Taylor, W., McLaurin, B., Higgins, T., and Quinn, W. (2006). Research and development of Las Vegas Valley VS(30) map. *Proceedings, 40th Annual Symposium on Engineering Geology and Geotechnical Engineering* [CD-ROM Murvosh1.pdf]. Pocatello, ID: Idaho State University.

Murvosh, H., Luke, B., Taylor, W., Liu, Y., and Jin, X. (2006). Characterizing shallow shear wave velocities in fabulous Las Vegas: processes and site selections. *Proceedings, 19th Annual Symposium on the Application of Geophysics to Engineering and Environmental Problems, Environmental and Engineering Geophysical Society*, Denver [CD-ROM P-153]. 1325-1333.

Luke, B., Twilley, K., **Murvosh, H.**, El-khater, R., Cheng, J., Yfantis, E., and Harris, D., (2003). Seismic Monitoring for Rockfall at Yucca Mountain: Concept Tests. In S. Elfass, G. Norris, and R. Watters (eds.) *Proceedings, 38th Annual Symposium Engineering Geology and Geotechnical Engineering* (pp. 281-288). Pocatello, ID: Idaho State University.

Twilley, K., **Murvosh, H.**, Cheng, J., Luke, B., Rock, D., and Tu, Y. (2003). Deployment of a Passive Seismic Array to Remotely Monitor for Rockfall in Underground Excavations. In S. Elfass, G. Norris, and R. Watters (eds.), *Proceedings, 38th Annual Symposium Engineering Geology and Geotechnical Engineering* (pp. 289-298). Pocatello, ID: Idaho State University.

Branagan, P., Vanderpool, W., and **Murvosh, H.** (2002). Defect Identification, Remediation, and Performance Monitoring of a Drilled-Shaft Foundation; A Case Study. *Proceedings, 37th Annual Symposium Engineering Geology and Geotechnical Engineering,* Idaho State University, Pocatello, ID.

Branagan, P., and **Murvosh, H.** (2001). Using Crosshole Sonic Logging To Assess the Integrity of Drilled-Shaft Concrete Foundations and Identify Construction Defects. In B. Luke, E. Jacobson, and J. Werle (eds.), *Proceedings, 36th Annual Symposium Engineering Geology and Geotechnical Engineering* (pp. 693-701). Pocatello, ID: Idaho State University.

Branagan, P., Vanderpool, W., **Murvosh, H.**, and Klein, M. (2000). CSL Defines CIDH Defects; Coring Confirms Results. Proceedings, Sessions of Geo-Denver 2000, Geotechnical Special Publication No. 100, *New Technological and Design Developments in Deep Foundations* (pp. 100-125). Restin, VA: American Society of Civil Engineers.

Thesis Title: Complex VS Profiles to 100 M Depth from Rayleigh Waves and 3-D VS Model for Las Vegas Valley

Thesis Examination Committee:

Chairperson, Barbara Luke, Ph. D., P.E., P.G.E., F. ASCE
Committee Member, Aly Said, Ph.D.
Committee Member, David James, Ph.D., P.E.
Committee Member, Carlos Calderón-Macías, Ph.D.
Graduate Faculty Representative, Wanda Taylor, Ph. D.